# MASTERARBEIT | MASTER'S THESIS

Titel | Title

A novel role for Spp1 and H3K4me3 in meiotic recombination

verfasst von | submitted by

Lisa Maria Kainz BSc

angestrebter akademischer Grad | in partial fulfilment of the requirements for the degree of

Master of Science (MSc)

Wien | Vienna, 2025

| | |
|---|---|
| Studienkennzahl lt. Studienblatt \| Degree programme code as it appears on the student record sheet: | UA 066 865 |
| Studienrichtung lt. Studienblatt \| Degree programme as it appears on the student record sheet: | Masterstudium Molecular Biology |
| Betreut von \| Supervisor: | Univ.-Prof. i.R. Dr. Franz Klein |

# Acknowledgments

I would like to thank everyone who contributed to this Master thesis and supported me along the way, with particular gratitude to the following people and groups.

First, I would like to thank my supervisor, Franz Klein, for giving me the opportunity to start out in his lab and for allowing me a lot of freedom, while working on a project that I am passionate about. This Master thesis would not have been possible without his continued support and guidance, and all the engaging discussions that shaped my work.

My sincere gratitude also goes to our collaborator Valerie Borde for her highly valuable feedback and contributions and to Akira Shinohara and Kim Nasmyth for kindly providing us with antibodies.

Moreover, I truly appreciate the friendly and supportive community in the Department of Chromosome Biology at Max Perutz Labs, and I also would like to thank the Max Perutz Labs BioOptics – Light Microscopy facility (Irmgard Fischer, Josef Gotzmann, and posthumously Thomas Peterbauer) and the Next Generation Sequencing Facility at Vienna BioCenter Core Facilities (VBCF), member of the Vienna BioCenter (VBC), Austria.

Of course, I would like to express my gratitude to all current and former members of the Klein lab for their friendship and creating such an excellent and fun working environment. Special thanks to Mustafa Alaabo, Martin Xaver, Claudia Kuntner, Max Benesch, Theresa Dangl and Julia Babel – I greatly enjoyed our coffee breaks, deep talks about science and everything else, and an awesome conference. Thanks also to Michele Paganini, with whom I co-planned the best-organized Advanced Genetic Engineering course ever. I am grateful to Doris Chen for her last-minute tutorial on data analysis and all her bioinformatic support, and to Magdalena Vesely for her irreplaceable technical skills and for always having an open ear. I would particularly like to thank Viktoria Prast, who taught me most of my practical lab skills, for sharing my humour and just being a pleasure to work with.

Finally, I thank my family and friends for all their love and support, which offered both balance and strength.

# Contents

# Abstract

Homologous chromosomes must be linked by crossovers in the first meiotic division to ensure faithful segregation. These crossovers arise from repair events following the formation of programmed DNA double-strand breaks (DSBs). DSBs occur primarily in active promoters enriched for H3K4me3 and located in chromatin loops, whereas the DSB machinery – Spo11 and its accessory proteins Rec114, Mei4 and Mer2 – is associated with the chromosome axis. The PHD finger protein Spp1 has been proposed as tether between future DSB sites and the DSB machinery by simultaneously binding H3K4me3 and Mer2. Interestingly, *spp1*Δ is synthetic lethal with the zmm$^-$ mutants (ZMM proteins: Zip1-4, Msh4-5, Mer3, Spo16), which promote DSB repair and crossover designation.

This Master thesis demonstrates that Spp1 and H3K4me3 contribute to meiotic DSB repair through a role that extends beyond DSB formation. Absence of Spp1 or H3K4me3 leads to pronounced delays in meiotic progression, indicating that DSB repair is compromised. STED microscopy revealed that in a background, where cells resort to the unregulated joint molecule (JM) pathway (*zmm*$^-$*, sgs1-mn*), formation of stable axial associations heavily relies on Spp1 and H3K4me3. The Mer2-Spp1 interaction, however, is dispensable for this stabilization. Cytological analysis and genome-wide Protec-seq emphasize that break number, timing and positioning cannot solely explain the defects in *spp1*Δ and *H3K4A* mutants. These mutants accumulate a considerable number of DSBs that can recruit repair factors, while altered DSB landscape alone only has minor effects.

Thus, we propose that, in the combined absence of ZMM proteins and H3K4me3/Spp1, helicases or nucleases gain inappropriate access to strand invasion intermediates, resulting in their destabilization and the loss of axial associations.

# 1 Introduction

## 1.1 Meiosis

For sexual reproduction, organisms depend on a specialized type of cell division called meiosis, in which the diploid chromosome content is faithfully reduced to a haploid one. Thereby enabling the eventual merging of two haploid germ cells, which inherited single recombined traits from their maternal and paternal chromosomes.

Meiosis consists of a single round of pre-meiotic DNA replication followed by two consecutive rounds of chromosome segregation. While meiosis I, the first meiotic division, separates the homologous chromosomes, meiosis II, the second meiotic division, divides the sister chromatids, resulting in four haploid germ cells from one diploid precursor. This achieves high genetic variation in the offspring, owed to meiotic recombination and random assortment of sister chromatids into the germ cells. The advantage of meiotic recombination is the ability of adapting to changing environmental conditions by creating novel genetic combinations. However, it is also a necessity for faithful chromosome segregation by connecting the homologous chromosomes prior to the first meiotic division.

Both, meiosis I and II, follow the order of prophase, metaphase, anaphase and telophase, with underlying mechanisms comparable to the vegetative cell division, mitosis. The prophase of meiosis I can be further divided into several substages: leptotene, zygotene, pachytene, diplotene and diakinesis, making it the longest phase of meiosis.

After meiotic DNA synthesis and at the beginning of leptotene, the two DNA strands of the sister chromatids start to become individualized through the combined activity of topoisomerases and structural maintenance of chromosome (SMC) complexes, condensin and cohesin (Hartsuiker, Bähler and Kohli, 1998; reviewed in Zickler and Kleckner, 2015). This was also shown for mitosis, where topoisomerase II and SMC complexes cooperate to facilitate chromosome condensation (reviewed in Nitiss, 2009). While type I topoisomerases nick dsDNA to relax supercoiled DNA, type II topoisomerases can cleave dsDNA strands and thus disentangle DNA (reviewed in Pommier *et al.*, 2016). Condensin is the SMC molecule that enables sister chromatid disentanglement, confers thread formation and longitudinal rigidity of meiotic chromosomes (Houlard *et al.*, 2015). During the condensation process the sister chromatids become organized into linear looped arrays, which are held together at their axis by the meiosis specific Rec8 cohesin (Klein *et al.*, 1999; Nasmyth, 2001). Recruitment of Red1 and Hop1, that later become lateral elements of the synaptonemal complex (SC) (Hollingsworth and Byers, 1989; Smith and Roeder, 1997), depend on the presence of Rec8 (Sun *et al.*, 2015). Red1 is required for maximal levels of meiotic recombination and normal formation of programmed meiotic DNA double strand breaks (DSBs) (Mao-Draayer *et al.*,

1996), while it also contributes to interhomolog bias (Schwacha and Kleckner, 1997). Hop1 directly interacts with Red1 (Smith and Roeder, 1997) and facilitates chromosome pairing, SC formation and crossover (CO) formation (Hollingsworth and Byers, 1989). At this stage the DSB machinery, made up by Spo11 and its accessory proteins Rec114, Mer2 and Mei4, is tethered to the chromosome axis via Red1 and Hop1 (Panizza *et al.*, 2011). Spo11 is a type II-topoisomerase-like transesterase, that confers the catalytic activity for DSB formation (Keeney, Giroux and Kleckner, 1997). The DSBs are further processed by 5' to 3' single-strand resection, after which the ssDNA tails form nucleoprotein filaments with Rad51 and Dmc1. Subsequently, the search for homologous DNA sequences is promoted through single strand invasion (Hong, Shinohara and Bishop, 2001; Ogawa *et al.*, 1993; Sung, 1994).

In the zygotene stage, pairing between the homologous chromosomes advances by homology search and SC formation, so that homologous recombination can eventually take place. In organisms that rely on SC formation for pairing and recombination, the proteinaceous structure polymerizes from recombination nodules in a zipper-like fashion. The SC consists of the lateral elements Red1 and Hop1, the transversal element Zip1, and the central elements Ecm11 and Gmc2. Emc11 is modified with the small ubiquitin-like modifier (SUMO), important for the assembly of Zip1. Thus, SUMO colocalizes with Zip1 and specifically promotes chromosome-associated SC polymerization (reviewed in Zickler and Kleckner, 2015).

The paired chromosomes condense even further, while the formed DSBs are repaired and homologous recombination is completed during pachytene. The exchange of segments between chromatids is called crossover (CO) and each pair of homologs must receive at least one. This obligatory CO ensures the correct segregation of homologous chromosomes in meiosis I and is therefore essential for successful meiotic division ("crossover assurance"). During meiosis, interhomolog bias exists to ensure that CO predominately form between the homologs (reviewed in Hunter, 2015). CO are a consequence of DSB repair for which there are three possibilities but only two yield CO. Even though, the repair through synthesis dependent strand annealing (SDSA) results in non-crossovers (NCO), DNA sequences can still be recombined between the homologs. Non-interfering CO (class II CO) are established through unregulated formation of double Holliday junctions (dHJs), which can also be cleaved in NCO depending on the cleavage orientation of each HJ. The ZMM pathway is responsible for 75-85% of CO in *Saccharomyces cerevisiae* and produces interfering CO (class I CO), that supress the formation of other CO in their proximity (reviewed in Pyatnitskaya, Borde and De Muyt, 2019).

During diplotene the SC is disassembled, whereas the homologous chromosomes remain connected via chiasmata, the visible consequence of CO. In the subsequent diakinesis stage, the last stage of prophase I, the chromosomes appear most condensed with chiasmata still

clearly visible. The nucleoli disappear, the nuclear membrane breaks down and meiotic spindle starts to form, resembling the prometaphase of mitosis (reviewed in Hunter, 2015).

With this, the prophase of the first meiotic division is completed and followed by metaphase I. The homologous pairs, which are connected through chiasmata, are aligned at the metaphase plate through microtubules attached to their kinetochores. The kinetochore microtubules attached to the kinetochores of the sister chromatids emanate from the same spindle pole. Tension is promoted through distal sister chromatid cohesion and at least one crossover to ultimately pull the homologs apart. Distal sister chromatid cohesion remains intact until anaphase I, where all chromosomes must be correctly bioriented for the cell to proceed. Although, cohesin at the arms of the sister chromatids is cleaved, centromeric cohesin stays protected by Shugoshin. The first meiotic division is complete, when the chromosomes have arrived at opposite poles during telophase I.

Immediately without DNA replication, prophase of the second meiotic division follows. Here, the sister chromatids are again condensed into shortened and thickened threads. In the subsequent metaphase, the kinetochore microtubules for one chromosome emanate from opposite spindle poles to attach at the sister chromatid kinetochores. Thus enabling the ultimate separation of the sisters and aligning the chromosomes at the metaphase plate, rotated 90 degrees from metaphase I in metaphase II. At this point, the centromeric cohesin is no longer protected and can be cleaved in anaphase II to finally separate the sister chromatids. In the second telophase of meiosis the nuclear envelopes are reformed, resulting in four haploid progeny (Alberts *et al.*, 2015).

## 1.2 DSB formation

### 1.2.1 Spo11

Meiotic recombination is initiated by the formation of programmed DNA double strand breaks (DSBs) at the onset of meiosis I. These programmed DSBs are introduced by the conserved transesterase Spo11, a homolog to the catalytic subunit of the archaeal type IIB topoisomerase VI. Spo11 was initially implicated in DSB formation by the purification of protein-DNA complexes from a specific mutant that accumulates breaks with a covalently attached protein (Keeney and Kleckner, 1995), later identified as Spo11. This observation strongly suggested, that meiotic DSBs are introduced via a topoisomerase-like transesterase mechanism (Keeney, Giroux and Kleckner, 1997). Independently, Bergerat *et al.* 1997 discovered a novel family of type II topoisomerases in the form of topoisomerase VI (Topo VI) from the archaeon *Sulfolobus shibatae* – type IIB. Spo11 shares similarities in structure and sequence with the catalytic A subunit of Topo VI, and a tyrosine in the 5Y-CAP motif conserved between the homologs was

identified as essential for Spo11 activity. Additionally, a Toprim domain with a metal-binding pocket presumably plays a role in the active site of type II topoisomerases (Berger *et al.*, 1998; Keeney, 2001; Keeney, 2008; Nichols *et al.*, 1999). Based on the homology of Topo VI and Spo11 and the known mechanism of action by type II topoisomerases, Spo11 was proposed as the catalytic subunit responsible for DSB formation in meiosis.

The mechanism by which Topo VI facilitates DNA breaks was first described over 30 years ago by Bergerat, Gadelle and Forterre, 1994. Like other topoisomerases, it catalyses DNA cleavage through a transesterification reaction, by which a tyrosine residue on the enzyme attacks the phosphorus in the DNA backbone. The enzyme then remains covalently bound to the DNA through a tyrosyl phosphodiester bond, which reversibly breaks the DNA and can later be religated. This mechanism is a hallmark of both type I and type II topoisomerases: type I enzymes cleave a single DNA strand, while type II enzymes cleave both strands in a duplex in concert, i.e. inserting a DSB (reviewed in Wang, 2002).

The archaeal topoisomerase VI is able to relax both positively (overwound) and negatively (underwound) supercoiled DNA and shows a strong decatenase activity, meaning that one DNA molecule is passed through the formed break of another DNA molecule. It acts as a heterotetrametric complex made up by two A subunits and two B subunits (Bergerat, Gadelle and Forterre, 1994). The A subunit carries the catalytic tyrosine responsible for DNA cleavage, while the B subunit is responsible for ATP hydrolysis (Bergerat *et al.*, 1997). Typical topoisomerases are essential for the relaxation of supercoiled DNA and the decatenation of DNA molecules during processes like DNA replication and transcription. The ability to re-ligate the breaks is an essential function. Even though, Spo11 resembles the A subunit of Topo VI it has evolutionary lost the ability to religate the broken DNA strands. Instead, Spo11 generates irreversible DSBs, while staying covalently bound to the 5’ ends of the DNA strands through a tyrosyl phosphodiester bond via the catalytic Tyr135. Hereby, Spo11 acts as a dimer and generates 5’ overhangs of two nucleotides (Liu, Wu and Lichten, 1995). Only after DSB processing through endo- and exonucleolytic strand resection, Spo11-oligonucleotides (protein-DNA complexes) are excised from the genome. Topoisomerase II-oligonucleotides can also be found in vegetative cells, if the relegation of a break fails, suggesting a general mechanism for repair of protein-linked DSBs. In the case of Spo11-oligonucleotides or Spo11-oligos, they either consist of estimated 21-37 nucleotides in length or <12 nucleotides (Keeney, Giroux and Kleckner, 1997; Neale, Pan and Keeney, 2005). These Spo11-oligos were later used to map DSB sites genome-wide (Pan *et al.*, 2011), which led to the observation that number and location of DSBs depend on the activity of DNA damage-responsive kinase Tel1 (ortholog of mammalian ATM). In a *tel1*$\Delta$ mutant the level of Spo11-oligos increases, while the

number of nucleotides in the DNA-protein complexes is altered, as well (Mohibullah and Keeney, 2017).

Recently, it has been discovered that concerted cuts by Spo11 dimers lead to DNA fragments that are capped on both ends by Spo11, when they are excised (Johnson *et al.*, 2021; Prieler *et al.*, 2021). These double DSB (dDSB) fragments can range from approximately 34 bp to several hundred bp, leaving gaps of the same size in the genome. The lengths of the fragments demonstrate a periodicity of about 10.4n + 3 bp, suggesting that Spo11 cuts on the same face of underwound DNA. In wild type, fragments up to 66 bp are stable, while fragments larger than 80 bp are degraded with a half-life of 22 min. Mapping the dDSB fragments using a genome-wide approach with single base-pair (Proteq-seq) showed that dDSBs increases are consistent with DSB hotspot sites. Furthermore, sites of dDSBs correlate with topoisomerase II-binding sites, indicating that topological stress and DNA crossings have a role in break formation. In addition, these sites show similarity to a DNA-bending motif, which points to the contribution of DNA bendability determining cleavage sites. Gaps generated through concerted cuts by Spo11, which make up estimated 20% of all initiation events, can give rise to deletions or insertions and offer an explanation for mismatch repair independent gene conversion events. However, whether dDSBs are a substantial source of evolutionary diversity or of pathogenic germline aberrations will require further investigation (Prieler *et al.*, 2021).

From the mechanism by which Topo VI introduces DNA breaks it was originally conferred how Spo11 must function mechanistically, since the protein seemed reluctant in biochemical reconstitution assays (Bergerat *et al.*, 1997). However, in three recent studies the reconstitution of Spo11's catalytic activity was finally achieved. While all three studies used the *Mus musculus* SPO11 (Oger and Claeys Bouuaert, 2025; Tang *et al.*, 2025; Zheng *et al.*, 2025), Oger and Claeys Bouuaert, 2025, could show that SPO11 alone without its accessory proteins was sufficient for break formation. SPO11 is monomeric in solution and dimerizes upon DNA binding when SPO11 is added in excess to the DNA substrate, thereby achieving high occupancy of the substrate by SPO11. The study further provides evidence that the target site selection by SPO11 depends on the sequence, bendability and topology of the DNA substrates and that SPO11 surprisingly can reseal single-stranded DNA nicks, which was confirmed by Zheng *et al*., 2025. Both Zheng *et al*., 2025, and Tang *et al*., 2025, used the mouse SPO11 bound to TOP6BL, the mouse orthologue of the archaeal Top6B subunit. In *Mus musculus*, TOP6BL interacts with Spo11 and forms a complex that is essential for meiotic DSB formation (Robert *et al.*, 2016). As for SPO11 alone, SPO11-TOP6BL is monomeric in solution and can bind to DNA, but only the dimeric complex is able to catalyse DNA cleavage. This suggests a model, where the weak intrinsic dimerization ability of SPO11 restrains its activity *in vivo*, therefore making it dependent on accessory proteins for catalysing break

formation (Zheng *et al.*, 2025). The SPO11-TOP6BL complex requires divalent metal ions, like $Mn^{2+}$, $Mg^{2+}$ or $Ca^{2+}$, for its catalytic activity, with $Mn^{2+}$ supporting the greatest activity (Tang *et al.*, 2025; Zheng *et al.*, 2025). Interestingly, DNA cleavage by the SPO11-TOP6BL complex is ATP independent (Tang *et al.*, 2025). Moreover, all three studies confirmed that SPO11 remains covalently bound to the 5' broken strands of the DNA.

### 1.2.2 Accessory proteins

Spo11 does not act alone, but in fact requires the help of several accessory proteins. In *S. cerevisiae*, this involves 9 other proteins that can be further grouped into four functional subgroups or subcomplexes (Spo11-Ski8, Rec102-Rec104, Rec114-Mei4-Mer2, and Mre11-Rad50-Xrs2). While it is clear that Spo11 exhibits the catalytic function and the MRX complex (Mre11-Rad50-Xrs2) is involved in DNA resection and repair after a DNA break occurred, the function of the other DSB proteins remains enigmatic. However, the absence of any of the accessory proteins prevents Spo11 from inducing DSBs. Several findings support the notion that these proteins are involved in coordinating DSB formation with chromatin, higher-order chromosome structure and replication (reviewed in Lam and Keeney, 2014). The interactions between these accessory proteins suggest that they form an interacting hub during DSB formation, called the pre-DSB recombinosome (Maleki *et al.*, 2007).

Ski8 directly interacts with Spo11 via a specific amino acid sequence on the surface of Spo11 and stabilizes its nuclear localization and chromatin association, and to a lesser extent that of Rec102-Rec104. In vegetative cells, Ski8 is involved in RNA metabolism, specifically mRNA decay in the cytosol, and interacts with Ski3 via a similar amino-acid motif (Arora *et al.*, 2004; Halbach *et al.*, 2013; Kee *et al.*, 2004; Prieler *et al.*, 2005).

Rec102 and Rec104 form a functional unit, that is essential for Spo11 dimerization, nuclear localization, chromatin association and binding to DSB hotspots (Kee *et al.*, 2004; Prieler *et al.*, 2005; Sasanuma *et al.*, 2007). The subcomplex resembles the B subunit of the archaeal topoisomerase VI without the ATPase domain (GHKL domain), which confers the dimerization ability to Topo VI (Claeys Bouuaert *et al.*, 2021b; Robert *et al.*, 2016). Since Rec102 and Rec104 interact directly with Spo11 and Ski8 and also with Mei4 and Rec114, they were proposed as a possible bridge between the subcomplexes Rec114-Mei4-Mer2 and Spo11-Ski8 (Arora *et al.*, 2004; Maleki *et al.*, 2007). Although Rec102 and Rec104 exhibit a preference for localisation to the chromosome axis, it is less prominent as for Rec114, Mei4 or Mer2. Therefore,. the subcomplex is possibly able to interact with both loop and axis sequences, while being more evenly distributed genome-wide (Kee *et al.*, 2004; Panizza *et al.*, 2011). Rec104 is phosphorylated and wild type phosphorylation levels depend on the presence of

Rec102, but not on other DSB proteins. This and the observation that Rec102 and Rec104 are degraded after DSB formation, indicate that the phosphorylation plays a role before DSB formation (Kee *et al.*, 2004).

Two-hybrid coimmunoprecipitation and cytological studies point to the formation of a complex consisting of Rec114, Mei4 and Mer2, abbreviated RMM complex. Each of the three proteins is absolutely required for Spo11-mediated DSB formation and DSB hotspots in *S. cerevisiae* (Arora *et al.*, 2004; Henderson *et al.*, 2006; Li, Hooker and Roeder, 2006; Maleki *et al.*, 2007; Panizza *et al.*, 2011). Biochemical evidence suggests that the proteins actually form two subcomplexes. The first subcomplex involves Mei4 and Rec114, where one Mei4 monomer interacts via its N-terminus with the C-terminus of a Rec114 homodimer. Mer2 on the other hand behaves as a homotetramer. Each subcomplex is monodispersed in solution, but forms nucleoprotein condensates in the presence of DNA (Claeys Bouuaert *et al.*, 2021a). Rec114, Mei4 and Mer2 associate with chromosome axis sites defined by Red1, Hop1 and Rec8 and the SC component Zip1 (Panizza *et al.*, 2011). DSBs, however, preferentially occur in the chromatin loops (Blat *et al.*, 2002; Kleckner, 2006), with DSB hotspots typically located in nucleosome depleted regions (NDR) at active promoter sites in *S. cerevisiae* (Pan *et al.*, 2011). Mer2 first associates with the axis components Red1 and Hop1 and can recruit Mei4 and Rec114 upon phosphorylation of serine 30 by S phase cyclin Clb5-, Clb6-dependent kinase (CDK-S). Moreover, axis localisation of the RMM complex is independent of Spo11's catalytic activity (Panizza *et al.*, 2011).

Although, the *MER2* gene is transcribed in meiosis as well as mitosis, only meiosis specific mRNA splicing yields a functional gene product. Its specific splicing factor Mer1 is only transcribed and expressed during meiosis (Engebrecht, Voelkel-Meiman and Roeder, 1991; Nandabalan and Roeder, 1995). The recruitment of Mer2 to the chromosome axis by Hop1 is likely evolutionary conserved (Kariyazono *et al.*, 2019; Panizza *et al.*, 2011; Tessé *et al.*, 2017; Wang *et al.*, 2023). However, only when Red1 is present can Mer2 bind to Hop1 in pull down experiments. Red1 potentially induces conformational changes in Hop1's HORMA domain, while Red1 alone and Mer2 do not interact. In vitro evidence suggests that Mer2 is able to interact with nucleosomes, likely in a 4:1 stoichiometry, and directly binds to Mre11 as well (Rousová *et al.*, 2021). During meiosis, Mer2 undergoes sequential phosphorylation modifications, first by the CDK-S at S30, which then enables subsequent phosphorylation on S29 by the Dbf4-dependent kinase Cdc7 (DDK). Both modifications are indispensable for DSB formation (Henderson *et al.*, 2006; Murakami and Keeney, 2008; Sasanuma *et al.*, 2008; Wan *et al.*, 2008). Other by DDK phosphorylated amino-terminal residues (S11, 15, 19, 22) allow normal levels of DSBs (Henderson *et al.*, 2006; Sasanuma *et al.*, 2008; Wan *et al.*, 2008). Besides these modifications, there is also the phosphorylation of S271, without any effect on

DSB formation (Henderson *et al.*, 2006). The phosphorylation of Mer2 enables the further enrichment and recruitment of Rec114, Mei4 and Xrs2 at chromosome axes (Henderson *et al.*, 2006; Sasanuma *et al.*, 2008; Panizza *et al.*, 2011). Mer2 has been proposed to coordinate premeiotic replication with DSB formation, because it is phosphorylated by replication-associated kinases (Murakami and Keeney, 2008). Hereby, DDK associates with the replisome-associated components Tof1 and Csm3, which recruit it to the replisome to phosphorylate Mer2 in the wake of the replication fork (Murakami and Keeney, 2014).

In contrast to Mer2, Rec114 is phosphorylated by the DNA damage signal transduction kinases Tel1 and Mec1 (ATM/ATR) only after DSB formation (Carballo *et al.*, 2013; Sasanuma *et al.*, 2008). Tel1 and Mec1 phosphorylate five serines and three threonines, seven of which located within two [S/T]Q cluster domains also found in several others of their targets. Replacing these eight S/T residues by alanine (*rec114-8A*), which is non-phosphorylatable, causes a modest increase in DSBs as measured by probing for specific loci with Southern blot assays in a resection (*com1Δ/sae2Δ, rad50S*) or recombination (*dmc1Δ*) deficient background. However, this effect could not be seen for all loci tested. Conversely, a phosphor-mimicking mutant, *rec114-8D*, shows a reduction in DSB levels from about 6% in wild type to nearly 0% in a *com1Δ/sae2Δ* background (Chr. III, YCL064C/CHA1 locus) and a reduction from about 25% to under 20% in a *dmc1Δ* background (Chr. VIII, YHL039W locus) after six hours in sporulation media. It has been proposed that the role of Rec114 phosphorylation is to mediate a negative feedback loop, that downregulates DSB formation (Carballo *et al.*, 2013).

Finally, DSB formation also depends on the MRX complex, which is composed of the endo- and exonuclease Mre11, the SMC-resembling protein Rad50, and Xrs2 (NBS1 in mammals) (Alani, Padmore and Kleckner, 1990; Ivanov, Korolev and Fabre, 1992; Keeney, 2001; Nairz and Klein, 1997). The MRX complex initiates strand resection after a break occurred through the catalytic activity of Mre11 and therefore plays a vital role in the repair and recognition of meiotic and mitotic DSBs as well (Casari *et al.*, 2019; Garcia *et al.*, 2011; Gobbini *et al.*, 2016; Moore and Haber, 1996; Paull and Gellert, 1998; Paull, 2018; Tisi *et al.*, 2020). Contrary to the RMM proteins, associated with the chromosome axes, MRX localises to DSB sites directly (Borde *et al.*, 2004; Pan *et al.*, 2011). Mre11 recruitment requires all other DSB proteins with the exception for Rad50 and might be facilitated through the interaction between Xrs2 and Mer2 after Mer2-phosphorylation by CDK-S, once Spo11 is prepared to catalyse the break (Arora *et al.*, 2004; Borde *et al.*, 2004; Henderson *et al.*, 2006). In addition, Xrs2 is responsible for nuclear localisation of Mre11-Rad50 and attracts Tel1 kinase to induce DNA damage signalling (Oh *et al.*, 2016; Tsukamoto *et al.*, 2005). Rad50 has ATPase activity and acts as dimer to tether the broken DNA ends together (de Jager *et al.*, 2001; Rojowska *et al.*, 2014). The *rad50S* mutant contains the single point mutation K81I. It demonstrates a separation of

function, where DSBs can form normally, but processing and repair are blocked, leading to accumulation of Spo11-DNA complexes (Alani, Padmore and Kleckner, 1990). In cooperation with Com1/Sae2 and Exo1's exonuclease activity, the MRX complex liberates Spo11-oligos from the resected DNA ends of the DSB through its initial endo- and exonuclease activity (Cannavo and Cejka, 2014; Neale, Pan and Keeney, 2005; Paull and Gellert, 1998; Prinz, Amon and Klein, 1997; Tsubouchi and Ogawa, 2000).

### 1.2.3 Spp1 and the Set1C/COMPASS complex

DSB formation and recombination preferentially occur between chromatin loops (Blat *et al.*, 2002). Since the DSB machinery and pre-DSB recombinosome are located at the chromosome axis (Kumar, Bourbon and de Massy, 2010; Panizza *et al.*, 2011), a tethered loop-axis complex (TLAC) has been proposed. The TLAC model suggests that future DSB sites in the loops can transiently interact with the DSB machinery at the axis to induce DSBs. The transient engagement of loop regions with the chromosome axis does not only play a role in DSB formation but also in ensuring inter-homolog bias during DSB repair (Blat *et al.*, 2002; Kim *et al.*, 2010; Kleckner, 2006; Panizza *et al.*, 2011). This spatial separation of the DSB machinery and the future DSB sites implies that there exists a physical mechanism that links these two components together for Spo11 to catalyse the break.

Genomic loci obtaining a high frequency of DSBs, the DSB hotspots, are not randomly distributed, but tend to be located in actively transcribed genes in nucleosome depleted regions (NDRs) in promoters of actively transcribed genes (Pan *et al.*, 2011). These promoter regions are marked by trimethylated K4 of histone H3 (H3K4me3) (Ng *et al.*, 2003; Pokholok *et al.*, 2005; Santos-Rosa *et al.*, 2002). In *S. cerevisiae*, the COMPASS (Complex Proteins Associated with Set1) complex or Set1C is exclusively responsible for the deposition of mono-, di-, and trimethylation at H3K4 (Dehé *et al.*, 2006; Ng, Dole and Struhl, 2003). One protein, which became central to the TLAC model, is the PHD finger-containing subunit of the COMPASS complex Spp1. Because Spp1 was shown to interact directly with H3K4me3 marks at DSB hotspots and with Mer2 of the RMM complex (also see **Section 1.2.2**), localized to the chromosome axis, it was proposed as the tether between the DSB machinery and future DSB sites (Acquaviva *et al.*, 2013; Sommermeyer *et al.*, 2013).

The COMPASS complex comprises eight subunits, with Set1 being the methyltransferase subunit and acting as a scaffold for Swd1, Swd2, Swd3, Bre2, Sdc1, Shg1 and Spp1 (Dehé *et al.*, 2006; Nagy *et al.*, 2002; Miller *et al.*, 2001). The study by Sommermeyer *et al.* from 2013 concluded that the recruitment of Spp1 to chromatin depends on Set1 but not on H3K4 methylation or its PHD finger. Therefore, it is important to understand how Set1 is directed to

promoter regions of actively transcribed genes. Set1 is recruited to transcription start sites (TSSs) by interacting with RNA polymerase II (RNAPII) after it has been phosphorylated at serine 5 of its C-terminal domain (CTD-Ser5P). Serine 5 is phosphorylated by the TFIIH-associated kinase Kin28 (Ng *et al.*, 2003). The interaction is facilitated via Set1's N-terminal domain, which interacts directly with the phosphorylated CTD of RNAPII and is dependent on the Swd2 subunit (Bae *et al.*, 2020). The phosphorylated form of RNAPII CTD-Ser5P marks the initial stages of transcriptional elongation and the recruitment of the COMPASS complex enables the continuous trimethylation at promoter-proximal sites (Soares *et al.*, 2017). Trimethylated H3K4, concentrated at the 5' portion of the coding region, strikingly correlates with Set1 occupancy, whereas dimethylation does so only poorly. The CTD of RNAPII is phosphorylated at the promoter region, Set1 however, is associated with the 5' portion of the mRNA coding region, indicating that CTD-Ser5P is not sufficient for Set1 targeting. Rtf1 and Paf1, factors interacting with RNA Pol II and implicated in elongation, are required for normal levels of trimethylated H3K4 and Set1 targeting (Ng *et al.*, 2003). Both factors are components of the RNA Pol II-associated Paf complex involved in transcriptional elongation (reviewed in Rosonina and Manley, 2005).

In addition, crosstalk between histone methylation and ubiquitylation plays a role for H3K4 methylation by Set1 and the targeting of the COMPASS complex. The ubiquitylation of histone H2B at lysine 123 (H2Bub) by the Rad6/Bre1 E3 ligase influences H3K4me3 and H3K4me2 levels and, to a lesser extent, levels of H3K4me1 (Dehé *et al.*, 2006; Dover *et al.*, 2002; Shahbazian, Zhang and Grunstein, 2005; Sun and Allis, 2002). Several studies could demonstrate how H2B ubiquitylation leads to the recruitment of COMPASS subunits, including Spp1, to actively transcribed genes. H2Bub was proposed for directing Swd2 to 5'ends of active genes, which later recruits other COMPASS subunits (Lee *et al.*, 2007). The ubiquitylation of histone H2B at lysine 123 appears to enhance methylation states in a Spp1 dependent manner. Set1 activity is stimulated because Spp1 interacts with Set1's N-SET domain (Kim *et al.*, 2013). Another study suggests that Rad6/Bre1 mediates ubiquitylation of H2B as well as Swd2 via an indirect mechanism. The ubiquitylation of Swd2 then leads to Spp1 recruitment, which can now increase the methyltransferase activity of Set1 (Vitaliano-Prunier *et al.*, 2008). Taken together these studies provide further explanation of how Spp1 is directed to promoter regions in the context of the COMPASS complex.

Because several studies demonstrated through immunoblotting that the absence of Spp1 leads to lower H3K4me3 levels, it was suggested to specifically promote trimethylation (Dehé *et al.*, 2006; Mersman *et al.*, 2012; Schneider *et al.*, 2005). However, upon loss of Spp1, significant H3K4me3 levels are retained specifically near promoters as indicated by ChIP-Seq data. In these mutants, H3K4me2 peak levels are elevated and correlate with H3K4me3 levels

in wild type, while their peak position shifts closer to the TSS. In addition, RNA transcript numbers in *spp1*Δ correlate to a greater extent with H3K4me2 levels than in wild type. These findings rather propose a model, where Spp1 affects Set1 activity more broadly and is not only required for normal levels of H3K4me3. Spp1 could influence the time Set1 remains tethered near a nucleosome, leading to regions that are normally trimethylated acquiring H3K4me2 and a redistribution of dimethylation patterns if Spp1 is absent (Soares *et al.*, 2017).

Deletion of *SET1, SWD3* or *SPP1* results in a delay of meiotic progression, in part caused by a compromised transcriptional program. Compared to wild type *S. cerevisiae, swd3*Δ and *spp1*Δ experience a 2 hour delay, while *set1*Δ even shows a delay of 3 hours, as demonstrated in the study by Sommermeyer *et al*. in 2013. Even though meiotic progression is affected in these COMPASS mutants, spore viability resembles wild type levels (97.9% *set1*Δ vs 98.2% WT). Quantification of DSBs at different DSB hotspots using Southern blots shows a reduction in DSB levels from 100% to approximately 20% for all three mutants. Interestingly, the COMPASS mutants obtain high levels of DSBs in two regions that typically have low DSB levels in wild type. Disrupting (Sommermeyer *et al.*, 2013) or deleting (Acquaviva *et al.*, 2013) Spp1's PHD finger domain results in the same DSB formation phenotype as *spp1*Δ without affecting H3K4me3 levels. Therefore, it was identified as the domain of Spp1, involved in promoting DSB formation. Mutating lysine 4 of histone H3 to alanine (*H3K4A*) has the same effect on DSBs as seen in *set1*Δ, *swd3*Δ and *spp1*Δ mutants. *H3K4A* also experiences a delay in meiotic progression comparable to *set1*Δ and has a slightly lower spore viability with 78.2%. While Set1 and Swd3 are essential for normal H3K4me3 levels based on immunoblotting, Spp1 is not strictly required and the absence of Spp1 leads to a reduction in H3K4me3 (Sommermeyer *et al.*, 2013). Thus, the loss of Spp1 or the deletion or disruption of its PHD finger severely affects DSB formation, even though H3K4me3 can still be detected (Acquaviva *et al.*, 2013; Sommermeyer *et al.*, 2013).

Mechanistically, Spp1 can bind to di- and trimethylated H3K4 via its plant homeodomain (PHD), provided that the second arginine residue of histone H3 (H3R2) is not asymmetrically dimethylated (Kirmizis *et al.*, 2007). PHD fingers are defined as tethering modules that can bind to methylated H3K4 and recruit or stabilize downstream factors. However, there is also evidence of PHD finger containing proteins that bind to unmethylated H3K4 (reviewed in Taverna *et al.*, 2007). PHD finger modules contain seven characteristically spaced cysteines and one histidine ($Cys_4$-His-$Cys_3$) binding two zinc ions (reviewed in Bienz, 2006) and the PHD finger of Spp1 is located towards its N-terminus (Rousová *et al.*, 2021). The module is structurally related to another metal-binding domain, the RING finger domain (Cys3-His-Cys4), which can associate with E2 ligases to mediate ubiquitylation (reviewed in Bienz, 2006). The Mer2 interacting motif, located at the C-terminus of Spp1, is predicted to contain a coiled-coil

domain (Rousová *et al.*, 2021). These domains, which consist of a bundle of at least two or more α-helices, are known to mediate protein-protein interactions and are common in proteins acting as molecular scaffolds for larger complexes. They can also serve as molecular rulers or spacers that position catalytic activities within enzymes or other proteins at fixed distances (reviewed in Truebestein and Leonard, 2016; Priyanka and Yenugu, 2021).

Separation of function mutants identified by two hybrid assays combined with pull down experiments and mass spectrometry revealed that Spp1 can exists within either the Set1 complex or the Mer2 complex. In this study, the mutations disrupting these interactions were included in Spp1's interacting partners Mer2 (*mer2-V195D*) or Set1 (five residues between amino acid 762-794 replaced by serines). Abolishing the interaction between Set1 and Spp1 does not affect meiotic DSB formation, however, Spp1's association with chromosome axis sequences is reduced (Adam *et al.*, 2018). This consistent with the fact that Mer2 is located at the chromosome axis (Panizza *et al.*, 2011) and Spp1 needs to interact with Mer2 to be associated with axis sequences (Adam *et al.*, 2018). The study could also confirm the observation that Spp1 needs to interact with Set1 for normal recruitment to TSSs using ChIP-Seq (Sommermeyer *et al.*, 2013; Adam *et al.*, 2018). When the interaction between Mer2 and Spp1 is disrupted, Spp1's axis localisation is strongly diminished, and the mutant mimics the DSB formation phenotype of *spp1*∆ (DSB levels at WT hotspots reduced and at COMPASS mutant hotspots increased) (Adam *et al.*, 2018). The observation of two distinct complexes is supported by another study where a *SPP1* mutant without the Mer2-interaction motif can no longer colocalize with Mer2, which was determined by immuno-fluorescence microscopy of chromosome spreads. The same study could also demonstrate that the deletion of Spp1's PHD finger is required for the colocalization of Spp1 and Mer2 (Karányi *et al.*, 2018). Surprisingly, the Spp1 interaction deficient Set1 mutant is able to maintain normal levels of H3K4me3 and only combining this mutant with a Spp1 mutant containing a disruptive mutation in the PHD finger module reduces H3K4me3 levels to *spp1*∆ levels. The authors conclude that this domain also plays role in maintaining H3K4me3 levels (Adam *et al.*, 2018).

Size exclusion chromatography coupled to multi-angle light scattering (SEC-MALS) revealed that Spp1 on its own is monomeric. However, in the Mer2:Spp1 complex, most likely obtains a 4:2 stoichiometry, indicating that the Mer2 tetramer plays a role in mediating the dimerization of Spp1 (Rousová *et al.*, 2021). As previously observed (Acquaviva *et al.*, 2013; Adam *et al.*, 2018), the binding affinity between Mer2 and Spp1 depends on Spp1's C-terminal domain, where the Mer2 interaction domain is located. Surprisingly, cross-linking the complex revealed that Spp1 interacts with Mer2 not via its Mer2 binding domain but rather with a region located immediately after its PHD finger domain. Comparison of binding affinities to modified mononucleosomes between the Mer2-Spp1 complex and dimerized Spp1, facilitated via a

GST-tag, the study found that Mer2-Spp1 exhibits a higher binding affinity, potentially indicating a direct contribution of Mer2 to nucleosome binding. In expending on this hypothesis the authors could confirm that Mer2 can bind nucleosomes on its own in a 4:1 stoichiometry (also see **Section 1.2.2**). Interestingly, cross-linking analysis revealed that Spp1 contains more internal contacts in the Mer2-Spp1-H3K4me3 conformation, than in the Mer2-Spp1 complex. This could either indicate that the two copies of Spp1 are located closer together when binding nucleosomes or that binding to H3K4me3 triggers internal rearrangement of Spp1. Unexpectedly, most contacts between Mer2-Spp1 and the nucleosomes are mediated via Mer2, which also strengthens the finding that Mer2 directly contributes to nucleosome binding (Rousová *et al.*, 2021).

In mammals, PRDM9, a histone methyltransferase, that contains a zinc finger and binds to DNA, determines DSB locations and recombination hotspots. The meiosis specific protein is responsible for histone H3 lysine 4 and 36 trimethylation in the vicinity of DSB hotspots of germline cells. In the absence of PRDM9, DSB hotspots are relocated to open chromatin regions particularly in gene promoters. However, these DSBs cannot be repaired efficiently, which results in pachytene arrest and ultimately causes sterility. This leads to the conclusion that other factors besides H3K4me3 marks are involved in determining DSB hotspots. Like Spp1, PRDM9 presumably tethers future DSB sites in the chromatin loops to the chromosome axis to facilitate breaks through the DSB machinery (reviewed in Paigen and Petkov, 2018).

## 1.3 DSB repair and SC formation

### 1.3.1 Resection and strand invasion

Before the DSBs inserted by Spo11 can be repaired as crossovers, the broken DNA ends must be processed through additional steps. Crossovers between the two homologous chromosomes lead to meiotic recombination and are essential for the correct segregation during the first meiotic division. Therefore, each chromosome pair should receive at least one crossover – the obligatory crossover.

The first critical step is strand resection, which can be separated into short and long range resection. Short range resection is initiated by the Mre11-Rad50-Xrs2 (MRX) complex (see also Section 1.2.2) in cooperation with Com1 (also called Sae2) (Prinz, Amon and Klein, 1997; McKee and Kleckner, 1997; Cannavo and Cejka, 2014; Neale, Pan and Keeney, 2005). Hereby, Com1 activates the Mre11 subunit of the MRX complex, which introduces an endolytic nick into the 5'-ending strands approximately 300 nts from the location of the DSB. Mre11 also possesses exonuclease activity and opens the nick up in 3'-5' direction, the direction of the break site (Neale, Pan and Keeney, 2005; Garcia *et al.*, 2011). The initial nick serves as an

entry point for the 5'-3' exonuclease Exo1, the helicase-nuclease pair Sgs1 (ortholog of BLM) and Dna2. In addition to Mre11, these proteins resect the DNA in 5'-3' direction (opposite of the break site). Together this activity produces 800-1000 nts of single-stranded DNA overhangs (long range resection), which act as a precursor for subsequent DNA repair reactions (Garcia *et al.*, 2011; Zhu *et al.*, 2008; Zakharyevich *et al.*, 2010; Mimitou, Yamada and Keeney, 2017; Tsubouchi and Ogawa, 2000).

Following strand resection, the single-stranded DNA overhangs are immediately coated by RPA to prevent the formation of secondary structures. RPA acts as a heterotrimer, consisting of Rfa1, Rfa2 and Rfa3 and is also already required for the generation of these overhangs by Exo1 and Sgs1-Dna2 (Chen, Lisby and Symington, 2013; Brill and Stillman, 1991). Subsequently, RPA is replaced by Rad51 and Dmc2, which are recombinases and vital for the next step of recombination, namely strand invasion. While Rad51 is also active during mitosis, Dmc1 is meiosis specific, promoting invasion of the homologous chromosome and providing interhomolog (IH) bias. Single-end invasion (SEI) results in D-loop formation, in which the invading 3' end pairs with its complementary sequence in the homolog (Schwacha and Kleckner, 1997; Hunter and Kleckner, 2001; Bishop *et al.*, 1992; Shinohara, Ogawa and Ogawa, 1992).

### 1.3.2 Meiotic DSB repair pathways (IH bias, Sgs1, pathway choice)

At the stage, where single-end invasion (SEI) has happened, the repair intermediates can either be dismantled, leading to synthesis-dependent strand annealing (SDSA), or be stabilized, leading to second-end capture and eventual double Holliday junction (dHJ) formation (reviewed in Hunter, 2015; Hunter and Kleckner, 2001; Allers and Lichten, 2001). Here, the bias towards the homologous chromosome as repair template reverses the mitotic trend of inter sister DSB repair, that would be lethal in meiosis, where pairing and CO formation with the homolog are the goal (Schwacha and Kleckner, 1997; Niu *et al.*, 2005; Hong *et al.*, 2013; reviewed in Zickler and Kleckner, 1998).

Inter homolog (IH) bias does not only involve recombinases Rad51 and Dmc1, but depends on the cooperation between these recombinases, axis proteins like Hop1 and Red1, and the meiosis specific kinase Mek1 (Schwacha and Kleckner, 1997; Cloud *et al.*, 2012; Hollingsworth, Ponte and Halsey, 1995). Hop1 and Red1, which assemble into the axial elements of the chromosome axes during meiosis, recruit Mek1 and Mek1/Tel1 phosphorylate Hop1. Phosphorylation of Hop1 prevents Dmc1 independent processing of DSBs and is required for normal levels of inter homolog recombination. Moreover, Hop1 phosphorylation is a prerequisite for the phosphorylation of Mek1 itself (Carballo *et al.*, 2008). Upon

phosphorylation Mek1 is activated and dimerizes in a Hop1-dependent manner (Niu *et al.*, 2005; Carballo *et al.*, 2008). By activating Mek1 in this manner, Mek1 binds to the chromosome axis (Niu *et al.*, 2007; Niu *et al.*, 2005) and phosphorylates downstream targets such as Hed1 and Rad54. Phosphorylated Hed1 inhibits Rad54, a Swi2/Snf2-like recombination repair protein that normally disassembles dsDNA filaments nucleated by Rad51. Through this mechanism, Mek1 blocks any further repair synthesis locally at the axis, close to the DSB site and indirectly supports Dmc1-mediated repair (Callender *et al.*, 2016; Niu *et al.*, 2009; Schwacha and Kleckner, 1997; Solinger, Kiianitsa and Heyer, 2002). However, Rad51 still contributes to Dmc1 filament formation as an accessory factor (Cloud *et al.*, 2012). Once the chromosomes have synapsed, Mek1 is normally removed from the chromosome. However, in the absence of Pch2, Mek1 persists on the chromosome axis and DSB repair is delayed, indicating that Mek1 creates a local environment that inhibits all repair. Before chromosomes have paired only inter sister repair interactions are impaired, however, when the homologs are in close proximity to each other, inter homolog repair can also be affected (Subramanian *et al.*, 2016)

When inter homolog bias has been established, the next critical step in meiotic recombination is the processing of the strand invasion intermediates. Here, the SEIs can now be repaired through two distinct mechanisms. In the first options, the SEI is dismantled, and the newly synthesized DNA anneals back with the second end of the break, resulting in non-crossover (NCO) products through synthesis-dependent strand annealing (SDSA) (Hunter and Kleckner, 2001; Allers and Lichten, 2001). Alternatively, the SEI is stabilized and undergoes second-end capture, producing a double Holliday junction (dHJ), which can then be resolved as a crossover (Allers and Lichten, 2001; Schwacha and Kleckner, 1995). These repair mechanisms are tightly regulated to secure at least one crossover per homologous chromosome pair (Borner, Kleckner and Hunter, 2004).

A key determinant of pathway choice in the budding yeast is the 3’-5’ RecQ helicase Sgs1, an ortholog of human BLM. The absence of Sgs1 results in a modest increase in crossover (CO) formation, because Sgs1 normally dismantles unstable SEIs, redirecting repair towards SDSA (Jessop *et al.*, 2006; Rockmill *et al.*, 2003). Sgs1 is responsible for disassembly of early SEI intermediates, while the remaining intermediates can become CO or NCO (De Muyt *et al.*, 2012). This activity limits the formation of irregular joint molecule (JM) structures, infrequent in wild type cells, including inter sister JMs, multichromatid JMs or recombinant JMs (two chromatids, where one already obtained a CO) (Jessop and Lichten, 2008; Oh *et al.*, 2008; Xaver *et al.*, 2013). Normally, Sgs1 acts in the context of the STR complex, where it collaborates with topoisomerase III (Top3) and Rmi1 to exhibit its function as early recombination intermediate chaperone (Kaur, De Muyt and Lichten, 2015; Tang *et al.*, 2015).

If the SEI intermediate is not dismantled by Sgs1, it can be committed to the ZMM pathway. This pathway involves the ZMM proteins (including Zip1–4, Msh4–5, Mer3, Spo16), which are a group of factors responsible to recognize and stabilize intermediates, that can become interfering CO, which are also required for SC formation (reviewed in Pyatnitskaya, Borde and De Muyt, 2019). The ZMM proteins, have antagonistic functions to Sgs1 by protecting repair intermediates from the anti-crossover activity of Sgs1 (Oh *et al.*, 2007). The decision whether a repair intermediate becomes a CO or NCO product happens early on, prior to stable strand exchange and independent of the SC. However, once a SEI intermediate has been reserved for the ZMM pathway it becomes embedded in patches of the SC (Borner, Kleckner and Hunter, 2004).

The antagonistic activities of the ZMM proteins and Sgs1 largely control the outcome of a SEI repair intermediate. In the absence of the ZMM proteins, these intermediates are dismantled by Sgs1, resulting in severely reduced crossover levels. If Sgs1 is eliminated in this background, dHJ accumulate in an unregulated manner, which can suppress the ZMM defects (Jessop *et al.*, 2006; Rockmill *et al.*, 2003). Here, cells resort to a third unregulated repair pathway, where dHJs form without the normal control mechanism, generating aberrant JMs (Oh *et al.*, 2008; Jessop and Lichten, 2008). Because of the large number of these unregulated events in *zmm⁻, sgs1-* mutants, chromosome axes align at a close distance even in the absence of Zip1, the lateral element of the SC, a phenomenon called pseudosynapsis (Rockmill *et al.*, 2003).

zmm⁻ mutants experience synapsis defects and reduced axial associations (Pyatnitskaya, Borde and De Muyt, 2019; Tsubouchi, Macqueen and Roeder, 2008; Rockmill *et al.*, 1995). This phenomenon was first described as a cytological feature for *zip1* mutants by Rockmill and colleagues (1995). In *zip1* mutants, the chromosomes can pair homologously but fail to synapse, instead, their axes appear connected at multiple sites along their length – an observation referred to as axial associations. Jessop and colleagues (2006) later demonstrated that *zmm⁻, sgs1⁻* double mutants, including *zip2, zip3, zip4* (B. Rockmill and G. S. Roeder, unpublished data) and *mer3*, experience an increase in crossovers (CO). They proposed that the increase in axial associations observed in these mutants represent cytological manifestations of those CO and thus likely correspond to joint molecules (JMs).

ZMM-dependent CO and CO resulting from unregulated repair events, differ in the way that they are resolved. The ZMM pathway yields class I CO or interfering CO, that can suppress other CO in their vicinity and CO from unregulated repair events are non-interfering and belong to the class II CO (reviewed in Pyatnitskaya, Borde and De Muyt, 2019). The two repair pathways differ specifically in the structure specific nucleases involved in the resolution of dHJs. ZMM-dependent CO (class I) are resolved by MutLγ endonucleases Mlh1-Mlh3 and also

depend on Sgs1 and Exo1. dHJs not stabilized by the ZMM proteins are resolved by other structure specific nucleases, such as Mus81-Mms4, Slx1-Slx4 and Yen1. In this unregulated pathway, which is quite minor in Sgs1 positive strains, JMs between sisters or homologs, as well as multi chromatid JMs may be converted to CO or NCO (Jessop and Lichten, 2008; de los Santos *et al.*, 2003; Cannavo *et al.*, 2020; Zakharyevich *et al.*, 2012).

### 1.3.3 The ZMM proteins

Genes are part of the ZMM pathway if they are essential for the formation of class I CO and are required for normal assembly of the synaptonemal complex (SC). Without them cells experience synapsis defects and typically a decrease in spore formation and viability, as well as delays in meiotic progression. The name ZMM derives from the fact that many of these genes begin with the letters Z or M. The ZMM (Zip/Msh/Mer) proteins include Zip1, which forms the transverse filament of the SC, Zip2/Zip4/Spo16, which bind branched DNA structures as the ZZS complex, the SUMO E3 ligase Zip3, Msh4 and Msh5, homologs of MutSɣ, the 5'-3' DNA helicase Mer3; and Ecm11 and Gmc2, forming the central element of the SC and required for regulating the distribution of interfering CO (reviewed in Pyatnitskaya, Borde and De Muyt, 2019). The ZMM proteins stabilize strand invasion intermediates against Sgs1 (Kaur, De Muyt and Lichten, 2015; Jessop *et al.*, 2006) allowing the formation of SEIs (Borner, Kleckner and Hunter, 2004). Afterwards, in a process called second end capture mediated by Rad52, the second 3'-end of the DSB anneals to the growing D-loop (Lao *et al.*, 2008), subsequently forming a dHJ (Schwacha and Kleckner, 1995), which is then exclusively resolved as CO by the MutLɣ resolvases Mlh1-Mlh3 (Borner, Kleckner and Hunter, 2004; Cannavo *et al.*, 2020; De Muyt *et al.*, 2012; Zakharyevich *et al.*, 2012).

In budding yeast, Zip1 makes up the transverse filament of the SC, bridging the two axial elements of the homologous chromosomes (also called lateral elements) within the SC at a spacing of about 100 nm (Sym, Engebrecht and Roeder, 1993; Tung and Roeder, 1998). Structurally, the protein contains a central coiled-coil region flanked by two globular domains. Within the SC, Zip1's C-terminal globular domain is oriented towards the lateral elements, while the N-terminal domains from two opposing Zip1 molecules interact with each other, forming the characteristic zipper-like structure of the SC (Dong and Roeder, 2000). Zip1 is recruited early on during meiotic recombination and its presence is a prerequisite for Zip3 localization to DSB sites (Serrentino *et al.*, 2013). Zip1 foci are still formed even if other ZMM proteins are absent (Agarwal and Roeder, 2000; Chua and Roeder, 1998; Shinohara *et al.*, 2008; Storlazzi *et al.*, 1996; Tsubouchi, Zhao and Roeder, 2006; Chen *et al.*, 2015). Following Zip1's recruitment the synapsis initiation complex (SIC) is assembled, which includes at least

Zip1, Zip2 and Zip3 and serves as a platform for Zip1 polymerization (Fung *et al.*, 2004). Zip1 interacts with the axial element Red1, likely mediated through poly-Smt3 (SUMO) chains (Cheng *et al.*, 2006; Lin *et al.*, 2010). Consistent with this, SUMO can be detected along the chromosome axes and synapsed regions, and several proteins required for meiotic recombination, including Zip1 and Red1, are SUMOylated or contain SUMO interactions motifs (SIMs) (Cheng *et al.*, 2006; Hooker and Roeder, 2006). Zip1 can self-assemble into large structures termed polycomplexes (PCs), typically located near the nucleolus. These PCs often retain an organization resembling the tripartite structure of the SC and can incorporate Rec8 or Red1 and other SC components (Klapholz, Waddell and Esposito, 1985; Sym and Roeder, 1995).

The ZZS complex composed of Zip2, Zip4 and Spo16 is a key subgroup of the ZMM proteins (Chua and Roeder, 1998; Shinohara *et al.*, 2008; Tsubouchi, Zhao and Roeder, 2006; De Muyt *et al.*, 2018; Perry, Kleckner and Börner, 2005). Even though, Zip2 and Spo16 are homologous to the structure-specific endonucleases XPF and ERCC1, respectively, neither protein exhibits endonuclease activity in vitro. Zip2 lacks the canonical XPF motif required for catalytical activity and no cleavage can be detected on branched DNA substrates (De Muyt *et al.*, 2018; Arora and Corbett, 2018; Macaisne *et al.*, 2008). Despite this, Zip2's XPF domain is essential for the CO-promoting function of the complex and the Zip2-Spo16 heterodimer can bind to branched DNA structures in vitro, which suggests a role in recognizing CO-prone intermediates and recruiting the full ZZS complex to these sites (De Muyt *et al.*, 2018; Arora and Corbett, 2018). The third member of the complex, namely Zip4, is a large TPR-containing protein (Tsubouchi, Zhao and Roeder, 2006; Perry, Kleckner and Börner, 2005). Tetratricopeptide repeats (TPR) are protein-protein interaction motifs that are frequent in proteins that mediate the assembly of multiprotein complexes (reviewed in D'Andrea and Regan, 2003). Consistently, Zip4 has been reported to interact with other ZMM proteins such as Zip3 and Msh4-Msh5, as well as with the axis proteins Red1 and Hop1, thereby possibly acting as an association hub within the recombination machinery (De Muyt *et al.*, 2018). Unlike Zip2 and Spo16, which localize to DSB sites relatively early during meiosis, Zip4 recruitment occurs slightly later, becoming first detectible 3 hours after meiotic induction and reaching maximum enrichment at 4-5 hours, overlapping with the formation of joint molecules (De Muyt *et al.*, 2018; Pyatnitskaya *et al.*, 2022).

Zip3 presumably functions as a SUMO E3 ligase, since it contains a C3HC4 zinc finger RING domain typical for this enzyme class (Agarwal and Roeder, 2000; Cheng *et al.*, 2006; Perry, Kleckner and Börner, 2005). Its recruitment to sites of DSB repair depends on the DNA damage checkpoint clamp formed by Rad17, Ddc1, and Mec3, in other organisms known as the 9-1-1 complex (Shinohara *et al.*, 2015). In budding yeast, SUMO (small ubiquitin-related

modifier) is encoded by the SMT3 gene and can be covalently attached to protein substrates in order to modulate their activity, localization or interactions (Mahajan *et al.*, 1997; Matunis, Coutavas and Blobel, 1996). Even though, specific SUMOylation targets of Zip3 have not been identified yet, the protein interacts with other ZMM proteins, including Msh4, Zip2 and Zip4, as well as Zip1, the transverse filament of the SC (Agarwal and Roeder, 2000; De Muyt *et al.*, 2018), suggesting that other ZMM proteins are targets of Zip3-dependent SUMOylation.

The heterodimer consisting of Msh4-Msh5 is also referred to as MutSγ and is homologous to the bacterial mismatch repair factor MutS (Hollingsworth, Ponte and Halsey, 1995; Pochart, Woltering and Hollingsworth, 1997; Ross-Macdonald and Roeder, 1994). However, Msh4-Msh5 lack the domain for recognizing base-pair mismatches and are therefore not involved in mismatch repair in yeast (reviewed in Manhart and Alani, 2016). In vitro recombinant human MSH4-MSH5 has a preference for binding recombination intermediates such as D-loops and dHJs (Snowden *et al.*, 2004). In *C. elegans*, MSH-5 forms two adjacent foci at CO sites (Woglar and Villeneuve, 2018), consistent with a model, where Msh4-Msh5 clamp each arm of a dHJ, thereby protecting the junctions from dissolution by the STR complex (Jessop *et al.*, 2006; Oh *et al.*, 2007). In mammals, MSH4-MSH5 interact with MutLγ (Santucci-Darmanin *et al.*, 2002), which might suggest that MutSγ promotes CO formation by stabilizing dHJs and recruiting MutLγ endonuclease (Mlh1-Mlh3) (reviewed in Gray and Cohen, 2016).

The 3′-5′ DNA helicase Mer3 (HFM1 in humans) was first identified in budding yeast (Nakagawa and Ogawa, 1999; Nakagawa, Flores-Rozas and Kolodner, 2001). Biochemical studies revealed that Mer3 can unwind DNA substrates with 3’ overhangs, D-loops and HJs, but can also only bind to D-loop structures in vitro (Nakagawa and Kolodner, 2002; Duroc *et al.*, 2017). The helicase promotes Rad51-mediated D-loop extension, supporting their stabilization into SEIs and thereby designating early ZMM-dependent crossovers (Borner, Kleckner and Hunter, 2004; Hunter and Kleckner, 2001; Mazina *et al.*, 2004). Additionally, Mer3 recruits the mismatch repair-related MutLβ complex (Mlh1-Mlh2), which constrains gene conversion tract length by limiting repair synthesis (Duroc *et al.*, 2017).

### 1.3.4 The SC and DSB down-regulation

To prevent excessive DNA damage through Spo11-induced DSBs, the formation of DSBs is tightly regulated. Recently, it was shown that SC formation triggers chromosome-autonomous feedback, which downregulates meiotic DNA break competence on individual chromosomes (Mu *et al.*, 2020). Interestingly, this regulation is chromosome size dependent, as larger chromosomes typically have lower DSB densities than smaller chromosomes in wild type (Pan *et al.*, 2011). This also affects the formation of crossovers, since smaller chromosomes have

more CO per length (Kaback *et al.*, 1992). However, this negative correlation breaks down in the ZMM mutant *zip3Δ*, which experiences synapsis defects, and DSB formation of larger chromosomes is no longer efficiently downregulated (Mu *et al.*, 2020; Thacker *et al.*, 2014).

A critical step before formation of the SC is chromatin compaction and condensation, primarily facilitated by the SMC molecules cohesin and condensin (Blat *et al.*, 2002; Ding *et al.*, 2006; Yu and Koshland, 2003). Meiotic chromosomes are organized into arrays of linear loops anchored by meiosis specific Rec8 cohesin (Klein *et al.*, 1999; Nasmyth, 2001). Together with Red1 and Hop1, Rec8 subsequently constitutes the lateral element of the SC (Hollingsworth and Byers, 1989; Klein *et al.*, 1999; Smith and Roeder, 1997). The chromosome axis provides a platform from which the axis-associated DSB machinery interacts with future DSB sites in the loops, forming the tethered loop-axis complex (TLAC) (Blat *et al.*, 2002; Kumar, Bourbon and de Massy, 2010; Panizza *et al.*, 2011). Cohesin is loaded onto DNA in a Scc2-Scc4 dependant manner, where it entraps the two sister DNAs within its ring and establishes sister chromatid cohesion (Gruber, Haering and Nasmyth, 2003; Ciosk *et al.*, 2000; Srinivasan *et al.*, 2018; Srinivasan *et al.*, 2019). The core cohesin is formed by the two coiled-coil proteins Smc1 and Smc3, which are connected by kleisin at their ATPase heads, Scc1 in mitosis (Michaelis, Ciosk and Nasmyth, 1997) and Rec8 in meiosis (Klein *et al.*, 1999), and can associate with the hook shaped HAWK proteins (heat repeat proteins associated with kleisins), Scc2, Scc3 and Pds5 (Wells *et al.*, 2017). During interphase, cohesin is responsible for the organization of chromatin into topological associated domains (TADs) (Fudenberg *et al.*, 2016; Rao *et al.*, 2017; Sanborn *et al.*, 2015), while condensin compacts mitotic chromosomes, likely through progressively expanding loops (Ganji *et al.*, 2018), a process termed loop extrusion (LE) (Goloborodko *et al.*, 2016; reviewed in Nasmyth, 2001; Naumova *et al.*, 2013). Cohesin can also extrude loops in vitro, but only in the presence of Scc2, which activates cohesin's ATPase activity and is essential for its dynamic loading (Davidson *et al.*, 2019; Kim *et al.*, 2019; Petela *et al.*, 2018). In order to be a key determinant of loop organization and compaction, also in SC formation, cohesin therefore requires its loader, namely Scc2.

Once SC formation is initiated, advancing synapsis directly downregulates Spo11-dependent DSBs chromosome autonomously. That chromosome size determines DSB density can be explained by the fact that smaller chromosomes synapse more rapidly and therefore lose DSB competence earlier, while larger chromosomes proceed slower. In mutants where homolog engagement (stable, synapsis-associated interactions between homologs) is impaired, Rec114 is retained longer on the chromosome axis, as shown by chromatin immunoprecipitation followed by quantitative PCR (ChIP-qPCR). This suggests that chromosomes spend more time in a DSB-competent state (Mu *et al.*, 2020). These findings are also supported by cytological observations that Rec114 foci seem dimmed and

subsequently disappear in synapsed chromosome regions, according to Zip1 staining (Panizza *et al.*, 2011). Mu and colleagues propose a scenario, where the $AAA^+$ ATPase Pch2 disrupts the interaction between Hop1 and Red1 (Kim *et al.*, 2014) in the context of the SC to remove the DSB machinery from the chromosome axis. $AAA^+$ ATPases are enzymes that can use the energy from ATP hydrolysis to mechanically remodel other proteins or macromolecules (reviewed in Khan, White and Brunger, 2022). Pch2 was shown to direct the relocalization of Hop1 after SC formation (Börner, Barot and Kleckner, 2008), with which the DSB machinery is associated (Panizza *et al.*, 2011). After chromosomes are synapsed other factors that promote Spo11 activity, such as Mei4, Rec102, Rec104, Rec114, and Red1 also dissociate (Keeney, Lange and Mohibullah, 2014). Taken together this could explain how synapsis downregulates DSB formation by remodelling the chromosome axis, followed by the dissociation of the DSB machinery (Mu *et al.*, 2020).

## 1.4 Aim of this study

In this study I set out to understand the synthetic lethal interaction between the ZMM pathway and Spp1, a protein previously thought to be involved only in meiotic DSB formation. This interaction was revealed in a synthetic lethality screen performed by Viktoria Prast (Prast, Master thesis, 2016). Therefore, the work in my Master thesis is based on Viktoria's initial observations and will help to elucidate a role for Spp1 and H3K4me3 in meiotic recombination.

Because DSB hotspots are typically located in chromatin loops (Blat *et al.*, 2002; Kleckner, 2006), while the DSB machinery is associated with the chromosome axis (Panizza *et al.*, 2011), a physical link between the two structures was proposed (Blat *et al.*, 2002; Kim *et al.*, 2010; Kleckner, 2006; Panizza *et al.*, 2011). Spp1 is thought to be that link, as it binds H3K4me3 marks near future DSB sites and interacts with Mer2, a component of the DSB machinery (Acquaviva *et al.*, 2013; Sommermeyer *et al.*, 2013). Although, Spp1 functions within the Set1C/COMPASS complex responsible for H3K4 methylation (Dehé *et al.*, 2006; Ng, Dole and Struhl, 2003), *spp1*Δ mutants surprisingly maintain wild type levels of sporulation and spore viability, but have a delay in meiotic progression (Acquaviva *et al.*, 2013; Sommermeyer *et al.*, 2013).

The synthetic lethality screen identified a group of deletion mutants that are primarily involved in DSB repair and pathway choice, namely the $zmm^-$ mutants. The deletion of *SPP1* in the absence of any ZMM protein (Zip1-4, Spo16, Msh4-5, Mer3) leads to a reduction in viable spore formation compared to $zmm^-$ single mutants. In this background *spp1*Δ does not accelerate meiotic progression (Prast, Master thesis, 2016), consistent with persistent DSB repair intermediates triggering the DNA damage checkpoint arrest (Börner, Kleckner and

Hunter, 2004). By contrast, the *rec114-8D* mutation, which downregulates DSB formation (Carballo *et al.*, 2013), accelerates progression and improves sporulation in zmm$^-$ mutants despite low spore viability (Prast, Master thesis, 2016). In addition, preliminary Calibrated Protec-seq data generated by Silvia Prieler and Doris Chen and published studies (Sommermeyer *et al.*, 2013; Bishop, 1994; Shinohara *et al.*, 1997; Gasior *et al.*, 1998) indicate that *spp1*Δ only causes a modest reduction in DSB levels. Together, these findings suggest that abnormal DSB formation alone cannot explain the synthetic interaction between s*pp1*Δ and zmm$^-$ mutants.

Typically, the detrimental effects of zmm$^-$ mutations can be suppressed by depleting Bloom's helicase Sgs1 (*sgs1-mn*), which promotes repair via the unregulated crossover pathway (Jessop and Lichten, 2008; Jessop *et al.*, 2006; Oh *et al.*, 2008). However, *sgs1-mn* failed to rescue the *zmm$^-$, spp1*Δ phenotype (Prast, Master thesis, 2016), implying that Spp1 plays a role specifically within this alternative repair pathway.

Using meiotic time course experiments to analyse progression, sporulation efficiency and spore viability, I confirmed and further substantiated these initial observations.

Based on these findings, my study aimed to determine why Spp1 becomes specifically important in the absence of the ZMM pathway, whether this requirement reflects its proposed tethering function between H3K4me3 and Mer2, or whether Spp1 contributes an independent activity to meiotic DSB repair. Furthermore, another goal was to evaluate whether changes in DSB distribution or global DSB levels contribute to the synthetic defects. To address these questions, I combined genetic assays in the form of meiotic time course experiments, high resolution microscopy, namely STED microscopy, and genome-wide Calibrated Protec-seq.

# 2 Material and Methods

Material and methods are partially described in my Bachelor thesis (Kainz, Bachelor thesis, 2022).

## 2.1 Yeast Methods

Throughout my Master thesis, I primarily used *Saccharomyces cerevisiae* SK1, which is known to sporulate rapidly and synchronously and therefore very suitable to study meiotic mechanisms (Kane and Roth, 1974).

With sufficient nutrients SK1 cells divide mitotically approximately every 100 minutes. However, diploid cells can undergo meiosis in an environment with pour carbon sources and no nitrogen, which results in four haploid progenies. The four haploid spores are contained in an ascus, where two belong to the MATa and two the MATα mating type. Normally, haploid cells can switch their mating type and become self-fertilized, for which they depend on the expression of the HO endonuclease (Haber, 2012; reviewed in Herskowitz, 1988).

All strains in this study contain a disrupted HO gene to prevent mating type switching and self-fertilization. Yeast handling was performed without the use of flame or laminar flow, and cultures were incubated at 30 °C unless stated otherwise. Yeast strains were patched or streaked on agar plates using autoclaved toothpicks, and liquid cultures were grown shaking at 200 rpm.

### 2.1.1 Yeast Media

In this section components used in the standard liquid and solid media for yeast cultivation are listed.

For routine yeast cultivation of haploid or diploid strains the nutrient rich YPD+ medium is employed. To detect *petite* mutants, which have mitochondrial defects (reviewed in Lipinski, Kaniak-Golik and Golik, 2010), YPG+ is used, as it contains a nonfermentable carbon source (glycerol). Before transferring diploid cell to minimal sporulation medium (SPM), the cells are grown in liquid pre-sporulation medium (SPS). For meiotic time courses, an amino acid mix is added to SPM. Typically, wild type cells sporulate very efficiently after 24 h in liquid SPM and at a slightly lower efficiency on SPM plates.

Synthetic drop out (SD-) media can select for specific auxotrophic genetic markers, and of course, media containing antibiotics selects for specific resistance conferring cassettes. The

resistance cassette KanMX encodes the aminoglyCOide phosphotransferase (APT) and confers resistance against Geneticin (G418) (Hadfield et al., 1990). Resistance against nourseothricin (ClonNAT) is conferred by the NatMX cassette, containing the nourseothricin N-acetyltransferase gene. The HphMX cassette encodes the hygromycin B phosphotransferase for resistance against Hygromycin B (Goldstein and McCusker, 1999).

To assess the mating type of haploid strains or detect diploid contaminations, strains are mated with mating type tester strains FKy515 and FKy516 on SM plates.

**YPD+ liquid – Rich medium (1L)**

| | |
|---|---|
| Yeast Extract ((Difco, 212750) | 10 g |
| Peptone (Difco, 211677) | 20 g |
| GluCOe | 20 g |
| Ade/Ura/Trp mix (5 g each) | 250 mg |
| $dH_2O$ | ad 1000 ml |

Sterilized using 0.2 µm MF75 Bottle-Top-Filter PES (Thermo Fisher, 3470570)

**YPD+ plates**

| | |
|---|---|
| Yeast Extract (Difco, 212750) | 10 g |
| Peptone (Difco, 211677) | 20 g |
| Agar (LabM, MC002-A) | 20 g |
| $dH_2O$ | 900 ml |

Autoclaved at 121°C for 20-30 min.

After autoclavation, add:

| | |
|---|---|
| GluCOe (20 g/L, sterilized using 0.2 µm MF75 Bottle-Top-Filter PES (Thermo Fisher, 3470570)) | 100 ml |
| Ade/Ura/Trp-Mix (5 g each) | 250 mg |

**YPG+ plates**

| | |
|---|---|
| Yeast Extract (Difco, 212750) | 10 g |
| Peptone (Difco, 211677) | 20 g |
| Agar (LabM, MC002-A) | 20 g |
| Gylcerol (3% v/v) | 30 ml |
| $dH_2O$ | ad 1000 ml |

Autoclaved at 121°C for 20-30 min.

**SPS liquid – Presporulation medium (1L)**

| | |
|---|---|
| Yeast Nitrogen Base w/o amino acids and w/o ammonium sulfate (Difco, 233520) | 1.7 g |
| Ammonium Sulfate | 10 g |
| Yeast Extract (Difco, 212750) | 5 g |
| Peptone (Difco, 211677) | 10 g |
| Potassium Acetate | 10 g |
| Potassium hydrogen phthalate (Merck, 1.04874.1000) | 10.2 g |
| $dH_2O$ | ad 1000.0 ml |

pH 5.5 using 10 M KOH

Sterilized using 0.2 µm MF75 Bottle-Top-Filter PES (Thermo Fisher, 3470570)

**SPM liquid (2% Potassium Acetate) – Sporulation medium (1L)**

| | |
|---|---|
| Potassium Acetate | 20 g |
| $dH_2O$ | ad 1000 ml |

Autoclaved at 121°C for 20-30 min.

Add amino acid mix before use of SPM (2 ml in 1 L SPM).

Amino acid mix for SPM liquid medium

| | |
|---|---|
| Uracil (Sigma Aldrich, U0750-100G) | 100 mg |
| L-Tryptophan (Sigma Aldrich, T0254-25G) | 100 mg |
| L-Histidine (Sigma Aldrich, H8000-100G) | 100 mg |
| L-Arginine monohydrochloride (Sigma Aldrich, A5131-100G) | 100 mg |
| L-Leucine (Sigma Aldrich, L8000-100G) | 100 mg |
| $dH_2O$ | ad 50 ml |

Sterilize by syringe filter (0.2 µm; Thermo Fisher, 10067860) and store at - 20 °.

**SPM Plates:**

| | |
|---|---|
| Potassium Acetate | 20 g |
| Agar (LabM, MC002-A) | 20 g |

| | |
|---|---|
| $dH_2O$ | ad 1000 ml |

Autoclaved at 121°C for 20-30 min.

**SD-ADE/-URA/-TRP plates – synthetic drop out media:**

For Dropout omit the appropriate ingredient.

| | |
|---|---|
| Yeast Nitrogen Base w/o amino acids and w/o ammonium sulfate (Difco, 233520) | 1.7 g |
| Ammonium Sulfate | 5.0 g |
| Casamino acids (Difco, 223120) | 11.0 g |
| Adenine | 55.0 mg (**omit for –ADE**) |
| Tyrosine | 55.0 mg |
| Uracil | 55.0 mg (**omit for –URA**) |
| $dH_2O$ | ad 1000.0 ml |
| pH 6 | |

| | |
|---|---|
| Agar (LabM, MC002-A) | 20.0 g |

Autoclaved at 121°C for 20-30 min.

After autoclaving, add:

| | |
|---|---|
| GluCOe (20 g/L, sterilized using 0.2 µm MF75 Bottle-Top-Filter PES (Thermo Fisher, 3470570)) | 100 ml |

When cooled down to 55-60°C add:

| | |
|---|---|
| Leucine (10 g/L, sterilized using 0.2 µm syringe filter) | 5 ml |
| Tryptophan (10 g/L, sterilized using 0.2 µm syringe filter) | 5 ml (**omit for -TRP**) |

**SD-ARG/-HIS/-LEU/-LYS plates – synthetic drop out media**

| | |
|---|---|
| Yeast Nitrogen Base w/o amino acids and w/o ammonium sulfate (Difco, 233520) | 1.7 g |
| Ammonium Sulfate | 5.0 g |
| Adenine | 55.0 mg |
| Tyrosine | 55.0 mg |
| Uracil | 55.0 mg |
| $dH_2O$ | ad 1000.0 ml |
| pH 6 | |

| | |
|---|---|
| Agar (LabM, MC002-A) | 20.0 g |

Autoclaved at 121°C for 20-30 min.

After autoclaving, add:

| | |
|---|---|
| GluCOe (20 g/L, sterilized using 0.2 µm MF75 Bottle-Top-Filter PES (Thermo Fisher, 3470570)) | 100 ml |

When cooled down to 55-60°C add:

| | |
|---|---|
| 100 x Amino Acid Drop out mix | 10 ml |

100 x Amino Acid Drop out mix:

Omit respective amino acid for dropout.

| | |
|---|---|
| L-Lysine (4 mg/L) | 400 mg (**omit for -LYS**) |
| L-Leucine (8 mg/L) | 800 mg (**omit for -LEU**) |
| L-Isoleucine (3 mg/L) | 300 mg |
| L-Methionine (2 mg/L) | 200 mg |
| L-Threonine (20 mg/L) | 2000 mg |
| L-Tryptophan (6 mg/L) | 600 mg |
| L-Phenylalanine (5 mg/L) | 500 mg |
| L-Histidine (2 mg/L) | 200 mg (**omit for -HIS**) |
| L-Arginine (2 mg/L) | 200 mg (**omit for -ARG**) |
| L-Serine (40 mg/L) | 4000 mg |
| L-Valine (14 mg/L) | 1400 mg |
| $dH_2O$ | ad 100 ml |

Sterilized using 0.2 µm syringe filter.

**YPD-G418/YPD-ClonNat/YPD-Hygromycin – antibiotic media**

| | |
|---|---|
| Yeast Extract (Difco, 212750) | 10 g |
| Peptone (Difco, 211677) | 20 g |
| Agar (LabM, MC002-A) | 20 g |
| $dH_2O$ | 900 ml |

Autoclaved at 121°C for 20-30 min.

After autoclaving, add:

| | |
|---|---|
| GluCOe (20 g/L, sterilized using 0.2 µm MF75 Bottle-Top-Filter PES (Thermo Fisher, 3470570)) | 100 ml |

When cooled down to 55-60°C add:

| | |
|---|---|
| respective Antibiotic stock solution | 1 ml |

Antibiotic stock solutions in $dH_2O$:

G-418 Disulphate (ForMedium, G4185) 200 mg/L

ClonNat (Werner BioAgents, 5001000) 100 mg/L

Hygromycin B (ForMedium, HYG5000) 100 mg/L

**SM plates – Synthetic minimal medium**

| | |
|---|---|
| Yeast Nitrogen Base w/o amino acids | |
| and w/o ammonium sulfate (Difco, 233520) | 1.7 g |
| Ammonium Sulfate | 5.0 g |
| $dH_2O$ | ad 1000.0 ml |

pH 5.5-6.0 using KOH

| | |
|---|---|
| Agar (LabM, MC002-A) | 20.0 g |

Autoclaved at 121°C for 20-30 min.

After autoclaving, add:

| | |
|---|---|
| GluCOe (20 g/L, sterilized using 0.2 µm MF75 Bottle-Top-Filter PES (Thermo Fisher, 3470570)) | 100 ml |

### 2.1.2 Storage of *S. cerevisiae* SK1 Strains

Diploid and haploid *S. cerevisiae* SK1 strains can be stored long term at -80 °C in 50 % Glycerol in YPD+. The cells were collected from patches on agar plates using toothpicks and carefully mixed with the appropriate amount of medium to prevent clumping in 2 ml screwcap cryotubes (typically 1 to 1.5 ml medium). To avoid sporulation, diploid strains were only frozen from fresh patches (not older than a day). While haploid strains can be stored at 4 °C over longer periods, they eventually run out of sufficient nutrients, leading to cell elongation. Therefore, haploid strains were also streaked out fresh and incubated o/n before freezing or other treatment. The most resilient are *S. cerevisiae* spores, which can be kept on SPM plates at 4 °C for months.

To revive cells, they were collected from their long-term storage tubes with a micropipette tip or toothpick and dropped onto YPD+ plates. Generally, diploid strains were streaked out for single colonies using a toothpick. Plates with cell droplets were either incubated at 30 °C o/n

or at room temperature (24 °C) for 1.5 days. Single colonies were grown two days at 30 °C or three days at RT.

### 2.1.3 Crossing of SK1 Strains

For a cross between a MATa and MATα strain, cells were revived from long-term storage or taken from fresh patches of strains stored at 4 °C as described above. Fresh strains do not have to undergo incubation before crossing.

To mate two haploid strains, equal amounts of cells were picked up with a toothpick and mixed on a small patch (~ 5 mm in diameter) on a YPD+ plate. The YPD+ plates were incubated o/n before transferring the cells to a SPM plate, where they would sporulate o/n. Spores were then dissected either immediately or stored at 4 °C.

### 2.1.4 Dissection of *S. cerevisiae* Asci

A culture of sporulated *S. cerevisiae* typically contains asci with four, three, two or one spores and unsporulated vegetative cells. Sporulated cells were either taken from a SPM plate and dissolved in 10 µl of $dH_2O$ prior to dissection, or 10 µl were taken from a liquid SPM culture. Liquid cultures of strains obtained from meiotic time courses that showed a low number of asci with four spores (in general *zip3*Δ or *zip4*Δ strains) were concentrated by centrifugation at 14,000 rpm for 10 sec. The spores were incubated with 182 µl of $dH_2O$, 5 µl of 0.5 M DDT and 3 µl of Zymolyase in a 1.5 ml epi for 20 min on a heat block at 30 °C. Afterwards, 25 µl of the mixture were dropped on a vertically held YPD+ plate, so that the drop would run down in a straight line across the plate.

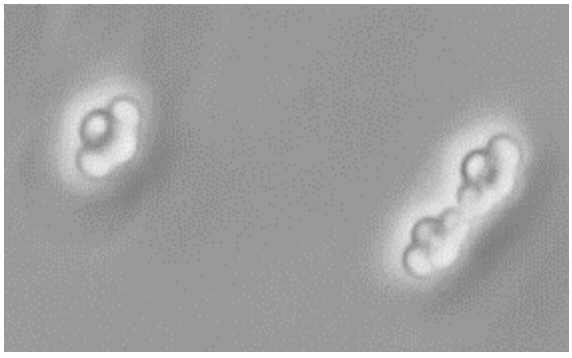

**Figure 2.1-1: Typical four-spored ascus form of *S. cerevisiae* SK1**. Three asci of the strain FKy8895 (*ubc9-K153R,K157R*) in phase contrast microscopy.

Only asci containing four spores were chosen for dissection (examples in **Figure 2.1-1**). Asci containing three, two or one spores are generally less stable and more prone to digestion of their ascus wall by Zymolase. The digestion therefore primarily leaves only asci with four spores, which can be dissected with a Leitz Micromanipulator. The four asCOpores were relocated on separate positions on the YPD+ plate for them to form isolated spore colonies. Plates were incubated until colonies became visible, usually at 30 °C for 2-3 days.

Zymolyase

10 mg/ml T100 Zymolyase (Seikagaku 120491) in $dH_2O$, stored at -20 °C.

0.5 M DTT

771 mg DL-Dithiothreitol (Sigma Aldrich, D-9779) in 10 ml $dH_2O$, stored in 1 ml aliquots at -20 °C.

### 2.1.5 Determination of Mating Type and Genetic Markers

Mating type and genetic markers were typically determined for crosses, where spores were previously dissected on YPD+ plates. First, these plates were replica plated onto autoclaved velvet spanned over a metal stamp. To determine the distribution of genetic markers in the four progenies, plates with suitable drop out media were then put onto the velvet. Additionally, YPG+ plates were used to test mitochondrial function. The mating type tester strains FKy515 (MATα) and FKy516 (MATa) were plated on separate YPD+ plates with autoclaved glass beads onto which spore colonies were replicated. Results for genetic markers were assessed after all plates were incubated at 30 °C for one to two days. The YPD+ plates used for the mating type test were replica plated onto SM plates and incubated again overnight. Only diploid strains contain all required marker for fast growth on the SM plates.

If strains contained the same genetic marker for different mutations, Colony PCR was employed for verification with one parental strain as positive and the other as negative control. Primers were chosen so that the new genetic construct could be distinguished from the parental strain. Point mutations or other mutations introduced by CRISPR/Cas9 were verified by sequencing after Colony PCR.

After candidates with the desired genotype were repatched onto YPD+ plates, they were stored at -80 °C as mentioned above (**Section 2.1.2**), while original plates were kept at 4 °C for as long as possible.

### 2.1.6 Isolation of Homozygous Diploid Strains

To generate zygotes from two fresh haploid strains of opposite mating types, equal amounts of each strain were mixed on a small patch (~ 5 mm in diameter) on a YPD+ plate using a toothpick. Progress was assessed by phase contrast microscopy, where SK1 zygotes can usually be identified by their characteristic propeller shape after 4-5 hours. At this point, cells were streaked out thinly to select and transfer zygotes to isolated positions on the plate with the Leitz Micromanipulator. Zygote incubation typically lasted 2-3 days, after which colonies became visible. Sporulation efficiency was assessed by patching the cells onto SPM plates and mitochondrial function was evaluated with YPG+ plates. To verify that the diploid strain was not contaminated with haploid cells tester strains FKy515 and FKy516 were employed as described above Additionally, phase-contrast microscopy can be used to examine the new strain: haploid cells are smaller and tend to clump together, while diploids are generally larger and more individually distributed. Before storage in 50% Glycerol in liquid YPD+, the homozygous diploid strain was restreaked on YPD+ and incubated at 30 °C overnight.

### 2.1.7 Genomic DNA Isolation for PCR

To isolate genomic yeast DNA the protocol of Harju et al. (2004) was followed. Hereby, one yeast colony of the strain of interest was resuspended in 200 µl Harju buffer and everything was vortexed shortly. Next, the solution was incubated at -20 °C for 2 min prior to incubation at 96 °C for 1 min. The freezing and heating cycle was repeated once, before vortexing for an additional 30 sec and the subsequent addition of 200 µl PCI. Thereafter, everything was vortexed for 2 min, prior to centrifugation for 3 min at full speed and RT. After centrifugation 2 phases should have formed. At this point the PCI should have denatured the proteins and they either remain insoluble in the upper, aqueous phase or are contained in the lower, organic phase. The upper phase, which should now contain the DNA, was transferred to a fresh 1.5 ml Eppendorf tube, where 400 µl of ice cold 96 % ethanol were added for DNA precipitation. The tube was either incubated at RT or at -20 °C for 5 min. The DNA was pelleted by centrifugation at full speed for 5 min at 4 °C and washed once with 70 % ethanol. Finally, the tube containing the DNA pellet was placed on the bench with the lid open to allow the remaining ethanol to evaporate before it was resuspended in 20 µl $dH_2O$. The concentration was measured using Nanodrop 2000 spectrophotometer (Thermo Scientific).

**Harju-Buffer:**

| | |
|---|---|
| Triton X-100 (2 %) | 1.0 ml |
| SDS 100 g/l (10g/l) | 5.0 ml |
| NaCl 5 M (100 mM) | 1.0 ml |
| Tris-HCl, pH 8, 1 M (10 mM) | 0.5 ml |
| EDTA o.5 M (1 mM) | 0.1 ml |
| dH2O | ad 50.0 ml |

sterilized using 0.2 µm syringe filter

**PCI (Phenol : Chloroform : Isoamylalcohol 25:24:1)**

| | |
|---|---|
| Phenol (Biomol 50734) | 25 ml |
| Chloroform (Merck 1.02445.2500) | 24 ml |
| Isoamylalcohol (Merck 1.00979.1000) | 1 ml |

stored at 4 °C under light protection

### 2.1.8 Genome Editing using the CRISPR/Cas9 System

CRISPR/Cas9 (clustered regularly interspaced short palindromic repeats/CRISPR associated 9) originates from an adaptive immune system of bacteria and archaea and has been developed into an efficient tool for genetic engineering (Jinek *et al.*, 2012). Bacteria and archaea use the CRISPR system to protect them against invading bacteriophages. spCas9 of *Streptococcus pyogenes* belongs to one of the best characterized CRISPR systems and introduces RNA-guided, site-specific DSBs. Multiple “spacers” flanked by short palindromic repeats make up the CRISPR array of bacteria. In a process called spacer acquisition these “spacers”, which derive from previously encountered intruders, are acquired and integrated into the CRISPR array (reviewed in McGinn and Marraffini, 2019).

The pre-crRNA is transcribed from the CRISPR array (reviewed in Wiedenheft, Sternberg and Doudna, 2012) before being further processed by RNase III into individual units, so-called guide RNAs (gRNAs). These gRNAs can hybridize with the tracrRNA (trans-activation crRNA) via their repeat sequence (Deltcheva *et al.*, 2011). The resulting RNA complex is bound by Cas9, which is then guided to the “protospacer” on the target sequence. The spacer on the gRNA is hereby complementary to the target DNA. To distinguish the target from the endogenous CRISPR locus, Cas9 requires a PAM site (protospacer adjacent motif, for spCas9: NGG) after the 3’ end of the protospacer. The DSB is then introduced 3-4 nucleotides upstream (5’ direction) of the PAM site by Cas9 (Jinek *et al.*, 2012).

For efficient processing without the need for hybridization between the tracrRNA and the gRNA, the two RNAs were synthetically fused for CRISPR/Cas9 applications – the synthetic guide RNA (or single guide RNA, sgRNA) (Jinek *et al.*, 2012). CRISPR/Cas9-mediated cleavage of DNA can be used to introduce scar-free and marker-free edits in the genome of many organisms with high efficiency. If a PAM site is available, Cas9 can cleave at any target locus. The DSB can then be repaired via nonhomologous end joining (NHEJ) or homologous recombination (HR) if a repair template containing the desired gene edit is supplied (Charpentier and Doudna, 2013).

**CRISPR plasmids**

Yeast mutants generated with CRISPR/Cas9 were mutated using episomal plasmids encoding for the sgRNA, Cas9 and the repair template. The plasmids were either directly assembled by yeast recombineering in the target strains or generated through Gibson assembly first, prior to transformation into the target strains. The sgRNA consists of the 20 bp gRNA and the chimeric gRNA scaffold, corresponding to the tracrRNA. The gRNA should be unique and located as close as possible to the site where the mutation is to be introduced. Of course, the location of the gRNA depends on the availability of PAM sites. To prevent re-cleavage of the edited genome or the plasmid itself, the PAM site should be mutated as a silent mutation in the repair template. For deletions the PAM site should ideally be located in the deleted portion of the genome. To later facilitate screening for correct candidates with a restriction digest, editing should either introduce or destroy a restriction site. This is especially important for point mutations. However, larger insertions or deletions can be differentiated through an analytical PCR based on their size difference to wild type. The inducible pCUP1 promoter controls the transcription of Cas9, while the pSNR51 promoter allows the constitutive expression of the sgRNA. For efficient HR, the desired mutation on the repair template should be flanked by 300-500 bp long homologies. An example for a CRISPR plasmid can be seen in **Figure 2.1-2**.

Following the yeast transformation protocol (**Section 2.1.10**), the CRISPR plasmid or the fragments for plasmid assembly by yeast recombineering were transformed into the target strain. After plating on selective medium, the plates were incubated for 2 days at 30 °C when selecting for antibiotic resistance and 3-4 days for auxotrophic selection. In general, no additional $CuSO_4$ was added, as the selective media contains enough for Cas9 expression. However, if required 23 µl $CuSO_4$ can be added to strongly express Cas9. Transformed candidates were checked for the correct edit using Phire Green colony PCR (usually 5-10 colonies). This could be followed by an analytical restriction digest if required. Initially, the

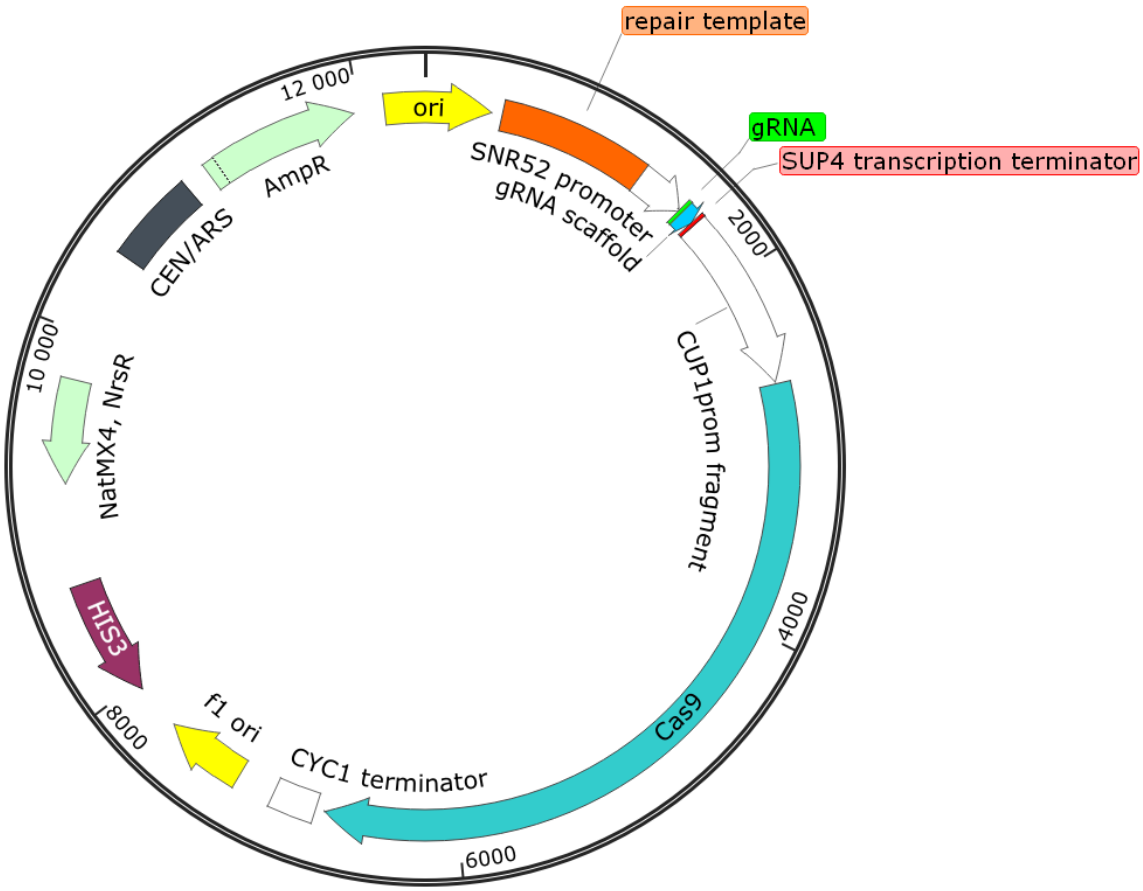


**Figure 2.1-2:** Example of a typical CRISPR plasmid. The plasmid contains an origin of replication for propagation in yeast (CEN/ARS) and bacteria (ori) and also selective markers for bacteria (AmpR) and yeast (NatMX4, a resistance cassette against ClonNat and auxotrophy marker His3). To introduce the edit into the yeast genome, the plasmid carries the repair template, containing 300-500 bp flanking the edit region and the altered PAM sequence, the sgRNA (gRNA, which can hybridize with the locus of interest, fused to the chimeric gRNA scaffold) under the control of the constitutive promoter pSNR52, as well as Cas9 under the control of the inducible promoter pCUP1.

obtained positive colonies are usually mosaic clones containing a mixture of edited and unedited cells. For plasmid loss, the candidates with the correct edit were restreaked thinly on YPD+ plates and incubated overnight at 30 °C. Cells were collected from these patches with a pipette tip and resuspended in 20 µl $dH_2O$, before adding $dH_2O$ to 1 ml. From this the cells were further diluted 1:100 and then 100 µl of the cell suspension were plated on YPD+ to obtain single colonies. The plates were incubated for 2 days at 30 °C, before replica plating them onto selective medium (incubated overnight at 30 °C). With colonies that had lost the CRISPR plasmid another analytical PCR was performed, followed by a restriction digest if required. Finally, correct clones were verified by sequencing and subsequently frozen.

### 2.1.9 Yeast Recombineering

*S. cerevisiae* has the capability to efficiently recombine dsDNA fragments with homologous ends *in vivo.* This allows the straightforward cloning of plasmids (Ma *et al.*, 1987; Oldenburg *et al.*, 1997; Orr-Weaver, Szostak and Rothstein, 1981). To employ yeast recombineering, 200-500 ng of the linearized vector backbone were mixed with the inserts in 2-5 x equimolar excess. It is important to gel-purify the linearized backbone to avoid contaminations with the closed plasmid. Otherwise, the closed plasmid would produce high numbers of false positive clones. The fragments should ideally contain around 50 bp large homologies, however, recombination can also be successful with homologies between 30 to 40 bp. For transformation, the standard yeast transformation protocol was followed as described below. To verify that positive clones contain the correct plasmid, primers spanning over one or more junctions were used for PCR. Verified plasmids were recovered using the Yeast plasmid mini prep kit (Zymoprep (#D2001)) and then isolated and amplified in *E. coli,* before performing an analytical restriction digest.

### 2.1.10 Yeast Transformation

In preparation for yeast transformation a single colony was inoculated in 10-15 ml YPD+ for an overnight culture (200 rpm, 30 °C). The overnight culture was added to 50 ml YPD+ with a final $OD_{600}$ of 0.1-0.2 nm at 30 °C and 200 rpm. Best transformative results are achieved, when cells are harvested during their exponential growth phase (Gietz and Schiestl, 2007). This is typically after 4.5 to 5 hours at an $OD_{600}$ of 0.4-0.8 on the DeNovix Photometer (optimal is an $OD_{600}$ of 0.6), where cells should have undergone at least two divisions. Cells were harvested by centrifugation at 3000 rpm and 4 min in a Falcon tube and then washed in 1 ml 0.1 M LiAc, before transferring them to a 2 ml Eppendorf tube. This step was followed by another centrifugation at 3000 rpm for 4 min, before careful resuspension in 150 -300 µl 1 M LiAc (300 µl 1 M LiAc per 50 ml culture of OD 0.8). Thereafter, 24 µl of the cells in 1 M LiAc were added to a master mix of 90µl 50% PEG 3350 and 8 µl ssDNA (salmon sperm DNA, boiled for 10 min at 98°C) already prepared beforehand. The master mix should be thoroughly mixed by vortexing. Because the cells are porous after the LiAc treatment, they should be handled with care by adding them to the master mix in a spiral pattern and gently flipping the tube. 8-15 µ DNA in $dH_2O$ were transferred to the mix in the same careful manner, pipetting in a spiral pattern and only gently flipping the tube. Everything was incubated for 45 min at room temperature (RT), before carefully adding 12 µl of 60 % glycerol. This was followed by an additional 45 min incubation at RT, before eventually heat shocking them at 42 °C for 10 min using a heat block at agitation at 600 rpm. When selecting for auxotrophic markers $dH_2O$ was immediately added afterwards to a final volume of 180-200 µl prior to plating with autoclaved

glass beads. When selecting for an antibiotic resistance, 1-2 ml YPD+ was added to the heat shocked cells, which were then incubated for four hours at 30 °C before reducing the volume to approximately 200 µl by brief centrifugation and plating. Alternatively, for incubation at room temperature overnight, cells were transferred to a 15 ml Falcon tube and 3 ml YPD+ were added (lid not fully closed). In this case the volume was reduced to 350-400 µl by short centrifugation if cells had not already sedimented to the bottom of the tube and plated on two plates. Typically, colonies became visible after three days at 30 °C.

To select for true transformants and against mitochondrial deficiencies, colonies were patched on another selective plate and a YPG+ plate according to their size, starting with the largest colonies. Colony PCR using suitable primers was employed to confirm genomic integration at the target site so that the new construct could be distinguished from the parental strain. This was followed by Sanger sequencing. To verify point mutations or other mutations introduced by CRISPR/Cas9, products of Colony PCR were also sequenced. Finally, the new strain was stored in 50 % glycerol in YPD+ at -80 °C after collecting the cells from a fresh cell patch.

0.1 M LiAc

Lithium acetate, dihydrate (Sigma Aldrich, L6883) 510 mg in $dH_2O$ ad 50 ml.

1 M LiAc

Lithium acetate, dihydrate (Sigma Aldrich, L6883) 1020 mg in $dH_2O$ ad 10 ml.

50 % PEG 3350

Polyethylenglycol 3350 (Sigma Aldrich, P3640) 5 g in $dH_2O$ ad 10 ml.

60 % Glycerol

Glycerol (Sigma Aldrich, G7757) 6 g in $dH_2O$ ad 10 ml.

The solutions were stored in plastic Falcon tubes at room temperature, once they were sterilized using a 0.2 µm syringe filter.

ssDNA

Salmon sperm DNA (Fluka, 31149) 100 µg/µl. Dissolved in $dH_2O$, sheared with a syringe, boiled at 98°C for 10 min and later stored at -20°C.

### 2.1.11 Plasmid Recovery from Yeast

Plasmids were typically recovered after yeast recombineering (described above, **Section 2.1.9**). To this aim, the Yeast Plasmid Miniprep I kit from Zymoprep (#D2001) was used according to the manufacturer's instructions.

### 2.1.12 Meiotic Time Course for *Saccharomyces cerevisiae* SK1 strains

A meiotic time course monitors meiotic progression of diploid strains over a period of several hours. Spore formation and spore viability can be assessed after at least 24 hours or more. For reliable results, yeast strains should undergo meiosis in a synchronized manner. To this aim several steps were taken in advance.

Homozygous diploid strains were streaked out for single colonies on YPD+ plates and either incubated at 30 °C for two days or at room temperature for three days. Using a micropipette tip a single colony was inoculated in 10-15 ml liquid YPD+ in an Erlenmeyer flask at 200 rpm and 30 °C overnight. The overnight culture was first diluted 1:10 in 1 ml SPS, and the diluted culture was then further diluted 1:700 or 1:300 in prewarmed SPS, resulting in a final dilution factor of 1:7,000 or 1:3,000. The diluted culture in SPS was then incubated for 18-16 hours at 200 rpm, 30 °C, until a cell density of 4 x $10^7$ cells/ml, corresponding to an $OD_{600}$ of 1.2-1.3 on the DeNovix Photometer. To harvest the cells the SPS culture was centrifuged for 4 min at 2000 rpm and washed once with prewarmed SPM or $dH_2O$. The cell pallet was resuspended in prewarmed SPM, where the cell density should be maintained at 4 x $10^7$ cells/ml ($OD_{600}$ of 1.2-1.3) before incubation at 200 rpm and 30 °C.

To ensure proper aeration in SPS and SPM, baffled flasks were used. Here, the content should not exceed 1/10 to 1/25 of the flask volume. PPG 1 % was added in 1:1000 dilution to prevent cells sticking to the flask and foam build up. An amino acid mix (**Section 2.1.1**) is added to the SPM shortly before use (2 ml to 1 L SPM).

PPG stock solution (0.1 g/L)

1 ml Polypropylene glycol, 1 % (v/v) (Fluka, 81380) with $dH_2O$ ad 100 ml.

### 2.1.13 Meiotic Time Course for *Saccharomyces kudriavzevii* strains

Prior to performing the meiotic time course, the diploid *S. kudriavzevii* strain was streaked out for single colonies on a YPD+ plate and incubated for 3 days at 23 °C. An overnight culture was prepared by inoculating a single colony in no more than 10 ml YPD+, which was shaken

at 200 rpm and 23 °C or RT for about 24 h. It is important that the culture reaches an $OD_{600}$ between 17 and 21, otherwise the stationary phase will not be reached, which is apparently a prerequisite for growth in SPS. Therefore, the volume of the YPD+ culture should not be increased, but rather several 10 ml overnight cultures should be prepared for larger SPS volumes, since approximately 10 ml overnight culture are required for 1 L SPS. The overnight culture was directly used to inoculate the SPS supplemented with 1:1000 of PPG 1 % at an $OD_{600}$ of 0.15 and then incubated at 200 rpm and 23 °C for 16 h. Before proceeding as described for a meiotic time course with *S. cerevisiae* SK1 (**Section 2.1.12**) and transferring the cells to SPM, the SPS culture should reach an $OD_{600}$ of 1.3-1.4 (DeNovix photometer). For *S. kudriavzevii* the SPM was not supplemented with an amino acid mix.

Samples were collected after 6 h in sporulation medium as calibration samples for dDSB Protec-seq. The quality of the samples was assessed by ChIP-qPCR.

## 2.2 Yeast Cytology

This section focuses on methods and techniques to evalutate meiotic progress, chromosome morphology and imaging techniques, like stimulated emission depletion (STED) microscopy. Furthermore, it includes how images were processed and how results were quntified and presented graphically.

### 2.2.1 DAPI Staining of Yeast Chromatin

Staining yeast chromatin with DAPI (4′,6-diamidino-2-phenylindole) was used to assess sporulation progress during meiotic time courses. To this aim, samples were collected hourly from a meiotic SPM culture (**Section 2.1.12**) typically starting at t4, and subsequently stained.

DAPI is an intercalating fluorescent dye that is DNA specific because it attaches to the minor groove of A-T rich DNA. The resulting fluorescent complex has a maximal absorption wave length of 358 nm (reviewed in Kapuscinski, 1995) and can be excited by ultraviolet light, which is detected through blue/cyan filters.

First, 100 µl of a sporulating culture in SPM were added to 500 µl of ice-cold 96% ethanol (Merck, 1.00971.2500) in a 1.5 ml Eppendorf tube. This step should preserve the cells in their current state and samples could therefore be stored at 4 °C overnight or processed immediately. Before adding the dye, the ethanol should be removed completely. Thus, the samples were centrifuged at 14,000 rpm for 10 sec, and most of the supernatant was pipetted off using a Gilson P1000. This was followed by another centrifugation step under the same conditions, after which the rest of the liquid was removed with a Gilson P200. Next, the tube

was incubated on the bench with an open lid to allow the remaining ethanol to evaporate, before 30 µl of DAPI $H_2O$ were added to the pellet. To resuspend the cells in the staining solution, sonication was employed for 1 sec (settings: 10 sec, cycle 1x10%, 70 % power). Typically, 100 cells were counted and classified as mono-, di- (post-M1), or tetranucleated (post-M2) cells. In our lab, wild-type cells usually reach 10-25 % post-M1 at t5, 20-30 % post-M2 at t6, and 80-100 % post-M2 at t8.

DAPI $H_2O$

DAPI (Sigma Aldrich, D9542) was dissolved in $dH_2O$ (0.2 µg/ml) and stored light protected at 4°C.

### 2.2.2 Spreading of Yeast Nuclei

The spreading of nuclei allows the expansion of chromatin without loss of chromatin-bound proteins, which is especially useful for yeast, because of its small size (Loidl, Klein and Engebrecht, 1998; Loidl, Nairz and Klein, 1991). Fluorescently stained chromosome spreads can then subsequently be imaged with fluorescence microscopy or STED microscopy.

For spreading, 1 ml samples were collected from a meiotic SPM culture (**Section 2.1.12**) at each considered timepoint and kept on ice. The samples should be processed immediately after collection by centrifugation at 14,000 rpm for 10 sec. Next, the supernatant was discarded, and the cell pellet was carefully resuspended by pipetting in 100 µl digestion solution. The digestion mix was incubated at 30 °C on a lab heat block until cells burst almost immediately upon contact with SarCOyl 1 %. Progress was assessed in phase-contrast by adding 5 µl SarCOyl 1 % to 5 µl digested cells directly under the coverslip. Optimally, the cell wall should then be digested enough to only leave spheroplasts. When digestion was considered successful, the tube was placed in ice water or spread immediately.

Nuclei were spread on ethanol cleaned slides or 24 mm x 40 mm coverslips by pipetting 5 or 4 µl of digested cells in the middle, respectively. Next, the 50 or 40 µl of spreading solution were distributed in small droplets around it. To connect the drops, form a gradient and spread the liquid over one third of the microscope slide or coverslip, an ethanol cleaned 5 ml glass pipette was used. Before further processing or storage at -80 °C, samples dried overnight on a clean, level bench.

**Digestion solution (for one sample)**

| | |
|---|---|
| DMEM + 1 M D-Sorbitol | 100 µl |
| 0.5M DTT | 2 µl |
| Zymolyase | 1.6 µl |

DMEM + 1 M D-Sorbitol

9.11 g D-Sorbitol (Merck, 1.07758) dissolved in 50 ml DMEM (Invitrogen, 41965-039). Sterilized using 0.2 µm syringe filter and stord at 4°C.

0.5 M DTT

771 mg DL-Dithiothreitol (Sigma Aldrich, D-9779) in 10 ml $dH_2O$, stored in 1 ml aliquots at -20°C.

Zymolyase

10 mg/ml T100 Zymolyase (Nacalai Tesque, 07665-55) in $dH_2O$, stored at -20°C.

**Spreading solution (for one slide)**

| | |
|---|---|
| Fixative | 30 µl |
| 1% Lipsol | 20 µl |
| 1% SarCOyl | 2-4 µl |

Varying concentration of SarCOyl 1% influences the appearance of spread nuclei. For most spreads 2 µl were used.

Fixative

| | |
|---|---|
| Paraformaldehyde (Sigma Aldrich, P-6148) | 4.0 ml |
| Sucrose (Merck, 1.07687.1000) | 3.4 g |
| $dH_2O$ | 100.0 ml |

Paraformaldehyde was dissolved at 70-80°C. The Fixative was stored at 4°C

1 % Lipsol

| | |
|---|---|
| Lipsol (LIP Ltd. Shipley, UK) | 500 µl |
| $dH_2O$ | ad 50 ml |

1 % SarCOyl

| | |
|---|---|
| N-lauroyl-sarCOine (Sigma Aldrich, L-5125) | 500 mg |
| $dH_2O$ | 50ml |

### 2.2.3 Immunostaining of Yeast Spreads

Immunostaining of spreads includes a primary antibody, which is protein specific, and a secondary antibody specific to the primary antibody, that is attached to a fluorescent dye.

First, the sorbitol in the spreading solution (described above) was dissolved in 1 x PBS. Hereby, the slides were put in a vertical staining jar filled with 1 x PBS to cover the spreading area. The individual coverslips were put in small empty media plates onto blotting paper with their spreading area facing upside, before they were covered with 1 x PBS. Slides and coverslips in their respective containers were placed on a shaker for 10 min. To remove excess 1 x PBS, the slides were briefly placed on a paper towel with the short side up after removing them from the vertical staining jar.

Spreads on slides were blocked for 10 min by picking up coverslips with 50 µl Blocking Buffer (BB) by connecting the surface of the slide with the droplet. After the coverslip was flicked off, the slide was directly incubated with 40 µl of the primary antibody diluted in BB on a fresh coverslip in the same way as before. Spreads on coverslips were placed on microscopy slide with 40 µl BB and also blocked for 10 min, before carefully removing them and placing them on new slides containing 35 µl of primary antibody in BB. Importantly, the formation of air bubbles was avoided as much as possible for an even staining and spreads were incubated in a humified box either at 4 °C overnight or at 37 °C for 2-6 hours. Next, the spreads were washed again with 1 x PBS for 10 min in the same manner as described above. Then, they were incubated with the secondary antibody diluted in BB (40 µl for slides and 35 µl for coverslips) in a humidified box at 4 °C overnight or at 37 °C for 2-6 hours. This was followed by another washing step in 1 x PBS for 10 min.

SYBR Green was used to stain chromatin for subsequent STED microscopy. Slides and coverslips were incubated with 40 and 35 µl of the dye, respectively, for approximately 15 min. While slides were dipped in 1 x PBS 3-4 times to remove any excess before being mounted with ProLong Diamond Antifade Mountant (Invitrogen, P36961), coverslips were mounted directly. Vectashield/DAPI (Szabo Scandic, H-1200) was used to mount spreads for fluorescence microscopy, therefore no incubation with SYBR Green was required. To remove excess mounting medium a Whatman drying block was used. The spreads could dry at room temperature in a microscopic slide box for 1-2 hours and were then either imaged immediately or stored at -80 °C.

**10 x PBS**

The following ingredients were dissolved in 800 ml $dH_2O$, after which $dH_2O$ was added to 1 L:

| | |
|---|---|
| NaCl | 80.0 g |
| KCl | 2.0 g |
| Dinatriumhydrogenphosphat (Na2HPO4) | 14.4 g |
| Kaliumdihydrogenphosphat (KH2PO4) | 2.4 g |

pH 7.4 (using HCl)

Sterilized by autoclaving. For 1 x PBS: dilute with $dH_2O$.

**Blocking Buffer (BB)**

Bovine Serum Albumin (Sigma Aldrich, A9647) 1 % and Gelatine from cold water fish skin (Sigma Aldrich, G7041) 1 % in 1 x PBS, sterile filtered.

**Table 2.2-1:** Primary and secondary antibodies for cytology

| FKab | Target (coupled to) | Dilution | Origin |
|---|---|---|---|
| **Primary antibodies:** | | | |
| 91 | Zip1 | 1:100 | mouse |
| 160 | Rad51 | 1:100 | mouse |
| 289 | Zip3 | 1:2,000 | rabbit |
| 314 | Rec8 | 1:1,000 | rabbit |
| 340 | Rec8 | 1:2,000 | guineapig |
| **Secondary antibodies:** | | | |
| 331 | rabbit (STAR RED) | 1:100 | |
| 332 | rabbit (STAR ORGANGE) | 1:200 | |
| 336 | mouse (STAR ORGANGE) | 1:100 | |
| 339 | guineapig (STAR RED) | 1:100 | |

### 2.2.4 Stimulated Emission Depletion Microscopy

Because stimulated emission depletion microscopy or STED microscopy can overcome Abbe's diffraction resolution limit, it belongs to the super-resolution microscopy (SRM) techniques. Here, a confocal excitation beam scans the region of interest in a raster pattern, while a doughnut shaped depletion laser is superimposed on it. The depletion laser prevents the outside of the focus from emitting fluorescence photons by forcing them back to the ground state. Therefore, fluorescence is only emitted from the middle of the focus, thereby overcoming the diffraction limit (Klar and Hell, 1999).

At Max Perutz Labs the Abberior Instruments STEDYCON was installed on the upright, manual Zeiss Axio Imager A2. The equipment includes two avalanche photodiode detectors for dual channel 2D STED microscopy in the orange and dark red spectral region and for conventional confocal imaging of three dyes in the green, orange and dark red spectral region.

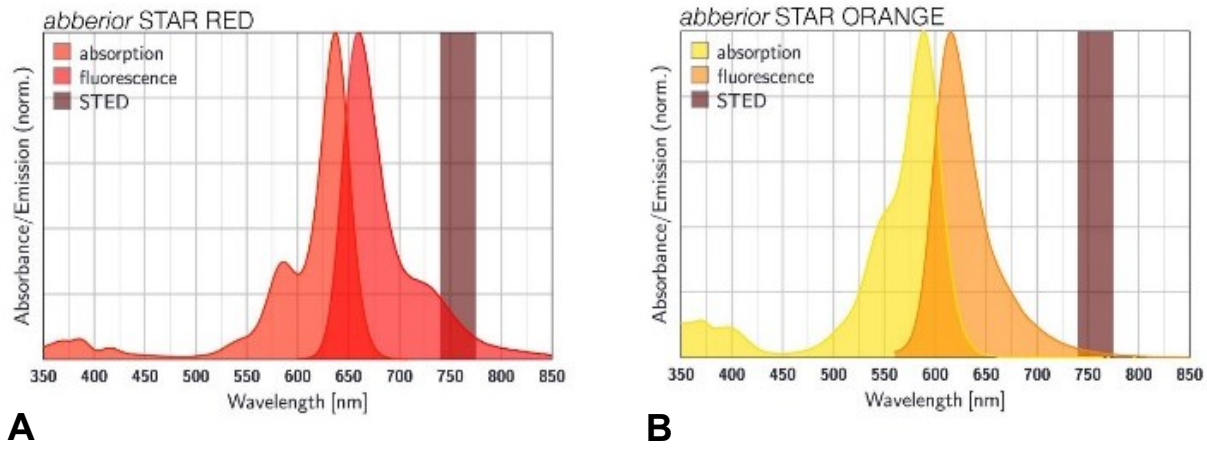


**Figure 2.2-1: Absorption and fluorescence spectrum** of (**A**) abberior STAR RED and (**B**) abberior STAR ORANGE label for STED microscopy (https://abberior.shop/abberior-STAR- 16.01.2022).

STED microscopy required special fluorophores that can withstand the power of the depletion laser. In my Master thesis, I primarily used secondary antibodies labelled with abberior STAR RED (excitation at 640 nm) and abberior STAR ORANGE (excitation at 561 nm) (**Figure 2.2-1,** Error! Reference source not found.). To image SYBR green by confocal microscopy, the 488 nm pulsed diode laser was used.

The excitation laser for STAR RED and SYBR Green was set to 10 %, respectively, and the laser for STAR ORANGE was set to 100 % using the STEDYCON Web interface, STEDYCON firmware 7.1.39. To achieve highest possible resolution the depletion laser was set to 100 %.

**Table 2.2-2:** Properties of Fluorescent Secondary Antibody Labels for STED Microscopy

| | STAR RED | STAR ORANGE |
|---|---|---|
| **Highest Theoretical Resolution Achievable** | 41 nm | 54 nm |
| **Excitation Range** | 630 - 650 nm | 550 - 610 nm |
| **Absorption $\lambda_{ex}$** | 638 nm | 589 nm |
| **Emission $\lambda_{em}$** | 655 nm | 616 nm |
| **Depletion** | 750 - 800 nm | |
| **Spectral Region** | dark red | Orange |

All fluorescent secondary antibodies are from abberior (Item number: STRED, STORANGE). The actual resolution achieved depends on sample quality.

The 100x oil objective alpha Plan-Apochromat 100x/1.46 Oil DIC M27 (WD 0.11 mm) was used for all imaging.

**Lasers for confocal excitation and depletion**

For green spectral region

488 nm: pulsed diode laser, output 0.2 mW at 40 MHz (max. 5 mW), > 3 pJ/pulse (< 150 ps)

For orange spectral region

561 nm: pulsed diode laser, 40 MHz

For dark red spectral region

640 nm: pulsed diode laser, output 1.2 mW at 40 MHz (max. 5 mW), > 20 pJ/pulse (< 150 ps)

STED laser

775 nm: pulsed, output 1.25 W, > 30 nJ/pulse (jitter < 100 ps)

**Detection System (STED/confocal)**

Avalanche photodiodes with gated detection and bandpass filters

APD1 for detection of STAR RED emission:
650-700 nm (Chroma 675/50 ET Bandpass)

APD2 for detection of fluorescence in the green spectral region (SYBR Green) and STAR ORANGE/580 emission:
500-550 nm and 580-625 nm (dual band, Semrock Em01-R488/568 + SP01-633RU)

Confocal beam scanner

QUAD beam scanner with 4 galvo mirrors (90 µm x 80 µm with the 100x objective), 512 x 512 pixel up to 1.1 fps; line frequency up to 800 Hz

Fixed confocal pinhole (1.1 Airy units for 100x/1.46 NA, 1.7 Airy units for 63x/1.4 NA)

The Zeiss Axio Imager A2 is also equipped for fluorescence microscopy with CoolLED pE-2 as widefield illumination source and a DAPI/FITC/TxRed nm LED Triple HC Filterset. This was used to initially find an appropriate z-focus.

Widefield illumination
CoolLED pE-2 (365, 470 and 550 nm)

Filters for fluorescence microscopy
DAPI/FITC/TxRed nm LED Triple HC Filterset (AHF F66-L412)
Semrock FF01-378/474/575
Semrock FF409/493/596
Semrock FF01-432/523/702

### 2.2.5 Image Processing and Statistics

The .obf files obtained through STED microscopy were converted from 16 bit to 8 bit .tif files using (Fiji Is Just) ImageJ 2.3.0/1.53q (Schindelin *et al.*, 2012; Schneider, Rasband and Eliceiri, 2012). ImageJ was also used for all further image analysis. Intensity was measured in the 16 .tif files, while measuring of aligned axes fragments was performed on 8 bit .tif files (**Section 5.6**). R version 4.1.3 (2022-03-10), RStudio 2022.07.1+554 and GraphPad Prism 10.6.1. (892), September 8, 2025, were used for graphical depiction and statistical analysis (R scripts in **Section 5.7**).

## 2.3 Bacterial Methods

*Escherichia coli* DH5α are commonly used to amplify plasmid because of their fast growth rates, high plasmid yields and transformation efficiency. Bacteria were incubated at 37 °C and liquid cultures were shaken at 200 rpm, if not otherwise stated.

### 2.3.1 Bacterial Media

2 x TY and LB media are standard culture media for the growth of *E. coli,* used for non-selective cultivation when no suitable antibiotics are added for selective conditions. Ingredients include water-soluble vitamins, amino acids and peptides.

**2 x TY liquid (1 L)**

| | |
|---|---|
| Trypton Pepton (Roth, 8986.4) | 16 g |
| Yeast extract (Difco, 212750) | 10 g |
| NaCl (Sigma Aldrich, 71382-1KG) | 5 g |
| $dH_2O$ | ad 1000 ml |

**LB liquid (1 L)**

| | |
|---|---|
| Trypton Pepton (Roth, 8986.4) | 10 g |
| Yeast extract (Difco, 212750) | 10 g |
| NaCl (Sigma Aldrich, 71382-1KG) | 10 g |
| $dH_2O$ | ad 1000 ml |

For both 2 x TY and LB, 20 g Agar agar (LabM, MC002-A) was added for plates. The pH was adjusted to 7.4 with NaOH. Autoclaving was performed at 121°C for 20-30 min for liquid and solid media. The medium was then stored at 4°C.

After autoclavation and cooling to ~50°C, 1 ml AMP stock (100 mg/ml) could be added to 1 L of 2 x TY or LB for selective cultivation.

AMP stock solution

Ampicillin, sodium salt (Sigma Aldrich, A9518) 100 mg/ml

in dH2O, sterilized using 0.2 µm syringe filter (Thermo Fisher, 10067860).

### 2.3.2 Bacterial Transformation

#### $CaCl_2$ method to produce competent *E. coli*

For approximately 20 aliquots of 100 µl competent *E. coli,* 250 µl of a 5 ml overnight culture (grown at 37 °C) were used to inoculate 50 ml of fresh LB, which was incubated at 200 rpm and 37 °C. After usually 2 hours when an $OD_{600}$ of 0.2-0.5 nm was reached, the culture was incubated on ice for 10 min, before harvesting the cells at 6000 rpm for 5 min and 4 °C. The pellet was carefully resuspended in 25 ml ice cold 0.1 M $CaCl_2$ by swirling. Subsequently, the cells were incubated on ice for 30 min, before pelleting them again through centrifugation at 6000 rpm for 5 min and 4 °C. To minimize shearing stress the tip for a Gilson P1000 was cut, before the cells were resuspended in 1 ml ice cold 0.1 M $CaCl_2$ and. Finally, 500 µl Glycerol (Sigma Aldrich, G7757-1L) were added and aliquots were frozen at -80 °C.

#### Transforming $CaCl_2$ competent *E. coli*

Competent *E. coli* DH5α were thawed on ice before adding DNA in a volume not exceeding 1/10 of the competent E. *coli*. DNA and bacteria were mixed carefully by gently flicking the tube. The cells were incubated with the DNA for 30 min on ice, before heat shocking them at 42 °C for 45 sec. 1 ml of pre-warmed LB medium was added immediately, which was followed by a 45 min incubation at 37 °C, where the bacteria should recover and express resistance. The volume was reduced to about 150 µl by centrifugation at 14,000 rpm for 10 sec, prior to plating the cells on plates with suitable selective media (generally 2 x TY AMP plates) and incubation overnight at 37 °C.

### 2.3.3 Gibson Assembly

The Gibson assembly, developed by Gibson *et al.*, 2009, is an in vitro cloning technique that allows up to eight DNA fragments to be reliably combined into a functional plasmid in a single reaction based on sequence identity. Further advantages of this technique include moderate insensitivity to internal repeats and seamless cloning (across restriction sites). The Gibson assembly is best suited for fragments longer than 500 bp with equal overlaps (at least 30 bp). However, in this study, assemblies with fragments smaller than 500 bp were also performed by adding them to the Gibson assembly mix at 3-5 times the equimolar concentration. Fragments used in the reactions were generated by PCR or restriction digest (generally for backbone). PCR products were purified using Monarch® Spin PCR & DNA Cleanup Kit (5 µg) and restriction digests were typically purified through gel extraction. Gibson assembly of

plasmids requires the concerted action of three enzymes: 5' exonuclease, a DNA polymerase, and a DNA ligase.

Typically, 70-100 ng of the backbone were mixed with the insert fragments in 3-5 fold equimolar excess. The final volume should not exceed 5 µl, if needed $dH_2O$ was used to increase the volume to 5 µl. The Gibson Master Mix was thawed on ice, before the fragment mix was added and all was mixed by pipetting. The reaction was incubated at 50 °C for one hour. To amplify the plasmid, 2-5 µl were transformed into competent *E. coli* DH5α. The bacteria were plated on appropriate selective media using autoclaved glass beads. After candidates were verified using PCR and Sanger sequencing, plasmids were extracted using plasmid mini or midi preparation (PureYield™ Plasmid Miniprep System or PureYield™ Plasmid Midiprep System). The plasmid was stored at -20 °C and the corresponding clone was kept at -80 °C in 50% glycerol in liquid LB.

**Gibson Master Mix**

| | |
|---|---|
| 5 x ISO reaction buffer | 100.0 µl |
| T5 Exonuclease (NEB, M0363), 1 U/µl (1:10 dilution in dH2O of original 10 U/µl) | 2.0 µl |
| Phusion (NEB, M0530), 2 U/µl | 6.2 µl |
| Taq ligase (NEB, M0208), 40 U/µl | 50.0 µl |
| $dH_2O$ (ad 375 µl) | 216.8 µl |

Aliquots of 15 µl can be stored at -20 °C.

5 x ISO reaction buffer

| | |
|---|---|
| Tris-HCl pH 7.5, 1 M (500 mM) | 1.5 ml |
| NAD (5 mM) | 10.0 mg |
| MgCl2, 1 M (50 mM) | 150.0 µl |
| dGTP, 100 mM (1 mM) | 30.0 µl |
| dATP, 100 mM (1 mM) | 30.0 µl |
| dTTP, 100 mM (1 mM) | 30.0 µl |
| dCTP, 100 mM (1 mM) | 30.0 µl |
| DTT, 0.5 M (50 mM) | 300.0 µl |
| PEG-8000 (250 g/L) | 750.0 mg |
| $dH_2O$ | ad 3.0 ml |

### 2.3.4 Plasmid Mini and Midi Preparation

Prior to plasmid mini or midi preparation a single colony of *E. coli* DH5α containing the plasmid of interest was inoculated in 20 ml (mini) or 50 ml (midi) LB with the appropriate antibiotic (generally 1:1000 diluted ampicillin stock solution (100 mg/ml)) and incubated overnight.

For the midi preparation, PureYield™ Plasmid Midiprep System (Promega, A2492) was employed according to the manufacturer's instructions. PureYield™ Plasmid Midiprep System (Promega, A1222) was used for plasmid mini preparation, following the alternative Protocol for Larger Culture Volumes. According to the manufacturer the protocol is suitable for cell culture volumes of 3 ml, however, all reagents were upscaled for 10 ml using two separate 1.5 ml microcentrifuge tubes. The supernatants of both tubes were transferred to the same PureYield™ Minicolumn.

Usually the centrifugation protocol was followed, but importantly, before the DNA was eluted, the binding columns were placed on the bench with an open lid to evaporate the remaining ethanol for at least two minutes. The plasmids were eluted in nuclease free water and DNA concentration was determined using Nanodrop 2000 spectrophotometer (Thermo Scientific) and were stored at -20 °C.

## 2.4 DNA Methods

### 2.4.1 Polymerase Chain Reaction (PCR)

Polymerase Chain Reaction (PCR) was invented by Kary Mullis in 1983 and is used to amplify DNA templates exponentially. A PCR reaction requires a DNA polymerase, suitable primers that bind to the DNA template and deoxidized nucleoside triphosphates (dNTPs).

The primers used for my Master thesis were designed with Snap Gene and ordered from Integrated DNA Technologies (IDT) or Mycrosynth. Preferably, the 3' end of the primer should be a guanine (G) or cytosine (C), since G-C forms three hydrogen bonds and is therefore more stably bonded compared to adenosine (A) - tyrosine (T) with two hydrogen bonds. The GC content of the primer should ideally be around 50 %. Primer lengths can of course vary but should at least contain 15 nt. Best results are obtained when the binding sequence of the primer had a length of 20 nt. Primers should have similar annealing temperatures for optimal outcome. To check annealing temperature, self-annealing ability and annealing between forward and reverse primer, Primer-BLAST of the National Library of Biotechnology Information (NCBI) was used. This should prevent primers to be titrated away from template amplification as much as possible.

**Preparative PCR**

Preparative PCR was usually used to generate DNA fragments that could subsequently be used for yeast recombineering or Gibson Assembly. Here, the Q5® Hot Start High-Fidelity DNA Polymerase (NEB, M0493L) was employed because of its ultra-low error rates. Final concentration of forward and reverse primers was usually 0.5 µM, respectively. However, preparative PCR was also performed using an inner primer set with a final concentration of 0.005 µM in addition to a primer set annealing to the first primers at a final concentration 0.5 µM. The reaction was set up as described in **Table** 2.4-1 and thermocycling conditions can be seen in **Table** 2.4-2. PCR products were either cleaned up using Monarch® Spin PCR & DNA Cleanup Kit (5 µg) or by agarose gel electrophoresis and DNA precipitation or agarose gel extraction.

**Table 2.4-1:** Reaction setup for Q5® Hot Start High-Fidelity DNA Polymerase

| **Component** | **50 µl Reaction** | **Final Concentration** |
|---|---|---|
| 5 x Q5® Reaction Buffer | 10 µl | 1 x |
| 2 mM dNTPs stock* | 5 µl | 200 µM |
| Primer mix, 10 µM each (and 0.1 µM)** | 2.5 µl | 0.5 µM (and 0.005µM) |
| Template DNA*** | variable | < 1,000 ng |
| Q5® Hot Start High-Fidelity DNA Polymerase | 0.5 µl | 0.02 U/µl |
| Nuclease-Free $H_2O$ | to 50 µl | |

*Working aliquots of at least 10 µl, prepared from 10 mM dNTPs (Promega, C1141) (1:5 dilution)

**10 µl of a 1:10 dilution prepared from 100 µM primer stock (and a 1:100 primer stock dilution when needed)

***About 25 ng of plasmid DNA, typically 2.5 µl

**Table 2.4-2**: Thermocycling conditions for Q5® Hot Start High-Fidelity DNA Polymerase

| Step | | Temperature | Time |
|---|---|---|---|
| Initial Denaturation | | 98°C | 30 s |
| Denaturation | | 98°C | 10 s |
| Annealing | 35 Cycles | Tm* | 30 s |
| Extension | | 72°C | 30 s/kb |
| Final Extension | | 72°C | 2 min |
| Hold | | 4–10°C | ∞ |

*The annealing temperature (Tm) was calculated with the online NEB Tm calculator.

**Colony PCR**

To specifically screen for certain genetic sequences of interest directly in bacterial or yeast colonies after transformation or crosses, Colony PCR was used. The Phire Green Hot Start II PCR Master Mix (Thermo Scientific, F126) is particularly useful in this respect, as it does not require prior isolation of the DNA. The Phire Hot Start II DNA Polymerase is already included in the master mix and does not need to be added separately. The Phire DNA polymerase is significantly faster than the Q5 DNA polymerase, though this comes at the COt of reduced accuracy.

A small amount of material from a single colony was collected using a sterile pipette tip and resuspended in 10-100 µl $dH_2O$ (20 µl work well) by vortexing and pipetting, prior to setting up the reaction (**Table 2.4-3**). Thermocycling conditions for Colony PCR using the Phire Green Hot Start II PCR Master Mix are listed in **Table** 2.4-4.

**Table 2.4-3:** Reaction setup with Phire Green Hot Start II PCR master mix

| Component | 20 µl Reaction | 30 µl Reaction |
|---|---|---|
| 2 x Phire Green Hotstart II Master Mix | 10 µl | 15 µl |
| Primer mix (10 µM each) | 1 µl | 1.5 µl |
| Cells resuspended in $dH_2O$ | 1 µl | 1.5 µl |
| Nuclease-Free $H_2O$ | 8 µl | 12 µl |

**Table 2.4-4:** Thermocycling conditions for PCR with Phire Green Hot Start II PCR master mix

| Step | | Temperature | Time |
|---|---|---|---|
| Initial Denaturation | | 98°C | 30 s |
| Denaturation | | 98°C | 5 s |
| Annealing | 35 Cycles | Tm* | 5 s |
| Extension | | 72°C | 15 s/kb |
| Final Extension | | 72°C | 1 min |
| Hold | | 4–10°C | ∞ |

*The annealing temperature (Tm) was calculated with the Thermo Fisher Scientific Tm calculator.

### 2.4.2 Restriction Digest

For analytical or preparative purposes, a restriction digest was set up to precisely cleave DNA (e. g. a PCR product or plasmid) with restriction enzymes. These reactions require site specific restriction enzymes that cleave the DNA at their restriction site. Snap Gene was used to design the restriction digests, and the reactions were set up according to the manufacturer's instructions (generally NEB or Thermo Fisher Scientific), typically incubated at 37 °C for 15-60

minutes. The digested products were analysed using agarose gel electrophoresis, which could be followed by gel extraction for Gibson Assembly or yeast recombineering.

### 2.4.3 Agarose Gel Electrophoresis

Agarose gel electrophoresis allows the separation of DNA fragments according to their size. DNA is negatively charged due to is phosphate backbone and can therefore migrate towards the positive pole of the electromagnetic field. The smaller a fragment the faster it runs on the gel. It is an ideal method to analyse restriction digests, PCR products or fragmentation of isolated DNA and it can also be used for preparative purposes.

The typical agarose concentrations used for gel electrophoresis in this study were in the range of 0.8-2 %. For this purpose, agarose was dissolved in 1 x TAE buffer in an Erlenmeyer flask by heating in a microwave for about 2 minutes, swirling the solution approximately every minute. This ensures that the agarose is distributed evenly and the process is accelerated, while preventing it from boiling over. Once all the agarose had dissolved and the solution was clear again, it was placed on the work bench to cool. As soon as the flask had cooled enough to be handled with bare hands, 20,000 x peqGREEN DNA/RNA binding dye was added. This is a dye that intercalates with nucleic acids and emits fluorescence upon excitation with UV or blue light.

For gel polymerization, the solution was poured into a casting chamber containing a gel tray with a suitable comb. The gels should have a thickness of 1-1.5 cm. The gel tray with the polymerized gel was then placed in a Sub-Cell® GT Cellsystems chamber and covered with 1x TAE buffer before the comb was removed. The surface of the gel should be covered completely by 1 x TAE before loading of the samples. 6 x orange gel loading dye was added to all samples, except PCR products of Colony PCR with Phire Green master mix, which already includes a loading dye. Additionally, a GeneRuler served as marker to determine fragment size, usually 6 µl of of GeneRuler 1 kb Plus DNA Ladder (Thermo Scientific, SM1331) or GeneRuler 50 bp DNA Ladder (Thermo Scientific, SM0372). The system was calibrated according to agarose concentration – higher concentrations require lower voltage but typically gels where run at 120 V for about 30 minutes. To separate larger fragments longer run times are required. Normally, 1 x TAE buffer was reused for analytical gels, but preparative gels were run in fresh buffer, and all equipment was thoroughly cleaned beforehand.

**Agarose Gel**

| | |
|---|---|
| 1 x TAE buffer | 240 ml |
| Agarose (Peqlab, 35-1020) | 1.92-4.8 g (0.8-2%) |

| | |
|---|---|
| 20,000 x peqGREEN DNA/RNA binding dye (VWR, 732-3196) | 12 µl |

This volume is sufficient for the Sub-Cell® GT Cellsystems chamber, half of it for a Mini-Sub-Cell® GT Cellsystems chamber (Biorad, 170-4404 or 170-4466).

50 x TAE buffer

The following ingredients were added to 900 ml dH2O:

| | |
|---|---|
| Tris (2 M) (Gerbu, 1018.4000) | 242.0 g |
| Acetic acid (5.7 % v/v) (Applichem Lifescience, A3686,2500) | 57.1 ml |
| EDTA disodium salt dihydrate (500 mM) (Gerbu, 1034.2500) | 18.6 g |
| $dH_2O$ | add to 1000 ml |

After setting pH to 7.9 and the buffer was autoclaved at 121 °C for 20-30 min. 50 x TAE was diluted with $dH_2O$ to 1 x TAE.

**6 x orange gel loading dye**

| | |
|---|---|
| Sucrose (40 % w/v) (Gerbu, 1331.5000) | 20 g |
| EDTA disodium salt dihydrate (60 mM) (Gerbu, 1034.2500) | 1.12 g |
| Orange G (3.3 mM) (Sigma Aldrich, O3756) | 75 mg |
| Tris (10 mM) (Gerbu, 1018.4000) | 60.6 mg |
| $dH_2O$ | ad 50 ml |

Sterilized by syringe filter (0.2 µm, Thermo Fisher, 10067860) and stored in aliquots at -20 °C.

### 2.4.4 Agarose Gel Extraction and DNA Elution

Gel extraction and gel elution ensure the removal of other molecules from PCR or restriction digests. After DNA fragments were separated according to their size by agarose gel electrophoresis as described above, DNA bands could be excised with a scalpel. To avoid cross contamination, the scalpel was ethanol cleaned and flame sterilized beforehand. During excision, the DNA bands were visualized with a Blue Light Transilluminator, since UV light can introduce mutation into DNA. For optimal results, the bands were cut out very precise, leaving as little gel as possible. The Monarch® DNA Gel Extraction Kit (NEB, T1020) was employed for gel elution according to the manufacturer's instructions. The DNA was eluted in $dH_2O$, usually 12 µl, and concentration was assessed using the Nanodrop 2000 spectrophotometer (Thermo Scientific). The DNA purified in this way could then be used for Gibson assembly or yeast recombineering.

### 2.4.5 DNA Precipitation

To increase the concentration of DNA in $dH_2O$ or purify DNA even further (e. g. PCR products or plasmids after midi preparation), DNA precipitation was performed. The DNA in solution was mixed with 3 M sodium acetate in a 1:10 ratio. Subsequently, ice cold 96% ethanol (Merck, 1.00971.2500) was added in two volumes of the original solution. Everything was incubated at -20 °C for several hours prior to centrifugation at 4 °C, 14,000 rpm for 15 minutes to recover the precipitated DNA.

### 2.4.6 Sanger Sequencing

Sanger sequencing was invented by Nicklen, and Coulson in 1977 and is based on the random incorporation of dideoxynucleotides by a DNA polymerase. Through the dideoxynucleotides the *in vitro* DNA replication is terminated. To analyse and verify plasmids or PCR products the Sanger Sequencing Service from Microsynth AG was used. Microsynth employs an adapted version of Sanger sequencing, where the dideoxynucleotides are coupled to fluorescent dyes that terminate chain elongation. The signal of migrating fragments of different sizes is measured in a capillary electrophoresis system. Reliable read length is approximately 1000 bases. Prior to preparing the samples for an Economic Run according to the User Guide, Sanger Sequencing (Microsynth AG), Exo-CIP™ Rapid PCR Cleanup Kit (NEB, E1050) was employed to purify PCR products.

## 2.5 Calibrated qChIP

The protocol for Calibrated qChIP is closely related to the protocol of Calibrated Protec-seq and based on Prieler et al. (2021). After dDSB fragments are excised from the genome by concerted cuts of Spo11, the protein remains covalently bound. For Calibrated qChIP, chromatin immunoprecipitation of Spo11-DNA complexes is performed, which is then followed by quantitative PCR (qPCR). Calibration relies on the deletion of one hotspot in the query strain (YFL022C) and the deletion of the query hotspot in the spike in strain – the calibration strain (INO2, YCR047). The concentration of the sample (S) is calculated like this: Quant(IP(S)) * Quant(WCE(C))/Quant(IP(C)) * Quant(WCE(S)).

For quality control of *Saccharomyces kudriavzevii* Protec-seq samples, no calibration strain was added.

All strains used for Calibrated qChIP contain Spo11-myc18. After sample collection, filter tips were used for all other steps.

### 2.5.1 Required Material

**Lysis buffer**

750 mM NaCl (5 M NaCl, Sigma Aldrich, 71386)
50 mM Hepes-KOH pH 7.5 (from 1 M Hepes-KOH pH 7.5 stock)
5 mM EDTA (0.5 M EDTA, Sigma Aldrich, E7889)
1 % Triton X-100 (from 10 % Triton™ X-100, Sigma Aldrich, X100 in ultrapure $dH_2O$)
0.1 %, Na-deoxycholate (from 10 % Na-deoxycholate, Sigma Aldrich, 30970 in ultrapure $dH_2O$)

filter sterilized, directly before use add 1 protease inhibitor tablet (Roche, Complete Protease Inhibitor Cocktail) per 50 ml lysis buffer

**High-salt lysis buffer**

1 M NaCl (5 M NaCl, Sigma Aldrich, 71386)
50 mM Hepes-KOH pH 7.5 (from 1 M Hepes-KOH pH 7.5 stock)
5 mM EDTA (0.5 M EDTA, Sigma Aldrich, E7889)
1 % Triton X-100 (from 10 % Triton™ X-100, Sigma Aldrich, X100 in ultrapure $dH_2O$)
0.1 %, Na-deoxycholate (from 10 % Na-deoxycholate, Sigma Aldrich, 30970 in ultrapure $dH_2O$)

filter sterilized, directly before use add 1 protease inhibitor tablet (Roche, Complete Protease Inhibitor Cocktail) per 50 ml lysis buffer

**Washing buffer**

10 mM Tris-HCl pH 8.0 (1 M Tris-HCl pH 8.0, Invitrogen™ UltraPure™, 10434742)
250 mM LiCl (from 5 M LiCl stock)
0.5 % NP-40 (from 10 % NP-40 stock)
0.5 % Na-deoxycholate (from 10 % Na-deoxycholate, Sigma Aldrich, 30970 in ultrapure $dH_2O$
10 mM EDTA (0.5 M EDTA, Sigma Aldrich, E7889)

filter sterilized, directly before use add 1 protease inhibitor tablet (Roche, Complete Protease Inhibitor Cocktail) per 50 ml lysis buffer

**1 x TE buffer**

10 mM Tris-HCl pH 8.0 (1M Tris-HCl pH 8.0, Invitrogen™ UltraPure™, 10434742)
1 mM EDTA (0.5 M EDTA, Sigma Aldrich, E7889)
filter sterilized

**Elution buffer (prepared freshly)**

50 mM Tris-HCl pH 8.0 (1M Tris-HCl pH 8.0, Invitrogen™ UltraPure™, 10434742)
10 mM EDTA (0.5 M EDTA, Sigma Aldrich, E7889)
1 % SDS (10 % SDS, Sigma Aldrich, 71736)

**Stock solutions:**

5 M LiCl: weighed in 50 ml Falcon, dissolved in approximately 30 ml for 3 h on shaker, before filling it up with ultrapure $dH_2O$ 50 ml mark, filter sterilized with 0.2 µm syringe (Herba Chemosan)

10 % NP-40: 5 ml IGEPAL (fill to 5 ml mark in 50 ml Falcon), add to 50 ml mark with ultrapure $dH_2O$

10 % Na-deoxycholate (Sigma Aldrich, 30970): weighed in 50 ml Falcon, dissolved in smaller volume before filled up to 50 ml mark with ultrapure $dH_2O$

1 M Hepes-KOH pH 7.5: Hepes, AppliChem, A3724, 0250 in ultrapure $dH_2O$, pH calibration with 10 M KOH, stored at 4 °C protected from light

**1 x TBS**

137 mM NaCl
2.7 mM KCl
24.8 mM Tris
pH 8.0 [HCl]

**1 x PBS**

137 mM NaCl
2.7 mM KCl
4.3 mM $Na_2HPO_4$
1.47 mM $KH_2PO_4$
pH 7.4 [NaOH]

**PBS/BSA**

1 x PBS with 5 mg/mL bovine serum albumin (SigmaAldrich, #A9647)

Glass beads, diameter 0.40-0.60 mm (Sartorius, BBI-8541701)

2 ml Screw cap tubes (Sarstedt, #72.693.005)

DynabeadsTM Pan Mouse IgG (Invitrogen via Thermofisher, #11041)

Proteinase K (20 mg/ml) (Roche via Merck/SigmaAldrich, RPROTK-RO, #3115828001)

DNase-free RNase (Roche via Merck/SigmaAldrich, RNASEA-RO #11119915001)

QIAquick Nucleotide removal kit (Qiagen, #28306)

Glycogen (10 mg/ml) (Roche via Merck/SigmaAldrich, #10901393001)

5 M NaCl (Sigma Aldrich, 71386)

**PCI (Phenol : Chloroform : Isoamylalcohol 25:24:1)**

| | |
|---|---|
| Phenol (Biomol 50734) | 25 ml |
| Chloroform (Merck 1.02445.2500) | 24 ml |
| Isoamylalcohol (Merck 1.00979.1000) | 1 ml |

stored at 4 °C under light protection

### 2.5.2 Sample Collection

Typically, two 50 ml samples (for calibration strain 25 ml) were collected per desired timepoint in 50 ml Falcon tubes from a meiotic time course culture (4 x $10^7$ cells/ml = $OD_{600}$ of 1.2-1.3). After centrifugation at 2000 rpm for 4 min at 4 °C, the samples were washed twice with cold 1 x TBS. Next, the sample was resuspended in 1 ml cold 1 x TBS and transferred to a 2 ml Eppendorf tube before centrifugation in a table top centrifuge (2000 rpm, 4 min, 4 °C). Thereafter, the supernatant was discarded, and the samples were frozen in liquid $N_2$.

### 2.5.3 Yeast Extract Preparation

The 25 ml pellets of the calibration strain were resuspended in 500 µl lysis buffer. If several samples were processed, all calibration strain pellets were mixed prior to using them to resuspend the query strain. To the 50 ml query strain pellets 360 µl of the calibration strain suspension and 640 µl lysis buffer were added. The final cell suspension was added to one 2 ml screw cap tube with 1 ml glass beads. The cells were broken using 4 cycles of 5.5 m/s for

30 sec at 4 °C in a Biomedicals™ FastPrep-24™ instrument with 5 min pause in between. The efficiency of cell breakage was assessed in phase contrast until 80% cells were broken.

For quality control of the *S. kudriavzevii* samples for Proteq-Seq, 50 ml pellets were resuspended in 1000 µl lysis buffer. Then they were transferred to 50 ml Falcon tubes containing 600 µl lysis buffer (1600 µl lysis buffer in total). Initially, all was transferred to one 2 ml screw cap tube containing 600 µl glass beads. To lyse the cells, 3 cycles of 5.5 m/s for 30 sec at 4 °C in a Biomedicals™ FastPrep-24™ instrument with 5 min pause were used. However, this proved inefficient, therefore the 1600 µl sample was split into 4 x 400 µl resuspended cells in 2 ml screw cap tubes with 600 µl glass beads. After another cycle of 5.5 m/s for 30 sec and 5 min rest, 80 % of the cells were broke. Therefore, it was concluded that cell breakage is more efficient when equal amounts of glass beads and cell suspension are used.

After poking a hole into the lid with a 23 G needle, the cell lysates were recovered by placing the inverted screw cap tubes into 15 ml Falcon tubes. The Falcon tubes were centrifuged for 1 min at 1700 rpm and 4 °C. All cell extracts were recombined in one Eppendorf tube, before centrifugation for 10 min at full speed and 4 °C. The supernatant was transferred to a fresh tube to remove the remaining cell debris. Of this, 20 µl were set aside in a separate tube to be processed as whole cell extract (WCE).

### 2.5.4 Chromatin Immunoprecipitation

For one 50 ml pellet of the query strain, 50 µl Pan mouse IgG magnetic Dynabeads were used. The beads were washed 3 times with 1 ml PBS/BSA. Per sample, 50 µl beads were resuspended in 200 µl PBS/BSA to which 50 µl FKab287 mouse-α-Myc antibody (9E11) (kind gift from Kim Naysmith) were added. The antibody was coupled to the beads for 4 or 6.5 h at 4 °C rotating on a turning wheel. The beads were then washed 3 times with 1 ml PBS/BSA and resuspended in 100 µl of PBS/BSA per sample.

For immunoprecipitation (IP), the prepared cell extracts (**Section 2.5.3**) were incubated with 100 µl antibody coupled beads in PBS/BSA for 3 h on a turning wheel at 4 °C. Subsequently, the beads were washed 2 x with lysis buffer, 2 x with high salt lysis buffer, 3x with washing buffer and 2 x with 10 mM Tris-HCl pH 8.0 (1 ml each) using a magnetic rack. After each washing step the beads were fixed to the side of the tube by using the magnetic rack. Finally, the beads were centrifuged shortly, 1000 rpm and 3 sec. To remove RNA and ssDNA, the samples were treated with ExoV and RNAse. Per sample a mix of 2.5 µL 10x NEBuffer 4 (NEB, B7004S), 2.5 µL 10 mM ATP (NEB, P0756S), 2.5 µL 500 µg/mL RNAse, DNAse-free (Roche, 1119915), 0.5 µL Exo V, RecBCD (NEB, M0345S) and 19.5 µl nuclease free $H_2O$ was

prepared (total volume 27.5 µl). The beads were incubated with the ExoV/RNAse mix for 30 min at 37 °C and 400 rpm and the reaction was stopped by adding 0.55 µl 0.5 M EDTA. Thereafter, the beads were washed 3 times with 1 ml 1x TE buffer and then Spo11-DNA complexes were eluted in 50 µl elution buffer for 30 min at 65° and 550 rpm. 44 µl 1x TE buffer were mixed with 6 µl Proteinase K per sample and incubated overnight at 50 °C and 550 rpm (final volume 100 µl). The next day, the beads were removed from the supernatant using the magnetic rack and the supernatant with the eluted DNA transferred to a new tube.

### 2.5.5 Whole Cell Extract (WCE) Preparation

The 20 µl whole cell extract (WCE), which was set aside after the preparation of cell extracts (**Section 2.5.3**), were typically processed during the incubation time of the IP (**Section 2.5.4**). First, 65 µl 1x TE and 5 µl RNAse, DNAse-free (500 µg/ml, Roche, 1119915) were added to the 20 µl WCE sample and everything was incubated for 30 min at 37 °C. Subsequently, 38 µl elution buffer and 12 ml Proteinase K were added to the solution and all was incubated at 50 °C and 550 rpm, overnight (final volume 140 µl).

### 2.5.6 DNA Purification

After IP (**Section 2.5.4**) and WCE preparation (**Section 2.5.5**), the DNA was purified using PCI and ethanol precipitation or the QIAquick Nucleotide removal kit (Qiagen, 28306). After DNA purification, all samples (WCE and IP) were stored at -20 °C.

#### PCI and ethanol precipitation

The lower phase of the PCI was added in 1:1 ratio to IP (100 µl) and WCE (140 µl). The solution was vortexed before centrifugation for 5 min at 14,000 rpm (RT) and the upper phase was transferred to a new tube. This step was repeated if the sample was still contaminated with the lower phase. Subsequently, 2.5 µl Glycogen (10 mg/ml), 4 µl 5 M NaCl and 250 µl -20 °C cold 96% ethanol per 90 µl sample were added to the solution. The volume of the individual components was adjusted based on the volume recovered after PCI purification. No master mix was prepared because NaOH would already precipitate in ethanol. The solution was incubated at -20 °C for 20 min and then centrifuged for 30 min at 14,000 rpm and 4 °C. After the supernatant was discarded, the DNA pellet was washed once with 1 ml -20 °C cold 70% ethanol. For this step care should be taken in not dissolving the pellet. Thereafter, the samples were centrifuged again for 5 min at 14,000 rpm and 4 °C and the supernatant was discarded.

The tube containing the DNA pellet was placed on the bench with an open lid to allow the remaining ethanol to evaporate before it was resuspended in 50 µl d$H_2O$ nuclease free $H_2O$.

**Column cleanup with QIAquick Nucleotide removal kit**

The QIAquick Nucleotide removal kit (Qiagen, 28306) was used according to the manufacturer's instructions. To the IP, 10 x volumes of PNI buffer were added and 6 x volume of PNI buffer were added to the WCE. The IP was eluted in 60 µl nuclease free $H_2O$ and the WCE in 100 µl nuclease free $H_2O$.

### 2.5.7 qPCR

**Preventing contaminations and sample handling**

To minimize contamination of the samples, LookOut® DNA Erase (L8917, Sigma Aldrich) was used prior to performing qPCR. The work bench was cleaned with 70 % ethanol and then with DNA Erase. All pipettes were taken apart and thoroughly cleaned with DNA Erase. In addition, they were either soaked in DNA Erase for several minutes to hours or overnight. For all steps, 1.5 ml low DNA binding microcentrifuge screw cap tubes were used and before opening any tube, the liquid was spun down. To ensure accurate pipetting, liquids were pipetted into one another by keeping the pipette tip at the surface tension interface. Through this the solution could be dispersed directly into the meniscus.

For all pipetting steps filter tips were used. Thermo Scientific™ ART™ Universal Pipette Tips were used for larger volumes (e. g. P200 and P1000 Gilson) and for small volumes long 10 µl filter tips (Biotix via Axonlab, #AL60X10).

**Preparation of standard samples**

To determine the concentration of any qPCR sample, standard samples with known concentrations are required, from which a standard curve can be derived. These standard samples were prepared through dilution from a template with a known concentration. Ideally, these templates should be larger than the PCR product of the qPCR primers. This should make template and dDSB fragments more comparable, since the dDSB fragments will also not precisely match the size of the qPCR amplicon. The templates were generated through preparative Q5 PCR (**Section 2.4.1**) and subsequent DNA purification through gel extraction and DNA elution (**Section 2.4.4**) using nuclease free $H_2O$. The primers used to generate qPCR templates for standard samples are listed in **Table 2.5-1**. The concentration (ng/µl) was determined using the Nanodrop 2000 spectrophotometer (Thermo Scientific). The NEBio Calculator was used to convert the mass of the dsDNA templates to moles. Then 200 µl of a

$10^{-2}$ pmol/µl dilution were prepared and everything was stored at -20 °C. From this stock, further dilutions ($10^{-4}$, $10^{-6}$, $10^{-8}$ and $10^{-10}$ pmol/µl) were freshly prepared immediately before use for qPCR. I tested several styles for dilution of the standard samples. Using the P200 and P1000 Gilson pipettes together with the Thermo Scientific™ ART™ Universal Pipette Tips proofed most accurate. The $10^{-4}$ dilution pmol/µl was prepared by adding 10 µl of $10^{-2}$ pmol/µl template to 990 µl nuclease free $H_2O$. Serial 1:10 dilutions were then prepared by transferring 100 µl of the previous dilution into 900 µl of nuclease free $H_2O$, generating the $10^{-5}$, $10^{-6}$, $10^{-8}$, $10^{-9}$ and $10^{-10}$ pmol/µl dilutions. In between each step, the tube was vortexed for 20 sec and then centrifuged shortly. For the standard curve only the $10^{-4}$, $10^{-6}$, $10^{-8}$ and $10^{-10}$ pmol/µl dilutions were used.

**Table 2.5-1:** Templates for qPCR standard samples, generated from genomic DNA

| FKo | strain specificity | region | size (bp) |
|---|---|---|---|
| 6176/6181 | *S. cerevisiae* | INO2 (DSB hotspot) | 94 |
| 6272/6273 | *S. cerevisiae* | INO2 (DSB hotspot) | 139 |
| 5028/4670 | *S. cerevisiae* | YCR047 (DSB hotspot) | 294 |
| 794/795 | *S. cerevisiae* | ADP1 (cold region for DSBs) | 130 |
| 5026/5027 | *S. cerevisiae* | YFL022 (DSB hotspot) | 143 |
| 6225/6226 | *S. cerevisiae* | YFL022 (DSB hotspot) | 954 |
| 4166/4167 | *S. kudriavzevii* | DSB hotspot | 148 |
| 4103/4104 | *S. kudriavzevii* | cold region for DSBs | 145 |

**qPCR reaction setup**

The Luna® Universal qPCR Master Mix (NEB, M3003) was used for qPCR according to the manufacturer's instructions. Importantly, the Luna® Universal qPCR Master Mix was carefully thawed on ice without vortexing. A master mix was prepared containing 10 µl Luna® Universal qPCR Master Mix, 7 µl nuclease free $H_2O$ and 1 µl primer mix (10 µM each) per 2 µl sample (IP or WCE) and put on ice. All primers used for qPCR are listed in **Table 2.5-2** and were chosen based on dDSB coverage in wild type. Prior to retrieving the $10^{-2}$ pmol/µl template from the -20 °C freezer, all screw cap tubes required for the serial dilutions were pre-filled with the

appropriate volumes of nuclease-free $H_2O$. Once the dilutions were prepared as described above, the qPCR master mix was added to an Eppendorf twin.tec® 96 real-time PCR Plate (Eppendorf, #30132513) (18 µl per 2 µl sample) using an Eppendorf Multipette® M4 - Repeating Pipette. Typically, all reactions were set up in duplicates. IPs were used either undiluted or 1:2 and WCEs in dilutions of 1:10, 1:20 or 1:30. With an Eppendorf Research® Plus G (0.1-2.5 µl), 2 µl of the samples or nuclease free $H_2O$ as a negative control were pipetted to the boarder of the well. Once all samples were added, the 96 well plate was sealed with a Microseal® 'B' PCR Plate Sealing Film from BioRad, #MSB1001, and then vortexed for 3 sec before centrifugation for 1 min at 1,500 rpm. All qPCR reactions were performed with an annealing temperature of 60 °C, as required for the DNA polymerase in the Luna® Universal qPCR Master Mix.

**Table 2.5-2:** Primers used for qPCR

| target | FKo | strain specificity | size (bp) |
|---|---|---|---|
| INO2 (DSB hotspot) | 6178/6179 | *S. cerevisiae* | 39 |
| INO2 (DSB hotspot) | 6178/6278 | *S. cerevisiae* | 80 |
| INO2 (DSB hotspot) | 6269/6270 | *S. cerevisiae* | 90 |
| YCR047 (DSB hotspot) | 4564/4565 | *S. cerevisiae* | 47 |
| YCR047 (DSB hotspot) | 6280/6281 | *S. cerevisiae* | 90 |
| ADP1 (cold region for DSBs) | 5788/5789 | *S. cerevisiae* | 52 |
| YFL022 (DSB hotspot) | 4513/4514 | *S. cerevisiae* | 45 |
| DSB hotspot | 4166/4167 | *S. kudriavzevii* | 148 |
| cold region for DSBs | 4103/4104 | *S. kudriavzevii* | 145 |

## 2.6 Calibrated Protec-seq

This method was developed by Prieler et al. (2021) to map dDSB fragments excised from the genome by coordinated cuts of Spo11. The protocol described here is from Prieler et al. (2021) with minor adaptations by Viktoria Prast. For all steps filter tips were used to minimize contamination. All strains for which Protec-seq was performed contain Spo11-myc18.

### 2.6.1 Required Material

**Lysis buffer**

150 mM NaCl (5 M NaCl, Sigma Aldrich, 71386)
50 mM Hepes-KOH pH 7.5 (from 1 M Hepes-KOH pH 7.5 stock)
5 mM EDTA (0.5 M EDTA, Sigma Aldrich, E7889)
1 % Triton X-100 (from 10 % Triton™ X-100, Sigma Aldrich, X100 in $H_2O$, Sigma Aldrich W402-1L)
0.1 %, Na-deoxycholate (from 10 % Na-deoxycholate, Sigma Aldrich, 30970 in $H_2O$, Sigma Aldrich W402-1L)

filter sterilized, directly before use add 1 protease inhibitor tablet (Roche, Complete Protease Inhibitor Cocktail) per 50 ml lysis buffer

**High-salt lysis buffer**

1 M NaCl
50 mM Hepes-KOH pH 7.5
5 mM EDTA
1 % Triton X-100
0.1 %, Na-deoxycholate

to produce the High-salt lysis buffer: 5 M NaCl was added to the lysis buffer (LB) to increase NaCl concentration to 1M (e.g. 10 ml to 50 ml LB = 0.2 x ml lysis buffer)

directly before use add 1 protease inhibitor tablet (Roche, Complete Protease Inhibitor Cocktail) per 50 ml lysis buffer

**Washing buffer**

10 mM Tris-HCl pH 8.0 (1 M Tris-HCl pH 8.0, Invitrogen™ UltraPure™, 10434742)
250 mM LiCl (from 5 M LiCl stock)
0.5 % NP-40 (from 10 % NP-40 stock)
0.5 % Na-deoxycholate (from 10 % Na-deoxycholate, Sigma Aldrich, 30970 in $H_2O$, Sigma Aldrich, W402-1L)
5 mM EDTA (0.5 M EDTA, Sigma Aldrich, E7889)

filter sterilized, directly before use add 1 protease inhibitor tablet (Roche, Complete Protease Inhibitor Cocktail) per 50 ml lysis buffer

**1 x TE buffer**

10 mM Tris-HCl pH 8.0 (1M Tris-HCl pH 8.0, Invitrogen™ UltraPure™, 10434742)
1 mM EDTA (0.5 M EDTA, Sigma Aldrich, E7889)
filter sterilized

**Elution buffer (prepared freshly)**

50 mM Tris-HCl pH 8.0 (1M Tris-HCl pH 8.0, Invitrogen™ UltraPure™, 10434742)
10 mM EDTA (0.5 M EDTA, Sigma Aldrich, E7889)
1 % SDS (10 % SDS, Sigma Aldrich, 71736)
filter sterilized

All flasks used, were washed without detergent (yellow top bottles in our lab) and autoclaved. In addition, the flasks were washed 2 x with ultrapure $dH_2O$ and 2 x with $H_2O$, Sigma Aldrich, W402-1L. 5 M LiCl, 10 % NP-40, 10 % Na-deoxycholate and 1 M Hepes-KOH pH 7.5 stock solutions were prepared. For 50 ml buffer, one protease inhibitor tablet was dissolved in 2 ml $H_2O$ Sigma Aldrich, W402.

**Stock solutions:**

5 M LiCl: weighed in 50 ml Falcon, dissolved in approximately 30 ml for 3 h on shaker, before filling it up with $H_2O$, Sigma Aldrich, W402 to 50 ml mark, filter sterilized with 0.2 µm syringe (Herba Chemosan)

10 % NP-40: 5 ml IGEPAL (fill to 5 ml mark in 50 ml Falcon), add to 50 ml mark with $H_2O$, Sigma Aldrich, W402

10 % Na-deoxycholate (Sigma Aldrich, 30970): weighed in 50 ml Falcon, dissolved in smaller volume before filled up to 50 ml mark with $H_2O$, Sigma Aldrich, W402

1 M Hepes-KOH pH 7.5: Hepes, AppliChem, A3724, 0250 weighed in yellow top bottles (washed 2 x with ultrapure $dH_2O$, 2x with $H_2O$, Sigma Aldrich, W402-1L), for pH calibration add 10 M KOH using filter tips, pH was measured by pouring out a small volume (0.5-3 ml) at a time and then dropping it onto pH strips, before finally pouring out 2 ml in 15 ml Falcon to measure with pH meter, stored at 4 °C protected from light

**1 x TBS**

137 mM NaCl
2.7 mM KCl
24.8 mM Tris
pH 8.0 [HCl]

**1 x PBS**

137 mM NaCl
2.7 mM KCl
4.3 mM $Na_2HPO_4$
1.47 mM $KH_2PO_4$
pH 7.4 [NaOH]

**PBS/BSA**

1 x PBS with 5 mg/mL bovine serum albumin (SigmaAldrich, #A9647)

Glass beads, diameter 0.40-0.60 mm (Sartorius, BBI-8541701)

2 ml Screw cap tubes (Sarstedt, #72.693.005)

DynabeadsTM Pan Mouse IgG (Invitrogen via Thermofisher, #11041)

Proteinase K (20 mg/ml) (Roche via Merck/SigmaAldrich, RPROTK-RO, #3115828001)

DNase-free RNase (Roche via Merck/SigmaAldrich, RNASEA-RO #11119915001)

QIAquick Nucleotide removal kit (Qiagen, #28306)

### 2.6.2 Sample Collection

For two samples, 200 ml were collected at the desired timepoints from a meiotic time course culture (4 x $10^7$ cells/ml = $OD_{600}$ of 1.2-1.3) using a measuring cylinder and a 500 ml centrifuge tube. The samples were centrifuged at 2000 rpm for 4 min at 4 °C and washed two times with cold 1x TBS (200 ml 1 x TBS per 200 ml sample). After the final washing step, the supernatant was discarded, and the pellet was resuspended in the remaining 1x TBS. The conical shape of the centrifuge tubes allows liquid to adhere. Therefore, if the supernatant is quickly discarded, a residue of liquid remains. The cell solution was divided into 2 x 2 ml Eppendorf

tubes (approximately 1.7 ml each), essentially leaving 100 ml samples, and centrifuged at 2000 rpm, 4 min, 4 °C in a table top centrifuge. Samples of *Saccharomyces kudriavzevii* were divided into 4 x 2 ml Eppendorf tubes (50 ml samples). Finally, the supernatant was removed completely, and the samples were frozen in liquid $N_2$.

### 2.6.3 Yeast Extract Preparation

One 50 ml sample needs to be resuspended in 1 ml lysis buffer. To this aim the samples were thawed on ice shortly. For 6 samples 6 pellets of 50 ml calibration strain (*S. kudriavzevii*) were resuspended in 1 ml lysis buffer each and mixed in a 50 ml Falcon tube. The 100 ml samples were also resuspended in 1 ml lysis buffer and then transferred to a 15 ml Falcon already containing 1 ml lysis buffer. Care should be taken to use reverse pipetting for resuspending the samples to prevent the formation of bubbles. To the 15 ml Falcons containing the 100 ml samples, 1 ml of resuspended calibration strain was added. The lysates of each sample was divided into 6 x 2 ml screw cap tubes containing 500 µl glass beads (approximately 560 µl per tube). The cells were broken using 3 cycles of 5.5 m/s for 30 sec at 4 °C in a Biomedicals™ FastPrep-24™ instrument with 5 min pause on ice in between. The progress of cell breakage was checked in phase contrast until 70-90 % of cells were lysed. Next, a hole was poked in the screw-cap tubes using a 23 G needle before these were turned upside down and placed in 15 ml tubes. To extract the cell lysates, everything was centrifuged 1 min at 1700 rpm at 4 °C. 3 cell lysates per samples were combined in a 2 ml Eppendorf tube (air bubbles should be avoided), resulting 2 x 2 ml tubes per sample. All tubes were centrifuged at full speed for 10 min at 4 °C to remove the remaining cell debris. The supernatant was transferred to a fresh 2 ml tube.

### 2.6.4 Chromatin Immunoprecipitation

For 6 samples, 6 x 300 µl Pan mouse IgG magnetic Dynabeads were washed 3 times with 1 ml PBS/BSA in 2 ml Eppendorf tubes, using a magnetic rack. Afterwards, 2 x 3 aliquots were pooled in one 2 ml Eppendorf tube by resuspending in one tube and then using that to resuspend the next and so on (900 µl Dynabeads per 2 ml tube). One tube was used to couple the antibody to the beads; the other was only incubated with PBS/BSA for pre-cleaning of the samples. It is important to minimize bubble formation; therefore, revers pipetting was used for resuspending the beads.

For coupling the antibody to the beads, the tube was resuspended in 900 µl PBS/BSA and 600 µl FKab287 mouse-α-Myc antibody (9E11) (kind gift from Kim Naysmith), rotating at 4 °C,

overnight on a turning wheel (for one 100 ml sample: 80 µl antibody and 120 µl beads). The other tube was incubated with 1500 µl PBS/BSA only also rotating at 4 °C, overnight. The next day, both the antibody coupled beads, and the pre-clearing beads were washed 3 times with 1 ml PBS/BSA before resuspending them in 1500 µl PBS/BSA each.

The completion of the extract preparation (**Section 2.6.3**) results in two cell extracts per sample. 100 µl of the pre-clearing beads were added to each of the two tubes of one lysed sample, which were then incubated for 1 h, 4 °C, rotating. After a short centrifugation (14,000 rpm, 10 sec), the supernatant was transferred to a new tube. For each sample, 2 x 20 µl were set aside and stored at -20 °C to be later processed as whole cell extract (WCE). For the immunoprecipitation (IP), the remaining sample was then incubated for 2 hours at 4 °C, rotating, with 100 µl of the antibody coupled beads in PBS/BSA (2 x for each sample). This finally results in 200 µl PBS/BSA of 80 µl antibody coupled to 120 µl beads per 100 ml sample.

Following the IP, the two corresponding samples were combined in one of the 2 ml tubes after the first washing step. The beads were washed 2 x with 1 ml lysis buffer, 2 x with 1 ml high-salt lysis buffer, 3 x with 1 ml washing buffer, 2 x with 1 ml 10 mM Tris-HCl pH 8.0. In between the washing steps, the beads were fixed to the side of the tube by using the magnetic rack. Ater the last washing step, the samples were spun shortly at 1000 rpm for 3 sec. Next, each sample was resuspended in 110 µl solution of ExoV and RNAse. Per sample the solution contains: 10 µL 10x NEBuffer 4 (NEB, B7004S), 10 µL 10 mM ATP (NEB, P0756S), 10 µL 500 µg/mL RNAse, DNAse-free (Roche, 1119915), 3 µL Exo V, RecBCD (NEB, M0345S) and 77 µl nuclease free $H_2O$. Everything was incubated for 30 min at 37 °C, shaking at 400 rpm. To stop the reaction 3.3 µl of 0.5 M EDTA were added and the beads washed 3 x with ice-cold 1 x TE. DNA-protein complexes were eluted in 100 ml elution buffer and incubated at 65 °C at 650 rpm, overnight. The next day, the samples were centrifuged shortly and the supernatant transferred to a new tube. To remove Spo11 from the DNA-protein complexes, 70.4 µl 1 x TE and 9.6 µl Proteinase K were added to each sample (final volume now 180 µl).

### 2.6.5 Whole Cell Extract (WCE) Preparation

The most convenient way to prepare the WCE is during the incubation of the IP. The two 20 µl WCE samples, which were set aside during chromatin immunoprecipitation (**Section 2.6.4**) were combined into one tube. To prepare the WCEs, the samples were first treated with RNAse and then with Proteinase K. For the RNAse digest, 50 µl 1 x TE and 10 µl RNAse, DNAse-free (500 µg/ml, Roche, 1119915) were added to the WCE sample. Everything, was placed on lab heat block for 30 min at 37 °C. Afterwards, 88 µl elution buffer and 12 µl Proteinase K were

added to the RNAse digest and everything was incubated at 50 °C and 550 rpm, overnight (final volume is now 200 µl).

### 2.6.6 DNA Purification

The DNA of IP and WCE samples was purified using the QIAquick Nucleotide removal kit (Qiagen, 28306) following the manufacturer's instructions. The 180 µl IP was transferred to a 2 ml Eppendorf tube, where 1,620 µl PNI buffer were added (corresponding to 10 x volumes). The 200 µl WCE was incubated with 1,000 µl PNI buffer (corresponding to 6 x volumes). The IP was eluted in 80 µl and the WCE in 50 µl of nuclease free $H_2O$. 2 µl of the IP were diluted 1:10 and stored at -20 °C for subsequent analysis using qPCR. With 2 µl the WCE a 1:100 dilution was prepared, subsequently frozen at -20 °C.

Before library preparation, the remaining WCE was fragmented using the Bioruptor in 0.2 ml Bioruptor tubes (Diagenode) with 10 cycles 30 sec on, 30 sec off, to produce 150-250 bp fragments.

### 2.6.7 TDP2 Digestion on IP samples

Before the purified DNA of the IP (**Section 2.6.6**) could be used for library preparation a TDP2 digest was performed. After removing Spo11 from the DNA-protein complexes with Proteinase K (**Section 2.6.4**) a tyrosyl residue remains bound to the DNA (5′-phosphotyrosyl DNA). This tyrosyl is digested by the enzyme TDP2 (Tyrosyl-DNA phosphodiesterase 2) (Schellenberg *et al.*, 2012). To this aim the IP was filled up to 77 µl using nuclease free $H_2O$. Then 20 µl of 5 x TDP2 reaction buffer and 3 µl TDP2 (His-GST-tags, 0.23 mg/ml, BPS Bioscience, 60702) were added and the solution was incubated at 25 °C for 60 minutes.

### 2.6.8 Library Preparation

Fully processed IP and WCE samples were used for library preparation with the NEBNext® Ultra™ II DNA Library Prep Kit for Illumina (NEB E7645) and NEBNext Multiplex Oligos for Illumina (Unique Dual Index UMI Adaptors DNA Set 1) (NEB E7395), according to the manufacturer's instructions. Prior to amplification and cleanup following the amplification, size selection was performed using AMPure® XP Beads (Beckman Coulter, Inc. A63881).

Further processing was performed by Viktoria Prast. The DNA was analysed and quantified after amplification using qPCR with the amplification primers from the Library Prep kit (P5: 5'-AATGATACGGCGACCACCGA 3' and P7: 5'- CAAGCAGAAGACGGCATACGAGAT-3'). In

addition, DNA concentration was measured by Qubit Flex Fluorometer (Thermo Fisher) using the Qubit™ dsDNA HS kit (Invitrogen via Thermo Fisher, #Q32851). The libraries were pooled according to results of the DNA quantification. Prior to sequencing of the multiplex libraries, insert sizes of 100-600 bp were selected using 2% dye free Agarose Cassettes (Sage Science CDF2003) on a PippinPrep instrument (Sage Science) by collecting fragments >200 bp. Sequencing of the multiplexed libraries was performed on the Illumina NovaSeq X according to the PE150 sequencing protocol at the Next Generation Sequencing Facility at Vienna BioCenter Core Facilities (VBCF), member of the Vienna BioCenter (VBC), Austria.

### 2.6.9 Analysis of Protec-seq Results

The Next Generation Sequencing Facility at Vienna BioCenter Core Facilities (VBCF), member of the Vienna BioCenter (VBC), Austria performed de-multiplexing on the sequencing results. Further bioinformatic processing, including the R scripts for data visualisation, was largely carried out as described in Prieler et al. (2021) by Doris Chen and my supervisor Franz Klein. For the maps of DSB hotspot signals (Spo11-oligos), the data is derived from Mohibullah and Keeney (2017) and mRNA transcriptome from Brar et al. (2012). For *S. cerevisiae* SK1 the GenBank accession GCA_002057885.1 (ASM205788v1, termed ‘ASMv1) and for *S. kudriavzevii* ZP591 the GenBank accession GCA_000167075.2 (Ports 1-16, ‘ultra-scaffolds’) were used for bioinformatic analysis.

# 3 Results

## 3.1 *spp1*∆ prevents suppression of zmm$^-$ mutant defects by *sgs1-mn*

Similar to *set1*∆*, spp1*∆ displays wild type levels of spore formation and viability, despite a noticeable delay in meiotic progression (Acquaviva *et al.*, 2013; Sommermeyer *et al.*, 2013). To identify additional factors involved in DSB formation, Viktoria Prast performed a synthetic lethality screen using the *Saccharomyces cerevisiae* deletion collection during her Master thesis in the Klein lab. However, rather than mutations contributing to DSB formation, the screen identified a group of deletion mutants that are primarily involved in DSB repair and pathway choice, namely the ZMM mutants. She demonstrated that deletion of *SPP1* in the absence of any ZMM protein (Zip1-4, Spo16, Msh4-5, Mer3) led to a reduction in viable spore formation (spore formation x spore viability) compared to zmm$^-$ single mutants. In this background the *SPP1* deletion does not accelerate meiotic progression, consistent with persistent DSB repair intermediates triggering the DNA damage checkpoint arrest. In contrast, the *rec114-8D* mutation, where DSB formation is downregulated (Carballo *et al.*, 2013), displays a drastic acceleration of progression in zmm$^-$ mutants, which results in increased sporulation efficiency, even though spore viability remains reduced (Prast, Master thesis, 2016). In addition, preliminary data from calibrated Protec-seq by Silvia Prieler and Doris Chen in the lab and published data from the Borde lab (Sommermeyer *et al.*, 2013; Bishop, 1994; Shinohara *et al.*, 1997; Gasior *et al.*, 1998) indicate only a modest overall reduction in DSBs in *spp1*∆*.* Based on these observations low DSB formation alone does not explain the importance of Spp1 in zmm$^-$ mutants.

The detrimental effects of zmm$^-$ mutants can be suppressed by the absence of Bloom's helicase Sgs1 (*pCLB2-SGS1*, "meiotic null", *sgs1-mn*, Jessop et al., 2006, Rockmill et al., 2003). Therefore, V. Prast tested whether the phenotype of *zmm$^-$, spp1*∆ double mutants could also be suppressed by *sgs1-mn*. Interestingly, this was not the case (Prast, Master thesis, 2016). Since Sgs1 depleted mutants, especially in a zmm$^-$ background, rely on the third less regulated cross over pathway (Jessop and Lichten, 2008; Jessop *et al.*, 2006; Oh *et al.*, 2008), Spp1 must play a role in this context.

Typically, *spp1*∆ delays progression about 2 hours (Sommermeyer et al., 2013, Prast, Master thesis, 2016). Adam and colleagues (2018) showed, that *spp1*∆ experiences a meiotic delay independent of its role in DSB formation. They proposed that this delay is related to the Set1 complex and arises in the context Set1-dependent transcription. The delay regards approximately 1 hour, while the rest is therefore, dependent on Spp1's role in meiotic recombination (Adam *et al.*, 2018).

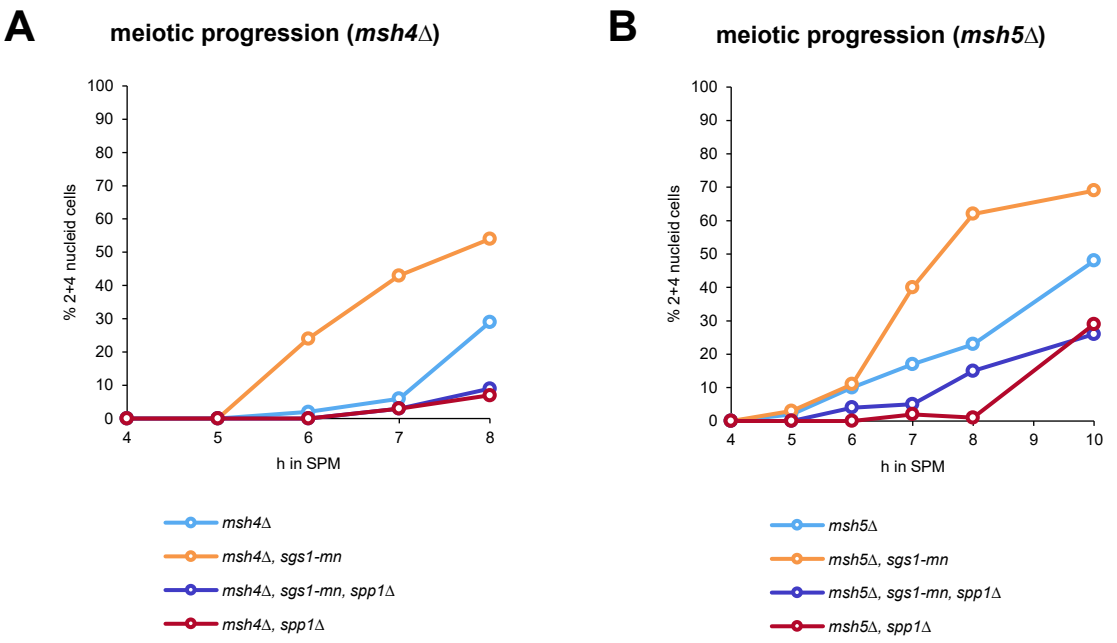


**C** spore formation, spore viability and viable spore yield (sf x sv/100) across ZMM mutants

| | Sgs1 | Spp1 | % spore formation | % spore viability | % viable spore yield |
|---|---|---|---|---|---|
| *msh4Δ* | + | + | 45.5 | 53.8 | 24.5 |
| | - | + | 80.4 | 85.0 | 68.3 |
| | - | - | 17.0 | 45.0 | 7.6 |
| | + | - | 9.4 | 3.8 | 0.4 |
| *msh5Δ* | + | + | 63.0 | 36.2 | 22.8 |
| | - | + | 86.0 | 83.8 | 72.0 |
| | - | - | 32.0 | 21.2 | 6.8 |
| | + | - | 14.0 | 0.0 | 0.0 |
| *zip4Δ* | + | + | 2.0 | 7.5 | 0.1 |
| | - | + | 16.4 | 75.0 | 12.3 |
| | - | - | 0.5 | 5.0 | 0.0 |
| | + | - | 1.5 | 0.0 | 0.0 |
| *zip3Δ* | + | + | 10.0 | | |
| | - | + | 20.0 | | |
| | - | - | 0.0 | | |



**Figure 1. Legend on the next page.**

**Figure 1. *spp1*Δ delays progression in *zmm*⁻, *sgs1-mn* mutants, and reduces spore formation, spore viability and viable spore yield.**

(**A**) and (**B**) meiotic progression of *sgs1-mn/sgs1-mn, spp1*Δ*/spp1*Δ in a *msh4*Δ and *msh5*Δ background, respectively.

(**C**) Heatmap showing spore formation (sf), spore viability (sv) and viable spore yield (sf x sv/100) of *sgs1-mn/sgs1-mn, spp1*Δ*/spp1*Δ in different zmm⁻ mutants (*msh4*Δ*, msh5*Δ*, zip4*Δ and *zip3*Δ).

Data from **TC2:** FKy6336 (*msh5*Δ), FKy6359 (*msh5*Δ*, sgs1-mn*), FKy6365 (*msh5*Δ*, sgs1-mn, spp1*Δ), FKy6290 (*msh5*Δ*, spp1*Δ), **TC5:** FKy8819 (*msh4*Δ), FKy8813 (*msh4*Δ*, sgs1-mn*), FKy8811 (*msh4*Δ*, sgs1-mn, spp1*Δ), FKy8812 (*msh4*Δ*, spp1*Δ), **TC9:** FKy6106 (*zip3*Δ), FKy5247 (*zip3*Δ*, sgs1-mn*), FKy6142 (*zip3*Δ*, sgs1-mn, spp1*Δ) and **TC11:** FKy6338 (*zip4*Δ), FKy6374 (*zip4*Δ*, sgs1-mn*), FKy6371 (*zip4*Δ*, sgs1-mn, spp1*Δ), FKy6296 (*zip4*Δ*, spp1*Δ).

Meiotic progression was followed by DAPI staining in a meiotic time course experiment at the indicated time points. For all mutants except the *zip4*Δ mutants, spore formation (sf) was assessed after 24 h in SPM (n = 100), spore viability (sv) was determined by tetrad dissection (n = 20) and incubation for 2 days at 30 °C or 3 days at RT, and viable spore yield is sf x sv/100.

sf, sv and viable spore yield of *zip4*Δ were analysed after 48 h SPM and tetrads also dissected after 48 h (n = 10, except FKy6374 (*zip4*Δ*, sgs1-mn*), where n = 20). For spore formation (sf) n = 200 per mutant.

For *zip3*Δ mutants spore viability and viable spore yield not analysed.

With meiotic time course experiments to analyse progression, sporulation efficiency and viability, I confirmed and further substantiated Viktoria Prast's initial observations in the course of my Master thesis (**Figure 1**).

Compared to other zmm⁻ mutants tested such as *zip3*Δ and *zip4*Δ*, msh4*Δ and *msh5*Δ single mutants display higher levels of sporulation efficiency and viability (**Figure 1 C**). In these less severe zmm⁻ mutants, absence of Sgs1 can rescue meiotic progression to a great extent. This suppression requires Spp1, since *spp1*Δ causes a pronounced delay in meiotic progression in the *msh4*Δ*/msh5*Δ*, sgs1-mn* double mutants. Furthermore, Spp1 is also required for progression in *msh4*Δ*/msh5*Δ single mutants, although it makes less difference (**Figure 1 A, B**). A similar trend can be observed for spore viability, spore formation and viable spore yield (sv x sf/100) in the *msh4*Δ and *msh5*Δ backgrounds. In these parameters, *spp1*Δ likewise prevents suppression of zmm⁻ mutant defects by *sgs1-mn*, a pattern that is also apparent for spore formation in the more detrimental zmm⁻ mutant *zip3*Δ. Again, Spp1 appears to contribute to sporulation and viability in the *msh4*Δ*/msh5*Δ single mutants, consistent with its role in meiotic progression. Notably, although complete suppression by the absence of Sgs1 is prevented, the triple mutants appear to perform better than the double mutants (*msh4*Δ*/msh5*Δ*, spp1*Δ). In contrast, the more severe zmm⁻ mutant *zip4*Δ does not display a similar pattern; here, the triple and double mutant, *zip4*Δ*, sgs1-mn, spp1*Δ and *zip4*Δ*, spp1*Δ*,* exhibit comparable sporulation efficiency and viability. Taken together, these observations indicate that Spp1 is required for suppression of the spore formation and viability defects in *zmm*⁻

mutants by depletion of Sgs1, where the requirement is absolute for *zip4*Δ and partial for *msh4*Δ or *msh5*Δ mutants (**Figure 1 C**).

In contrast to *msh4*Δ and *msh5*Δ meiotic progression is much slower in *zip3*Δ and *zip4*Δ, as well as *zip3*Δ, *sgs1-mn* and *zip4*Δ, *sgs1-mn* double mutants. Deletion of *SPP1* seems not to delay that progression further, in fact there is a slight acceleration for the *zip4*Δ, *sgs1-mn* background (**Figure 2 A, B)**. However, this improvement does not include spore formation, spore viability, or viable spore yield (**Figure 1 C)**. In contrast, as stated above, *SPP1* deletion abolishes any suppression of these *zip4*Δ defects.

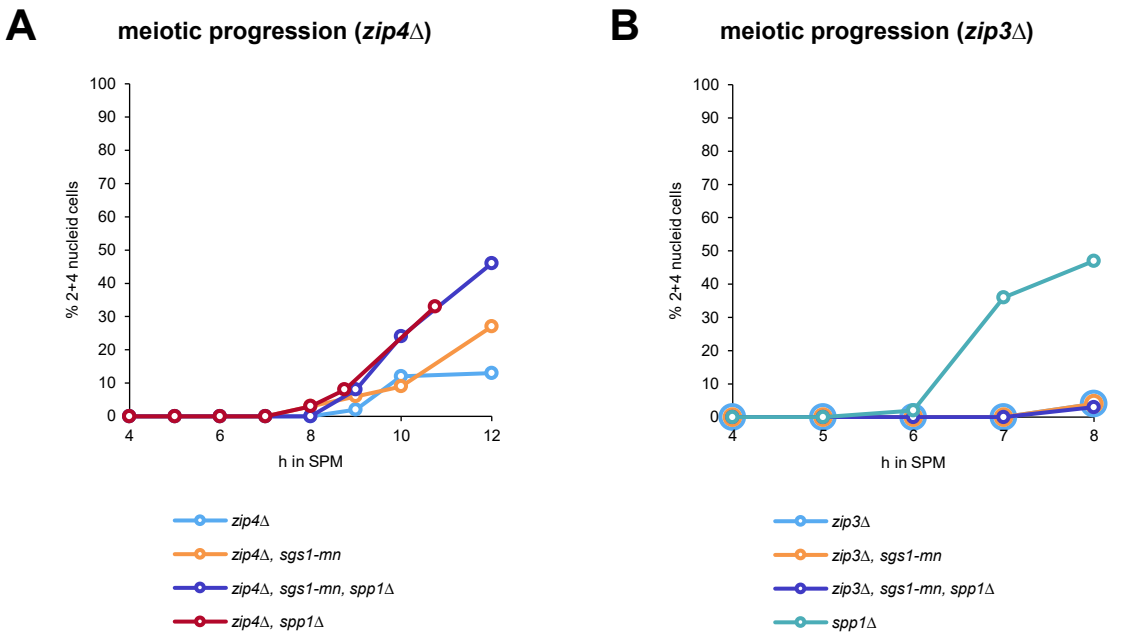


**Figure 2. After 8 h in SPM, *spp1*Δ can slightly accelerate meiotic progression of *zip4*Δ +/- Sgs1. However, this minor improvement is not mirrored by spore formation, spore viability or viable spore yield. The deletion of *SPP1* cannot enhance progression of *zip3*Δ in 8 h of SPM.**

(**A**) Meiotic progression of *sgs1-mn/sgs1-mn, spp1*Δ*/spp1*Δ in a *zip4*Δ background.

(**B**) Meiotic progression of *sgs1-mn* and *sgs1-mn, spp1*Δ in a *zip3*Δ background and additionally *spp1*Δ single mutant.

Data from **TC9:** FKy6106 (*zip3*Δ), FKy5247 (*zip3*Δ, *sgs1-mn*), FKy6142 (*zip3*Δ, *sgs1-mn, spp1*Δ), FKy5539 (*spp1*Δ) and **TC11:** FKy6338 (*zip4*Δ), FKy6374 (*zip4*Δ, *sgs1-mn*), FKy6371 (*zip4*Δ, *sgs1-mn, spp1*Δ), FKy6296 (*zip4*Δ, *spp1*Δ).

Meiotic progression was followed by DAPI staining in a meiotic time course experiment at the indicated time points.

## 3.2 Spp1 is required for axial associations, likely representing JMs, in *zip3*Δ and *zip4*Δ mutants

Initially, we wanted to separate a mechanistic role of Spp1 in tethering of the DSB machinery from its role in H3K4me3. Therefore I constructed an *SPP1*-allele for auxin inducible degradation, *SPP1-AID**, to conditionally deplete Spp1 after DSB formation in order to separate a potential repair phenotype from its role in DSB formation. The adapted auxin-inducible degron system (AID*) employs a smaller version of the AID tag designed to interfere less with protein function (Morawska and Ulrich, 2013). However, depletion of Spp1 proved insufficient, and the tag appeared to compromise Spp1 function. This project was later continued by Viktoria Prast and Armela Jahic (Bachelor student in the Klein lab) using the full-length AID-tag (Nishimura *et al.*, 2009), but similar limitations were encountered. In particular, Spp1-AID seemed hypomorphic and also a single dose of Auxin (4 mM) only suppressed Spp1 for a few hours. Therefore this experiment still needs to be improved and repeated.

Following a different approach I asked whether differences in the chromosomal structures could be observed between zmm$^-$ mutants +/- Spp1. To obtain the best possible resolution, I employed Stimulated Emission Depletion (STED) microscopy to analyse the effect of *spp1*Δ on pachytene chromosomes in *zip3*Δ and *zip4*Δ mutants. zmm$^-$ mutants typically are devoid of synapsis and show very few axial associations (Pyatnitskaya, Borde and De Muyt, 2019; Tsubouchi, Macqueen and Roeder, 2008; Rockmill *et al.*, 1995). Suppression of zmm$^-$ mutant defects by depletion of Sgs1 (Jessop *et al.*, 2006; Rockmill *et al.*, 2003), is characterized by pseudosynapsis – where axes align closely, due to an abundance of axial associations, but without incorporation of Zip1 (Rockmill *et al.*, 2003).

**Figure 3. Spp1 is required for stable axial associations in *zip4*Δ and *zip4*Δ*, sgs1-mn* backgrounds, as evidenced by the analysis of aligned axes fragments.**

(**A**) Representative STED images showing Rec8-stained chromosome spreads in different *zip4*Δ mutant backgrounds after 6 h in SPM, with *spp1Δ* at 5 h as indicated.

(**B**) Quantification of the total length of associated axial fragments per nucleus across different mutants (whiskers: min to max, individual data points shown).

(**C**) Distribution of the lengths of individual associated axial fragments for each mutant (one outlier was excluded for *zip4*Δ*, sgs1-mn*; whiskers: mean +/- SD, individual data points shown).

(**D**) Manual measurement of associated axial fragments (presumably JMs), defined as axis regions closely aligned with one another, visualized by Rec8 staining. Example image shows the measurement of 27 associated stretches with a total length of ~24 µm and an average length of ~1 µm.

Number of nuclei analysed: *zip4*Δ (n = 36); *zip4*Δ*, sgs1-mn* (n = 35); *zip4*Δ*, sgs1-mn, spp1*Δ (n = 36); *zip4*Δ*, spp1*Δ (n = 35); *spp1*Δ (n = 20).

Data from TC9: FKy5539 (*spp1*Δ) and TC11: FKy6338 (*zip4*Δ), FKy6374 (*zip4*Δ*, sgs1-mn*), FKy6371 (*zip4*Δ*, sgs1-mn, spp1*Δ), FKy6296 (*zip4*Δ*, spp1*Δ).

Only relevant significant comparisons shown. Data was analysed using one-way ANOVA with Tukey's multiple comparisons test. Brightness adjusted for better visualisation.

Antibodies: 1st FKab314 rabbit α-Rec8 1:1,000, 2nd FKab331 α-rabbit STAR RED 1:100

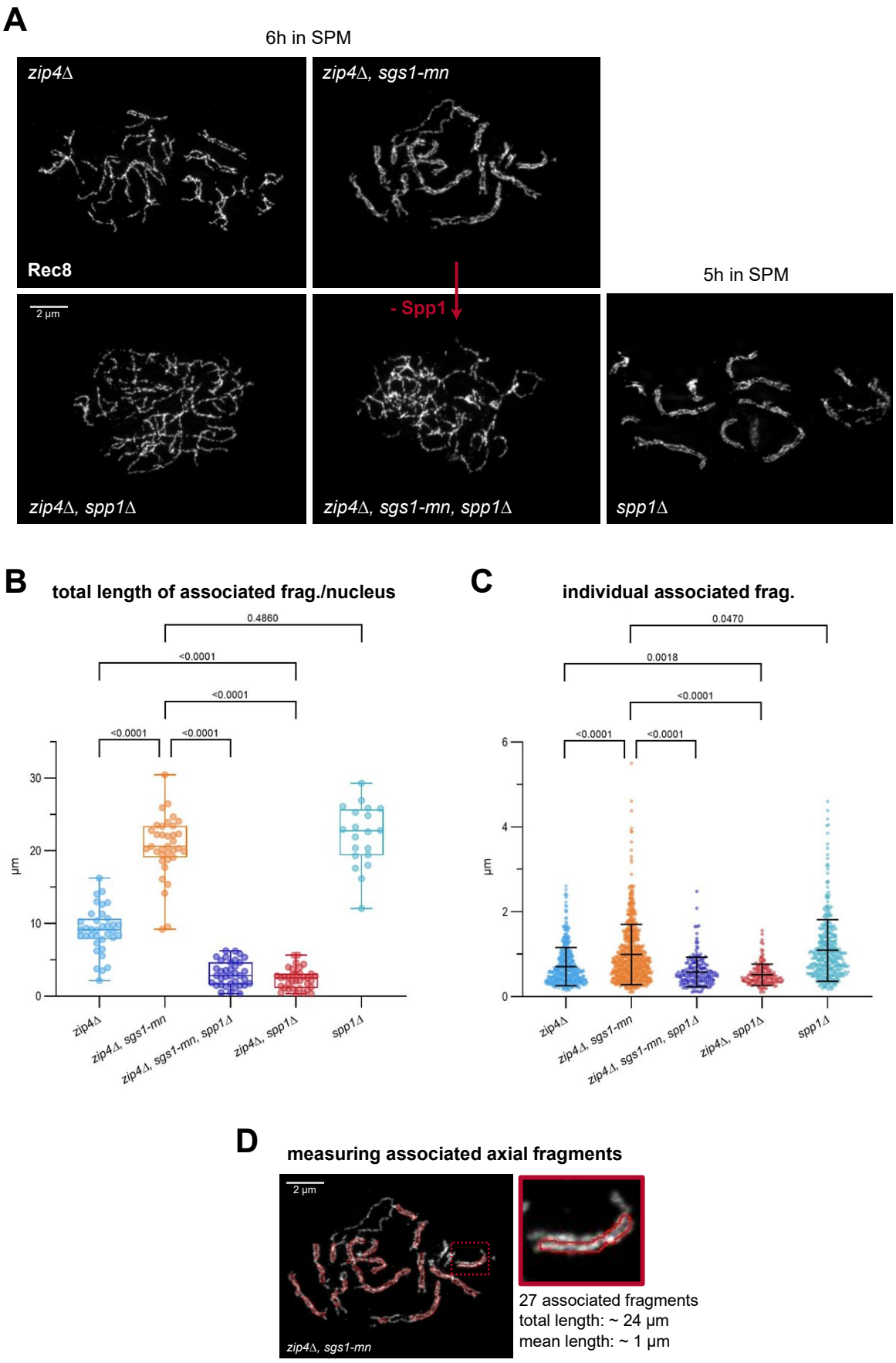


**Figure 3. Legend on the previous page.**

*zip3*Δ and *zip4*Δ single mutants display very few axial associations per homolog after 6 h in SPM by STED microscopy (**Figure 3 A**). Compared to Zip3, Zip4 may play a less critical role in homology search, as *zip4*Δ single mutants appear to pair predominantly with the correct homolog. In the absence of Sgs1, chromosome axes visualized by Rec8 staining appear tightly aligned (**Figure 3 A**), consistent with the pseudosynapsis phenotype. Zip1 is essential for synapsis, the close alignment of axial elements at a distance of 100 nm. It cannot be incorporated between axes in *zip3*Δ and *zip4*Δ mutants. Pseudosynapsis arises from high abundance of axial associations due to the loss of Sgs1. Deleting Spp1 in these backgrounds reduced axial associations and eliminated pseudosynapsis (**Figure 3 A, Figure 5 A**).

Even in *zip4*Δ single mutants Spp1 is required for the few residual axial associations observed. This is consistent with the above-mentioned observation that *msh4*Δ and *msh5*Δ single mutant phenotypes, such as meiotic progression, sporulation efficiency and spore viability, are also aggravated by the deletion of *SPP1* (**Section 3.1, Figure 1**). The *zip4*Δ*, spp1*Δ double mutant closely resembles the phenotype of the triple mutant (*zip4*Δ*, sgs1-mn, spp1*Δ) regarding the loss of axial associations (**Figure 3 A**). In contrast, the *spp1*Δ single mutant had no discernible defect in SC formation, as demonstrated by Zip1 staining (**Figure 6 B**).

To quantitatively assess these observations, I developed an ImageJ-based analysis tool, in which the user manually marks closely aligned chromosome axes (“associated axial fragments”) (script in **Section 5.6.4**). The script measures the length of each marked region and determines the total number of associated stretches per nucleus (example nucleus shown in **Figure 3 D**).

### In absence of Spp1, Sgs1 depletion does not detectably suppress *zip4*Δ axes association defects

Quantitative analysis of the summed lengths of all associated stretches per nucleus revealed that *zip3*Δ*, sgs1-mn* and *zip4*Δ*, sgs1-mn* mutants contain significantly more associated axes than their respective single mutants. Conversely, loss of Spp1 causes a drastic reduction in the total length of associated stretches per nucleus, indicating that Spp1 is required for the establishment or maintenance of axial associations in these backgrounds (**Figure 3 B, Figure 5 B**). Quantitative analysis shows that both double and triple mutants contain significantly fewer aligned chromosome axes than the *zip4*Δ single mutant, suggesting that Spp1 contributes to axial associations even in the single mutant context (**Figure 3 B**). Analysis of individual stretch lengths supports similar conclusions in terms of significant differences but reveals that in all strains a majority of short axial fragments dominates (**Figure 3 C, Figure 5 C**). This could be due to the inherent fragility of the axes, or alternatively, could be due to a

lack of synchrony, where early stage nuclei, with small axes fragments, are part of the studied population.

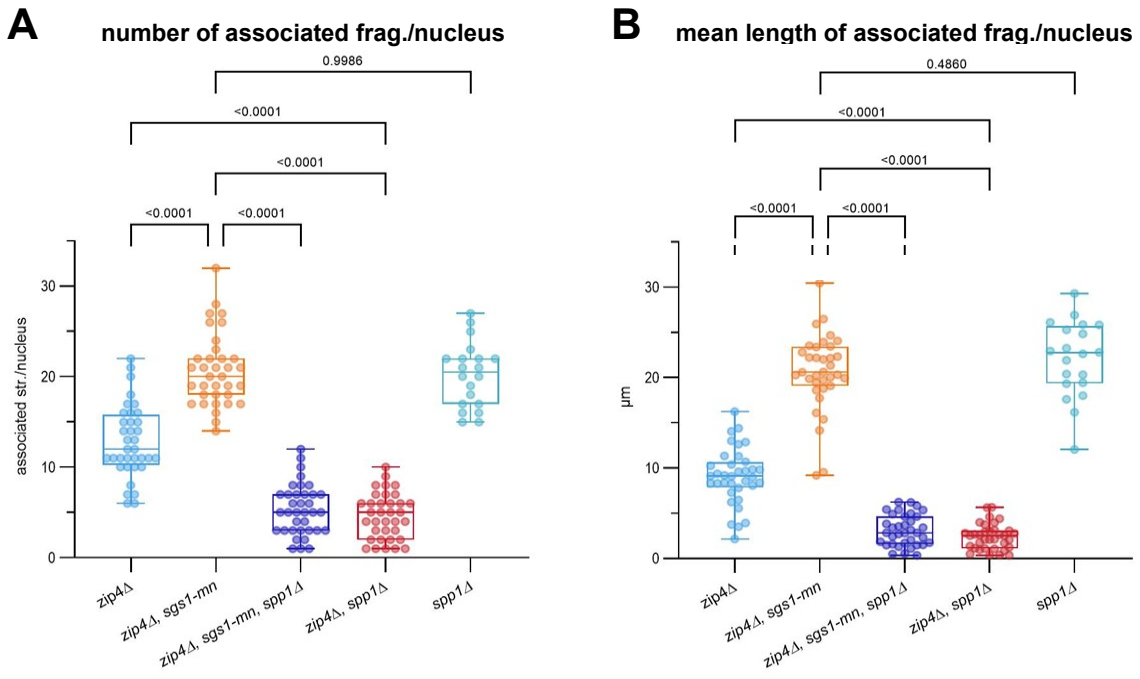


**Figure 4. Independent of Sgs1, *zip4*Δ, *spp1*Δ shows a significant decrease in the number of associated axial fragments per nucleus. The mean length of these stretches is also reduced.**

(**A**) shows the distribution of the number of associated axial fragments per nucleus.

(**B**) presents the average length of these associated axial fragments (one outlier excluded for *zip4*Δ, *sgs1-mn, spp1*Δ).

Number of nuclei analysed: *zip4*Δ (n = 36); *zip4*Δ, *sgs1-mn* (n = 35); *zip4*Δ, *sgs1-mn, spp1*Δ (n = 36); *zip4*Δ, *spp1*Δ (n = 35); *spp1*Δ (n = 20).

Data from **TC9:** FKy5539 (*spp1*Δ) and **TC11:** FKy6338 (*zip4*Δ), FKy6374 (*zip4*Δ, *sgs1-mn*), FKy6371 (*zip4*Δ, *sgs1-mn, spp1*Δ), FKy6296 (*zip4*Δ, *spp1*Δ). Only most relevant significant comparisons shown (all differ significantly from *spp1*Δ single mutant). Data was analysed using one-way ANOVA with Tukey's multiple comparisons test.

Antibodies: 1st FKab314 rabbit α-Rec8 1:1,000, 2nd FKab331 α-rabbit STAR RED 1:100

## Both, elongation and an increase in the number of associated stretches contributed to the suppression of *zip3*Δ and *zip4*Δ axis association defects

For all *zip4*Δ mutants, surprisingly the number of associated stretches parallels the increase in total length of associated axes (**Figure 4**). This means, that some of the increase in length is due to generation of more short, aligned axes fragments and not only to the fusion of short associated axes, which would in fact reduce numbers. Similarly, analysis of total lengths in the *zip3*Δ mutants also correspond largely with the numbers of associated stretches between the *zip3*Δ, *sgs1-mn* double mutant and the *spp1*Δ single mutant. However, the cohort representing the Zip3 plus, *spp1*Δ strain performs stronger in length than in numbers. (**Figure 5 D versus**

**C and E**). While the total lengths of associated stretches differ significantly, the number of stretches does not, indicating that long robust axes form rather in Zip3 plus than in the *zip3*Δ mutants and that suppression works more through addition of short fragments (**Figure 5 B, D**).

The mean length of associated stretches between *zip3*Δ single and *zip3*Δ*, sgs1-mn, spp1*Δ triple mutant is similar, also arguing that observed differences in total length derive from an increase in short associations (**Figure 5 D**, **E**). The suppression of *zip3*Δ due to Sgs1 depletion again works through both, elongation and increase in numbers (**Figure 5 D**, **E**), but the elongation is not as strong as in *zip4*Δ (**Figure 3 B, C**), perhaps suggesting more robust axes in *zip4*Δ than in *zip3*Δ.

**Figure 5. *spp1*Δ also reduces stable axial associations in *zip3*Δ*, sgs1-mn* mutants.**

(**A**) Representative STED images showing Rec8-stained chromosome spreads in different *zip3*Δ mutant backgrounds after 5 h in SPM. The increase of the polycomb (PC) complex signal can be attributed to bleed-through from the red (Zip1, not shown) to the far-red (Rec8) channel.

(**B**) Quantification of the total length of associated axial fragments per nucleus across different mutants (whiskers: min to max, individual data points shown).

(**C**) Distribution of the lengths of individual associated axial fragments for each mutant (whiskers: mean +/- SD, individual data points shown).

(**D**) shows the distribution of the number of associated axial fragments per nucleus.

(**E**) presents the average length of these associated axial fragments.

Number of nuclei analysed: *zip3*Δ (n = 18); *zip3*Δ*, sgs1-mn* (n = 37); *zip3*Δ*, sgs1-mn, spp1*Δ (n = 15); *spp1*Δ (n = 20).

Data from **TC9** FKy6106 (*zip3*Δ), FKy5247 (*zip3*Δ*, sgs1-mn*), FKy6142 (*zip3*Δ*, sgs1-mn, spp1*Δ), FKy5539 (*spp1*Δ). Only most relevant significant comparisons shown (all differ significantly from *spp1*Δ single mutant). Data was analysed using one-way ANOVA with Tukey's multiple comparisons test. Brightness adjusted for better visualisation.

Antibodies: 1st FKab314 rabbit α-Rec8 1:1,000, 2nd FKab331 α-rabbit STAR RED 1:100

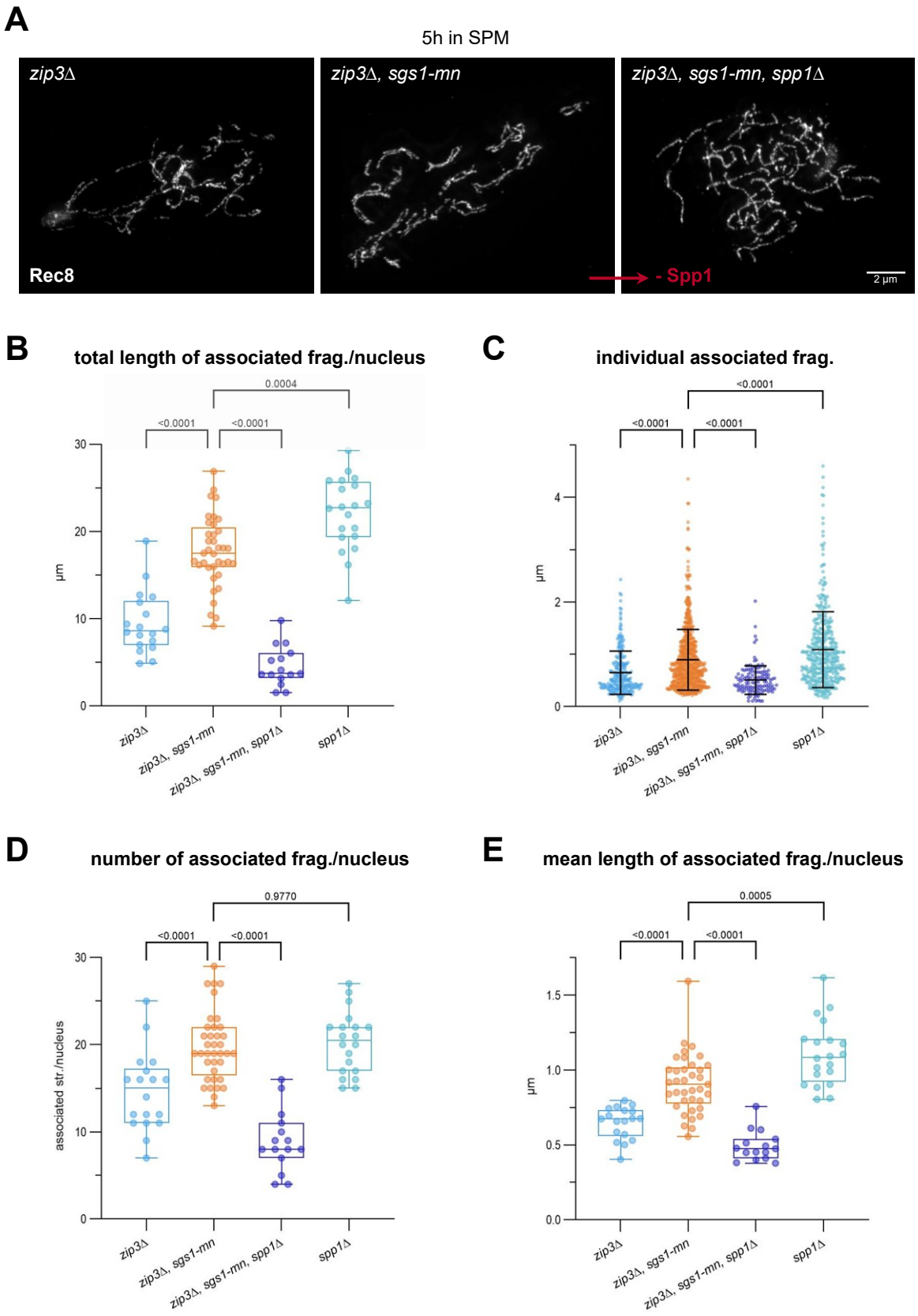


**Figure 5. Legend on the previous page.**

*zip3*Δ and *zip3*Δ*, sgs1-mn* double mutants lack full synapsis but still display individual Zip1 foci, which may correspond to Zip1's role within recombination foci (Fung *et al.*, 2004). Deletion of *SPP1* did not abolish these Zip1 foci (**Figure 6 A**). Given the near complete absence of axial associations in some of these mutants, we conclude that in these cases Zip1 foci may not actually correspond to JMs. *spp1*Δ single mutant, of course, showed normal synapsis (**Fig, 6 B**).

Loss of Spp1 disrupts pseudosynapsis in the *zip3*Δ*, sgs1-mn* and the *zip4*Δ*, sgs1-mn* background, as disorganized chromosome axes were observed. These results indicate that Spp1 is required for the establishment and/or maintenance of axial associations, likely representing JMs, in these backgrounds. This is also true in *zip4*Δ single mutants, although there are already few axial associations to begin with, suggesting that Spp1 also is important for the few remaining axial associations in zmm$^-$ single mutants.

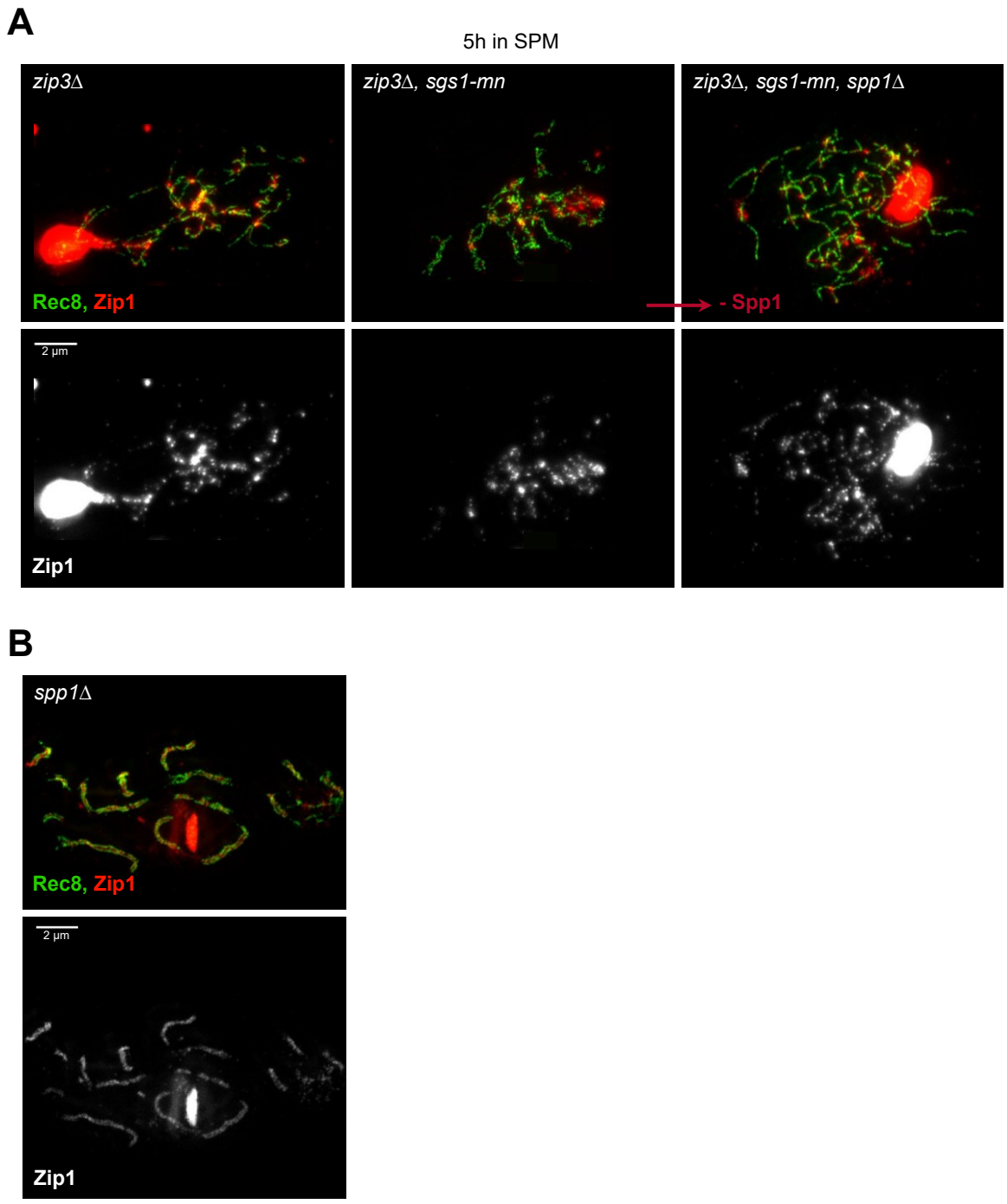


**Figure 6. *spp1*Δ disrupts axis alignment in the *zmm*$^{-}$*, sgs1-mn* background, but has no detectable effect in wild type background.**

(**A**) Representative STED images showing Rec8, Zip1-stained chromosome spreads in different *zip3*Δ mutant backgrounds after 5 h in SPM. None of the mutants achieve synapsis, as indicated by the Zip1 staining. No distinct polycomb complex was observed for the *zip3*Δ*, sgs1-mn* nucleus, likely due to its loss during the spreading procedure.

(**B**) shows that *spp1*Δ single mutant in contrast achieves full synapsis, as indicated by the continuous Zip1 staining.

Data from TC9 FKy6106 (*zip3*Δ), FKy5247 (*zip3*Δ*, sgs1-mn*), FKy6142 (*zip3*Δ*, sgs1-mn, spp1*Δ), FKy5539 (*spp1*Δ). Brightness adjusted for better visualisation.

Antibodies: 1st FKab314 rabbit α-Rec8 1:1,000 and FKab91 mouse α-Zip1 1:100, 2nd FKab331 α-rabbit STAR RED 1:100 and FKab336 α-mouse STAR ORGANGE 1:100.

## 3.3 High amounts of Rad51 foci in *zip4*Δ*, sgs1-mn* +/- Spp1 suggest no dramatic loss of DSBs in *spp1*Δ

To initially address whether a potential reduction in DSBs in the absence of Spp1 accounts for the loss of axial associations, I analysed Rad51 foci in chromosome spreads as a cytological proxy for DSB formation (**Figure 7 A**). Since Rad51 is a recombinase involved in homologous recombination (HR) (Shinohara, Ogawa and Ogawa, 1992), its accumulation in discrete nuclear foci can be used as marker for ongoing DSB repair (Bishop, 1994; Shinohara *et al.*, 1997; Gasior *et al.*, 1998). As evidenced by staining of chromosome spreads after 6 h in SPM and subsequent analysis by STED microscopy, all examined mutants contain meiosis specific Rad51 foci. This indicates that all mutants, including those carrying the *spp1*Δ mutation, are capable of forming meiosis specific DSBs that recruit Rad51 (**Figure 7 A**).

Although the number of Rad51 foci is slightly but significantly reduced in the *spp1*Δ mutants compared to *zip4*Δ single mutant, no significant difference can be observed between the *zip4*Δ*, sgs1-mn* double mutant and the *zip4*Δ*, sgs1-mn, spp1*Δ triple mutant (**Figure 7 B**). In contrast, individual foci intensities are highly variable between the mutants, with all strains displaying significant differences, suggesting that this is not an optimal feature for comparison (**Figure 7 C**). Nevertheless, the overall trend in total Rad51 foci intensity per nucleus follows that of the foci numbers. All double and triple mutants are reduced compared to the *zip4*Δ single mutant and differ significantly from it, but not from each other (**Figure 7 D**). Analysis of the mean Rad51 foci intensity per nucleus further reveals that the triple mutant contains a higher proportion of low-intensity foci and differs significantly from both the *zip4*Δ*, spp1*Δ double mutant and the *zip4*Δ single mutant (**Figure 7 E**). These changes reflect that introduction of the *sgs1-mn* and/or *spp1*Δ mutation in the *zip4*Δ background leads to a reduction in the number and intensity of Rad51 foci. The small observed differences in Rad51 foci intensities could be due to experimental variation or might indeed reflect biological context. However, the reduction is small and cannot explain the pronounced loss of axial associations in the *zip4*Δ*, spp1*Δ +/- Sgs1 mutants. In addition, the presence of Rad51 foci in the *spp1*Δ mutants, suggests that DSBs still occur in reasonable numbers in the absence of Spp1.

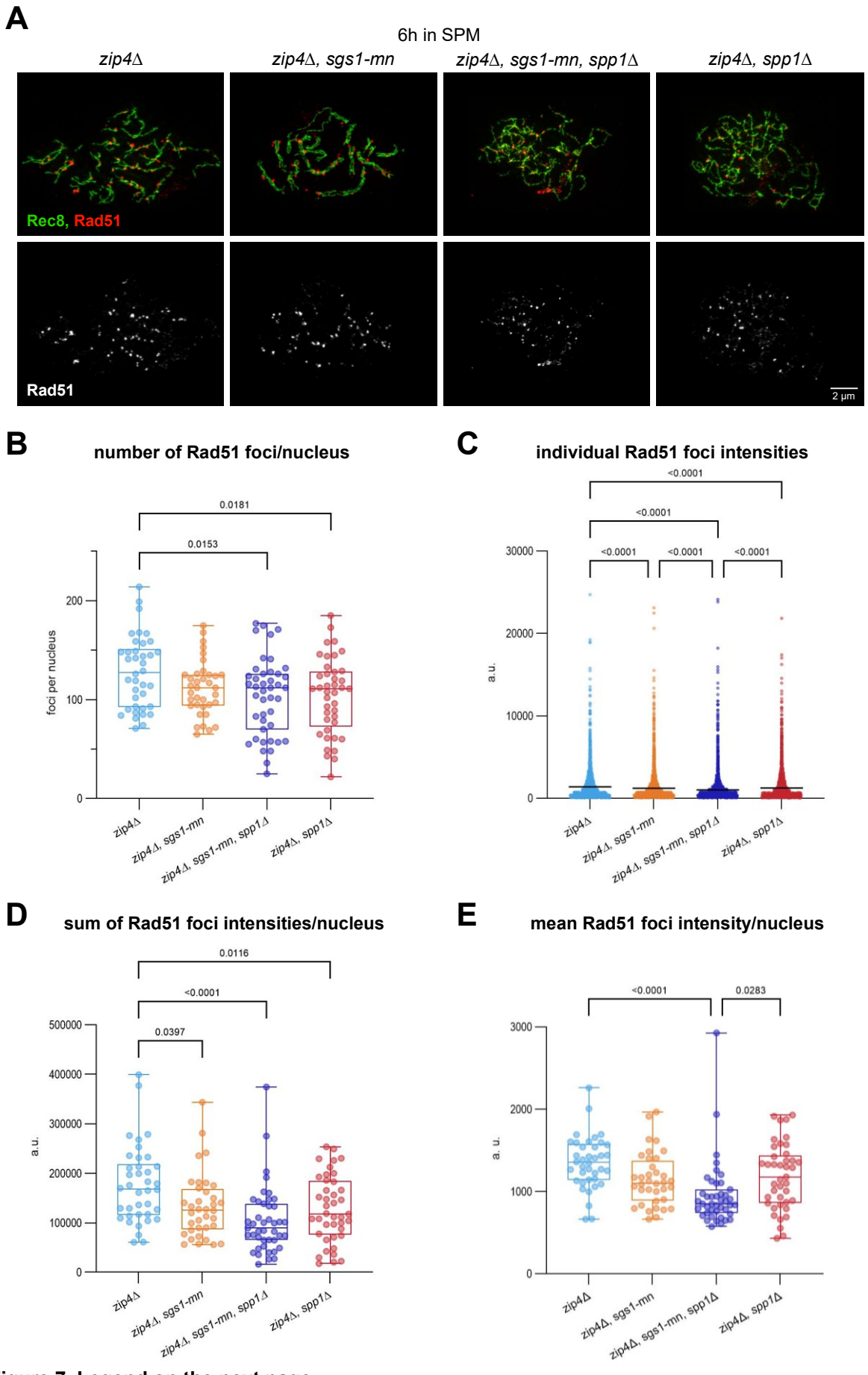


**Figure 7. Legend on the next page.**

**Figure 7. Rad51 foci show no variation that can explain dramatic loss of axial associations in the *zip4*Δ*, sgs1-mn, spp1*Δ mutant.**

(**A**) Representative STED images showing Rec8, Rad51-stained chromosome spreads in different *zip4*Δ mutant backgrounds after 6 h in SPM.

(**B**) Rad51 foci number per nucleus across all mutants.

(**C**) Distribution of all individual Rad51 foci intensities for each mutant (mean, individual data points).

(**D**) Added up Rad51 foci intensities per nucleus for the different mutants.

(**E**) presents the average intensity of these Rad51 foci per nucleus.

Number of nuclei analysed: *zip4*Δ (n = 36); *zip4*Δ*, sgs1-mn* (n = 35); *zip4*Δ*, sgs1-mn, spp1*Δ (n = 36); *zip4*Δ*, spp1*Δ (n = 35).

Data from TC11: FKy6338 (*zip4*Δ), FKy6374 (*zip4*Δ*, sgs1-mn*), FKy6371 (*zip4*Δ*, sgs1-mn, spp1*Δ), FKy6296 (*zip4*Δ*, spp1*Δ).

Only relevant significant comparisons shown. Data was analysed using one-way ANOVA with Tukey's multiple comparisons test. Brightness adjusted for better visualisation.

Box plots: whiskers from min to max, individual data points shown.

Antibodies: 1st FKab314 rabbit α-Rec8 1:1,000 and FKab160 mouse α-Rad51 1:100, 2nd FKab331 α-rabbit STAR RED 1:100 and FKab336 α-mouse STAR ORGANGE 1:100

Figures 8 through 11 show a more detailed quantitative analysis of Rad51 foci in the four *zip4*Δ mutant backgrounds (**Figure 8-11**). They show a bar plot (**A**), heatmap (**B**), density plot (**C**) and box plot (**D**), which all demonstrate different aspects of the frequency and intensity of Rad51 foci. The *zip4*Δ single mutant shows a relatively wide distribution in the number of foci per nucleus (mean = 127.9; SD = +/- 36.58), indicating some variability among individual cells. The corresponding class frequency plot demonstrates that most nuclei contained between 90 and 150 Rad51 foci, suggesting that *zip4*Δ mutant form numerous recombination intermediates (**Figure 8 A**). Similar distributions can be observed in the other mutants: *zip4*Δ*, sgs1-mn* (mean = 111.7, SD = +/- 27.54) (**Figure 9 A**), *zip4*Δ*, sgs1-mn, spp1*Δ (mean = 103.6, +/- 39.26) (**Figure 10 A**), *zip4*Δ*, spp1*Δ (mean = 127.9, SD = +/- 36.58) (**Figure 11 A**). Based on the standard deviations (SD), *zip4*Δ*, sgs1-mn* shows the least variability among individual cells, whereas the triple mutant displays the highest variability. In this strain meiotic DSBs are successfully repaired, which may prevent formation of strongly variable foci. The mean and median Rad51 foci numbers are comparable between the four strains, indicating that none of them has dramatically different DSB numbers.

For all mutants, foci intensity distributions per foci class frequency show a similar pattern: most foci exhibit low intensity, with only a small fraction displaying high intensity (**Figure 8-11 B**).

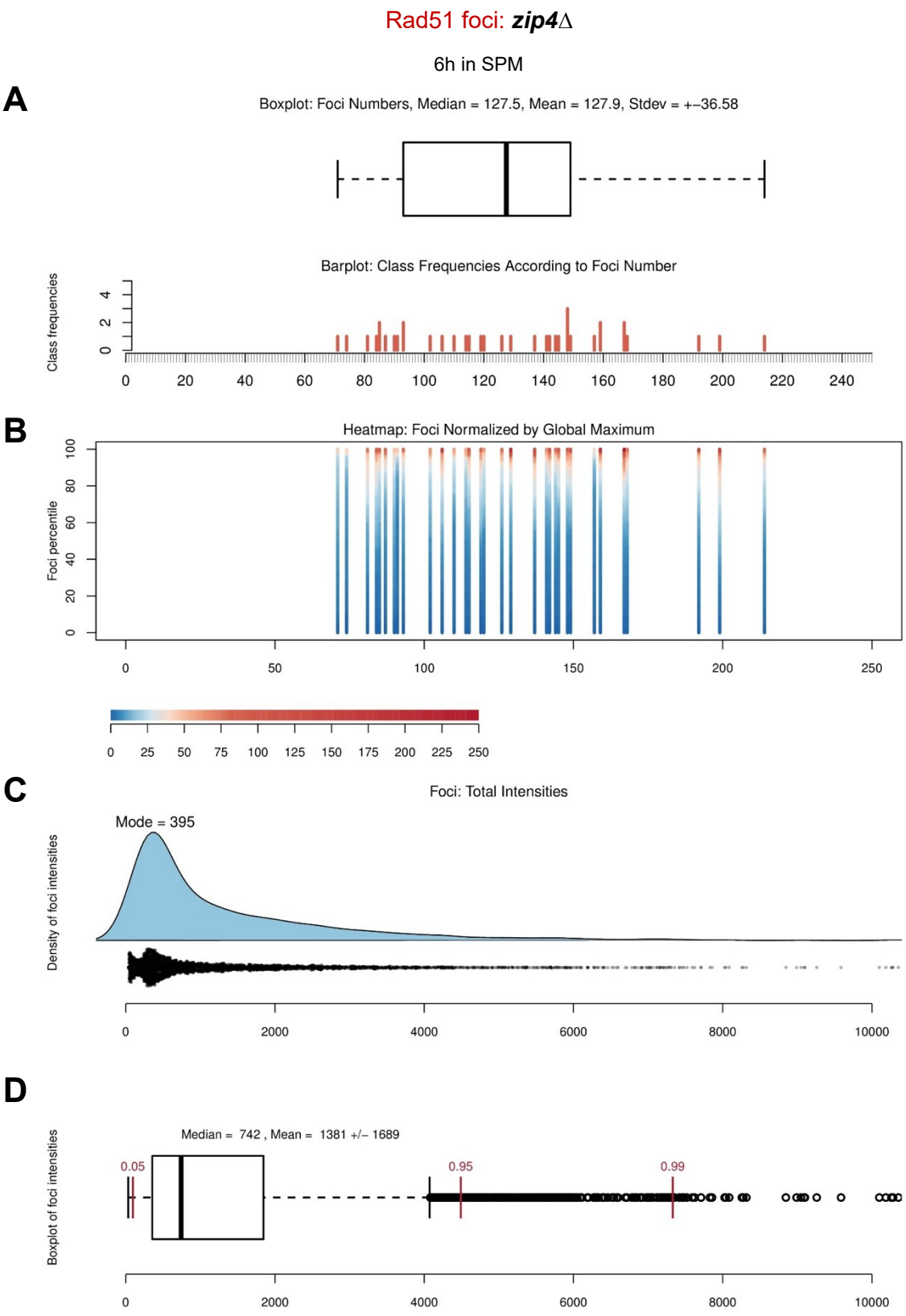


**Figure 8. Legend after Figure 11.**

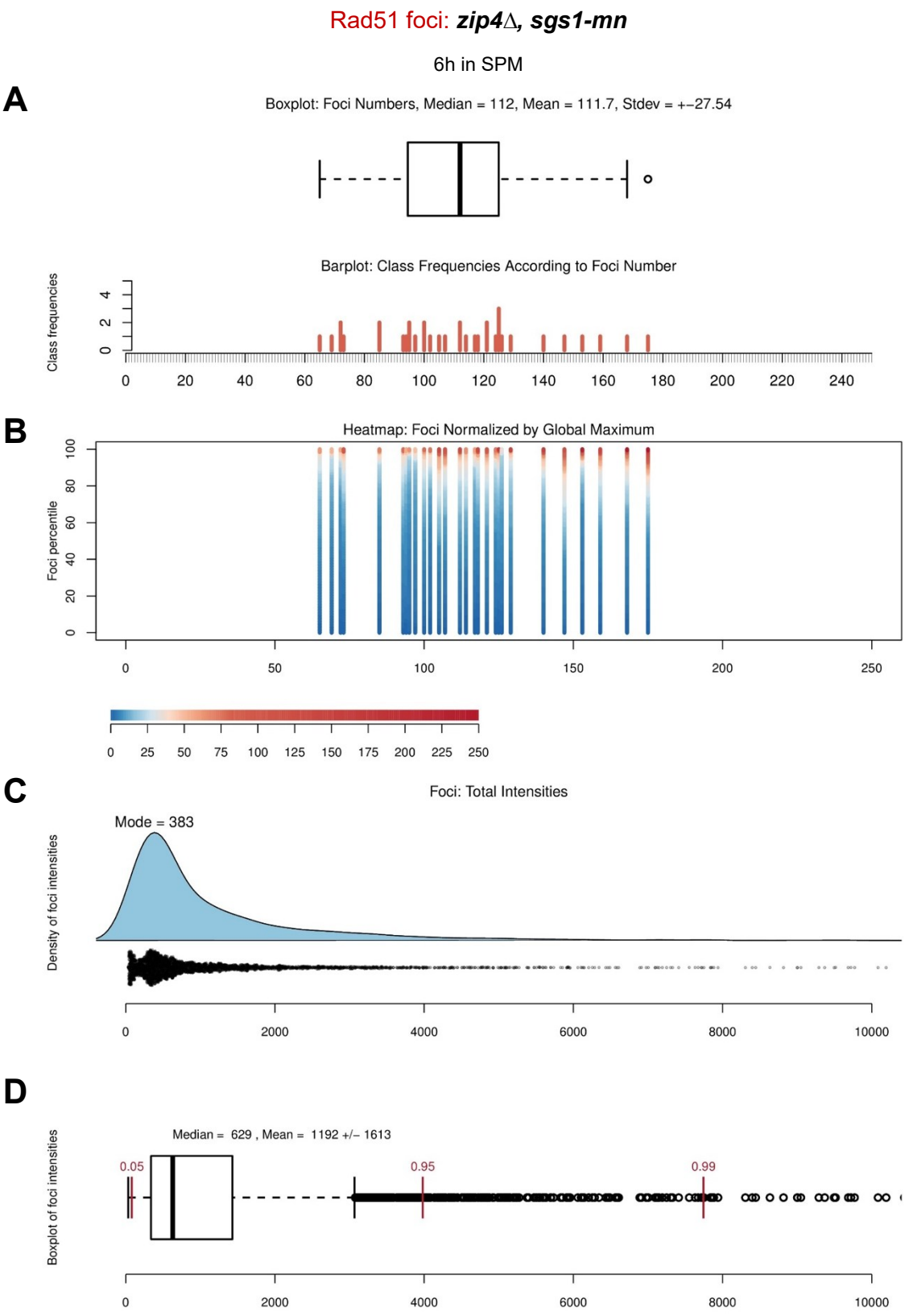


**Figure 9. Legend after Figure 11.**

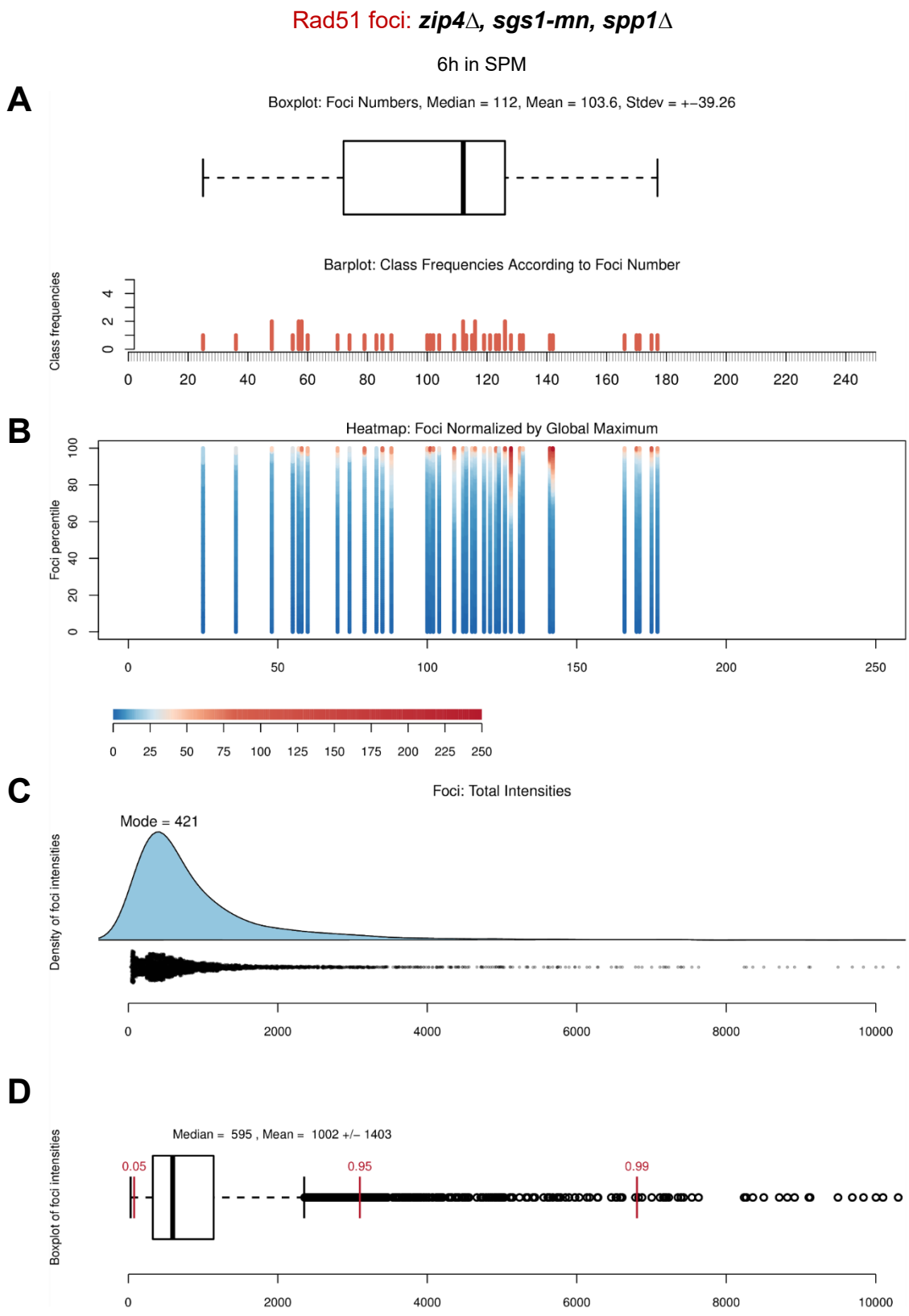


**Figure 10. Legend after Figure 11.**

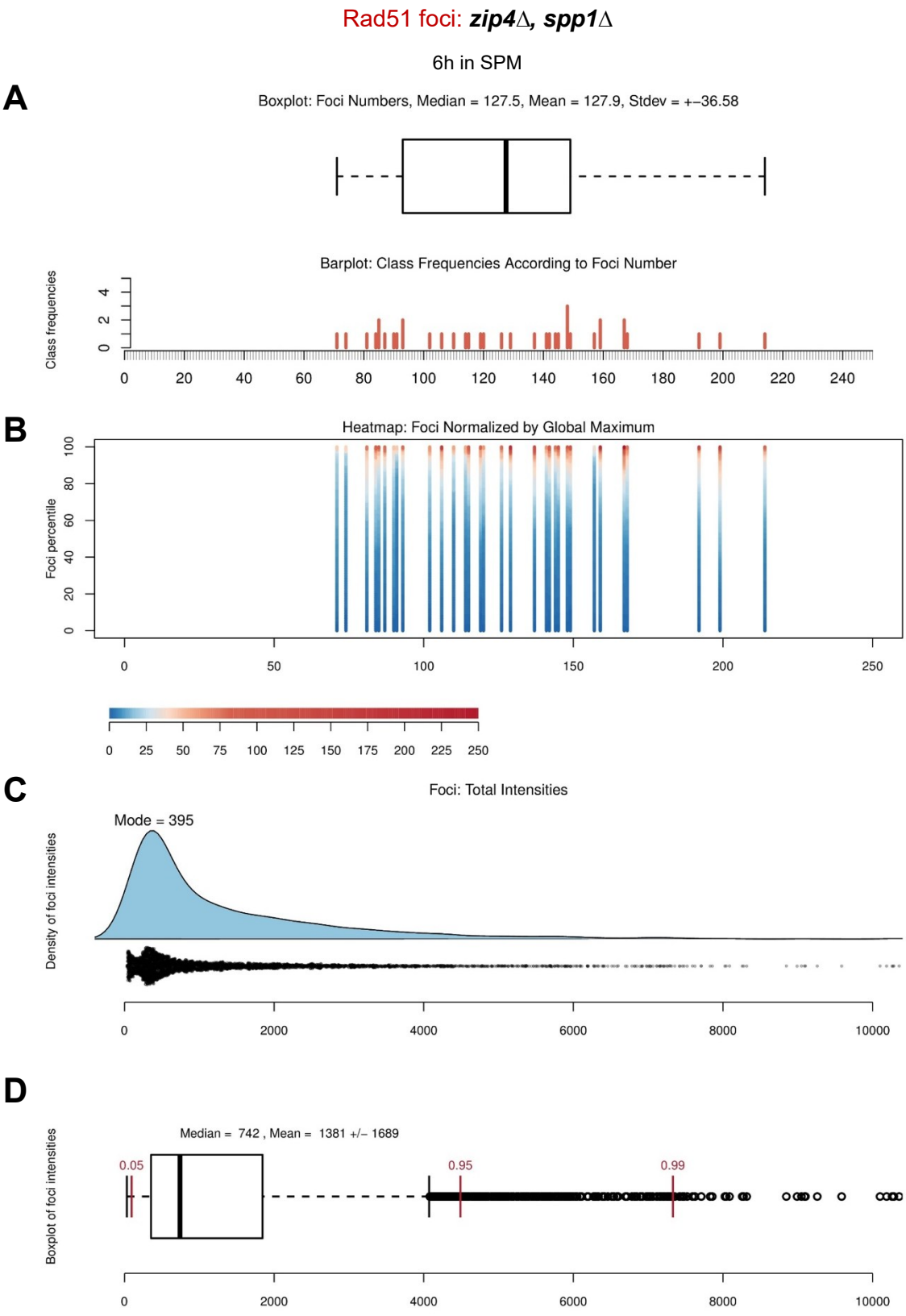


**Figure 11. Legend on the next page.**

**Figure 8-11. Quantitative analysis of Rad51 foci for *zip4*Δ (n = 36); *zip4*Δ*, sgs1-mn* (n = 35); *zip4*Δ*, sgs1-mn, spp1*Δ (n = 36) and *zip4*Δ*, spp1*Δ (n = 35) mutants after 6 h in SPM.**

(**A**) The boxplot shows the distribution of Rad51 foci numbers per nucleus, providing median, mean and standard deviation. The bar plot below represents the class frequency of foci numbers across the different nuclei.

(**B**) displays the normalized intensity distribution of Rad51 foci per class, with colour coding indicating intensity levels (x-axis = foci number, y-axis = foci percentile).

(**C**) The density plot shows the overall distribution of total foci intensities together with the mode. The scatter plot below it shows the corresponding individual intensity values (in arbitrary units).

(**D**) shows a boxplot for the total foci intensities. Red bars indicate 0.05, 0.95 and 0.99 quantile of all data points. The black whiskers of the box plot range from Q1 - 1.5 x IQR to Q3 + 1.5 x IQR.

Data from TC11: FKy6338 (*zip4*Δ), FKy6374 (*zip4*Δ*, sgs1-mn*), FKy6371 (*zip4*Δ*, sgs1-mn, spp1*Δ), FKy6296 (*zip4*Δ*, spp1*Δ). Raw grayscale values (0–65,535 for 16-bit images) using Fiji (ImageJ) = arbitrary units.

Antibodies: 1st FKab160 mouse α-Rad51 1:100, 2nd FKab336 α-mouse STAR ORGANGE 1:100

## 3.4 *rec114-8D* and *spp1*Δ behave differently in genetic interaction with zmm$^-$ mutants

### 3.4.1 *spp1*Δ delays, while *rec114-8D* accelerates progression in zmm$^-$ backgrounds

The *rec114-8D* mutation was previously shown to downregulate DSB formation (Carballo *et al.*, 2013). The zmm$^-$ mutants *msh5*Δ and *zip4*Δ experience a delay in meiotic progression due to the prolonged activation of DNA damage checkpoint (Börner, Kleckner and Hunter, 2004). *msh5*Δ*, rec114-8D* and *zip4*Δ, *rec114-8D* double mutants display a dramatically accelerated meiotic progression relative to the single zmm$^-$ mutants, consistent with the reduction in DSBs (**Figure 12 A, B**). In contrast, deletion of *SPP1* either does not accelerate (*zip4*Δ) or even delays meiotic progression (*msh5*Δ) (**Figure 12 A**).

Spore viability does not differ strongly between double mutants with *spp1*Δ or *rec114-8D* for both *msh5*Δ and *zip4*Δ (**Figure 12 C, D**), although 5 % viable spores were found for *msh5*Δ*, rec114-8D* but none for *msh5*Δ, *spp1*Δ*.* Spore formation is more reduced in *msh5*Δ*, spp1*Δ (14 %), as opposed to the *msh5*Δ*, rec114-8D* mutant (82 %) (**Figure 12 C**). Similarly, spore formation in *zip4*Δ*, rec114-8D* is two-fold higher than in *zip4*Δ*, spp1*Δ (**Figure 12 D**).

Taken together, these observations suggest that although both *spp1*Δ and *rec114-8D* reduce spore viability, the underlying cause differs: in *rec114-8D*, the defect likely arises from an insufficient number of DSBs, while in *spp1*Δ the pronounced delay in meiotic progression suggests a continued activation of the DNA damage checkpoint due to a defect in DSB repair.

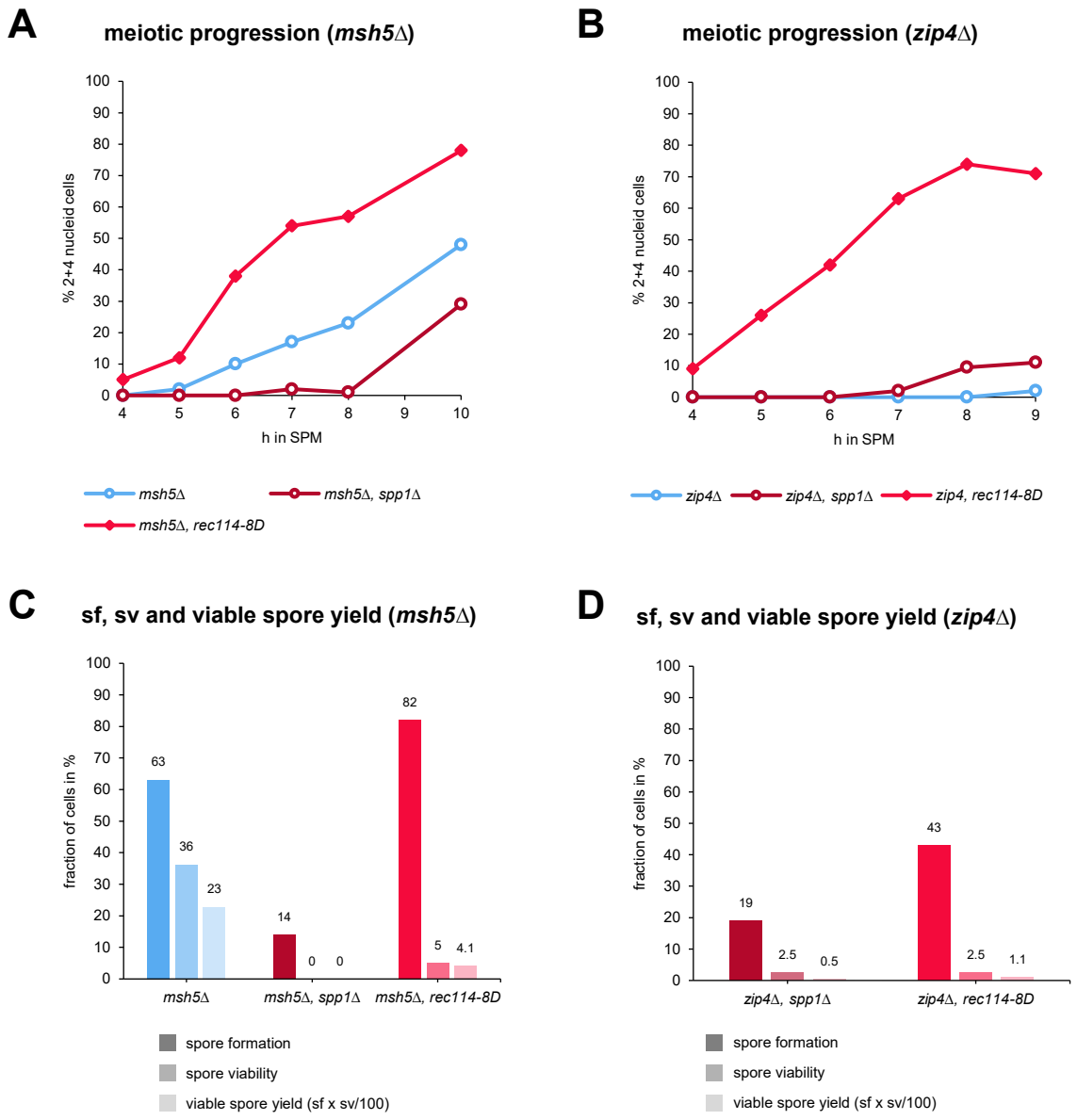


**Figure 12. Unlike *spp1*Δ, *rec114-8D* drastically accelerates meiotic progression and increases spore formation of *zmm*⁻ mutants, while spore viability remains decreased.**

(**A**) Meiotic progression of *spp1*Δ or *rec114-8D* in a *msh5*Δ background, compared to *msh5*Δ single mutant.

(**B**) Same as (A) just in a *zip4*Δ background.

(**C**) Spore formation (sf), spore viability (sv) and viable spore yield of *spp1*Δ or *rec114-8D* in a *msh5*Δ background, compared *msh5*Δ single mutant.

(**D**) Same as (A) just in a *zip4*Δ background.

Data from **TC2:** FKy6336 (*msh5*Δ), FKy6290 (*msh5*Δ*, spp1*Δ), FKy6362 (*msh5*Δ*, rec114-8D*) and **TC11:** FKy6338 (*zip4*Δ); **TC23:** FKy6296 (*zip4*Δ*, spp1*Δ), FKy6377 (*zip4*Δ*, rec114-8D*).

Meiotic progression was followed by DAPI staining in a meiotic time course experiment at the indicated time points. Spore formation (sf) was assessed after 24 h in SPM (n = 100), spore viability (sv) was determined by tetrad dissection (n = 20) and incubation for 2 days at 30 °C or 3 days at RT, and viable spore yield is sf x sv/100.

sf, sv and viable spore yield of *zip4*Δ were not included in (B) because sf was analysed after 48 h SPM and tetrads were only dissected after 48 h, as well.

The triple mutant *zip4*Δ*, sgs1-mn, rec114-8D* behaves like the double mutant *zip4*Δ*, rec114-8D* in regard to meiotic progression (**Figure 13 A**), suggesting a reduced number of DSBs in this background. In contrast, the *zip4*Δ*, sgs1-mn, spp1*Δ triple mutant displays a prolonged meiotic progression (**Figure 13 B**), comparable to the *zip4*Δ*, sgs1-mn* double mutant.

While the introduction of *sgs1*-mn does not affect meiotic progression of the *zip4*Δ*, rec114-8D* or *zip4*Δ*, spp1*Δ double mutant (**Figure 13 A, B**), the same does not apply to sporulation efficiency and spore viability (**Figure 13 C**). In contrast to the *zip4*Δ*, spp1*Δ mutants, depletion of Sgs1 in the *zip4*Δ*, rec114-8D* background can modestly suppress spore formation and spore viability defects in the *zip4*Δ*, rec114-8D* double mutant (**Figure 13 C**).

Similar trends are observed in other zmm$^-$ mutants (*mer3*Δ*, msh5*Δ*, zip2*Δ) (**Figure 13 D, E**). Overall, spore formation is much higher in all *zmm*$^-$*, rec114-8D* mutants than *zmm*$^-$*, spp1*Δ mutants (**Figure 13 D**). However, while spore formation is rescued by *sgs1-mn* in *mer3*Δ*, rec114-8D*, it is reduced in *msh5*Δ and *zip2*Δ (**Figure 13 D**). A more consistent trend is observed for spore viability, which is suppressed by *sgs1-mn* in *zmm*$^-$*, rec114-8D* mutants double mutants (**Figure 13 E**). The only exception is *msh5*Δ*, spp1*Δ, which shows slightly elevated levels of spore viability in the absence of *sgs1-mn* (**Figure 13 E**).

**Figure 13. Absence of Sgs1 improves spore viability for *rec114-8D* in *zmm*$^-$ mutants but not for *spp1*Δ but does not further improve progression.**

(**A**) Meiotic progression of *rec114-8D* in the *zip4*Δ and *zip4*Δ*, sgs1-mn* backgrounds.

(**B**) Same as (A) just with *spp1*Δ.

(**C**) Spore formation (sf), spore viability (sv) and viable spore yield of all strains in (A) and (B).

(**D**) Shows spore formation in % for *mer3*Δ*, msh5*Δ and *zip2*Δ. Either with *rec114-8D* or *spp1*Δ and plus/minus Sgs1 (- Sgs1 = *sgs1-mn*).

(**E**) Same as (D) with spore viability in %.

Data from **TC23** (Fig. 13 A-C): FKy6374 (*zip4*Δ*, sgs1-mn*), FKy6368 (*zip4*Δ*, sgs1-mn, rec114-8D*), FKy6377 (*zip4*Δ*, rec114-8D*), FKy6371 (*zip4*Δ*, sgs1-mn, spp1*Δ), FKy6296 (*zip4*Δ*, spp1*Δ).

Data for (D) and (E) from Viktoria Prast's Master thesis (2016) (all except *, which are from TC2: FKy6362 (*msh5*Δ*, rec114-8D*), FKy6365 (*msh5*Δ*, sgs1-mn, spp1*Δ), FKy6290 (*msh5*Δ*, spp1*Δ)).

Meiotic progression was followed by DAPI staining in a meiotic time course experiment at the indicated time points. Spore formation (sf) was assessed after 24 h in SPM (n = 100), spore viability (sv) was determined by tetrad dissection (n = 20) and incubation for 2 days at 30 °C or 3 days at RT, and viable spore yield is sf x sv/100.

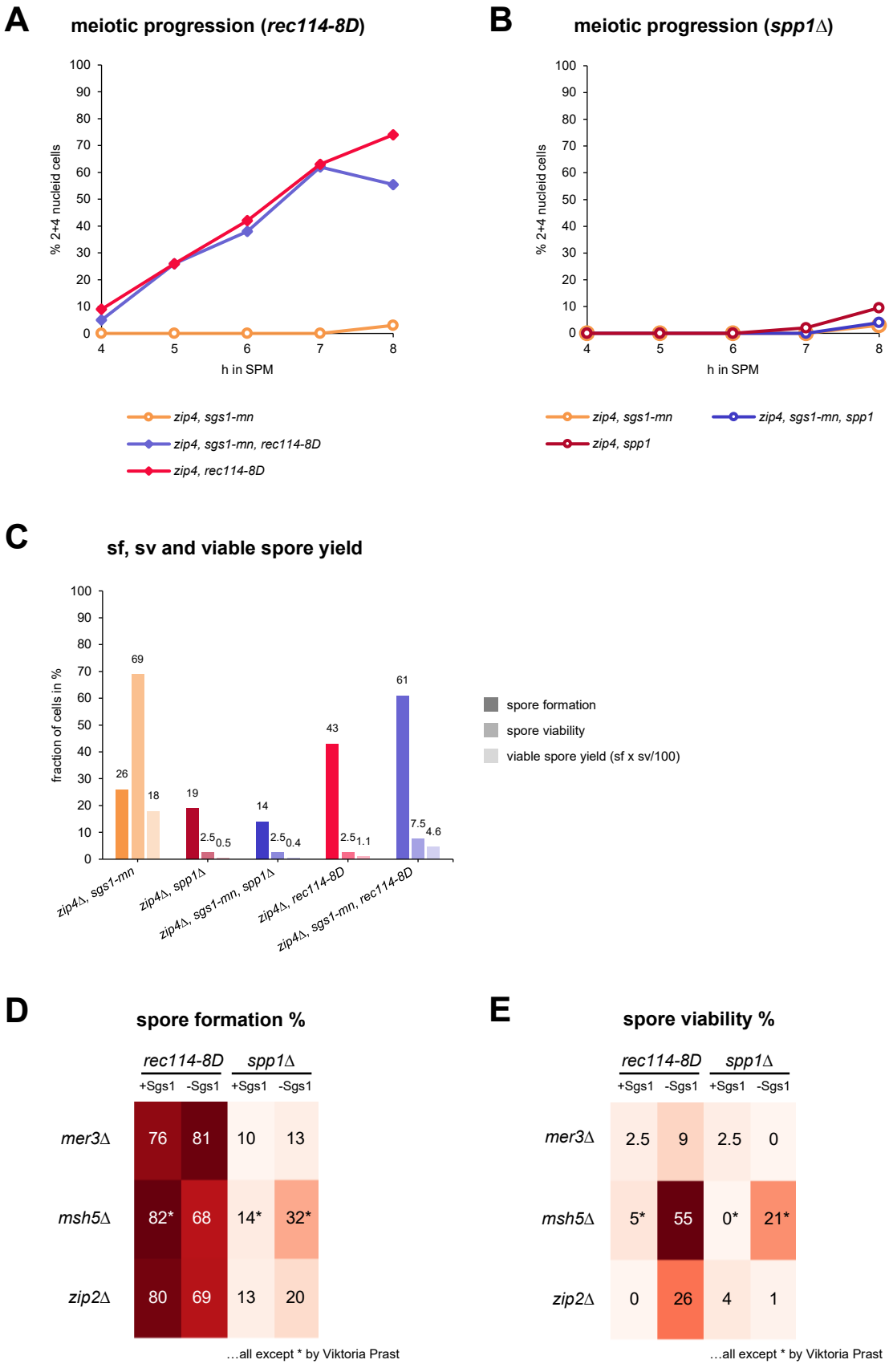


**Figure 13. Legend on the previous page.**

### 3.4.2 Axial associations are reduced in both, *spp1*Δ and *rec114-8D*, mutants

In order to further investigate the reason for the delay in meiotic progression chromosome morphology was analysed by STED microscopy (**Figure 14 A**). Since the *zip4*Δ*, rec114-8D* +/- Sgs1 mutants progress faster through meiosis than the *zip4*Δ*, spp1*Δ +/- Sgs1 mutants, the former were analysed after 4 h and the latter after 6 h in SPM, to catch the strains when they have optimal numbers of nuclei displaying axial elements. After 4 h in SPM, the *zip4*Δ*, rec114-8D* double mutant appears to contain less Rad51 foci than the *zip4*Δ*, sgs1-mn, rec114-8D* triple mutant at 6 h (**Figure 14 A**). However, the *zip4*Δ*, sgs1-mn, rec114-8D* and the *zip4*Δ*, spp1*Δ +/- Sgs1 mutants show a considerable number of Rad51 foci (**Figure 14 A**). No obvious differences between the *rec114-8D* and *spp1*Δ mutants in the alignment of chromosome axes could be observed in the STED images (**Figure 14 A**). This result is confirmed by the quantitative analysis of the aligned axes fragments (**Figure 14 B, C** and **Figure 15 A, B**). All mutants that contain the *rec114-8D* or *spp1*Δ mutation have significantly reduced axial associations per nucleus compared to the *zip4*Δ*, sgs1-mn* double mutant (**Figure 14 B**). While the *rec114-8D* mutants display a modest increase in axis alignment per nucleus relative to the *spp1*Δ mutants, the difference is not significant (**Figure 14 B**). Quantification of the individual aligned fragments revealed that the aligned axis segments are overall shorter in *rec114-8D* mutants than in the *spp1*Δ mutants (**Figure 14 C**). The *rec114-8D* mutants contain a higher number of aligned axes fragments than *spp1*Δ, especially in the *zip4*Δ*, sgs1-mn* background (**Figure 15 A**). The increase in total length of aligned axes fragments in the *rec114-8D* mutants results from an elevated number of associated stretches and not an increase in the length of these aligned axis stretches – an assessment further supported by the mean length of the associated fragments, which is shortest in the *rec114-8D* mutants (**Figure 15 B**).

When comparing Rad51 foci in the *rec114-8D* mutants after 4 h (**Figure 14 A**) and 5 h (**Figure 16 A**) in SPM, a higher number of foci can be observed in the *zip4*Δ*, rec114-8D* double mutant after 5 h SPM. Overall, both the *zip4*Δ*, rec114-8D* double mutant and the *zip4*Δ*, sgs1-mn, rec114-8D* triple mutant retain a considerable number of Rad51 foci after 5 h in SPM, suggesting the existence of unrepaired lesions (**Figure 16**). We did not expect to find so many Rad51 foci, because it was shown by Southern blotting in *com1*Δ*/sae2*Δ strains and by Spo11 ChIP-seq that DSBs are reduced in *rec114-8D* (Carballo *et al.*, 2013). However, by meiotic progression, spore viability and spore formation *rec114-8D* behaves as reported as a DSB hypomorph. We therefore stick with this working hypothesis, but future experiments should clarify the significance of the observed Rad51 foci numbers.

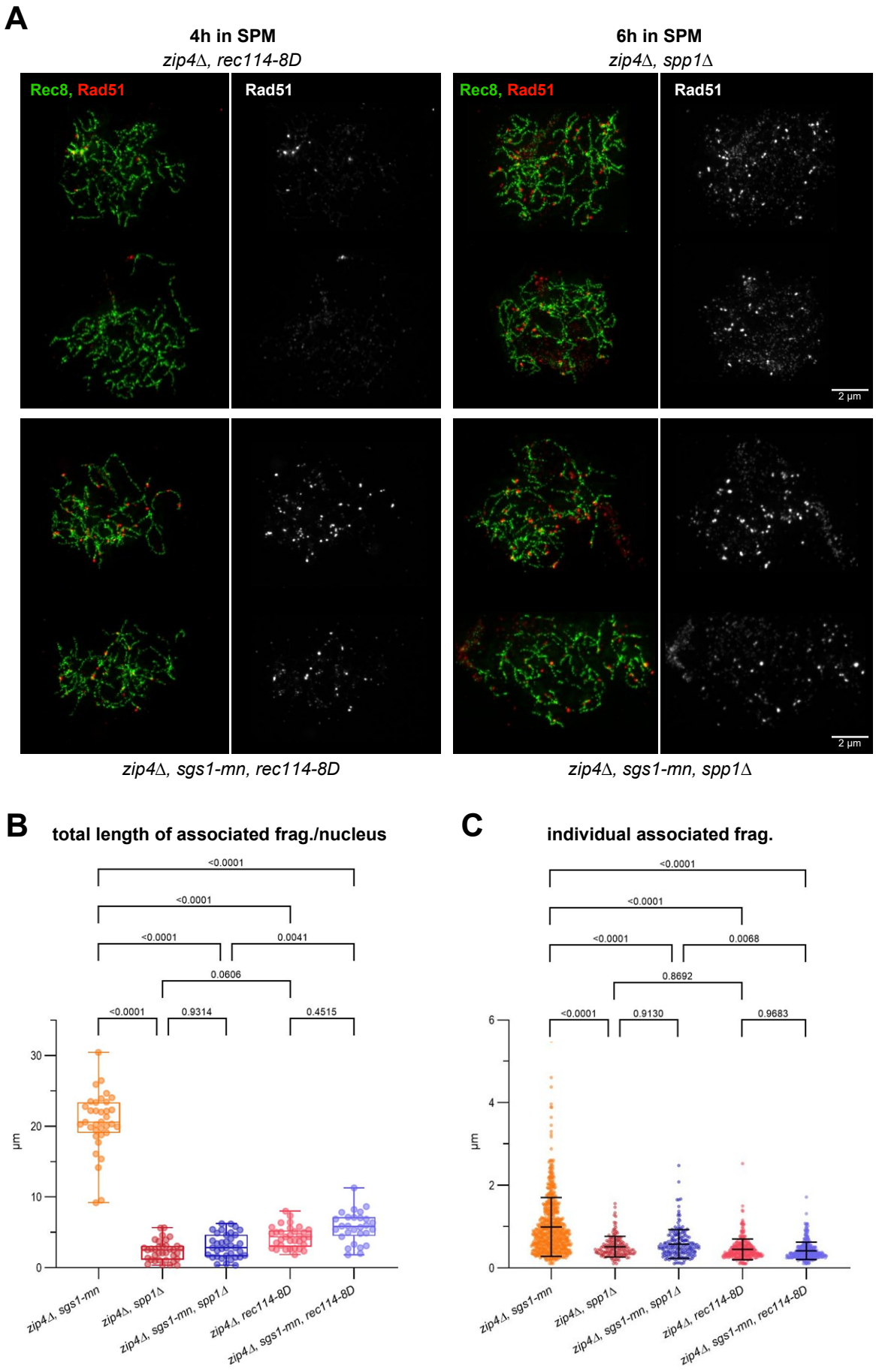


**Figure 14. Legend on the next page.**

**Figure 14. Chromosome spreads reveal a similar phenotype for *spp1*Δ or *rec114-8D* in *zip4*Δ +/- Sgs1 mutants. However, analysis of axial associations suggests that *sgs1-mn* slightly rescues *zip4*Δ, *rec114-8D* but not *zip4*Δ, *spp1*Δ.**

(**A**) Representative STED images showing Rec8 and Rad51-stained chromosome spreads for *zip4*Δ, rec114-8D and *zip4*Δ, sgs1-mn, rec114-8D at 4 hours in SPM and for *zip4*Δ, *spp1*Δ and *zip4*Δ, sgs1-mn, *spp1*Δ at 6 hours in SPM (n = 2 for each).

(**B**) Quantification of the total length of associated axial fragments per nucleus across different mutants (whiskers: min to max, individual data points shown).

(**C**) Distribution of the lengths of individual associated axial fragments for each mutant background (one outlier was excluded for *zip4*Δ, *sgs1-mn*; whiskers: mean +/- SD, individual data points shown).

Data for (A) from **TC23:** FKy6377 (*zip4*Δ, *rec114-8D*), FKy6368 (*zip4*Δ, *sgs1-mn, rec114-8D*), FKy6296 (*zip4*Δ, *spp1*Δ), FKy6371 (*zip4*Δ, *sgs1-mn, spp1*Δ).

Brightness was adjusted for Rec8-staining for better visualisation but not for Rad51-staining.

Data for (B) and (C) from **TC11:** FKy6374 (*zip4*Δ, *sgs1-mn*), FKy6296 (*zip4*Δ, *spp1*Δ), FKy6371 (*zip4*Δ, *sgs1-mn, spp1*Δ) (6 h in SPM) and **TC23:** FKy6377 (*zip4*Δ, *rec114-8D*), FKy6368 (*zip4*Δ, *sgs1-mn, rec114-8D*) (4 h in SPM).

Number of nuclei analysed (B-C): *zip4*Δ, *sgs1-mn* (n = 35); *zip4*Δ, *spp1*Δ (n = 35); *zip4*Δ, *sgs1-mn, spp1*Δ (n = 36); *zip4*Δ, *rec114-8D* (n = 33); *zip4*Δ, *sgs1-mn, rec114-8D* (n = 28).

Only most relevant significant comparisons shown. Data was analysed using one-way ANOVA with Tukey's multiple comparisons test.

Antibodies: 1st FKab314 rabbit α-Rec8 1:1,000 and FKab160 mouse α-Rad51 1:100, 2nd FKab331 α-rabbit STAR RED 1:100 and FKab336 α-mouse STAR ORGANGE 1:100

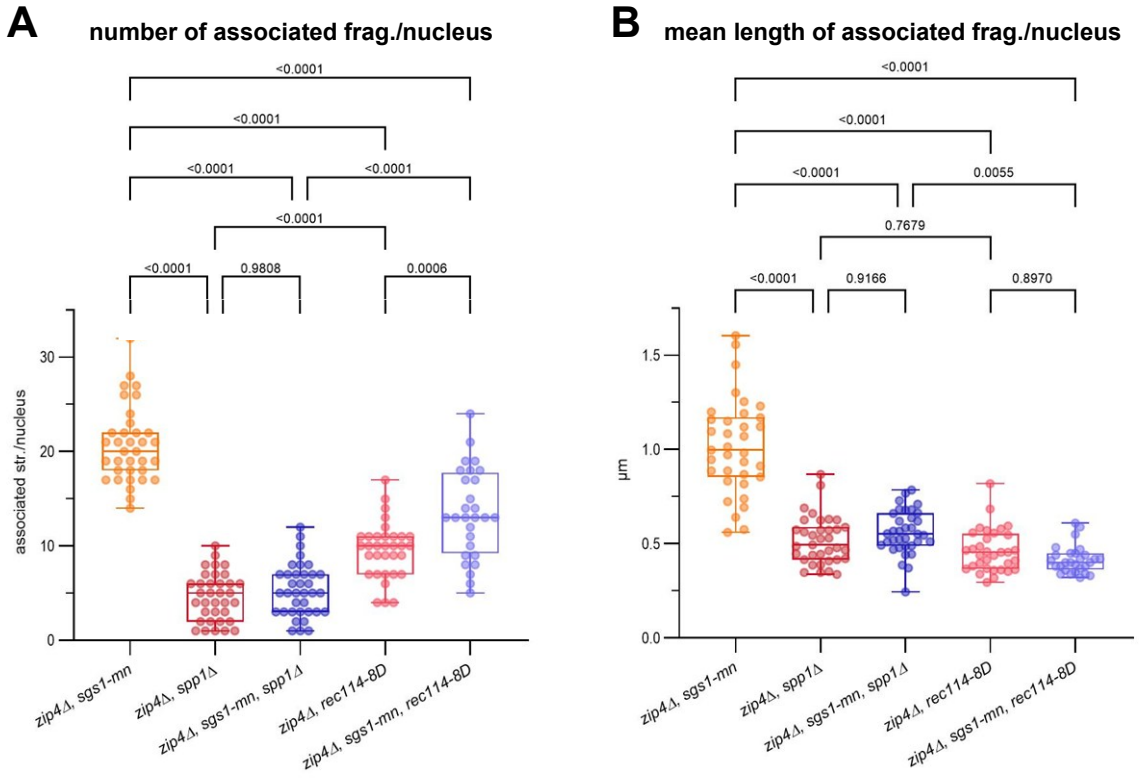


**Figure 15. Legend on the next page.**

**Figure 15. Number of associated stretches per nucleus is significantly increased by absence of Sgs1 in *zip4*Δ, *rec114-8D,* but not in *zip4*Δ, *spp1*Δ. The mean length of associated stretches remains comparable across all mutants, except *zip4*Δ, *sgs1-mn*.**

(**A**) shows the distribution of the number of associated axial fragments per nucleus.

(**B**) presents the average length of these associated axial fragments (one outlier excluded for *zip4*Δ, *sgs1-mn, spp1*Δ).

Data from TC11: FKy6374 (*zip4*Δ, *sgs1-mn*), FKy6296 (*zip4*Δ, *spp1*Δ), FKy6371 (*zip4*Δ, *sgs1-mn, spp1*Δ) (6 h in SPM) and TC23: FKy6377 (*zip4*Δ, *rec114-8D*), FKy6368 (*zip4*Δ, *sgs1-mn, rec114-8D*) (4 h in SPM).

Only most relevant significant comparisons shown. Data was analysed using one-way ANOVA with Tukey's multiple comparisons test.

Number of nuclei analysed: *zip4*Δ, *sgs1-mn* (n = 35); *zip4*Δ, *spp1*Δ (n = 35); *zip4*Δ, *sgs1-mn, spp1*Δ (n = 36); *zip4*Δ, *rec114-8D* (n = 33); *zip4*Δ, *sgs1-mn, rec114-8D* (n = 28).

Antibodies: 1st FKab314 rabbit α-Rec8 1:1,000, 2nd FKab331 α-rabbit STAR RED 1:100

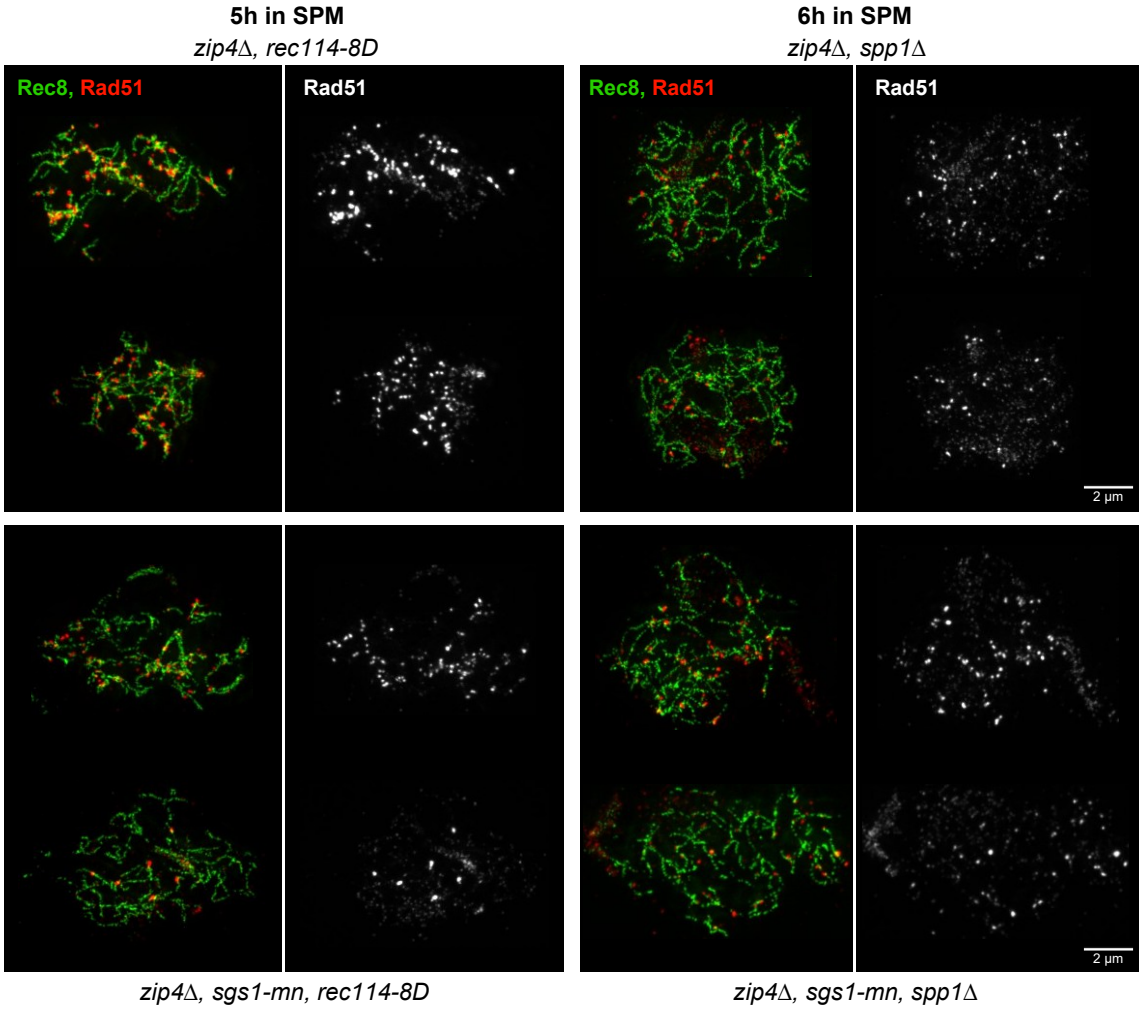


**Figure 16. Legend on the next page.**

**Figure 16. Rad51 foci in *spp1*∆ and *rec114-8D* in the *zip4*∆ +/- Sgs1 background after 5 h in SPM.**

Representative STED images showing Rec8 and Rad51-stained chromosome spreads for *zip4*∆, *rec114-8D* and *zip4*∆, *sgs1-mn, rec114-8D* at 5 hours in SPM and for *zip4*∆, *spp1*∆ and *zip4*∆, *sgs1-mn, spp1*∆ at 6 hours in SPM (n = 2 for each).

Data from TC23: FKy6377 (*zip4*∆, *rec114-8D*), FKy6368 (*zip4*∆, *sgs1-mn, rec114-8D*), FKy6296 (*zip4*∆, *spp1*∆), FKy6371 (*zip4*∆, *sgs1-mn, spp1*∆).

Brightness was adjusted for Rec8-staining for better visualisation but not for Rad51-staining.

Antibodies: 1st FKab314 rabbit α-Rec8 1:1,000 and FKab160 mouse α-Rad51 1:100, 2nd FKab331 α-rabbit STAR RED 1:100 and FKab336 α-mouse STAR ORGANGE 1:100

### 3.4.3 *rec114-8D* is epistatic to *spp1*∆ concerning meiotic progression

Introduction of the *rec114-8D* allele in the *zip4*∆, *spp1*∆ +/- Sgs1 mutant background, accelerates meiotic progression to levels comparable to the progression of *zip4*∆, *rec114-8D* +/- Sgs1 mutants (**Figure 17 A**). This observation shows that phosphorylated Rec114 acts upstream of Spp1. If the delay in *spp1*∆ meiotic progression were caused by changes in the transcriptional program *spp1*∆ should be epistatic to *rec114-8D*. If, however, the delay were caused by unrepaired DSBs, the reduction of DSB formation in *rec114-8D* should accelerate the progression. As we observe a dramatic improvement in progression, we conclude that the reduction in DSB formation is responsible.

Interestingly, spore formation of *zip4*∆, *rec114-8D, spp1*∆ +/- Sgs1 does not reach the levels observed in *zip4*∆, *rec114-8D* +/- Sgs1 and spore viability is abolished, consistent with repair defects introduced by *spp1*∆. Both the triple mutant, *zip4*∆, *rec114-8D, spp1*∆, and the quadruple mutant, *zip4*∆, *sgs1-mn, rec114-8D, spp1*∆, produced no viable spores (**Figure 17 B**). Thus, while meiotic progression is accelerated by reduced DSBs in *rec114-8D,* spore formation and spore viability are strongly defective in each mutant, *rec114-8D* and *spp1*∆.

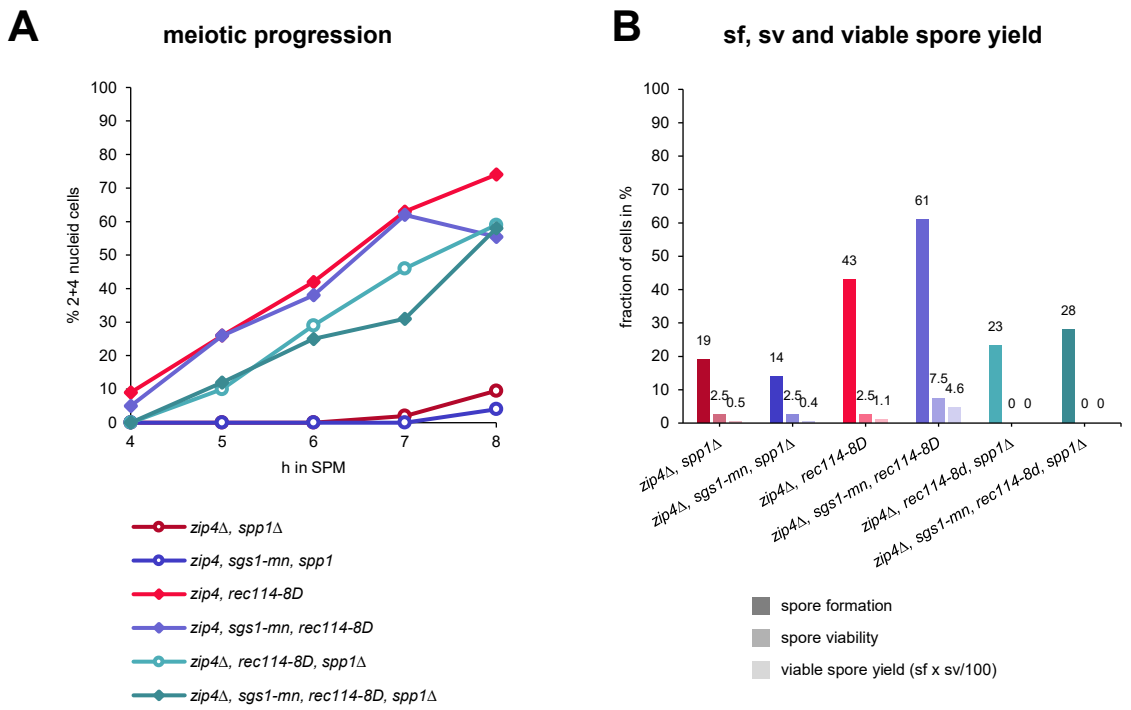


**Figure 17. *rec114-8D* improves meiotic progression of *zip4*Δ, *spp1*Δ and *zip4*Δ, *sgs1-mn, spp1*Δ mutants, while spore formation and spore viability remain reduced.**

(**A**) Meiotic progression of *rec114-8D* and/or *spp1*Δ in *zip4*Δ or *zip4*Δ, *sgs1-mn* mutant backgrounds.

(**B**) Spore formation (sf), spore viability (sv) and viable spore yield of all strains in (A).

Meiotic progression was followed by DAPI staining in a meiotic time course experiment at the indicated time points. Spore formation (sf) was assessed after 24 h in SPM (n = 100), spore viability (sv) was determined by tetrad dissection (n = 20) and incubation for 2 days at 30 °C or 3 days at RT, and viable spore yield is sf x sv/100.

Data from **TC23:** (FKy6374 (*zip4*Δ, *sgs1-mn*), FKy6368 (*zip4*Δ, *sgs1-mn, rec114-8D*), FKy6377 (*zip4*Δ, *rec114-8D*), FKy6371 (*zip4*Δ, *sgs1-mn, spp1*Δ), FKy6296 (*zip4*Δ, *spp1*Δ) and **TC32:** FKy9416 (*zip4*Δ, *rec114-8D, spp1*Δ), FKy9413 *(zip4*Δ, *sgs1-mn, rec114-8D, spp1*Δ).

## 3.5 Zip3 foci frequency and intensity is largely independent of Spp1 in the *zip4*Δ background

To determine if deletion of *SPP1* affects the formation of repair intermediates reserved for the ZMM pathway in *zip4*Δ +/- Sgs1 mutants, I analysed the number and intensity of Zip3 foci as a cytological marker. In wild type Zip3 foci mark ZMM-dependent recombination intermediates, reflecting sites where class I CO designation has occurred (Agarwal and Roeder, 2000; Tsubouchi, Zhao and Roeder, 2006). In the *zip4*Δ mutant Zip3 foci also are found predominantly at axial association sites. STED microscopy of chromosome spreads after 6 h in SPM revealed that all analysed mutants exhibit a substantial number of Zip3 foci, indicating that deletion of *SPP1* does not reduce Zip3 foci formation (**Figure 18 A**).

Compared to the *zip4*Δ single mutant and the *zip4*Δ*, spp1*Δ double mutant, the number of Zip3 foci are elevated in the *zip4*Δ*, sgs1-mn* double mutant and the *zip4*Δ*, sgs1-mn, spp1*Δ triple mutant. However, this increase reached statistical significance only in comparison to the *zip4*Δ*, spp1*Δ double mutant (**Figure 18 B**). Analysis of individual Zip3 foci intensities shows that the *zip4*Δ*, spp1*Δ mutant displays the weakest foci intensities, whereas the *zip4*Δ*, sgs1-mn* double mutant exhibits the highest intensities, closely followed by the *zip4*Δ*, sgs1-mn, spp1*Δ triple mutant (**Figure 18 C**). This trend is also reflected in the summed Zip3 foci intensities per nucleus, with *the zip4*Δ*, spp1*Δ double mutant showing the lowest number (**Figure 18 B**) and the weakest cumulative Zip3 foci signal (**Figure 18 D**). There is hardly a difference between the mean foci intensities between the different strains (**Figure 18 E**).

**Figure 18. Frequency and intensity of Zip3 foci increase in the absence of Sgs1 and the presence of Spp1 in a *zip4*Δ background**

(**A**) Representative STED images showing Rec8, Zip3-stained chromosome spreads in different *zip4*Δ mutant backgrounds after 6 h in SPM.

(**B**) Zip3 foci number per nucleus across all mutants.

(**C**) Distribution of all individual Zip3 foci intensities for each mutant (mean, individual data points).

(**D**) Added up Zip3 foci intensities per nucleus for the different mutants.

(**E**) presents the average intensity of these Zip3 foci per nucleus.

Number of nuclei analysed: *zip4*Δ (n = 37); *zip4*Δ*, sgs1-mn* (n = 36); *zip4*Δ*, sgs1-mn, spp1*Δ (n = 36); *zip4*Δ*, spp1*Δ (n = 34).

Data from TC11: FKy6338 (*zip4*Δ), FKy6374 (*zip4*Δ*, sgs1-mn*), FKy6371 (*zip4*Δ*, sgs1-mn, spp1*Δ), FKy6296 (*zip4*Δ*, spp1*Δ).

Only significant comparisons shown. Data was analysed using one-way ANOVA with Tukey's multiple comparisons test. Brightness adjusted for better visualisation.

Box plots: whiskers from min to max, individual data points shown.

Antibodies: 1st FKab340 guineapig α-Rec8 1:2,000 and FKab289 rabbit α-Zip3 1:2,000, 2nd FKab339 α-guineapig STAR RED 1:100 and FKab332 α-rabbit STAR ORGANGE 1:200

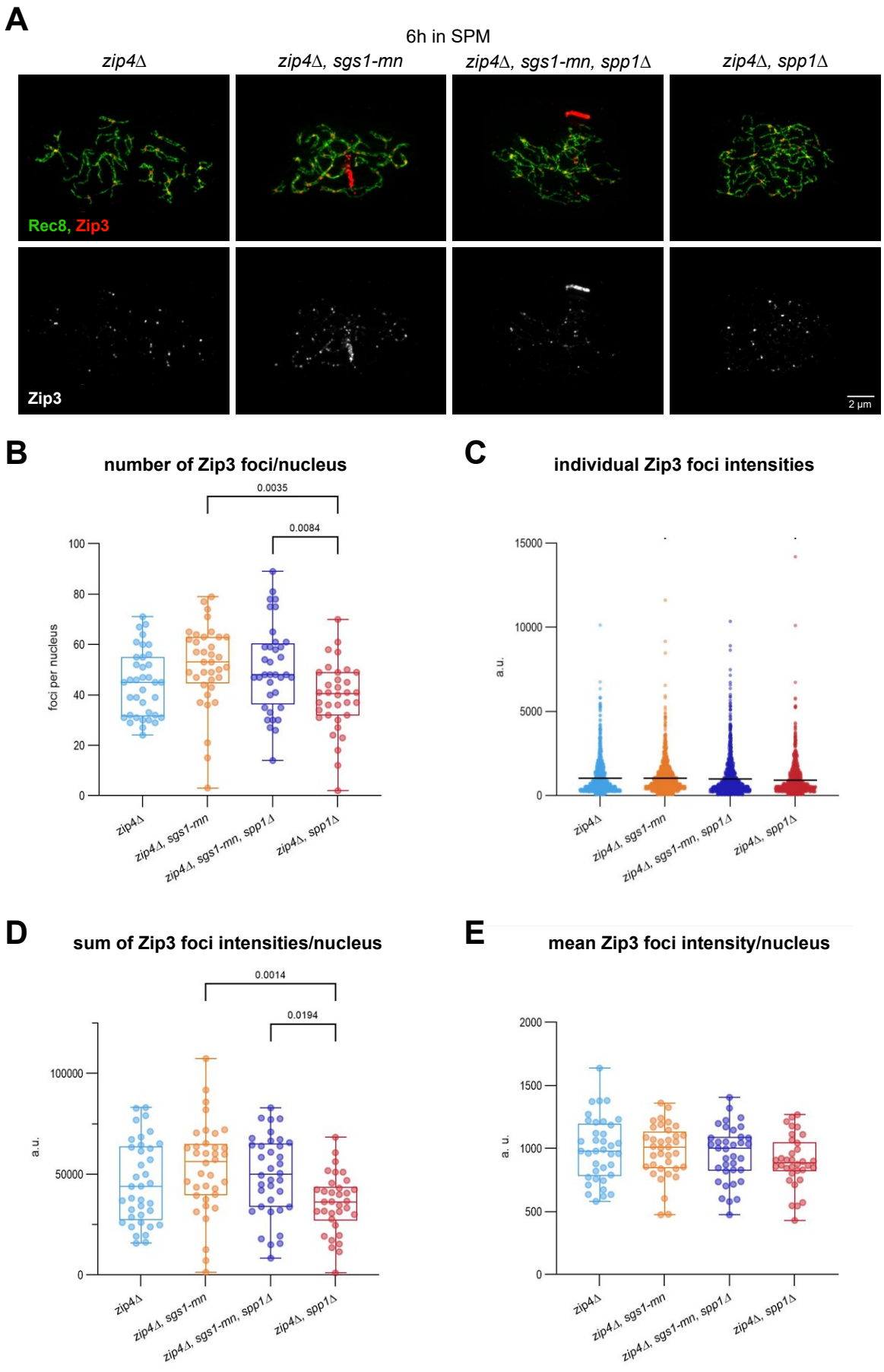


**Figure 18. Legend on the previous page.**

The lowest variability in Zip3 foci number was observed in the *zip4*Δ single mutant (range: 24-71; mean = 44.5; SD = +/- 13.11; **Figure 19 A**). The *zip4*Δ, *spp1*Δ double mutant exhibits comparable variability (mean = 38.9, SD = +/- 13.82) (**Figure 22 A**). In contrast, introduction of the *sgs1-mn* mutation increases variability in the *zip4*Δ, *sgs1-mn* double mutant (mean = 51.7, SD = +/- 16.21) (**Figure 20 A**) and the *zip4*Δ, *sgs1-mn, spp1*Δ triple mutant (mean = 50.7, SD = +/- 17.49) (**Figure 21 A**). Taken together, these results suggest that the absence of Sgs1 and the presence of Spp1 enhances mainly Zip3 foci numbers.

The corresponding heatmap of the foci intensities per foci class revealed that the *zip4*Δ single mutant contains the most high-intensity foci per class (**Figure 19 B**) compared to all other examined mutants (**Figure 19-22 B).** The *zip4*Δ, *sgs1-mn* double mutant (**Figure 20 B**) and the *zip4*Δ, *sgs1-mn, spp1*Δ triple mutant (**Figure 21 B**) retain a higher proportion of strong Zip3 foci relative to the *zip4*Δ, *spp1*Δ double mutant (**Figure 22 B**). Across all mutants, the majority of Zip3 foci exhibit relatively low intensities, with only a minor subset displaying higher intensity (**Figure 19-22 C, D**). Overall the intensities are variable, as shown through the following SDs: *zip4*Δ (mean = 1026, SD = +/- 976) (**Figure 19 D**), *zip4*Δ, *sgs1-mn* (mean = 1028, SD = +/- 890) (**Figure 20 D**), *zip4*Δ, *sgs1-mn, spp1*Δ (mean = 973, SD = +/- 1024) (**Figure 21 D**), *zip4*Δ, *spp1*Δ (mean = 911, SD = +/- 928) (**Figure 22 D**).

**Figure 19-22. Quantitative analysis of Zip3 foci for *zip4*Δ (n = 37); *zip4*Δ, *sgs1-mn* (n = 36); *zip4*Δ, *sgs1-mn, spp1*Δ (n = 36) and *zip4*Δ, *spp1*Δ (n = 34) mutants after 6 h in SPM.**

(**A**) The boxplot shows the distribution of Zip3 foci numbers per nucleus, providing median, mean and standard deviation. The bar plot below represents the class frequency of foci numbers across the different nuclei.

(**B**) displays the normalized intensity distribution of Zip3 foci per class, with colour coding indicating intensity levels (x-axis = foci number, y-axis = foci percentile).

(**C**) The density plot shows the overall distribution of total foci intensities together with the mode. The scatter plot below it shows the corresponding individual intensity values (in arbitrary units).

(**D**) shows a boxplot for the total foci intensities. Red bars indicate 0.05, 0.95 and 0.99 quantile of all data points. The black whiskers of the box plot range from Q1 - 1.5 x IQR to Q3 + 1.5 x IQR.

Data from TC11: FKy6338 (*zip4*Δ), FKy6374 (*zip4*Δ, *sgs1-mn*), FKy6371 (*zip4*Δ, *sgs1-mn, spp1*Δ), FKy6296 (*zip4*Δ, *spp1*Δ). Raw grayscale values (0–65,535 for 16-bit images) using Fiji (ImageJ) = arbitrary units.

Antibodies: 1st FKab289 rabbit α-Zip3 1:2,000, 2nd FKab332 α-rabbit STAR ORGANGE 1:200

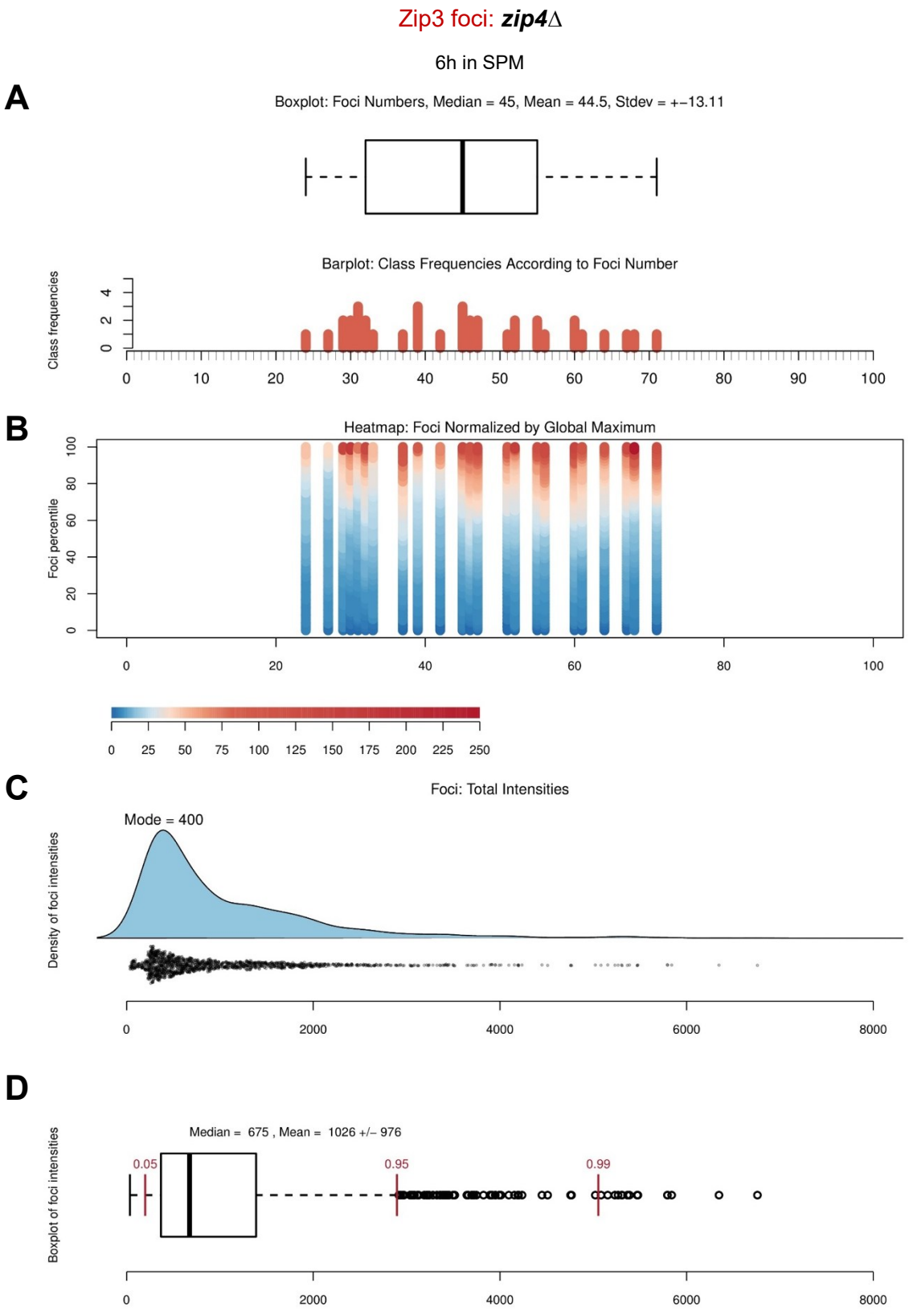


**Figure 19. Legend on the previous page.**

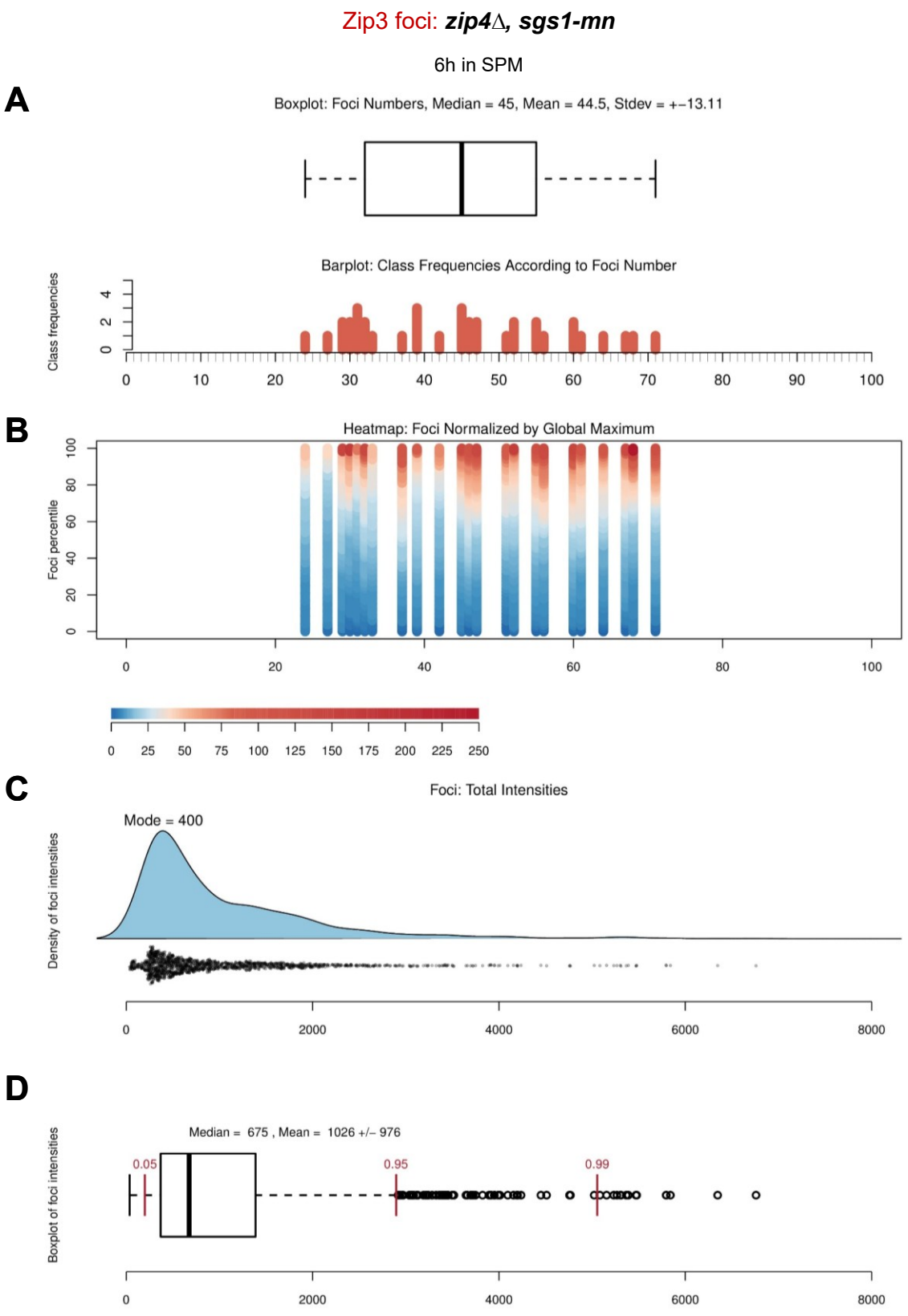


**Figure 20. Legend before Figure 19.**

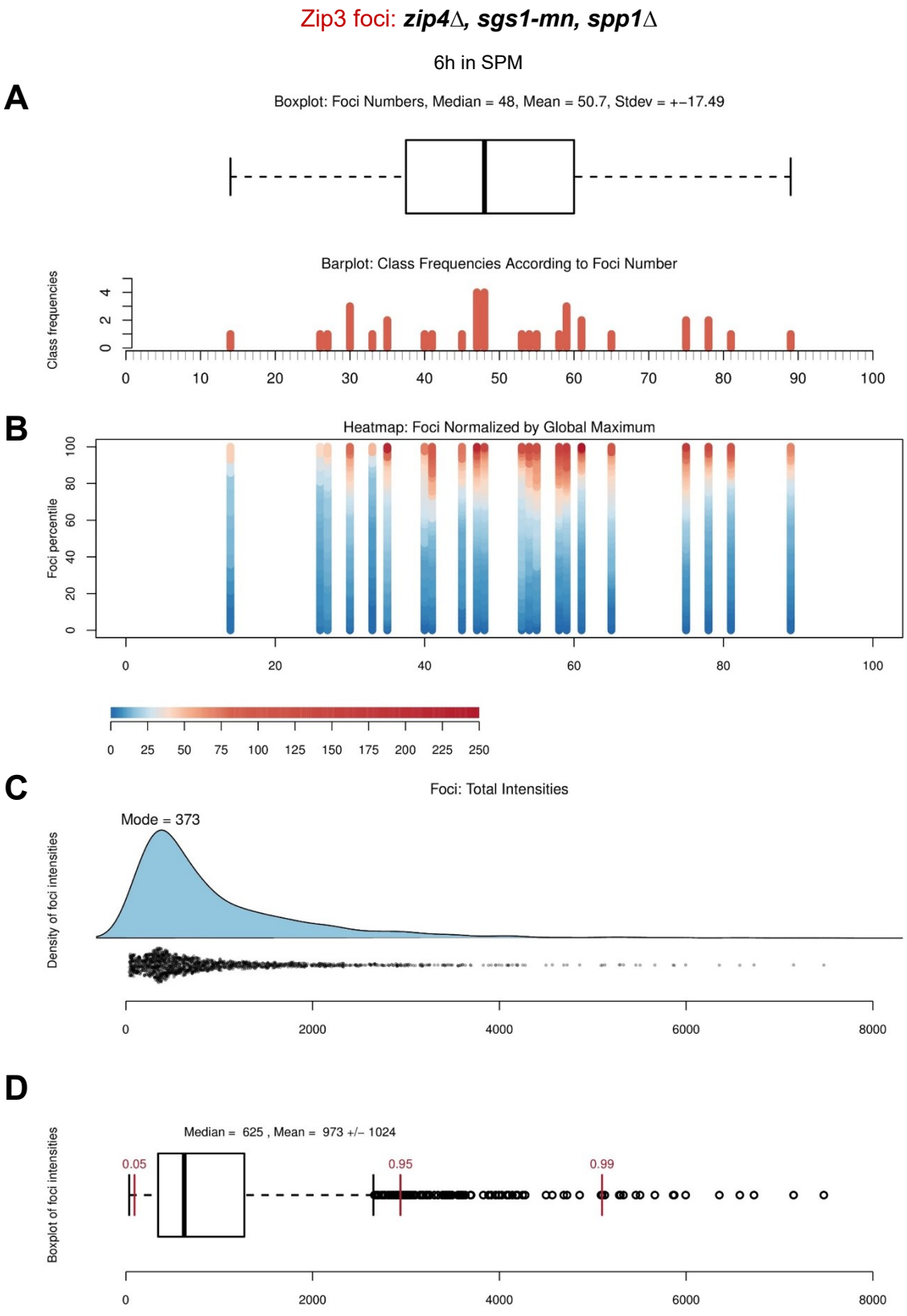


**Figure 21. Legend before Figure 19.**

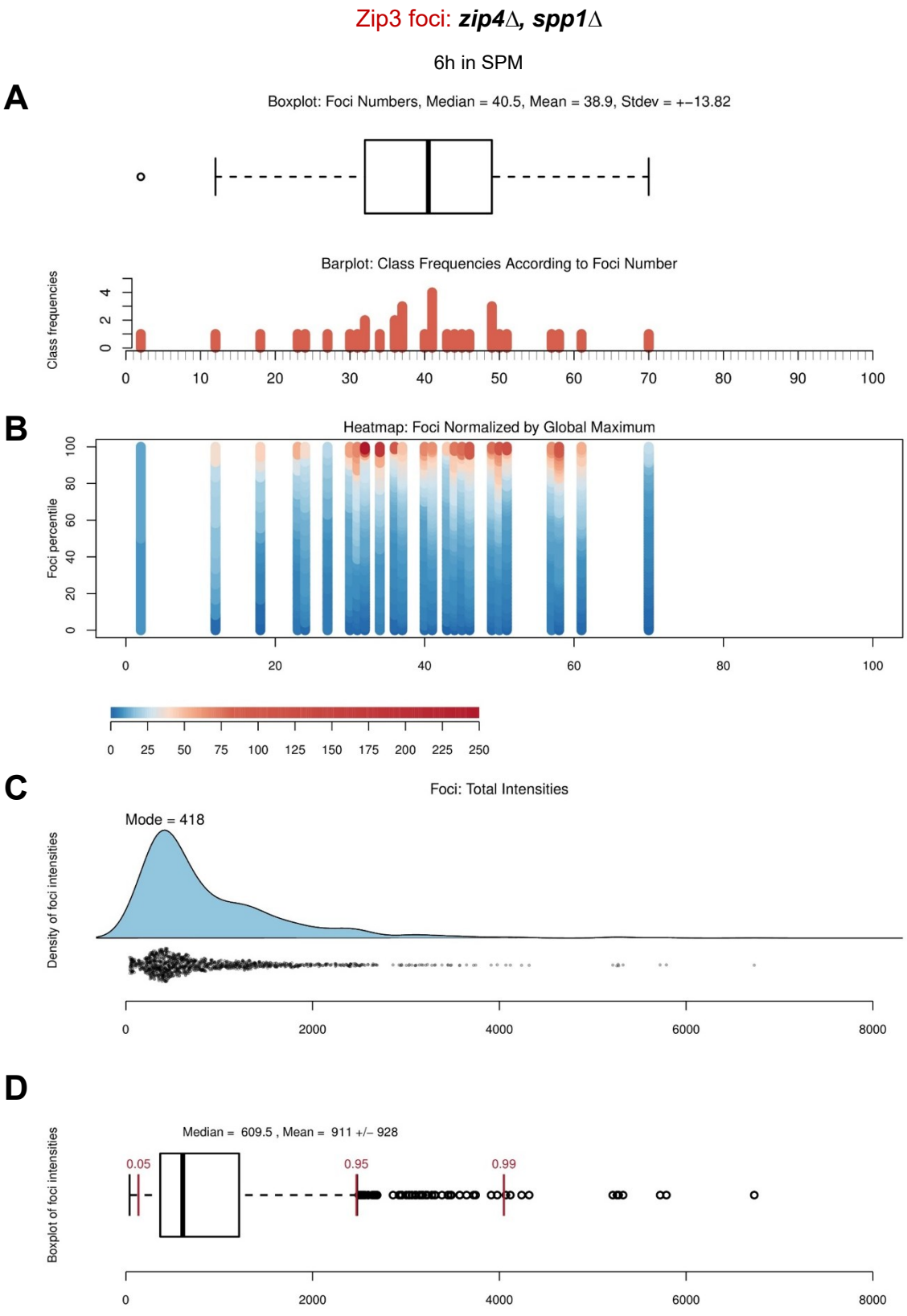


**Figure 22. Legend before Figure 19.**

## 3.6 Axial associations in the absence of Sgs1 also depend on H3K4me3

To examine if Spp1's anchor point H3K4me3 is also required for the establishment of axial associations in a *zmm⁻, sgs1-mn* background, I mutated lysine 4 to alanine in both copies of histone H3 using CRISPR/Cas9. From this point forward *H3K4A* will refer to the double mutation *hht1-K4A, hht2-K4A*. The *H3K4A* mutation has been characterized in previous studies, which reported wild type like sporulation efficiency and spore viability (Govin *et al.*, 2010).

In my experiments, the *H3K4A* mutant copied Spp1's phenotype regarding meiotic progression and is delayed to 6 h in SPM before first meiotic divisions (**Figure 23 A, B**). Like *spp1*Δ*, H3K4A* does not accelerate meiotic progression of *zip3*Δ*, sgs1-mn* (**Figure 23 A**) and *zip4*Δ*, sgs1-mn* (**Figure 23 B**). Spore formation and viability of *spp1*Δ and *H3K4A* single mutants were largely similar (**Figure 23 C, D**), with the *H3K4A* mutant performing slightly worse than *spp1*Δ single mutant. Introducing the *H3K4A* mutation increases spore formation levels in the *zip3*Δ*, sgs1-mn* and *zip4*Δ*, sgs1-mn* backgrounds (**Figure 23 C,D**). As with *spp1*Δ*,* the *H3K4A* mutation prevents the suppression of spore formation and viability defects by the absence of Sgs1 (**Figure 23 C, D**). Spore viability in the *zip4*Δ*, sgs1-mn* context depends on the availability of H3K4 (**Figure 23 D**).

**Figure 23. *H3K4A* mirrors *spp1*Δ in meiotic progression, spore formation and spore viability in the *zip3*Δ*, sgs1-mn* and *zip4*Δ*, sgs1-mn* backgrounds.**

(**A**) compares meiotic progression of *H3K4A* and *spp1*Δ in the *zip3*Δ*, sgs1-mn* background with the *zip3*Δ*, sgs1-mn* double mutant. *spp1*Δ and *H3K4A* single mutants serve as control.

(**B**) Same as (A) just in the *zip4*Δ background.

(**C**) Spore formation (sf) after 24 h SPM of the different mutants in (A) in the *zip3*Δ background.

(**D**) Spore formation (sf), spore viability (sv) and viable spore yield of the different mutants in (A) in the *zip4*Δ background.

Data from **TC9**: FKy5247 (*zip3*Δ*, sgs1-mn*), FKy6142 (*zip3*Δ*, sgs1-mn, spp1*Δ), FKy5539 (*spp1*Δ); **TC15**: FKy9196 (H3K4A, SPO11-myc), FKy9198 (zip3Δ, sgs1-mn, H3K4A); **TC23**: FKy6374 (*zip4*Δ*, sgs1-mn*), FKy6371 (*zip4*Δ*, sgs1-mn, spp1*Δ) and **TC34**: FKy9303 (*zip4*Δ*, sgs1-mn, H3K4A)*.

*spp1*Δ single mutant (FKy5539) in (D) is from Viktoria Prast's Master thesis (2016).

Meiotic progression was followed by DAPI staining in a meiotic time course experiment at the indicated time points. Spore formation (sf) was assessed after 24 h in SPM (n = 100), spore viability (sv) was determined by tetrad dissection (n = 20) and incubation for 2 days at 30 °C or 3 days at RT, and viable spore yield is sf x sv/100.

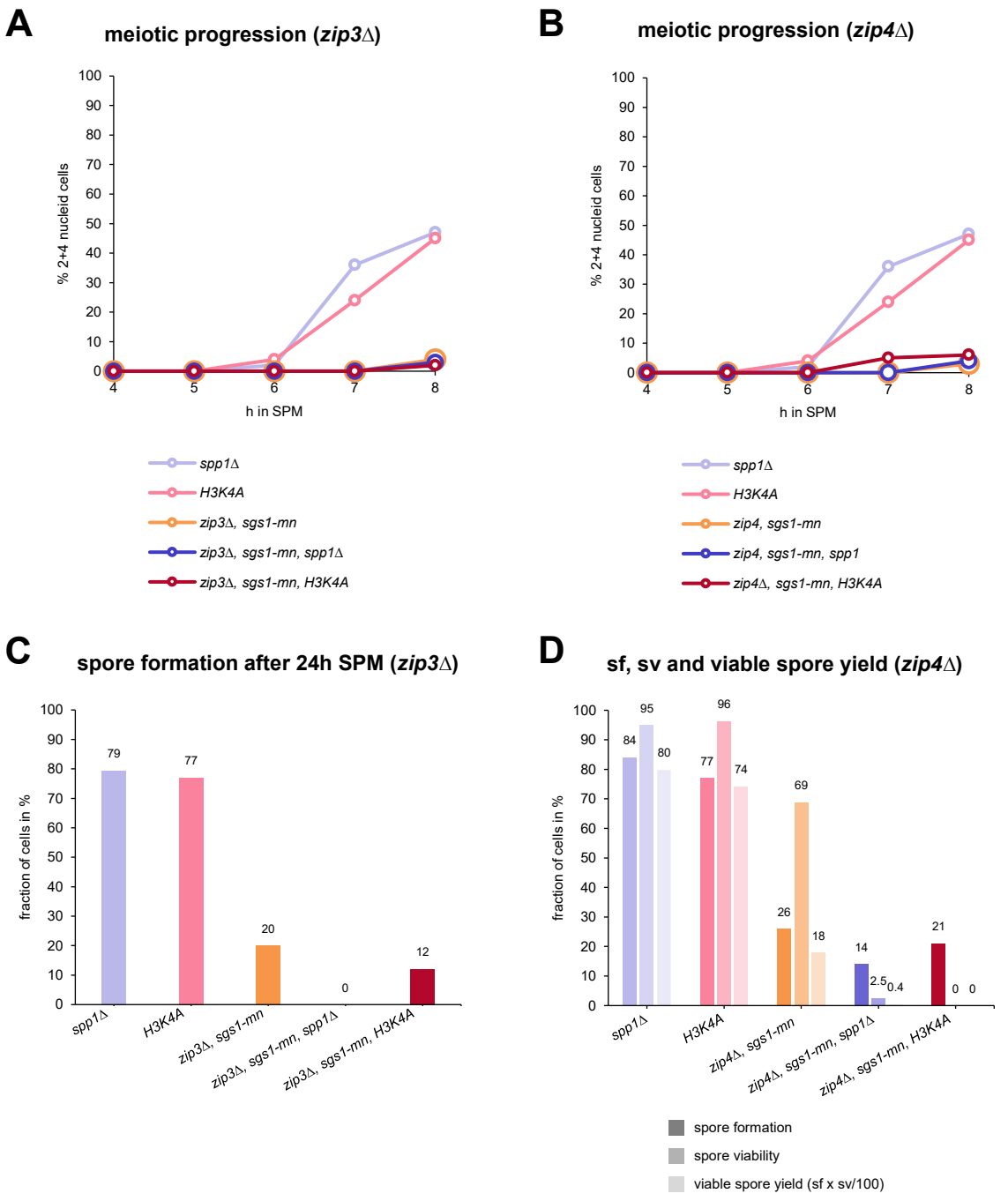


**Figure 23. Legend on the previous page.**

STED microscopy could demonstrate that H3K4 is required for axial associations in *zip3Δ, sgs1-mn* and *zip4Δ, sgs1-mn* double mutants similarly to Spp1 (**Figure 24**). *H3K4A* abolishes pseudosynapsis in both *zip3Δ, sgs1-mn* (**Figure 24 A**) and *zip4Δ, sgs1-mn* (**Figure 24 B**) double mutants. Quantitative analysis of STED images confirmed these observations (**Figure 25**). The *zip3Δ, sgs1-mn, H3K4A* mutant displays an even shorter total length of aligned axes fragments per nucleus than the *zip3Δ, sgs1-mn, spp1Δ* triple mutant (**Figure 25 A**). Moreover, the *zip3Δ, sgs1-mn, H3K4A* mutant contains the shortest aligned axes overall (**Figure 25 B**). The aligned fragments in the *zip3Δ, sgs1-mn, H3K4A* mutant have a comparable size to the

aligned axes fragments in the *zip3*Δ*, sgs1-mn, spp1*Δ triple mutant (**Figure 25 D**). However, the former also contains a reduced number of these fragments (**Figure 25 C**).

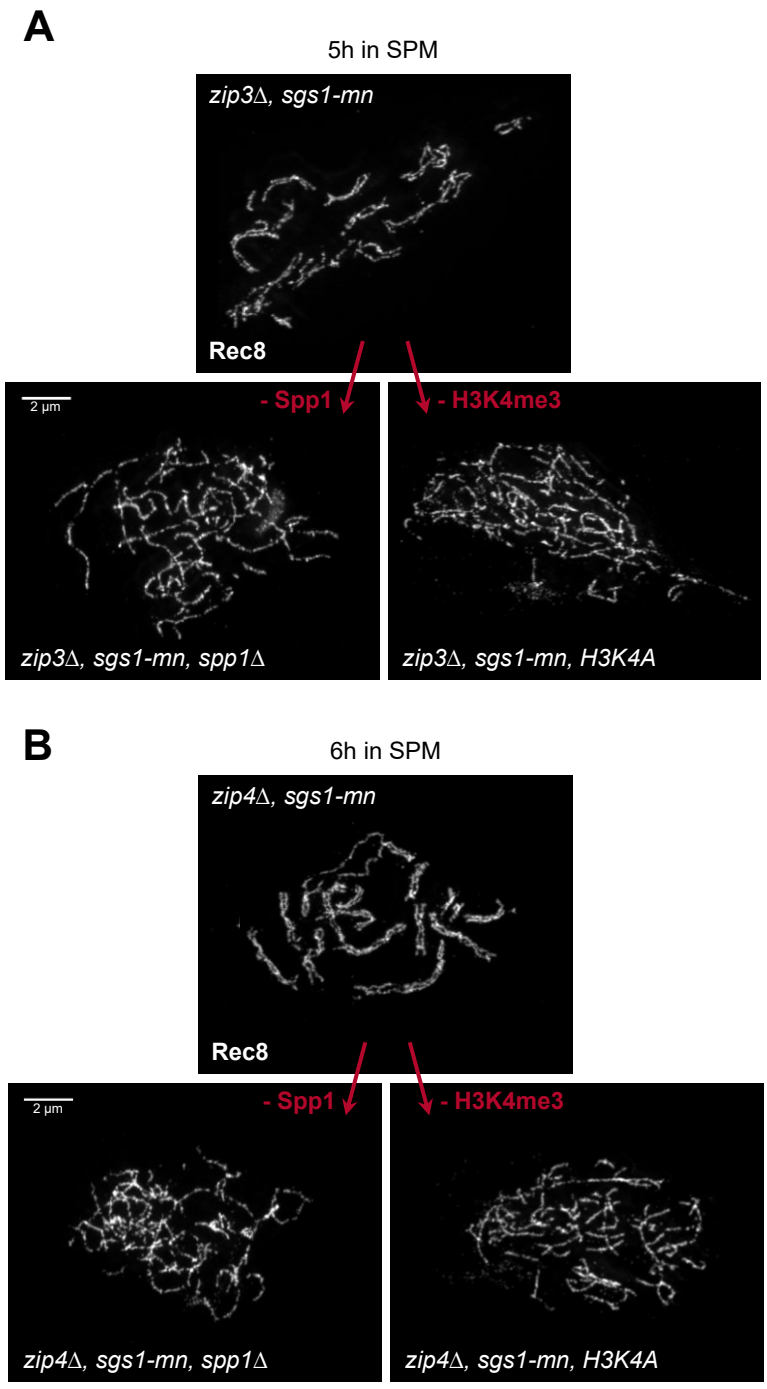


**Figure 24. Like *spp1*Δ*, H3K4A* abolishes Sgs1 sensitive axial associations in *zip3*Δ and *zip4*Δ.**

(**A**) Representative STED images showing Rec8-stained chromosome spreads in different *zip3*Δ mutant backgrounds after 5 h in SPM.

(**B**) Same as (A) but in the *zip4*Δ background and after 6 h in SPM.

Data from **TC9**: FKy5247 (*zip3*Δ*, sgs1-mn*), FKy6142 (*zip3*Δ*, sgs1-mn, spp1*Δ); **TC15**: FKy9198 (*zip3*Δ*, sgs1-mn, H3K4A*); **TC11**: FKy6374 (*zip4*Δ*, sgs1-mn*), FKy6371 (*zip4*Δ*, sgs1-mn, spp1*Δ) and **TC34**: FKy9303 (*zip4*Δ*, sgs1-mn, H3K4A)*.

Brightness adjusted for better visualisation.

Antibodies: 1st FKab314 rabbit α-Rec8 1:1,000, 2nd FKab331 α-rabbit STAR RED 1:100

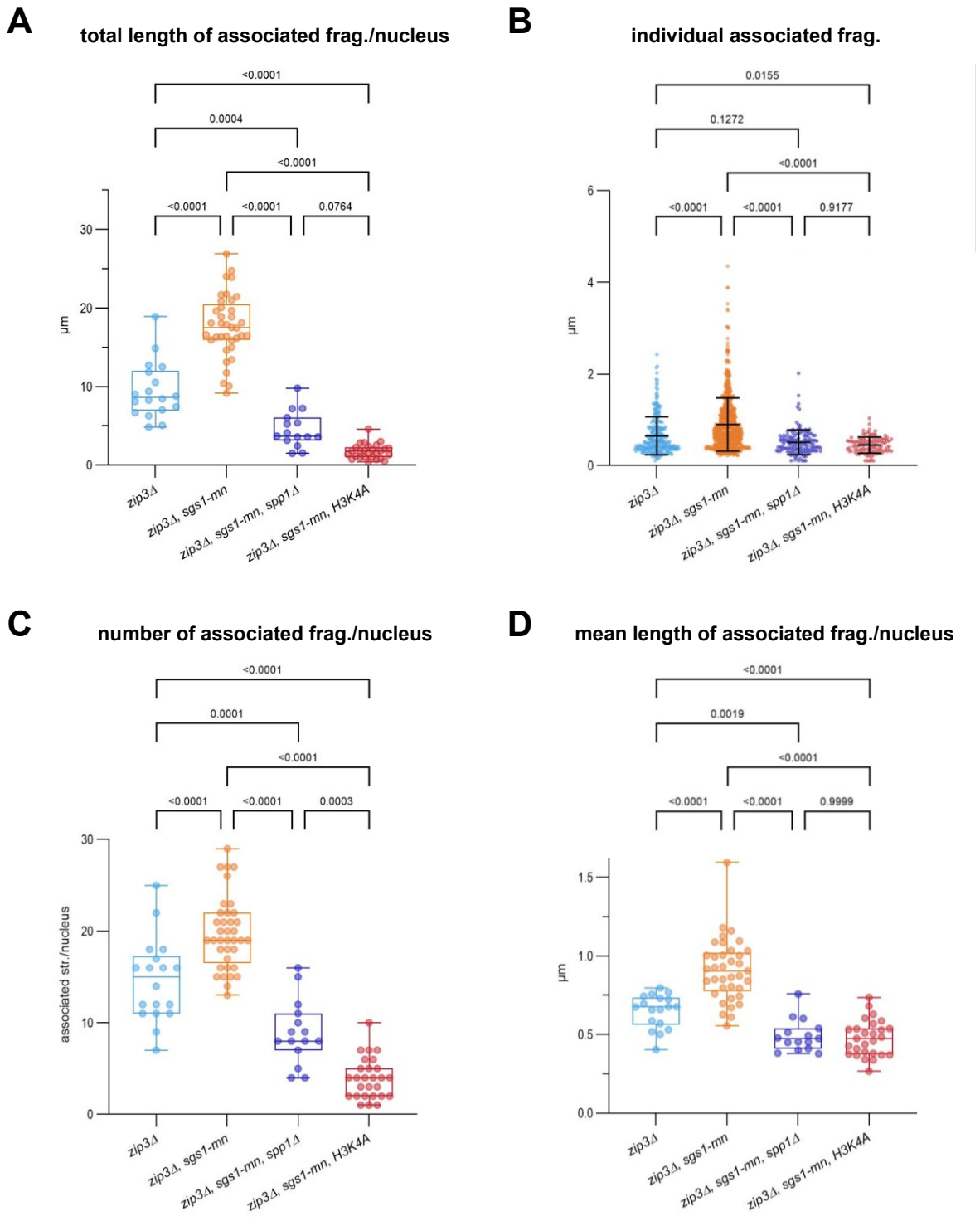


**Figure 25. Legend on the next page.**

**Figure 25. Quantification confirms that *H3K4A* also reduces associated axial fragments in the *zip3*Δ*, sgs1-mn* background.**

(**A**) Quantification of the total length of associated axial fragments per nucleus across different mutants (whiskers: min to max, individual data points shown).

(**B**) Distribution of the lengths of individual associated axial fragments for each mutant (whiskers: mean +/- SD, individual data points shown).

(**C**) shows the distribution of the number of associated axial fragments per nucleus.

(**D**) presents the average length of these associated axial fragments.

Number of nuclei analysed: *zip3*Δ (n = 18); *zip3*Δ*, sgs1-mn* (n = 37); *zip3*Δ*, sgs1-mn, spp1*Δ (n = 15); *zip3*Δ*, sgs1-mn, H3K4A* (n = 27).

Data from **TC9**: FKy6106 (*zip3*Δ), FKy5247 (*zip3*Δ*, sgs1-mn*), FKy6142 (*zip3*Δ*, sgs1-mn, spp1*Δ) and **TC15**: FKy9198 (*zip3*Δ*, sgs1-mn, H3K4A*).

Only most relevant significant comparisons shown. Data was analysed using one-way ANOVA with Tukey's multiple comparisons test. Brightness adjusted for better visualisation.

Antibodies: 1st FKab314 rabbit α-Rec8 1:1,000, 2nd FKab331 α-rabbit STAR RED 1:100

## 3.7 The Mer2-Spp1 interaction deficient mutant *mer2-V195D* (*mer2-sid*) does not eliminate axial associations in zmm$^-$ mutants

Spp1 binds to H3K4me3 marks in active promoters and Mer2 of the DSB machinery to anchor future DSB sites to the chromosome axis (Acquaviva *et al.*, 2013; Sommermeyer *et al.*, 2013). To test whether the physical tethering through Spp1 between H3K4me3 and Mer2 is required for axial associations in a *zip4*Δ*, sgs1-mn* background, I used the Mer2-Spp1 interaction deficient mutant *mer2-V195D* (*mer2-sid* for Spp1 interaction deficient) (Adam *et al.*, 2018). The mutation was introduced into the relevant mutant backgrounds using CRISPR/Cas9.

Adam and colleagues (2018) reported that *mer2-sid* single mutant exhibits wild type like meiotic progression, sporulation efficiency and spore viability. In my hands, the single mutant *mer2-sid* starts first meiotic divisions after 5 h in SPM (**Figure 26 A**), compared to 4 h as previously reported (Adam *et al.*, 2018). A similar shift was observed for the *spp1*Δ single mutant, which also progressed more slowly than reported in that study (**Figure 26 A**, Adam et al., 2018, Figure 6 G). Therefore, the behaviour of *mer2-sid* and *spp1*Δ appears to be consistent with previously published data. Absence of Spp1 and H3K4 causes an additional 1 h delay in meiotic progression relative to the *mer2-sid* (**Figure 26 A**). Comparisons among *spp1*Δ*, H3K4A,* or *mer2-sid* in the *zip4*Δ*, sgs1-mn* background do not reveal any differences. Similar to *spp1*Δ and *H3K4A, mer2-sid* does not accelerate meiotic progression in the *zip4*Δ*, sgs1-mn* background (**Figure 26 B**). The *mer2-sid* single mutant displays the highest sporulation efficiency and spore viability compared to the *spp1*Δ and *H3K4A* single mutants (**Figure 26 C**). This trend extends to the triple mutants. In contrast to the *zip4*Δ*, sgs1-mn, spp1*Δ or *zip4*Δ*, sgs1-mn, H3K4A* mutants, *zip4*Δ*, sgs1-mn, mer2-sid* has spore formation and spore viability levels comparable to *zip4*Δ*, sgs1-mn* double mutant or higher (**Figure 26 C**).

**Figure 26. *mer2-sid* performs differently in meiotic progression, spore formation and spore viability than *H3K4A* or *spp1*Δ in the *zip4*Δ*, sgs1-mn* background.**

(**A**) compares meiotic progression of *mer2-sid, H3K4A* or *spp1*Δ single mutants.

(**B**) compares meiotic progression of *mer2-sid, H3K4A* or *spp1*Δ in the *zip4*Δ*, sgs1-mn* background with the *zip4*Δ*, sgs1-mn* double mutant. The *mer2-sid* single mutant serves as control.

(**C**) Spore formation (sf), spore viability (sv) and viable spore yield of the different mutants in (A) and (B).

Data from **TC9**: FKy5539 (*spp1*Δ); **TC15**: FKy9196 (*H3K4A, SPO11-myc*); **TC23**: FKy6374 (*zip4*Δ*, sgs1-mn*), FKy6371 (*zip4*Δ*, sgs1-mn, spp1*Δ); **TC26**: FKy9344 (*zip4*Δ*, sgs1-mn, mer2-sid*); **TC32** FKy9338 (*mer2-sid*) and **TC34**: FKy9303 (*zip4*Δ*, sgs1-mn, H3K4A)*.

*spp1*Δ single mutant (FKy5539) in (C) is from Viktoria Prast's Master thesis (2016).

Meiotic progression was followed by DAPI staining in a meiotic time course experiment at the indicated time points. Spore formation (sf) was assessed after 24 h in SPM (n = 100), spore viability (sv) was determined by tetrad dissection (n = 20) and incubation for 2 days at 30 °C or 3 days at RT, and viable spore yield is sf x sv/100.

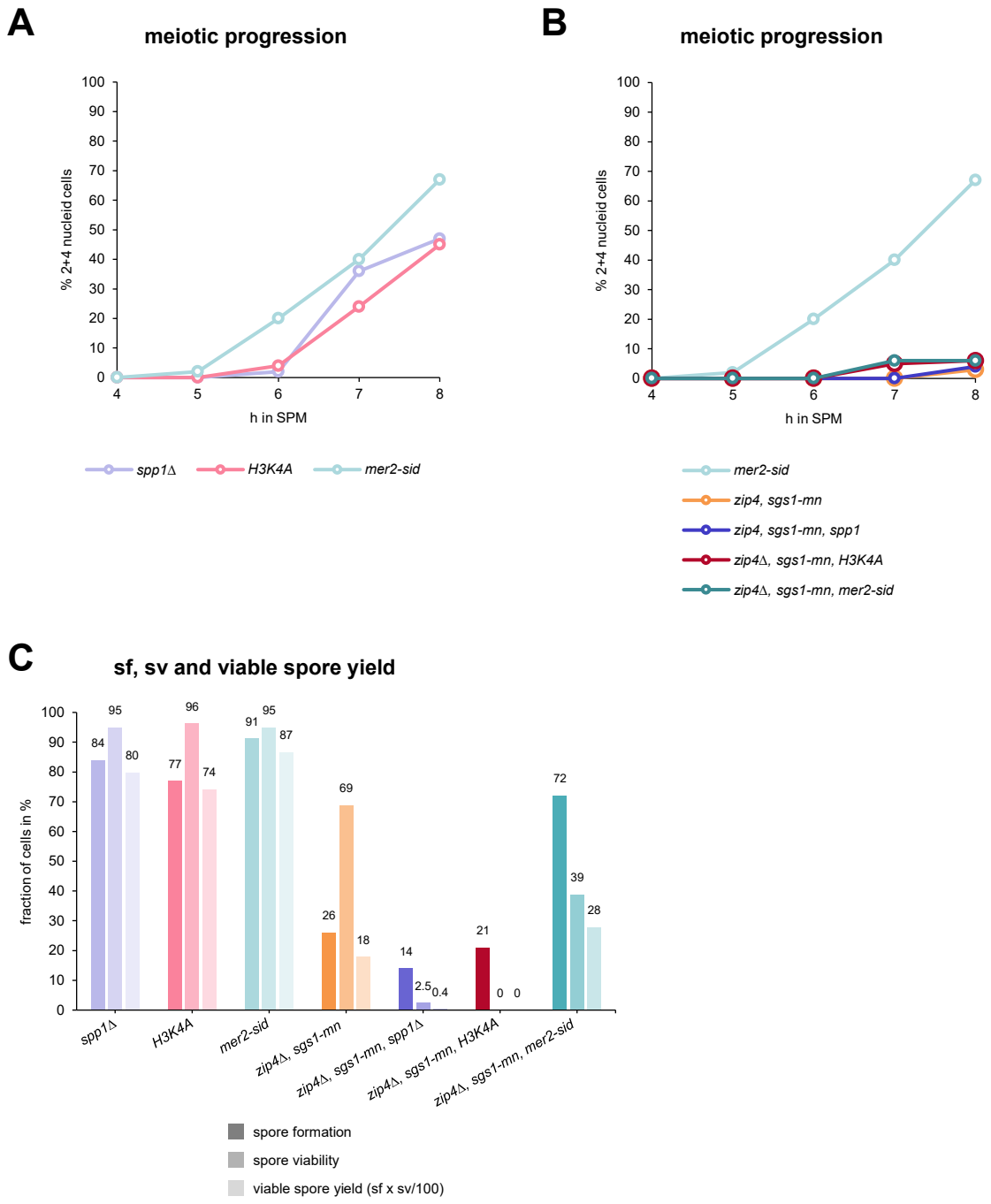


**Figure 26. Legend on the previous page.**

The double mutants *zip4Δ, mer2-sid* has similar levels of spore formation and spore viability as *zip4Δ, spp1Δ* (**Figure 29 B**). *sgs1-mn* can therefore partly rescue the *zip4Δ, mer2-sid* phenotype.

Using STED microscopy, I determined that *mer2-sid* does not abolish axial associations in the *zip4Δ, sgs1-mn* background, contrary to *spp1Δ* and *H3K4A* (**Figure 27 A**). In fact, where axes are aligned in the *zip4Δ, sgs1-mn, mer2-sid* mutant, they seem to be tighter associated with each other than in the *zip4Δ, sgs1-mn* mutant. Some nuclei also display an interwoven

appearance of chromosome axes (**Figure 27 A, *mer2-sid***). This result indicates that the interaction between Mer2 and Spp1 is not required for axial associations to the same extent as Spp1 and H3K4. Quantitative analysis of aligned axes fragments supports this initial observation (**Figure 27 B, C; Figure 28**). The triple mutant *zip4*Δ*, sgs1-mn, mer2-sid* displays greater total length of aligned fragments than the *zip4*Δ*, sgs1-mn, spp1*Δ triple mutant. While *mer2-sid* allows for more extensive axes alignment than *spp1*Δ in the same background, it does not reach levels of the *zip4*Δ*, sgs1-mn* double mutant (**Figure 27 B**). Thus, *mer2-sid* partly diminishes suppression by *sgs1-mn* in the *zip4*Δ background but does not completely prevent it like *spp1*Δ. Individual stretches of aligned axes are significantly reduced in the *zip4*Δ*, sgs1-mn, mer2-sid* triple mutant relative to the *zip4*Δ*, sgs1-mn* mutant (**Figure 27 C**). The number of aligned fragments in the *zip4*Δ*, sgs1-mn, mer2-sid* mutant resembles the number of fragments in the double mutant *zip4*Δ*, sgs1-mn* (**Figure 28 A**). The mean length of these fragments is more similar between the *zip4*Δ*, sgs1-mn, mer2-sid* triple mutant, the *zip4*Δ single mutant and the *zip4*Δ*, sgs1-mn, spp1*Δ double mutant (**Figure 28 B**). This indicates that the decrease in the total length of aligned axes in *zip4*Δ*, sgs1-mn, mer2-sid* results from a reduced length of the associated axes fragments rather than a lower number of fragments compared the *zip4*Δ*, sgs1-mn* double mutant.

**Figure 27. The Mer2-Spp1 interaction is not as crucial as Spp1 or H3K4me3 to stabilize associated axial fragments in the *zip4*Δ*, sgs1-mn* background.**

(**A**) Representative STED images showing Rec8-stained chromosome spreads in different *zip4*Δ mutant backgrounds after 6 h in SPM.

(**B**) Quantification of the total length of associated axial fragments per nucleus across different mutants (whiskers: min to max, individual data points shown).

(**C**) Distribution of the lengths of individual associated axial fragments for each mutant (one outlier was excluded for *zip4*Δ*, sgs1-mn*; whiskers: mean +/- SD, individual data points shown).

Number of nuclei analysed: *zip4*Δ (n = 36); *zip4*Δ*, sgs1-mn* (n = 35); *zip4*Δ*, sgs1-mn, spp1*Δ (n = 36); *zip4*Δ*, sgs1-mn, mer2-sid* (n = 38).

Data from **TC11**: FKy6338 (*zip4*Δ), FKy6374 (*zip4*Δ*, sgs1-mn*), FKy6371 (*zip4*Δ*, sgs1-mn, spp1*Δ); **TC26**: FKy9344 (*zip4*Δ*, sgs1-mn, mer2-sid*) and **TC34**: FKy9344 (*zip4*Δ*, sgs1-mn, mer2-sid*), FKy9303 (*zip4*Δ*, sgs1-mn, H3K4A*).

Only relevant significant comparisons shown. Data was analysed using one-way ANOVA with Tukey's multiple comparisons test. Brightness adjusted for better visualisation.

Antibodies: 1st FKab314 rabbit α-Rec8 1:1,000, 2nd FKab331 α-rabbit STAR RED 1:100

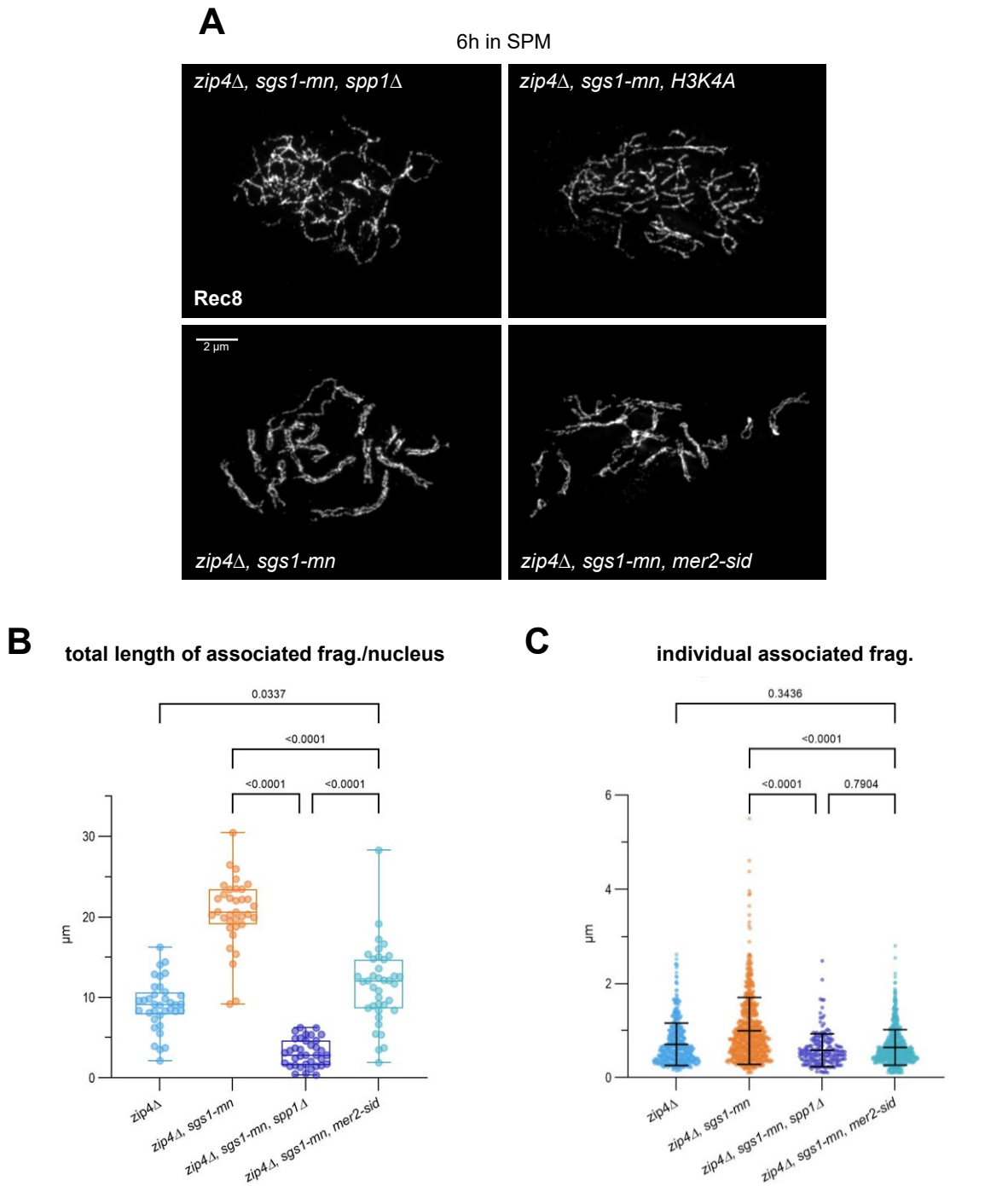


**Figure 27. Legend on the previous page.**

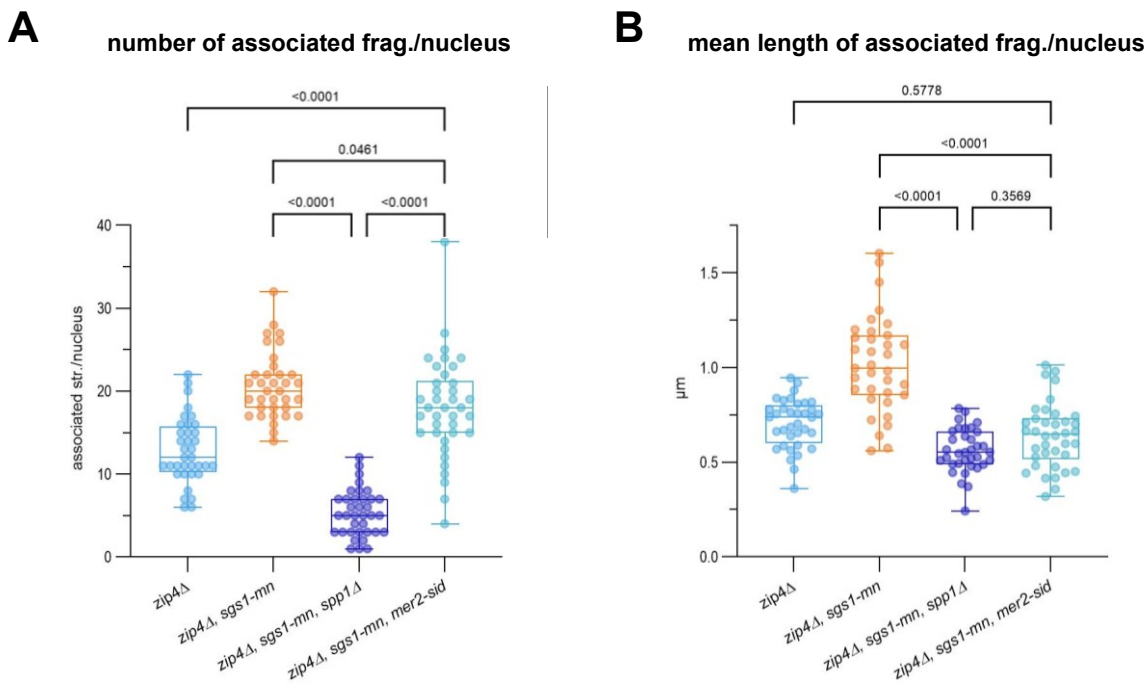


**Figure 28. The number of associated axial fragments in *zip4*Δ*, sgs1-mn, mer2-sid* reaches *zip4*Δ*, sgs1-mn* levels, but the mean fragment length resembles *zip4*Δ*, sgs1-mn, spp1*Δ.**

(**A**) shows the distribution of the number of associated axial fragments per nucleus.

(**B**) presents the average length of these associated axial fragments (one outlier excluded for *zip4*Δ*, sgs1-mn, spp1*Δ).

Number of nuclei analysed: *zip4*Δ (n = 36); *zip4*Δ*, sgs1-mn* (n = 35); *zip4*Δ*, sgs1-mn, spp1*Δ (n = 36); *zip4*Δ*, sgs1-mn, mer2-sid* (n = 38).

Data from **TC11**: FKy6338 (*zip4*Δ), FKy6374 (*zip4*Δ*, sgs1-mn*), FKy6371 (*zip4*Δ*, sgs1-mn, spp1*Δ); **TC26**: FKy9344 (*zip4*Δ*, sgs1-mn, mer2-sid*) and **TC34**: FKy9344 (*zip4*Δ*, sgs1-mn, mer2-sid*).

Only relevant significant comparisons shown. Data was analysed using one-way ANOVA with Tukey's multiple comparisons test. Brightness adjusted for better visualisation.

Antibodies: 1st FKab314 rabbit α-Rec8 1:1,000, 2nd FKab331 α-rabbit STAR RED 1:100

Meiotic progression of the double mutant *zip4*Δ*, mer2-sid* is comparable to *zip4*Δ*, spp1*Δ (**Figure 29 A**). Therefore, progression is not accelerated by the loss of the Mer2-Spp1 interaction in the *zip4*Δ background. Spore formation and spore viability of the *zip4*Δ*, mer2-sid* double mutant experience a reduction similar to *zip4*Δ*, spp1*Δ levels. However, these defects can be suppressed by the absence of Sgs1, unlike the defects of the *zip4*Δ*, spp1*Δ mutant (**Figure 29 B**). Analysis of axes alignment determined by STED microscopy (**Figure 29 C**) supports these results: the *zip4*Δ*, mer2-sid* double mutant resembles the *zip4*Δ*, spp1*Δ double mutant, while the triple mutant *zip4*Δ*, sgs1-mn, mer2-sid* displays more axes alignment than the *zip4*Δ*, sgs1-mn, spp1*Δ triple mutant and the *zip4*Δ*, mer2-sid* or the *zip4*Δ*, spp1*Δ double mutants (**Figure 29 C**).

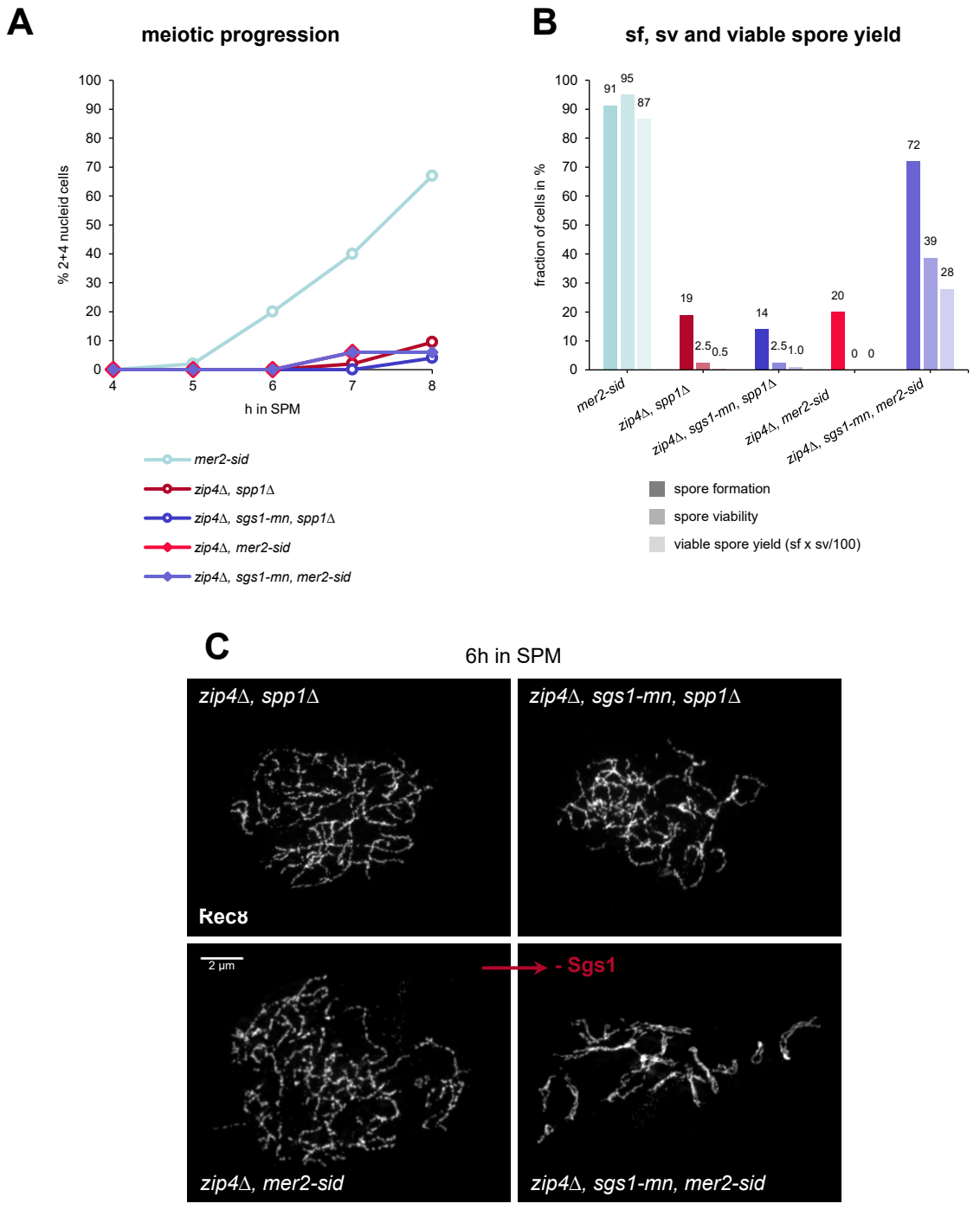


**Figure 29. Legend on the next page.**

**Figure 29. Absence of Sgs1 can supress *mer2-sid*, but not *spp1*Δ, spore formation, spore viability and axial associations defects in the *zip4*Δ background.**

(**A**) compares meiotic progression of *spp1*Δ and *mer2-sid* in the *zip4*Δ and *zip4*Δ*, sgs1-mn* background. The *mer2-sid* single mutant serves as control.

(**B**) Spore formation (sf), spore viability (sv) and viable spore yield of all mutants in (A).

(**C**) Representative STED images showing Rec8-stained chromosome spreads in the different *zip4*Δ mutant backgrounds after 6 h in SPM.

Data from **TC11**: FKy6296 (*zip4*Δ*, spp1*Δ), FKy6371 (*zip4*Δ*, sgs1-mn, spp1*Δ); **TC26:** FKy9341 (*zip4*Δ*, mer2-sid*), FKy9344 (*zip4*Δ*, sgs1-mn, mer2-sid*) and **TC32** FKy9338 (*mer2-sid*)

Meiotic progression was followed by DAPI staining in a meiotic time course experiment at the indicated time points. Spore formation (sf) was assessed after 24 h in SPM (n = 100), spore viability (sv) was determined by tetrad dissection (n = 20) and incubation for 2 days at 30 °C or 3 days at RT, and viable spore yield is sf x sv/100.

Brightness was adjusted for better visualisation.

Finally, to determine whether Spp1 and H3K4 are required upstream of the Mer2-Spp1 interaction, the *mer2-sid* mutation was introduced into *zip4*Δ*, sgs1-mn, spp1*Δ and *zip4*Δ*, sgs1-mn, H3K4A* triple mutants, generating quadruple mutants. The *zip4*Δ*, sgs1-mn, spp1*Δ*, mer2-sid* quadruple mutant initiates first meiotic divisions earlier than all other examined mutants, but only marginally so relative to the *zip4*Δ*, sgs1-mn, mer2-sid* and *zip4*Δ*, sgs1-mn, H3K4A* triple mutants (**Figure 30 A**). After 9 h in SPM, the *zip4*Δ*, sgs1-mn, mer2-sid* triple mutant and the *zip4*Δ*, sgs1-mn, H3K4A, mer2-sid* were the most advanced in meiotic progression (**Figure 30 A**). Moreover, *mer2-sid* can modestly suppress the detrimental effect that *H3K4A* and *spp1*Δ have on spore formation in the *zip4*Δ*, sgs1-mn* background and for *H3K4A* also spore viability (**Figure 30 B**). Chromosome axes of the quadruple mutants resemble the axes organization of the corresponding triple mutants (**Figure 30 C**), suggesting that Spp1 and H3K4me3 are epistatic to the Mer2-Spp1 interaction.

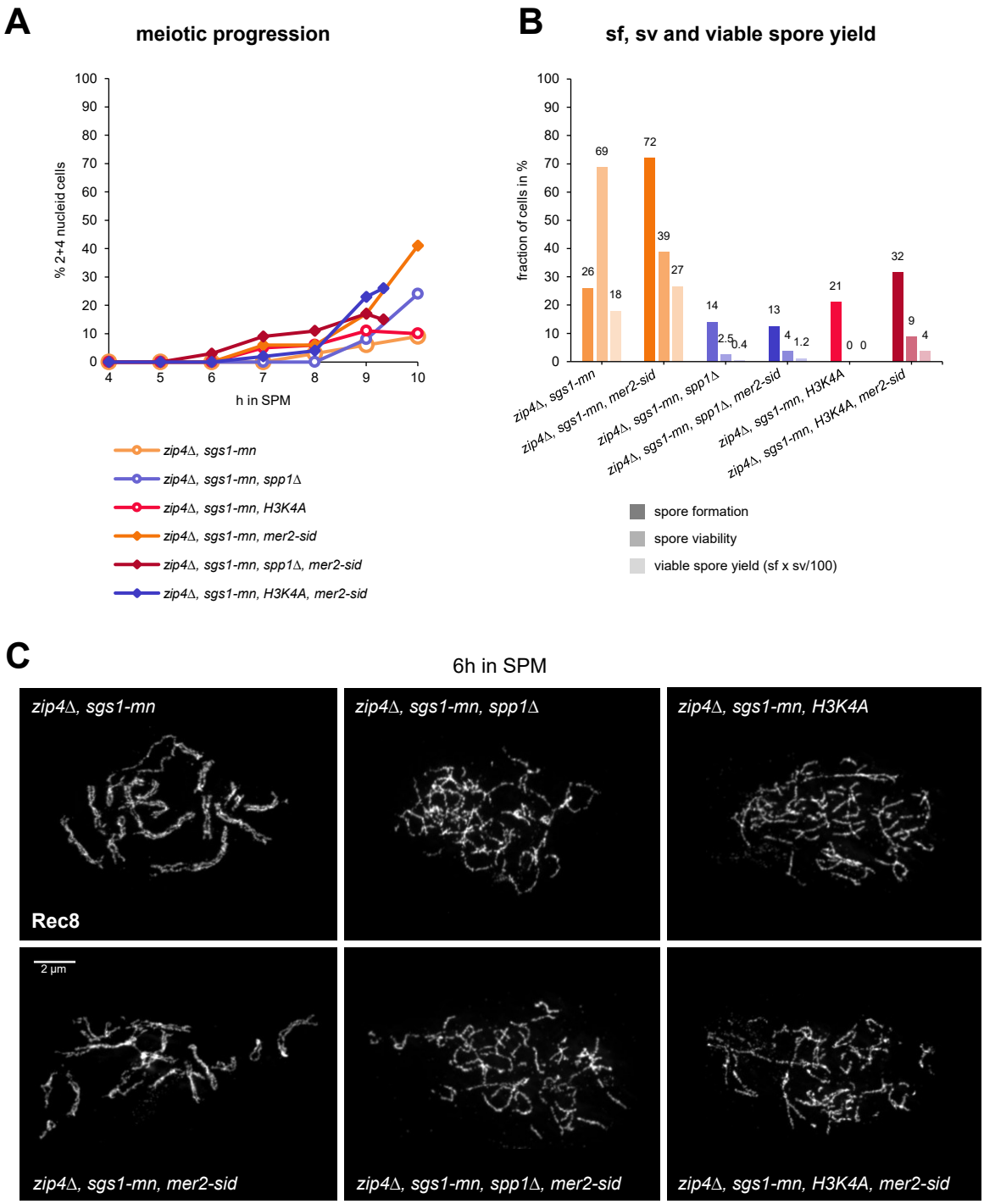


**Figure 29. Legend on the next page.**

**Figure 30. Quadruple mutants reveal that *H3K4A* and *spp1*∆ are epistatic to *mer2-sid*. Although, *mer2-sid* can slightly improve spore formation and spore viability of *spp1*∆ or *H3K4A* in *zip4*∆, *sgs1-mn* mutants.**

(**A**) compares meiotic progression of *spp1*∆*, H3K4A* or *mer2*-sid, as well as *spp1*∆*, mer2-sid* or *H3K4A, mer2-sid* in the *zip4*∆*, sgs1-mn* background with the double mutant *zip4*∆*, sgs1-mn.*

(**B**) Spore formation (sf), spore viability (sv) and viable spore yield of all mutants in (A).

(**C**) Representative STED images showing Rec8-stained chromosome spreads in different *zip4*∆ mutant backgrounds after 6 hours in sporulation medium (SPM).

Data in (A) and (B) from **TC23**: FKy6374 (*zip4*∆*, sgs1-mn*), FKy6371 (*zip4*∆*, sgs1-mn, spp1*∆) and **TC34**: FKy9303 (*zip4*∆*, sgs1-mn, H3K4A*), FKy9344 (*zip4*∆*, sgs1-mn, mer2-sid*), FKy9396 (*zip4*∆*, sgs1-mn, mer2-sid, H3K4A*), FKy9404 (*zip4*∆*, sgs1-mn, mer2-sid, spp1*∆)

Data for (C) from **TC11**: FKy6374 (*zip4*∆*, sgs1-mn*), FKy6371 (*zip4*∆*, sgs1-mn, spp1*∆), **TC26:** FKy9344 (*zip4*∆*, sgs1-mn, mer2-sid*) and **TC34**: FKy9303 (*zip4*∆*, sgs1-mn, H3K4A)*, FKy9396 (*zip4*∆*, sgs1-mn, mer2-sid, H3K4A*), FKy9404 (*zip4*∆*, sgs1-mn, mer2-sid, spp1*∆)

Meiotic progression was followed by DAPI staining in a meiotic time course experiment at the indicated time points. Spore formation (sf) was assessed after 24 h in SPM (n = 100), spore viability (sv) was determined by tetrad dissection (n = 20) and incubation for 2 days at 30 °C or 3 days at RT, and viable spore yield is sf x sv/100.

Brightness was adjusted for better visualisation.

Antibodies: 1st FKab314 rabbit α-Rec8 1:1,000, 2nd FKab331 α-rabbit STAR RED 1:100

## 3.8 Genome-wide dDSB maps show that both *spp1*Δ and *H3K4A* alter the DSB landscape similarly

To analyse how Spp1 and its interaction with trimethylated H3K4 contribute to DSB formation genome-wide, calibrated Protec-seq maps were generated for wild type, *spp1*Δ, and the histone mutant *H3K4A*. Preliminary Protec-seq data generated in the lab by Silvia Prieler and Doris Chen in a background that also contained *REC104-FRB* suggested comparable dDSB levels for wild type and *spp1*Δ, but due to this confounding tag, which can easily affect DSB levels, the experiment had to be repeated. I performed meiotic time courses in a *SPO11-myc18* wild type background and generated Protec-seq libraries in collaboration with Viktoria Prast. An additional calibrated Protec-seq library for *H3K4A* was generated by Viktoria Prast, enabling direct comparisons. These experiments have not yet been fully evaluated, so only a preview of the analysis is shown here (quality control of calibration strain *S. kudriavzevii* in **S Figure 1, Section 5.1**).

Across the genome, wild type and *zip4*Δ, *sgs1-mn* display highly similar Protec-seq profiles (**Figure 31**). Hotspot clustering and relative peak intensities of individual hotspots are similar in these mutants, consistent with a limited or absent role of Sgs1 and Zip4 in DSB formation. In contrast, the dDSB landscapes of the *spp1*Δ and the *H3K4A* mutants markedly differ from wild type (**Figure 31**). Expectedly, the *spp1*Δ single mutant and the *zip4*Δ, *sgs1-mn, spp1*Δ triple mutant exhibit virtually indistinguishable patterns of hotspot clustering and relative intensity of individual peaks (**Figure 31**). Most altered regions in the *spp1*Δ mutants relative to wild type are reproduced by *H3K4A* (**Figure 31**, dashed boxes), consistent with the model that the change in DSB landscape reflects the loss of Spp1-H3K4me3 interaction.

**Figure 31** and **Figure 32** highlight *CYS3/DEP1* and *PES4*, two hotspots, that have been shown to differ between *SPP1* wild type and *spp1*Δ. At the *CYS3/DEP1* hotspot (at 131 kb on Chr. I) at least two studies have reported a reduction in DSB levels in *spp1*Δ (Acquaviva *et al.*, 2013; Sommermeyer *et al.*, 2013). Indeed, wild type strains show two peaks matching the DSB-oligo signals by Mohibullah and Keeney (2017), while *spp1*Δ and *H3K4A* mutants display a reduction in signal in our Protec-seq profiles. In contrast, the *PES4* region on Chr. VI is known to be induced specifically in *spp1*Δ and *H3K4A* mutants (Sommermeyer *et al.*, 2013). Again, our profiles recapitulate this finding, with strong signals in the *spp1*Δ and *H3K4A* strains and weak ones in wild type (**Figure 32**). Other differences, in which the mutants reduce DSBs relative to wild type include peaks at 49, 60, 62, 167 and 194 kb on Chr. I. In contrast, *spp1*Δ and *H3K4A* mutants excel at 19, 25, 32, 33, 36, 105, 113, 153, 176, and 212 kb on Chr. I (**Figure 31**). Obviously, more repeats will be required to allow a completely systematic comparison of the altered peaks, and whether they are really closely related in these mutants genome-wide.

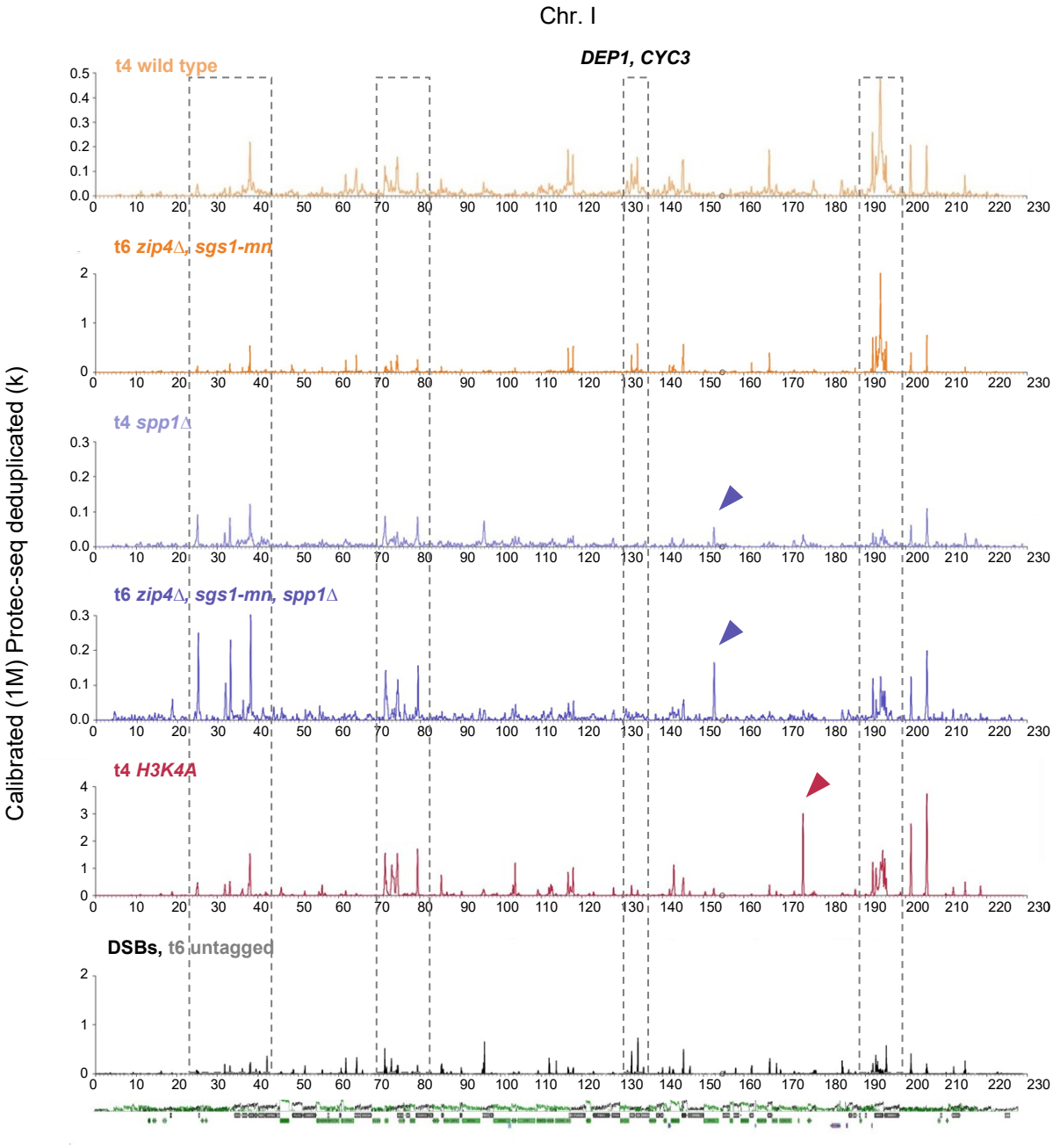


**Figure 31. dDSB landscape is altered by *spp1*Δ and *H3K4A* in a similar manner. Chr. I is shown as an example.**

Shows Calibrated Protec-seq profiles (chromosome I) for t4 wild type, t6 *zip4*Δ*, sgs1-mn*, t4 *spp1*Δ, t6 *zip4*Δ*, sgs1-mn, spp1*Δ, t4 *H3K4A* and t6 untagged together with Spo11-oligos (DSBs) from Mohibullah and Keeney (2017). mRNA transcript levels derived from Brar et al. (2012). Dashed boxes show similarities between H3K4A and *spp1*Δ mutants, dashed arrow heads highlight differences between the mutants.

Protec-seq IDs: **vp053.IP**, FKy1358 (t4*, SPO11-myc18,* wt); **vp055.IP**, FKy5525 (t4*, SPO11-myc18, spp1Δ*); **vp056.IP**, FKy9407 (t6, *SPO11-myc18, zip4Δ, sgs1-mn*); **vp057.IP,** FKy9410 (t6, *SPO11-myc18, zip4Δ, sgs1-mn, spp1Δ*); **vp083.IP**, FKy9196 (t4, *SPO11-myc18, H3K4A*) and **vp063**.IP, FKy3088 (t6, untagged, wt). For more details see Appendix.

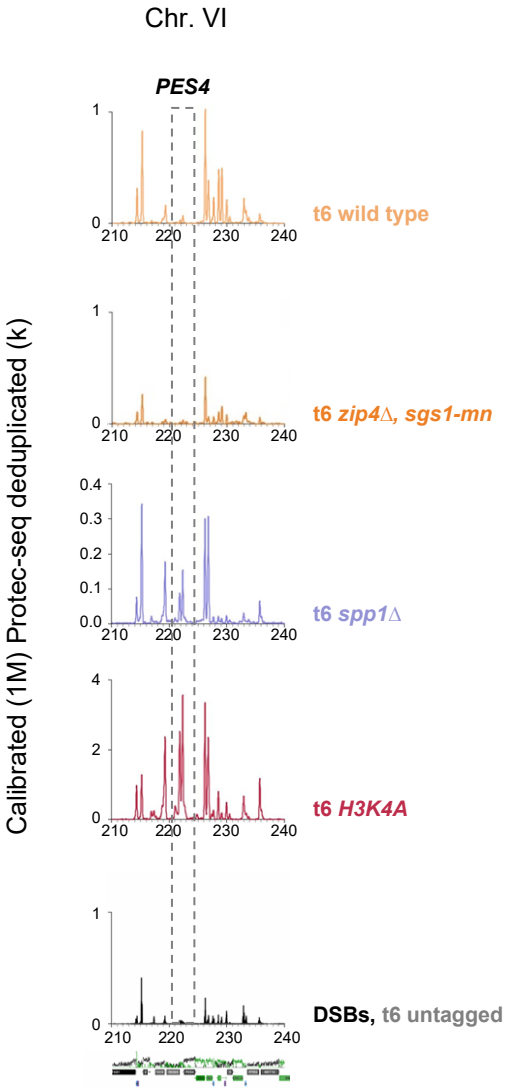


**Figure 32. The *PES4* region on Chr. VI is induced by *spp1*Δ and *H3K4A* at 6 h in SPM.**

Shows Calibrated Protec-seq profiles (chromosome VI) for t6 wild type, t6 *zip4Δ, sgs1-mn*, t6 *spp1*Δ, t6 *H3K4A* and t6 untagged together with Spo11-oligos (DSBs) from Mohibullah and Keeney (2017). mRNA transcript levels derived from Brar et al. (2012). The dashed box highlights the *PES4* region.

Protec-seq IDs: **vp059.IP**, FKy1358 (t6, *SPO11-myc18,* wt); **vp061.IP**, FKy5525 (t6, *SPO11-myc18, spp1Δ*); **vp056.IP**, FKy9407 (t6, *SPO11-myc18, zip4Δ, sgs1-mn*); **vp084.IP**, FKy9196 (t6, *SPO11-myc18, H3K4A*) and **vp063**.IP, FKy3088 (t6, untagged, wt). For more details see Appendix.

In some genomic regions *spp1*Δ and *H3K4A* display unique dDSB features. *spp1*Δ mutants, for instance have relatively strong peaks between at 25, 32, 33 kb on Chr. I, where *SPP1* wild type and *H3K4A* signals are relatively weak and a peak at 155 kb (**Figure 31**, blue arrow heads), where wild type and *H3K4A* have none. On the other hand, *H3K4A* exhibits a high, isolated peak at 175 kb, which is weak in *spp1*Δ and completely absent in *SPP1* wild type strains (**Figure 31,** red arrow head). Genome wide similarities will be quantified by Pearson and Spearman correlations once more robust profiles are available. The observed isolated differences in dDSBs likely reflect local variations in gene expression in the mutants compared.

## 3.9 *spp1*∆ accumulated overall dDSBs up to 30-40 % of wild type with some delay

To visualize the temporal dynamics of DSB formation, calibrated Protec-seq profiles were generated for *spp1*∆ and wild type after 3.5, 4, 5 and 6 h in SPM (**Figure 33**). Although *spp1*∆ showed reduced dDSB at each time point, both wild type and *spp1*∆ display a gradual increase in dDSB signal throughout examined timepoints. By 6 h in SPM, *spp1*∆ reached its highest dDSB levels, reflecting a substantial accumulation of dDSB fragments over time (**Figure 33**). Thus, while our particular *spp1*∆ cells were quite strongly delayed relative to wild type in these time courses, it eventually caught up to decent dDSB levels. In contrast, *H3K4A* displayed already high levels of dDSBs after 4 h in SPM, even higher than wild type (**Figure 31, Figure 34**). The difference in dDSB levels and timing can, at least in part, be due to variation between experiments. In the wild type and *spp1*∆ strains cells exhibited slower meiotic progression than usual (**S Figure 2, Section 5.1**), which might be related to their lower dDSB levels at 4 h in SPM.

Number and intensity of Rad51 foci did not differ between the double mutant *zip4*∆*, sgs1-mn* and the triple mutant *zip4*∆*, sgs1-mn, spp1*∆ (**Figure 7 B, D**) as analysed by STED microscopy. Because dDSB fragments up to 70 bp are very stable (Prieler *et al.*, 2021), Protec-seq captures most dDSBs generated during the time course, independent of repair. The apparent discrepancy between the overall lower levels of dDSBs in *spp1*∆ and the similar number of Rad51 foci could be explained if some Rad51 foci represented unrepaired DSBs. However, Rad51 foci are not accurate measures of DSBs, while ProtecSeq is. In the future we plan to repeat and extend these experiments to include *mer2-sid* to finally solve the enigma of the changed DSB landscapes in the tethering mutants.

**Figure 33. *spp1*∆ accumulates a substantial amount of dDSBs after 6 h in SPM, while wild type dDSB levels were not reached.**

Compares Calibrated Protec-seq profiles (chromosome I) for t3.5, t4, t5, t6 wild type and t3.5, t4, t5, t6 *spp1*∆. The dashed box highlights the *DEP1/CYC3* hotspot.

Protec-seq IDs:

wild type: **vp052.IP**, FKy1358 (t3.5, *SPO11-myc18*, wt); **vp053.IP**, FKy1358 (t4, *SPO11-myc18,* wt); **vp058.IP**, FKy1358 (t5, *SPO11-myc18,* wt); **vp059.IP**, FKy1358 (t6, *SPO11-myc18,* wt)

*spp1Δ:* **vp054.IP**, FKy5525 (t3.5, *SPO11-myc18, spp1Δ*); **vp055.IP**, FKy5525 (t4, *SPO11-myc18, spp1Δ*); **vp060.IP**, FKy5525 (t5, *SPO11-myc18, spp1Δ*); **vp061.IP**, FKy5525 (t6, *SPO11-myc18, spp1Δ*).

For more details see Appendix.

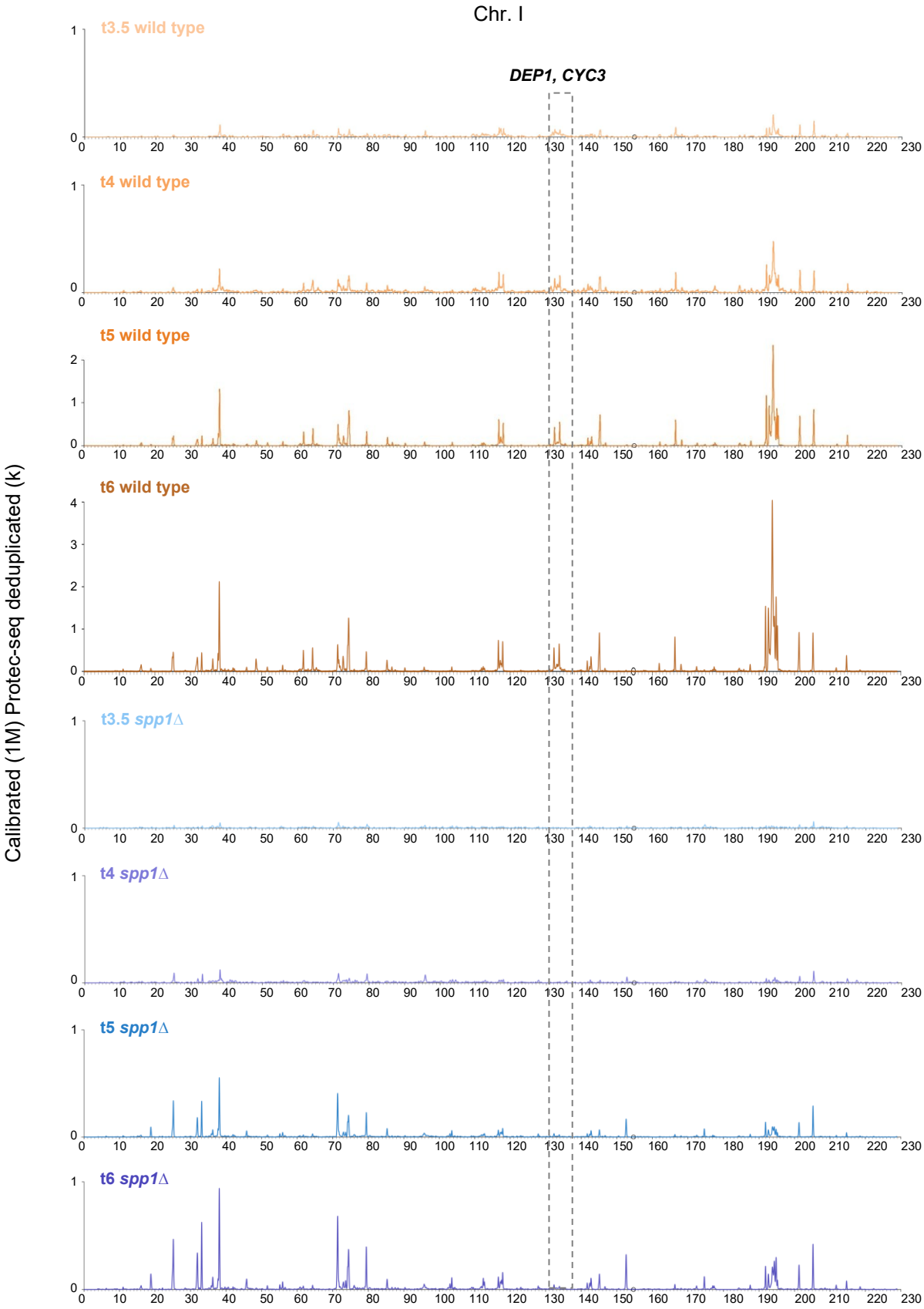


**Figure 33. Legend on the previous page.**

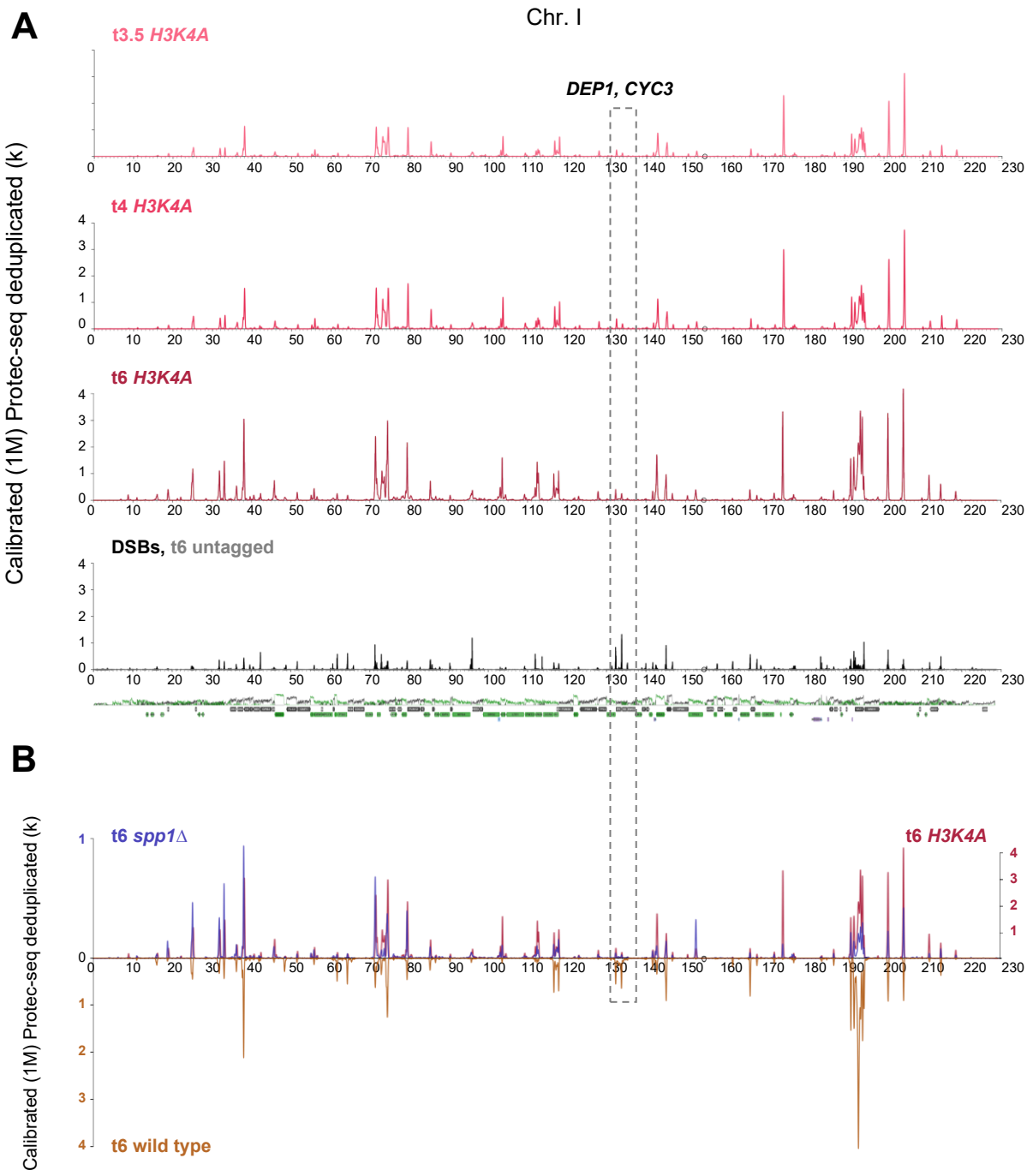


**Figure 34. Preliminary data suggests that *H3K4A* reaches higher dDSB levels than *spp1*Δ.**

(**A**) shows how breaks accumulate over time in *H3K4A* (t3.5, t4, t6) and t6 untagged together with Spo11-oligos (DSBs) using Protec-seq profiles (Chr. I).

(**B**) comparison of wild type, *spp1*Δ and *H3K4A* after 6 h in SPM (Chr. I).

Calibrated Protec-seq profiles (chromosome I) for t3.5, t4, t6 *H3K4A*, t6 wild type and t6 *spp1*Δ. Spo11-oligos (DSBs) are derived from Mohibullah and Keeney (2017). mRNA transcript levels derived from Brar et al. (2012). The dashed box highlights the *DEP1/CYC3* hotspot.

Protec-seq IDs: **vp082.IP**, FKy9196 (t3.5, *SPO11-myc18, H3K4A*); **vp083.IP**, FKy9196 (t4, *SPO11-myc18, H3K4A*); **vp084.IP**, FKy9196 (t6, *SPO11-myc18, H3K4A*); **vp059.IP,** FKy1358 (t6, *SPO11-myc18*, wt); **vp061.IP, FKy5525** (t6, *SPO11-myc18, spp1Δ*) and **vp063.IP,** FKy3088 (t6, untagged, wt)

For more details see Appendix.

# 4 Discussion

Given that Spp1 has been regarded primarily as a factor required for DSB formation, the findings described in this Master thesis emphasize a conceptually new role for Spp1 and H3K4me3 in the repair of meiotic DSBs. Here, I would like to summarize the main findings:

I. Spp1 is required for timely repair of DSBs in zmm$^-$ mutants

II. The stabilization of axial associations depends on Spp1 and H3K4me3

III. The interaction between Mer2-Spp1 is not crucial for the DSB repair function

IV. Abnormal DSB formation alone fails to explain *spp1*∆ or *H3K4A* defects when ZMM and Sgs1 are non-functional

- Number of DSBs: Both mutants accumulate a substantial amount of DSBs, which can recruit downstream repair factors. A mutant with downregulated levels of DSBs behaves differently from *spp1*∆ and *H3K4A.*
- Timing of DSBs: Same phenotype of *spp1*∆ and *H3K4A* in *zmm$^-$, sgs1-mn* double mutant background, but DSBs are strongly delayed only in *spp1*∆*.* This observation argues against aberrant timing as the key explanation for their defects.
- Positioning of DSBs: The repair defect can be decoupled from Mer2-Spp1 tethering because *mer2-sid* is required for positioning, but not for repair.

## 4.1 When the canonical ZMM pathway fails, Spp1 becomes crucial for DSB repair

The synthetic lethality screen performed by Viktoria Prast revealed that *spp1*∆ is synthetic with zmm$^-$ mutants, indicating that Spp1 becomes especially important if the predominant pathway for meiotic recombination is compromised (Prast, Master Thesis, 2016). During my Master thesis, I expanded on these findings and could also observe that *spp1*∆ prevents the well-established suppression of zmm$^-$ defects by depletion of Sgs1. This suppression was originally described for zmm$^-$ mutants (Jessop *et al.*, 2006; Rockmill *et al.*, 2003) and could be attributed to the absence of the anti-recombinase activity by Sgs1 (De Muyt *et al.*, 2012; Xaver *et al.*, 2013). In wild type, Sgs1 disassembles SEI intermediates that are not stabilized by the ZMM proteins (Oh *et al.*, 2007), thereby restricting repair through alternative pathways such as SDSA or the unregulated JM pathway (Jessop and Lichten, 2008; Jessop *et al.*, 2006; Oh *et al.*, 2008; Rockmill *et al.*, 2003). Without Sgs1, JMs resulting from unregulated repair events can persist and are resolved by structure specific nucleases such as Mus81-Mms4, Slx1-Slx4 and Yen1, which are also required in mitotic homologous recombination (Jessop and Lichten,

2008; de los Santos *et al.*, 2003; Cannavo *et al.*, 2020; Zakharyevich *et al.*, 2012). The fact that *spp1*Δ abolishes this suppression, strongly suggests that Spp1 is required for successful repair via this alternative, mitotic-like repair pathway.

In zmm$^-$ mutants with comparably milder defects such as *msh4*Δ and *msh5*Δ, Spp1 is required for the acceleration of meiotic progression by depletion of Sgs1 (*sgs1-mn*). It also prolongs meiotic prophase of the single mutants *msh4*Δ and *msh5*Δ. Consistent with previous studies (Acquaviva *et al.*, 2013; Adam *et al.*, 2018; Karányi *et al.*, 2018; Sommermeyer *et al.*, 2013), the *spp1*Δ single mutant displayed a moderate meiotic delay. Importantly, however, the delay in the milder *zmm*$^-$, *spp1*Δ double and the *zmm*$^-$, *sgs1-mn, spp1*Δ triple mutants is substantially greater than in *spp1*Δ alone. In more severe zmm$^-$ mutants like *zip3*Δ and *zip4*Δ, which already show extensive delays on their own, *spp1*Δ does not further delay meiotic progression. As prolonged meiotic arrest is a hallmark for continued activation of the DNA damage checkpoint (Börner, Kleckner and Hunter, 2004), these observations suggest the presence of unrepaired lesions in *zmm*$^-$, *spp1*Δ and *zmm*$^-$, *sgs1-mn, spp1*Δ mutants.

Deletion of *SPP1* also further decreases spore formation and spore viability of the *msh4*Δ, *msh5*Δ and *zip4*Δ single mutants (n. a. for *zip3*Δ). The suppression by *sgs1-mn* of these zmm$^-$ defects is completely abolished by *spp1*Δ, resulting in a reduction to *zmm*$^-$, s*pp1*Δ double mutant levels. In zmm$^-$ mutants, low spore formation after the prolonged arrest in meiotic prophase is caused by missegregation of chromosomes as a result of synapsis and recombination defects (San-Segundo and Roeder, 1999). The additional decrease by *spp1*Δ in these backgrounds hints at a repair or a recombination problem.

Together, these observations suggest that Spp1 is not exclusively required for DSB formation through its H3K4me3-Mer2 tethering function (Acquaviva *et al.*, 2013; Sommermeyer *et al.*, 2013), but instead may serve a dedicated function in DSB repair. When cells resort to repair via the unregulated JM pathway because ZMM and Sgs1 are non-functional, Spp1's role becomes visible. While it may be possible that Spp1 acts by releasing intermediates from the failed attempts of the compromised ZMM pathway, it is much more likely that it is directly or indirectly facilitating repair in the alternative pathway.

## 4.2 Spp1 and H3K4me3 are required for stable axial associations in zmm$^-$ mutants

In *zip1* mutants, chromosomes can pair homologously, but they fail to synapse, while their axes seem only connected at distinct sites, called axial associations (Rockmill *et al.*, 1995). For *zip1* and several other zmm$^-$ mutants, such as *zip3, mer3* (Jessop *et al.*, 2006), *zip2* and *zip4* (B. Rockmill and G. S. Roeder, unpublished data), it has been established that depletion

of Sgs1 leads to the close alignment of chromosome axes. This phenomenon, referred to as pseudosynapsis (Rockmill *et al.*, 2003), is caused by a high number of axial associations, which probably represent joint molecules, and increase due to the absence of Sgs1 (Jessop *et al.*, 2006; Rockmill *et al.*, 2003).

Using super-resolution microscopy, I found that Spp1 is required for the establishment of stable axial associations, presumably interhomolog JMs, in *zip3*Δ and *zip4*Δ mutants. The effect of Spp1 becomes especially apparent in *zmm*$^{-}$*, sgs1-mn* backgrounds: while *zip3*Δ*, sgs1-mn* and *zip4*Δ*, sgs1-mn* mutants typically display extensive axial associations and pseudosynapsis (as previously described by Jessop et al., 2006 and Rockmill et al., 2003), the corresponding *zip3*Δ*, sgs1-mn, spp1*Δ and *zip4*Δ*, sgs1-mn, spp1*Δ mutants are nearly devoid of any alignment of axial segments. This implies that the stabilization of JMs formed in the absence of Sgs1 depend on Spp1.

This requirement is not restricted to Sgs1-depleted backgrounds. The *zip4*Δ single mutant already contains a very low number of axial associations, however deletion of *SPP1* in this background significantly further reduces the number and length of associated axes fragments. This indicates that the small number of ZMM-independent JMs that remain in a *zip4*Δ background also require Spp1 for stabilization. Those JMs may have escaped the anti-recombinase activity of Sgs1 and may require Spp1 for further protection.

The histone mutant *H3K4A,* where H3K4-trimethylation is abolished, was shown to alter the DSB landscape at certain genomic loci such as *CYS3, DEP1* or *PES4 s*imilarly to *spp1*Δ (Sommermeyer *et al.*, 2013). Here we confirmed and extended this observation by genome wide Protec-seq. Indeed, both, *spp1*Δ and *H3K4A* dDSB sites are similar, but different from wild type. While *spp1*Δ signals are overall weaker than wild type, especially in the early time points, signals in the *H3K4A* background are robust and strong. There are some positions, in which *H3K4A and spp1*Δ signals differ, but overall there is strong similarity.

The similarity is not unexpected. The currently favoured model proposes that Spp1 binds to H3K4me3 marks in promoter regions of actively transcribed genes to tether future DSB sites to the DSB machinery (Acquaviva *et al.*, 2013; Sommermeyer *et al.*, 2013). As a component of the Set1C/COMPASS complex, Spp1 is also required for normal levels of H3K4me3 (Dehé *et al.*, 2006; Mersman *et al.*, 2012; Schneider *et al.*, 2005). Importantly, *H3K4A* phenocopies *spp1*Δ in all important aspects in the *zmm*$^{-}$*, sgs1-mn* background. It affects spore viability and progression equally as *spp1*Δ and most strikingly *H3K4A* abolishes axial associations as much or more as *spp1*Δ in the *zip3*Δ*, sgs1-mn* and *zip4*Δ*, sgs1-mn* backgrounds. The markedly prolonged meiotic prophase in the *zmm*$^{-}$*, sgs1-mn, H3K4A* strains indicates that unrepaired lesions activate the DNA damage checkpoint also in these backgrounds. This suggests that, like Spp1, H3K4me3 is required for the timely completion of DSB repair. Furthermore, spore

viability and spore formation in *zip4*Δ*, sgs1-mn* mutants not only depend on Spp1, but also on H3K4me3. This trend could also be observed in *zip3*Δ*,* sgs1-mn mutants, where H3K4A severely reduced spore formation.

## 4.3 Abnormal DSB formation alone does not explain the severe defects of *spp1*Δ and *H3K4A* in zmm$^-$ mutants

*spp1*Δ*, H3K4A* (Acquaviva *et al.*, 2013; Sommermeyer *et al.*, 2013) and the Mer2-Spp1 interaction deficient mutant *mer2-sid* (Adam *et al.*, 2018) have been reported to alter the DSB levels at certain loci (e. g. *CYS3, DEP1* or *PES4*). Therefore, a central question is whether the defects in meiotic progression, spore viability and axial associations in *zmm*$^-$*, spp1*Δ*, zmm*$^-$*, sgs1-mn, spp1*Δ and *zmm*$^-$*, sgs1-mn, H3K4A* mutants can be attributed to abnormal DSB formation rather than a direct role in DSB repair. Three conservative explanations need to be considered. First, that simply too few DSBs are formed in these mutants, second, that transcriptional defects in *spp1*Δ and *H3K4A* mutants leads to wrongly timed DSB formation, and third, that the altered DSB positions prevent the efficient recruitment of repair factors. However, several independent observations argue against these explanations.

### 4.3.1 *spp1*Δ and *H3K4A* mutants form considerable amounts of DSBs and behave differently from a mutant with substantial DSB reduction

Another strong indicator that low number of DSBs is not the reason for *spp1*Δ defects in *zmm*$^-$ and *zmm*$^-$*, sgs1-mn* mutants is the different behaviour of *rec114-8D* in the same backgrounds, as this phosphor mimicking mutant is known to drastically downregulate meiotic DSBs (Carballo *et al.*, 2013).

In zmm$^-$ mutants such as *msh5*Δ and *zip4*Δ introduction of *rec114-8D* accelerates meiotic progression dramatically – exactly as expected for a reduction in checkpoint-triggering DSBs (Börner, Kleckner and Hunter, 2004). This phenotype is not affected by the absence of Sgs1. In contrast, *spp1*Δ delays meiotic progression even further in milder zmm$^-$ mutants like *msh5*Δ or does not accelerate it for more server zmm$^-$ mutants like *zip4*Δ. This fundamentally different behaviour clearly contradicts the explanation of low DSB numbers causing the *spp1*Δ phenotype and instead reinforces the conclusion of persistent unrepaired lesions that activate the DNA damage checkpoint.

Another difference between *spp1*Δ and *rec114-8D* lies in the high levels of spore formation of *zmm*$^-$*, rec114-8D* mutants. While *zmm*$^-$*, rec114-8D* mutants display elevated levels of spore formation relative to *zmm*$^-$ single mutants, it is dramatically reduced in *zmm*$^-$*, spp1*Δ. However,

both mutations result in critically low levels of spore viability in different *zmm*$^{-}$ backgrounds. Interestingly, viability defects are moderately suppressed by the absence of Sgs1 for *zmm*$^{-}$*, rec114-8D* but not in *zmm*$^{-}$*, spp1*Δ mutants. This observation suggests that the low number of DSBs in *zmm*$^{-}$*, sgs1-mn, rec114-8D* mutants can be repaired via the unregulated JM pathway, DSBs in *zmm*$^{-}$*, sgs1-mn, spp1*Δ*,* however, cannot. This conclusion is also incompatible with a simple DSB reduction model: if low DSBs were the problem in *spp1*Δ, the two mutants should behave the same.

In cytological assays, both *rec114-8D* and *spp1*Δ displayed short and infrequent associated axes fragments in *zip4*Δ or *zip4*Δ*, sgs1-mn* backgrounds. However, based on the observations described above, we assume different reasons for this similar phenotype: in *rec114-8D* mutants low number of DSBs results in loss of axial associations, and *spp1*Δ mutants are unable to stabilize formed axial associations. More Rad51 foci were observed in *rec114-8D* mutants than expected from published evidence of reduced DSB formation. This contrasts with reported Southern blotting in *com1*Δ*/sae2*Δ backgrounds and by Spo11 ChIP-seq data (Carballo *et al.*, 2013). As *rec114-8D* still behaves as a DSB hypomorph in our assays, we retain this interpretation, but the basis of the Rad51 foci signal remains to be clarified.

Importantly, when *rec114-8D* is combined with *spp1*Δ in the *zip4*Δ or *zip4*Δ*, sgs1-mn* background, meiotic progression becomes accelerated – like for *rec114-8D* alone, indicating that *rec114-8D* is epistatic to *spp1*Δ*.* However, spore formation of the *zip4*Δ*, rec114-8D, spp1*Δ mutant is not elevated to the level of the *zip4*Δ*, rec114-8D* mutant and no suppression by the absence of Sgs1 was observed. Furthermore, no viable spores were detected, which suggests that *spp1*Δ still contributes to the defects observed in these mutants.

As an alternative strategy for a mutant impaired in DSB formation, we could employ hypomorphic *spo11* alleles, such as *spo11-Y135F/spo11-3HA* (heterozygously), which also exhibit reduced DSB levels (Keeney, Giroux and Kleckner, 1997; Neale *et al.*, 2002; Pan *et al.*, 2011). This would circumvent the ambiguous readout associated with the substantial amount of Rad51 foci in *rec114-8D* mutants.

**The substantial amount of DSBs generated in *spp1*Δ mutants recruits DSB repair factors**

If *zmm*$^{-}$*, spp1*Δ and *zmm*$^{-}$*, sgs1-mn, spp1*Δ mutants had insufficient DSBs, one would expect reduced recruitment of downstream repair or recombination factors. However, this was not the case as revealed by immunostaining for Rad51 and Zip3.

Rad51 foci remained abundant in *zip4*Δ*, spp1*Δ and *zip4*Δ*, sgs1-mn, spp1*Δ mutants and no dramatic reduction was detected compared to *zip4*Δ single and *zip4*Δ*, sgs1-mn* double mutants 6 h after induction of meiosis. Intensities of individual foci are highly variable in all backgrounds

with nuclei typically displaying a smaller portion of high intensity foci and a lot of low intensity foci. These observations indicate that DSBs are formed in the absence of Spp1 that are competent to recruit Rad51, which is required for strand invasion and recombination (Bishop, 1994; Schwacha and Kleckner, 1997). Thus, the presence Rad51 foci is inconsistent with the idea that *spp1*Δ defects in zmm$^-$ mutants arise from too few DSBs that are recombination competent.

Although the ZMM pathway is blocked in *zip4*Δ mutants, Zip3 foci remained abundant in all examined backgrounds. Zip3 signals were consistently robust in *zip4*Δ and *zip4*Δ*, sgs1-mn* strains, indicating that neither the depletion of Sgs1 nor the loss of Spp1 markedly reduces Zip3 foci formation. The slight increase in Zip3 foci in Sgs1-depleted mutants could indicate that strand invasion intermediates are more stable in this background, providing additional opportunities for Zip3 recruitment. However, while Zip3 foci were localized to axial associations in the *zip4*Δ single mutant, they were found in regions that lack visible axial associations in the *zip4*Δ*, spp1*Δ and *zip4*Δ*, sgs1-mn, spp1*Δ mutants. As Zip3 is a well-established cytological marker for class I CO designation (Agarwal and Roeder, 2000; Tsubouchi, Zhao and Roeder, 2006), these intermediates either ultimately fail to become stable JMs or *spp1*Δ prevents normal CO designation.

Because microscopy provides only snapshots of meiotic nuclei, it cannot capture the turnover or repair dynamics of unrepaired lesions. Hence, it remains possible that DSBs are repaired more rapidly in *zip4*Δ and *zip4*Δ*, sgs1-mn* than in *zip4*Δ*, spp1*Δ or *zip4*Δ*, sgs1-mn, spp1*Δ*.* This explanation is supported by the analysis of genome-wide Protec-seq profiles, which showed that *spp1*Δ mutants are delayed in DSB formation, although they accumulate a considerable number of DSBs over time. The estimated 30-40% of wild type DSBs in *spp1*Δ mutants are clearly sufficient for meiotic recombination as progenies of the *spp1*Δ single mutant are completely viable and spore formation is not reduced. *H3K4A* also generated a considerable amount of DSBs, also inconsistent for too few DSBs as an explanation for the *zmm*$^-$*, sgs1-mn, H3K4A* mutant defects. Even if *spp1*Δ does never reach the same DSB levels as *H3K4A,* the nearly indistinguishable defects exhibited by both mutants in a *zmm*$^-$*, sgs1-mn* background strongly argue against reduced DSB formation as the underlying cause.

### 4.3.2 *H3K4A* does not share *spp1*Δ's delay in DSB formation, while being equally defective in axial associations

Both *spp1*Δ and *H3K4A* show a very similar phenotype in all assays performed during this study. Meiotic progression is delayed in the single mutants and even more so in *zmm*$^-$*, spp1*Δ double or *zmm*$^-$*, sgs1-mn, spp1*Δ and *zmm*$^-$*, sgs1-mn, H3K4A* triple mutants. Like Spp1,

H3K4me3 seems to be required for the stable formation of axial associations. In their absence spore formation and spore viability of *zmm⁻, sgs1-mn* mutants are similarly reduced. Furthermore, genome-wide dDSB landscape of *spp1*Δ and *H3K4A* highly resemble each other in most regions, although there are some loci where they behave differently. While they are very comparable in all these aspects, they differentiate in the timing of DSBs. *H3K4A* shows higher levels of dDSBs after 4 h than *spp1*Δ after 6 h in SPM. Even though, in the time course used for Protec-seq, both wild type and *spp1*Δ were moderately delayed, it is possible that *spp1*Δ has a greater delay in accumulating DSBs than *H3K4A.* If true, this would indicate that the wrongly timed DSBs cannot explain *spp1*Δ defects in *zmm⁻* and *zmm⁻, sgs1-mn* mutants since *H3K4A* shows the same phenotype but clearly produces DSBs in a timely manner. To validate this hypothesis in the future, Protec-seq samples from *H3K4A* and *spp1*Δ should be collected from the same meiotic time course for better comparability.

Both H3K4me3 and Spp1 are required for normal gene expression (Cruz *et al.*, 2018; Santos-Rosa *et al.*, 2002), raising the concern that reduced transcription of meiotic genes in *spp1*Δ and *H3K4A* delays the meiotic program in zmm⁻ mutants even further. However, this explanation is unlikely. A key observation is that phospho-mimetic activation of Rec114 (*rec114-8D*), which functions upstream of Spp1, restores meiotic progression even in *zip4*Δ*, spp1*Δ +/- Sgs1 backgrounds. Because *rec114-8D* bypasses the delay without correcting any transcriptional defects, these findings support the conclusion that *spp1*Δ affects DSB repair in a direct capacity rather than through transcriptional defects.

In addition, Rad51 and Zip3 foci could be detected and were not reduced in *spp1*Δ backgrounds, arguing against the possibility of insufficiently expressed meiotic repair proteins. However, this interpretation could be substantiated by future ChIP-seq experiments.

### 4.3.3 The Mer2-Spp1 tether is required for DSB positioning but not for axial associations in *zmm⁻, sgs1-mn* mutants

In the currently favoured model Spp1 is proposed to tether H3K4me3 marks to the DSB machinery via its interaction with Mer2 (Acquaviva *et al.*, 2013; Sommermeyer *et al.*, 2013). *spp1*Δ and *H3K4A* both reposition DSBs as first described for certain loci (Sommermeyer *et al.*, 2013) and now, based on our Protec-seq profiles, shown to occur genome-wide. The Mer2-Spp1 interaction deficient mutant *mer2-V195D* (*mer2-sid*) also alters hotspot activity at *CYS3, DEP1* and *PES4* (Adam *et al.*, 2018), like *spp1*Δ and *H3K4A* (Sommermeyer et al., 2013). Adam and colleagues (2018) demonstrated using yeast-2-hybrid assays, pull-down experiments and mass-spec based approaches that Mer2-sid does not interact with Spp1,

while H3K4me3 levels are not compromised. Thus, the mutation does not affect binding of Spp1 to H3K4me3 but completely disrupts the Mer2-Spp1 interaction.

Several observations demonstrate that *mer2-sid* does not copy the *spp1*Δ and *H3K4A* phenotype in a *zmm*$^{-}$*, sgs1-mn* background, although DSB positioning is affected in all three mutants.

The *mer2-sid* single mutant did not display the same meiotic delay as *spp1*Δ and *H3K4A*, but showed similarly high spore formation and spore viability, consistent with previous reports (Acquaviva *et al.*, 2013; Adam *et al.*, 2018; Sommermeyer *et al.*, 2013). Like *spp1*Δ and *H3K4A, mer2-sid* did not accelerate progression of the *zip4*Δ single*, zip4*Δ*, sgs1-mn* double or *zip3*Δ*, sgs1-mn* double mutants. Interestingly, while spore formation and spore viability in *zip4*Δ*, mer2-sid* double mutants were similarly reduced as for *zip4*Δ*, spp1*Δ mutants, these defects could be notably suppressed by the absence of Sgs1. So the Mer2-Spp1 interaction is not required for suppression of zmm$^{-}$ defects by *sgs1-mn*. It may be interesting to test how *mer2-sid* affects progression, sporulation efficiency and spore viability of milder zmm$^{-}$ mutants such as *msh4*Δ or *msh5*Δ*,* where *spp1*Δ even increases the defects.

The most compelling evidence that the Mer2-Spp1 interaction can be separated from the potential function of Spp1 and H3K4me3 in repair was revealed by cytological analysis. *mer2-sid* does not eliminate axial associations in *zip4*Δ*, sgs1-mn* strains to the extent of *spp1*Δ or *H3K4A*. The Mer2-Spp1 interaction deficient mutant supports much more aligned axes fragments than *spp1*Δ in the same background (*H3K4A* not quantified in *zip4*Δ*, sgs1-mn*), while staying slightly below *zip4*Δ*, sgs1-mn, MER2*. This implies that the Mer2-Spp1 interaction is not as important for stabilisation of axial associations as Spp1-H3K4me3 interaction. We rationalize this puzzling result by proposing that Spp1 and H3K4me3 may have a direct mechanistic role in stabilizing intermediates, while Mer2-Spp1 may only work via shaping the landscape. Because the landscape under the conditions tested uses the same hotspots, albeit with a different set of weights, the effect of *mer2-sid* may be much milder than the abrogation of the recruitment of a stabilizer in *H3K4A*.

In contrast to the *zip4*Δ*, sgs1-mn, mer2-sid* triple mutant, the double mutant *zip4*Δ*, mer2-sid* resembles *zip4*Δ*, spp1*Δ*,* that is, it does slightly aggravate the *zip4*Δ phenotype. Together with the slight defect seen in the triple mutant background, this argues that the Mer2-Spp1 interaction may be required for full protection of repair intermediates in zmm$^{-}$ mutants, although the effects of Spp1 and H3K4me3 are more important.

Another difference to *spp1*Δ and *H3K4A* in *zmm*$^{-}$*, sgs1-mn* mutants is the appearance of the chromosome axes. The axes fragments, which are aligned in the *zip4*Δ*, sgs1-mn, mer2-sid* mutant, seem to be tighter associated with each other than in *zip4*Δ*, sgs1-mn*. Chromosomes

appear interwoven, which resembles entanglements arising in *mer3* mutants of *Sordaria* in early prophase (Storlazzi *et al.*, 2010). Spore formation and spore viability of the *zip4Δ, sgs1-mn, mer2-sid* are ambiguous. In our experiment, *mer2-sid* even improved spore formation, but reduced spore viability. If this holds true, *mer2-sid* might affect some DNA damage surveillance, leading to faster, but error prone meiosis. Viable spore yield was even slightly improved in *zip4Δ, sgs1-mn, mer2-sid* over *zip4Δ, sgs1-mn* suggesting that overall the lack of Mer2-Spp1 is either compensated for, or of less importance.

The cytology of the quadruple mutants *zip4Δ, sgs1-mn, mer2-sid, spp1Δ* and *zip4Δ, sgs1-mn, mer2-sid, H3K4A* resemble their corresponding triple mutants without *mer2-sid*. *mer2-sid* seems to slightly improve meiotic progression and slightly increase spore formation and spore viability in both backgrounds. This unexpected result could again point at a role of Mer2 in the DNA damage checkpoint, where surveillance might be relaxed in *mer2-sid.* Of course, this role could be mediated by modulation of its DSB promoting activity.

Overall, the differences between the *mer2-sid* and *spp1Δ* or *H3K4A* in the *zmm⁻, sgs1-mn* background suggest that tethering between Mer2 and Spp1 is less required for stabilisation of axial associations than Spp1-H3K4me3 tethering. Based on the modified DSB levels at certain loci in *mer2-sid* (Adam *et al.*, 2018; Sommermeyer *et al.*, 2013), this suggests that changing the DSB landscape alone has a milder defect than *spp1Δ* and *H3K4A*, or in other words, that the latter mutations do not act via landscape changes alone. It will be important to extend the *mer2-sid* DSB maps to genome-wide, which we would like to do by Protec-seq.

## 4.4 Potential roles for Spp1 and H3K4me3 in DSB repair

If tethering of H3K4me3 to Mer2 was required for establishing stable axial associations, *mer2-sid* should behave the same way as *spp1Δ* and *H3K4A,* since it also severs the tethering. However, that is not the case, showing that tethering of the DSB machinery is not the main mechanism for CO repair. Since *H3K4A* and *spp1Δ* share the same defects, it is quite likely that the mechanism involves binding of Spp1 to H3K4me3. In other words, the active mark may recruit factors that stabilize non-ZMM repair intermediates for stable joint molecule formation, and this recruitment requires Spp1 and H3K4me3. What might this stabilization entail?

In principle, any repair process after DSB formation, such as 5'- resection, Dmc1/Rad51-filament formation and strand invasion, as well as repair DNA-synthesis could be affected. The constraint is, that it only seems to matter in a *zmm⁻* background, that is, when ZMM proteins fail to protect the strand invasion intermediate.

*spp1*Δ was also shown to be synthetically defective for viable spore formation with *vpr1*Δ, a novel member of the Shu complex (Prast, Master thesis, 2016). The Shu complex (Csm2-Psy3-Shu1-Shu2 and now Vpr1 (Prast, Master thesis, 2016) promotes the formation of Rad51 filaments by stabilising Rad51 on RPA-coated ssDNA and indirectly supports Dmc1-mediated interhomolog strand invasion (Sasanuma *et al.*, 2013; Shor, Weinstein and Rothstein, 2005). Rad51 foci still form normally in *spp1*Δ strains, including in the *zip4*Δ*, sgs1-mn* background, which indicates that Rad51 loading is not severely impaired. In contrast, markedly less Rad51 foci were detected for *vpr1*Δ after 5 hours in SPM (Prast, Master thesis, 2016). Furthermore, Shu-complex mutants alone display recombination defects (Shor, Weinstein and Rothstein, 2005), whereas the *spp1*Δ defects become only visible in zmm$^-$ mutants. The Shu complex is also thought to be antagonistic to the Srs2 helicase (Bernstein *et al.*, 2011) possibly implying control over anti-recombinogenic factors in the defect. The synthetic defect actually argues that *spp1*Δ and *vpr1*Δ reduce joint molecule formation in different ways.

Normally, ZMM proteins protect early recombination intermediates from Sgs1's anti-recombination activity. However, when the ZMM proteins do not function properly, these intermediates remain unprotected unless Sgs1 is removed (Oh *et al.*, 2008; De Muyt *et al.*, 2012; Jessop and Lichten, 2008). We therefore speculate that the ZMM proteins may also protect intermediates against other helicases or nucleases. In particular, Mph1 and Srs2 are both known to be able to destabilize strand invasions.

Mph1 was shown to dismantle D-loops through 3'-5' helicase activity and channels repair into the SDSA pathway, while limiting crossover formation in mitotic recombination (Prakash *et al.*, 2009; Tay, Sidebotham and Wu, 2010). Biochemical experiments demonstrate that Mte1 (Mph1-associated telomere maintenance protein 1) inhibits the disassembly of D-loops by Mph1 (Silva *et al.*, 2016). Mph1 also interacts with the conserved histone fold MHF complex that structurally resembles the histone H3 and H4 heterotetramer (Yang *et al.*, 2012; Daee *et al.*, 2012; Singh *et al.*, 2010; Yan *et al.*, 2010). The MHF complex promotes Mph1-mediated repair of damaged replication forks. However, while *mph1*Δ does increase crossover formation, MHF mutants have no effect on outcomes of DSB repair events (Xue *et al.*, 2015). Both Mte1 and the MHF complex are also expressed during meiosis and constitutively bind to Mph1 (Wild *et al.*, 2019). In meiosis, strand exchange between sister chromatids is prevented through Mph1, while D-loops between homologs can mature into recombination intermediates if protected by Zip1 (Sandhu *et al.*, 2020). Thus Mph1 is active in meiosis and is actively participating in JM quality control by preventing inter sister cross overs and regulated by the ZMM pathway. Because Mph1 is regulated by a histone fold protein, it is a really attractive candidate to be controlled by H3K4me3.

The 3'-5' helicase Srs2 has anti-recombination activity by disrupting Rad51 filaments to inhibit strand exchange. Mutations in SRS2 lead to DNA damage mediated checkpoint arrest, indicating that unrepaired DSBs persist, slow growth, chromosome loss and hyper-recombination in vegetative cells (Krejci *et al.*, 2003; Veaute *et al.*, 2003). Interaction between Rad51 and the C-terminal region of Srs2 stimulates ATPase hydrolysis within the Rad51 filament through which Rad51 dissociates from DNA (Antony *et al.*, 2009). Srs2 activity therefore channels repair into the SDSA pathway and towards formation of non-crossovers in mitotic recombination (Robert *et al.*, 2006; Saponaro *et al.*, 2010). In addition, biochemical experiments revealed that removal of Rad51 from the DNA by Srs2 stimulates structure specific nucleases Mus81-Mms4 (Chavdarova *et al.*, 2015). In meiosis, *srs2*$^{-}$ mutants accumulate persistent Rad51 aggregates and aberrant recombination intermediates, resulting in delayed meiotic progression and reduced spore viability (Sasanuma *et al.*, 2019; Hunt *et al.*, 2019). Hunt and colleagues (2019) used a meiotic null allele of *SRS2* (*srs2-md*) and reported that it maintains wild type crossover levels. Spp1 and H3K4me3 controlling Srs2 activity could explain the synthetic effect between *vpr1*Δ and *spp1*Δ (Prast, Master thesis, 2016), as the Shu complex is required for Rad51 filament formation and antagonizes Srs2 (Sasanuma *et al.*, 2013; Shor, Weinstein and Rothstein, 2005).

Recently, Ghaddar and colleagues (2023) reported that Spp1 restricts Exo1-mediated resection of nascent DNA at stalled replication forks in mitotic cells. They suggest that Spp1 protects nascent DNA after fork reversal by masking H3K4me3 in the parental chromatin, thereby inhibiting other histone readers that would recruit Exo1. However, in meiosis Exo1's 5'-3' activity is required for strand resection to enable subsequent 3' end invasions (Zakharyevich *et al.*, 2010), so there is no reason to assume that eliminated Exo1 activity would eliminate CO. H3K4me3/Spp1 could however inhibit 3'-5' nucleases like Mre11 (Neale, Pan and Keeney, 2005; Garcia *et al.*, 2011) via an analogous mechanism.

Ghaddar et al (2023) proposed that binding of Spp1 to H3K4me3 could result in masking the histone mark, but this should result in antagonistic phenotypes. However, we observe the same phenotype for the two players, indicating that they work together. More likely, therefore, H3K4me3/Spp1 recruit additional factors, which then inhibit helicases or nucleases.

Taken together, this leads to our current working hypothesis in which H3K4me3/Spp1 protect repair intermediates redundantly with the ZMM proteins from destabilizers. This could either be facilitated via an indirect or direct mechanism, while Sgs1 remains largely unaffected by H3K4me3/Spp1. We propose that helicases or nucleases gain access to strand invasions in the absence of both, ZMM and H3K4me3/Spp1. In our future work we will try to test this hypothesis, by depleting the candidates in the triple mutant background, to see, whether loss of axial associations can be suppressed.

H3K4me3 may aid DSB repair also in higher eukaryotes. In mice, the dual H3K4me3/H3K36me3 reader ZCWPW1 is required for the efficient repair of PRDM9-dependent DSBs (Huang *et al.*, 2020; Wells *et al.*, 2020; Mahgoub *et al.*, 2020). Although, $PRDM9^{-/-}$ mice still form abundant DSBs, these occur close to PRDM9-independent H3K4me3 chromatin lacking H3K36me3, do not recruit ZCWPW1 and are not repaired efficiently, resulting in persistent DNA damage, pachytene arrest and sterility (Hayashi, Yoshida and Matsui, 2005; Brick *et al.*, 2012). This resembles vaguely the situation in yeast, with Spp1 resembling ZCWPW1 and H3K4me3 in yeast playing the role of H3K4me3/H3K36me3 in mice. An important difference is that in yeast *spp1*Δ and *H3K4A* have nearly no defect on their own, so it is questionable, how close the systems are related.

The Set1C/COMPASS complex, including Spp1, is of course active in vegetative cells, since H3K4me3 is required for normal gene expression (Briggs *et al.*, 2001; Santos-Rosa *et al.*, 2002). Since Spp1 and H3K4me3 are particularly important when cells rely on the alternative, mitotic-like pathway during meiosis, we speculate that they also could be important in mitotic DSB repair. Mitotic repair follows principles similar to this pathway: the 3'-5' helicases Srs2, Mph1 and Sgs1 suppress the accumulation of toxic or aberrant repair intermediates and promote SDSA (Krejci *et al.*, 2003; Liu *et al.*, 2017; Prakash *et al.*, 2009; Mazón and Symington, 2013; Fabre *et al.*, 2002), while the same structure specific nucleases – Mus81-Mms4, Slx1-Slx4 and Yen1 – are required to resolve recombination intermediates (Ho *et al.*, 2010; Matos *et al.*, 2011; Fricke and Brill, 2003; Blanco *et al.*, 2010).

In summary, we have identified a condition in meiosis (*zmm*$^{-}$*, sgs1-mn*) in which H3K4me3 and Spp1 are essential for JM formation. This identifies a previously unknown essential role for these two factors in DSB repair. Future work is required to elucidate the mechanism by which they exert this function.

# 5 Appendix

## 5.1 Supplementary Figures

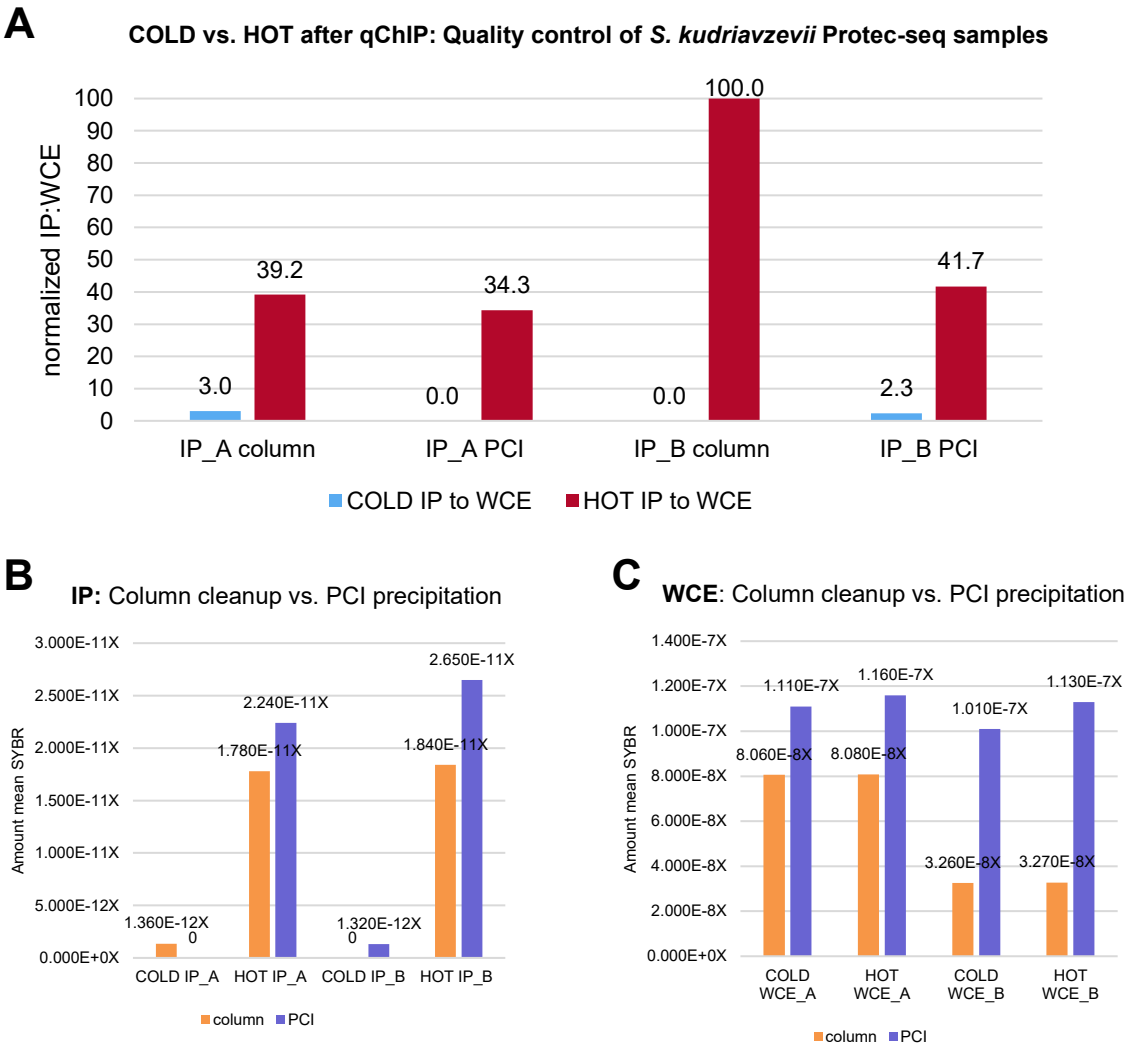


**S Figure 1. ChIP-qPCR of Protec-seq calibration strain samples reveals strong signals for a DSB hotspot and low signals at a DSB cold region, indicating that meiosis was sufficiently induced. Furthermore, two methods of DNA purification, column clean up and PCI precipitation, were compared in two technical replicates.**

(**A**) DSB hotspot vs. DSB cold region for the two technical replicates A and B. For each replicate PCI precipitation and column clean up using the QIAquick Nucleotide removal kit as described in Section for Calibrated qChIP were performed.

(**B**) IP values measured in qPCR were plotted for the DSB cold region and the DSB hotspot, also comparing column cleanup vs. PCR precipitation per replicate (A and B). The signal for the cold region is reduced in column and PCI, while the signal for DSB hotspots is increased.

(**C**) Same as (B) just for the WCEs. WCEs should theoretically be very similar, however, there is some variation. Column cleanup shows bigger differences than PCR precipitation.

Data from TC28: FKy6634 (*SPO11-myc18*), *S. kudriavzevii*

FKo4166/4167: DSB hotspot, FKo4103/4104: cold region for DSBs

Samples from the same time course were used as calibration strain for Protec-seq.

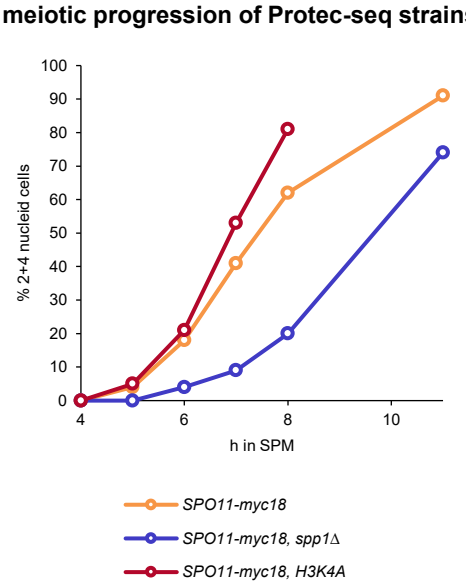


**S Figure 2. Wild type and *spp1*Δ strains were more delayed in meiotic progression than usual.**

Data from TC33: FKy1358 (*SPO11-myc18*), FKy5525 (*SPO11-myc18, spp1*Δ) and TCVP: FKy9196 (*SPO11-myc18, H3K4A*)

## 5.2 Strains used in this Study

**Table 5.2-1:** All strains used in meiotic time course experiments, which were mentioned in this study

| FKy | Species | MAT | Genotype |
|---|---|---|---|
| 1358 | *S. c.* | a/α | *ho::LYS2, ura3, trp1::hisG, leu2::hisG, SPO11-myc18::TRP1*<br>*ho::LYS2, ura3, trp1::hisG, leu2::hisG, SPO11-myc18::TRP1* |
| 5247 | *S. c.* | a/α | *ho::LYS2, ura3, leu2::hisG, his3::hisG,*<br>*ho::LYS2, ura3, leu2::hisG, his3::hisG,*<br>*arg4Δ(eco47III-hpa1),*<br>*ARG4,*<br>*zip3Δ::KanMX, sgs1::KanMX::pCLB2-3HA-SGS1*<br>*zip3Δ::KanMX, sgs1::KanMX::pCLB2-3HA-SGS1* |
| 5525 | *S. c.* | a/α | *ho::LYS2, ura3, leu2::hisG, trp1::hisG, his3::hisG,*<br>*ho::LYS2, ura3, leu2::hisG, trp1::hisG, his3::hisG,*<br>*SPO11-myc18::TRP1, spp1Δ::HphMX4*<br>*SPO11-myc18::TRP1, spp1Δ::HphMX4* |
| 5539 | *S. c.* | a/α | *ho::LYS2, lys2, ura3, leu2::hisG, trp1::hisG, his3::hisG,*<br>*ho::LYS2, lys2, ura3, leu2::hisG, trp1::hisG, his3::hisG,*<br>*spp1Δ::HphMX4*<br>*spp1Δ::HphMX4* |
| 6106 | *S. c.* | a/α | *ho::LYS2, lys2, ura3, leu2::hisG, trp1::hisG, his3::hisG,*<br>*ho::LYS2, lys2, ura3, leu2::hisG, trp1::hisG, his3::hisG,*<br>*zip3Δ::KanMX*<br>*zip3Δ::KanMX* |
| 6142 | *S. c.* | a/α | *ho::LYS2, lys2, ura3, trp1::hisG, LEU2, HIS3,*<br>*ho::LYS2, lys2, ura3, trp1::hisG, leu2::hisG, his3::hisG,*<br>*ARG4*<br>*arg4Δ(eco47III-hpa1)*<br>*his4Δ(Sa1-Cla1)::URA3-Δ(Sma1-Eco47III)-arg4-EcPal(1691)*<br>*his4Δ(Sa1-Cla1)::URA3-Δ(Sma1-Eco47III)-arg4-EcPal(1691)*<br>*zip3Δ::KanMX, sgs1::KanMX::pCLB2-3HA-SGS1, spp1Δ::HphMX*<br>*zip3Δ::KanMX, sgs1::KanMX::pCLB2-3HA-SGS1, spp1Δ::HphMX* |
| 6290 | *S. c.* | a/α | *ho::LYS2, lys2, ura3, leu2::hisG, trp1::hisG, his3::hisG,*<br>*ho::LYS2, lys2, ura3, leu2::hisG, trp1::hisG, his3::hisG,*<br>*spp1Δ::hphMX, msh5Δ::KanMX*<br>*spp1Δ::hphMX, msh5Δ::KanMX* |
| 6296 | *S. c.* | a/α | *ho::LYS2, lys2, ura3, leu2::hisG, trp1::hisG, his3::hisG,*<br>*ho::LYS2, lys2, ura3, leu2::hisG, trp1::hisG, his3::hisG,*<br>*spp1Δ::hphMX, zip4Δ::KanMX*<br>*spp1Δ::hphMX, zip4Δ::KanMX* |
| 6336 | *S. c.* | a/α | *ho::LYS2, lys2, ura3, leu2::hisG, trp1::hisG, his3::hisG,*<br>*ho::LYS2, lys2, ura3, leu2::hisG, trp1::hisG, his3::hisG,*<br>*msh5Δ::KanMX*<br>*msh5Δ::KanMX* |
| 6338 | *S. c.* | a/α | *ho::LYS2, lys2, ura3, leu2::hisG, trp1::hisG, his3::hisG,*<br>*ho::LYS2, lys2, ura3, leu2::hisG, trp1::hisG, his3::hisG,*<br>*zip4Δ::KanMX*<br>*zip4Δ::KanMX* |
| 6359 | *S. c.* | a/α | *ho::LYS2, lys2, ura3, leu2::hisG, trp1::hisG, his3::hisG,*<br>*ho::LYS2, lys2, ura3, leu2::hisG, trp1::hisG, his3::hisG,*<br>*msh5Δ::KanMX, sgs1::KanMX::pCLB2-3HA-SGS1*<br>*msh5Δ::KanMX, sgs1::KanMX::pCLB2-3HA-SGS1* |
| 6362 | *S. c.* | a/α | *ho::LYS2, lys2, ura3, trp1, his3::hisG, leu2::hisG, arg4Δ(eco47III-hpa1)*<br>*ho::LYS2, lys2, ura3, trp1, his3::hisG, leu2::hisG, arg4Δ(eco47III-* |

| | | | |
|---|---|---|---|
| | | | *hpa1)*<br>*msh5Δ::KanMX, rec114-8D::HphMX*<br>*msh5Δ::KanMX, rec114-8D::HphMX* |
| 6365 | *S. c.* | a/α | *ho::LYS2, lys2, ura3, trp1, his3::hisG, leu2::hisG,*<br>*ho::LYS2, lys2, ura3, trp1, his3::hisG, leu2::hisG,*<br>*sgs1::KanMX::pCLB2-3HA-SGS1, msh5Δ::KanMX, spp1Δ::hphMX*<br>*sgs1::KanMX::pCLB2-3HA-SGS1, msh5Δ::KanMX, spp1Δ::hphMX* |
| 6368 | *S. c.* | a/α | *ho::LYS2, lys2, ura3, leu2::hisG, trp1::hisG, his3::hisG,*<br>*ho::LYS2, lys2, ura3, leu2::hisG, trp1::hisG, his3::hisG,*<br>*zip4Δ::KanMX, sgs1::KanMX::pCLB2-3HA-SGS1, rec114-8D::HphMX*<br>*zip4Δ::KanMX, sgs1::KanMX::pCLB2-3HA-SGS1, rec114-8D::HphMX* |
| 6371 | *S. c.* | a/α | *ho::LYS2, lys2, ura3, leu2::hisG, trp1::hisG, his3::hisG,*<br>*ho::LYS2, lys2, ura3, leu2::hisG, trp1::hisG, his3::hisG,*<br>*zip4Δ::KanMX, sgs1::KanMX::pCLB2-3HA-SGS1, spp1Δ::HphMX*<br>*zip4Δ::KanMX, sgs1::KanMX::pCLB2-3HA-SGS1, spp1Δ::HphMX* |
| 6374 | *S. c.* | a/α | *ho::LYS2, lys2, ura3, leu2::hisG, trp1::hisG, his3::hisG, ARG4,*<br>*ho::LYS2, lys2, ura3, leu2::hisG, trp1::hisG, his3::hisG,*<br>*arg4Δ(eco47III-hpa1),*<br>*sgs1::KanMX::pCLB2-3HA-SGS1, zip4Δ::KanMX*<br>*sgs1::KanMX::pCLB2-3HA-SGS1, zip4Δ::KanMX* |
| 6377 | *S. c.* | a/α | *ho::LYS2, lys2, ura3, leu2::hisG, trp1, his3::hisG, arg4Δ(eco47III-hpa1),*<br>*ho::LYS2, lys2, ura3, leu2-RV::URA3-Δ(Sma1-Eco47III)-[ARG4], trp1, his3::hisG, ARG4,*<br>*zip4Δ::KanMX, rec114-8D::HphMX*<br>*zip4Δ::KanMX, rec114-8D::HphMX* |
| 6634 | *S. k.* | a/α | *SPO11-myc18::HphMX*<br>*SPO11-myc18::HphMX* |
| 8811 | *S. c.* | a/α | *ho::hisG, LYS2/ho::LYS2, lys2, leu2::hisG, ura3, his3::hisG, cyh2-z, trp1::hisG*<br>*ho::hisG, lys2, leu2::hisG, ura3, his3::hisG, trp1::hisG,*<br>*msh4Δ::NatMX, spp1Δ::HphMX, sgs1::KanMX::pCLB2-3HA-SGS1*<br>*msh4Δ::NatMX, spp1Δ::HphMX, sgs1::KanMX::pCLB2-3HA-SGS1* |
| 8812 | *S. c.* | a/α | *ho::hisG, lys2, leu2::hisG, ura3, his3::hisG,*<br>*ho::hisG, LYS2/ho::LYS2, lys2, leu2::hisG, ura3, his3::hisG, cyp2-z,*<br>*msh4Δ::NatMX, spp1Δ::HphMX*<br>*msh4Δ::NatMX, spp1Δ::HphMX,* |
| 8813 | *S. c.* | a/α | *ho::hisG, LYS2 or ho::LYS2, lys2, leu2::hisG, ura3, his3::hisG, trp1::hisG,*<br>*ho::LYS2, LYS2, leu2::hisG, ura3, his3::hisG, trp1::hisG,*<br>*msh4Δ::NatMX, sgs1::KanMX::pCLB2-3HA-SGS,*<br>*msh4Δ::NatMX, sgs1::KanMX::pCLB2-3HA-SGS,* |
| 8819 | *S. c.* | a/α | *ho::LYS2, lys2, ura3, leu2::hisG, trp1::hisG, his3::hisG,*<br>*ho::LYS2, lys2, ura3, leu2::hisG, trp1::hisG, his3::hisG,*<br>*msh4Δ::NatMX*<br>*msh4Δ::NatMX* |
| 8895 | *S. c.* | a/α | *ho::LYS2, lys2, ura3, trp1::hisG, his3::hisG, ho::LYS2, lys2, ura3, trp1::hisG, his3::hisG, leu2::hisG,*<br>*ubc9-K153R,K157R*<br>*ubc9-K153R,K157R* |
| 8909 | *S. c.* | a/α | *ho::LYS2, lys2, ura3, trp1::hisG, leu2::hisG, arg4Δ(eco47III-hpa1),*<br>*ho::LYS2, lys2, ura3, trp1::hisG, leu2::hisG, ARG4*<br>*SPO11-myc18::TRP1, zip3Δ::KanMX, sgs1::KanMX::pCLB2-3HA-SGS1*<br>*SPO11-myc18::TRP1, zip3Δ::KanMX, sgs1::KanMX::pCLB2-3HA-SGS1* |
| 9196 | *S. c.* | a/α | *ho::LYS2, ura3, trp1::hisG, leu2::hisG,*<br>*ho::LYS2, ura3, trp1::hisG, leu2::hisG,*<br>*SPO11-myc18::TRP1, hht1-K4A, hht2-K4A* |

| | | | |
|---|---|---|---|
| | | | *SPO11-myc18::TRP1, hht1-K4A, hht2-K4A* |
| 9198 | *S. c.* | a/α | *ho::LYS2, ura3, leu2::hisG, his3::hisG*, arg4Δ(eco47III-hpa1)*<br>*ho::LYS2, ura3, leu2::hisG, his3::hisG*, ARG4*<br>*zip3Δ::KanMX, sgs1::KanMX::pCLB2-3HA-SGS1, hht1-K4A, hht2-K4A*<br>*zip3Δ::KanMX, sgs1::KanMX::pCLB2-3HA-SGS1, hht1-K4A, hht2-K4A* |
| 9217 | *S. c.* | a/α | *ho::LYS2, lys2?, ura3, trp1::hisG, leu2::hisG, arg4Δ(eco47III-hpa1)*<br>*ho::LYS2, lys2?, ura3, trp1::hisG, leu2::hisG, ARG4*<br>*SPO11-myc18::TRP1, zip3Δ::KanMX, sgs1::KanMX::pCLB2-3HA-SGS1, SPO11-myc18::TRP1, zip3Δ::KanMX, sgs1::KanMX::pCLB2-3HA-SGS1,*<br>*hht1-K4A, hht2-K4A*<br>*hht1-K4A, hht2-K4A* |
| 9338 | *S. c.* | a/α | *ho::LYS2, lys2, ura3, leu2::hisG, trp1::hisG, his3::hisG,*<br>*ho::LYS2, lys2, ura3, leu2::hisG, trp1::hisG, his3::hisG,*<br>*mer2-sid(V192D)*<br>*mer2-sid(V192D)* |
| 9341 | *S. c.* | a/α | *ho::LYS2, lys2, ura3, leu2::hisG, trp1::hisG, his3::hisG,*<br>*ho::LYS2, lys2, ura3, leu2::hisG, trp1::hisG, his3::hisG,*<br>*zip4Δ::KanMX, mer2-sid(V192D)*<br>*zip4Δ::KanMX, mer2-sid(V192D)* |
| 9344 | *S. c.* | a/α | *ho::LYS2, lys2, ura3, leu2::hisG, trp1::hisG, his3::hisG,*<br>*arg4Δ(eco47III-hpa1)*<br>*ho::LYS2, lys2, ura3, leu2::hisG, trp1::hisG, his3::hisG, ARG4,*<br>*zip4Δ::KanMX, sgs1::KanMX::pCLB2-3HA-SGS1, mer2-sid(V192D)*<br>*zip4Δ::KanMX, sgs1::KanMX::pCLB2-3HA-SGS1, mer2-sid(V192D)* |
| 9396 | *S. c.* | a/α | *ho::LYS2, lys2, ura3, leu2::hisG, trp1::hisG, his3::hisG,*<br>*arg4Δ(eco47III-hpa1),*<br>*ho::LYS2, lys2, ura3, leu2::hisG, trp1::hisG, his3::hisG, ARG4*<br>*zip4Δ::KanMX, sgs1::KanMX::pCLB2-3HA-SGS1, hht1-K4A, hht2-K4A,*<br>*zip4Δ::KanMX, sgs1::KanMX::pCLB2-3HA-SGS1, hht1-K4A, hht2-K4A,*<br>*mer2-sid(V192D)*<br>*mer2-sid(V192D)* |
| 9404 | *S. c.* | a/α | *ho::LYS2, lys2, ura3, leu2::hisG, trp1::hisG, his3::hisG,*<br>*ho::LYS2, lys2, ura3, leu2::hisG, trp1::hisG, his3::hisG,*<br>*sgs1::KanMX::pCLB2-3HA-SGS1, zip4Δ::KanMX, spp1Δ::hphMX,*<br>*sgs1::KanMX::pCLB2-3HA-SGS1, zip4Δ::KanMX, spp1Δ::hphMX,*<br>*mer2-sid(V192D)*<br>*mer2-sid(V192D)* |
| 9407 | *S. c.* | a/α | *ho::LYS2, lys2, ura3, leu2::hisG, trp1::hisG, his3::hisG,*<br>*ho::LYS2, lys2, ura3, leu2::hisG, trp1::hisG, his3::hisG,*<br>*zip4Δ::KanMX, sgs1::KanMX::pCLB2-3HA-SGS1, SPO11-myc18::TRP1*<br>*zip4Δ::KanMX, sgs1::KanMX::pCLB2-3HA-SGS1, SPO11-myc18::TRP1* |
| 9410 | *S. c.* | a/α | *ho::LYS2, lys2, ura3, leu2::hisG, trp1::hisG, his3::hisG*<br>*ho::LYS2, lys2, ura3, leu2::hisG, trp1::hisG, his3::hisG*<br>*zip4Δ::KanMX, sgs1::KanMX::pCLB2-3HA-SGS1, spp1Δ::hphMX,*<br>*zip4Δ::KanMX, sgs1::KanMX::pCLB2-3HA-SGS1, spp1Δ::hphMX,*<br>*SPO11-myc18::TRP1*<br>*SPO11-myc18::TRP1* |
| 9413 | *S. c.* | a/α | *ho::LYS2, lys2, ura3, leu2::hisG, trp1::hisG, his3::hisG*<br>*ho::LYS2, lys2, ura3, leu2::hisG, trp1::hisG, his3::hisG*<br>*zip4Δ::KanMX, sgs1::KanMX::pCLB2-3HA-SGS1, spp1Δ::hphMX,*<br>*zip4Δ::KanMX, sgs1::KanMX::pCLB2-3HA-SGS1, spp1Δ::hphMX,*<br>*rec114-8D::HphMX4*<br>*rec114-8D::HphMX4* |

| | | | |
|---|---|---|---|
| 9416 | *S. c.* | a/α | *ho::LYS2, lys2, ura3, leu2::hisG, trp1::hisG, his3::hisG,*<br>*ho::LYS2, lys2, ura3, leu2::hisG, trp1::hisG, his3::hisG,*<br>*zip4Δ::KanMX, spp1Δ::hphMX, rec114-8D::HphMX4*<br>*zip4Δ::KanMX, spp1Δ::hphMX, rec114-8D::HphMX4* |

## 5.3 Primers used in this Study

**Table 5.3-1:** Primers used for qPCR or generating qPCR templates in *S. cerevisiae* SK1

| FKo | Sequence (5'-3') | Target | Purpose |
|---|---|---|---|
| 794 | GGTGATGATTGCTCTCTGCC | ADP1 | template |
| 795 | CGTCACAATTGATCCCTCCC | ADP1 | template |
| 4513 | TAGTGTTAGTGCCGGTGCAGC | YFL022 | qPCR |
| 4514 | TGGTGGCTGTTAGTACCAGCG | YFL022 | qPCR |
| 4564 | CGGCCGTGGTTGGACTCG | YCR047 | qPCR |
| 4565 | GGGTCTGCTGGGTGCTATTGTTC | YCR047 | qPCR |
| 4670 | CGTTATCGTACGTGACCGAATGC | YCR047 | template |
| 5026 | ATCATTGCGTCCGACCACAG | YFL022 | template |
| 5027 | TGTGCGACTCATAGTGCTGTT | YFL022 | template |
| 5028 | TCTGGCTTGGCCATCAAATACC | YCR047 | template |
| 5788 | CCATCCGTTATCACAATGAC | ADP1 | qPCR |
| 5789 | GGATCGTCCCATAAGAGCAC | ADP1 | qPCR |
| 6176 | CCGGCGAATTTTTTACC | INO2 | template |
| 6178 | TTAGGTTGGTTCCATCTGC | INO2 | qPCR |
| 6179 | GAATCACCCTCCATAGTGC | INO2 | qPCR |
| 6181 | CACTTCCTGCGCCTTTTCC | INO2 | template |
| 6225 | TGTCATCGAGGTCGTTGTTG | YFL022 | qPCR |
| 6226 | ACGTACTTGGCGCCATAATC | YFL022 | qPCR |
| 6269 | TTGGTTCCATCTGCCGCA | INO2 | qPCR |
| 6270 | TGTCTTTCAACATGCTGC | INO2 | qPCR |
| 6272 | CGATTTCCCAACAATGTC | INO2 | template |
| 6273 | GCGAATTTTTTACCTCCTGC | INO2 | template |
| 6278 | ttatttacttgagactggcatcgcaatggaaaatccaACGGGTATTCTAAGGCAGGTTTC | INO2 | qPCR |
| 6280 | TAAGAAGGACGAGCGTGGTG | YCR047 | qPCR |

| | | | |
|---|---|---|---|
| 6281 | TTTGGCGCTCTTGCTGCAAG | YCR047 | qPCR |

**Table 5.3-2:** All primers were used for both, generating qPCR templates and qPCR, for *S. kudriavzevii*

| **FKo** | **Sequence (5'→3')** | **Target** |
|---|---|---|
| 4103 | GAAGTTGCGAGAGAGGCACAG | cold region |
| 4104 | GTTCAAGCAAGGCGCTGACAG | cold region |
| 4166 | CCTGATCGTGCAAATGTGCC | DSB hotspot |
| 4167 | TGGGTGAGCATTGAACTCGG | DSB hotspot |

## 5.4 $OD_{600}$ prior to Meiotic Time Courses

Numbering of meiotic time courses (TC) corresponds to numbering on VBC server (\\share.mfpl.ac.at\vbc\CHROM\KLEIN\Lisa_VBC\time courses). Typical volumes in SPS and SPM were 20 to 45 ml, except for Protec-seq TCs (TC28, TC31 and TC33), where larger volumes were used (2 x 200 ml or 4 x 300 ml in baffled flasks).

**Table 5.4-1:** $OD_{600}$ in SPS and SPM before meiotic time course experiments

| TC (date) | FKy | Genotype (short) | Species | SPS $OD_{600}$ | SPM $OD_{600}$ |
|---|---|---|---|---|---|
| **TC2 (2021-03-05)** | 6336 | *msh5*Δ | *S. c.* | 1.30 | 1.07 |
| | 6359 | *msh5*Δ*, sgs1-mn* | *S. c.* | 1.23 | 1.09 |
| | 6365 | *msh5*Δ*, sgs1-mn, spp1*Δ | *S. c.* | 1.36 | 1.07 |
| | 6290 | *msh5*Δ*, spp1*Δ | *S. c.* | 1.32 | 0.97 |
| | 6362 | *msh5*Δ*, rec114-8D* | *S. c.* | 1.16 | 1.03 |
| **TC5 (2021-04-09)** | 8819 | *msh4*Δ | *S. c.* | 1.64 | 0.90 |
| | 8813 | *msh4*Δ*, sgs1-mn* | *S. c.* | 1.44 | 0.88 |
| | 8811 | *msh4*Δ*, sgs1-mn, spp1*Δ | *S. c.* | 0.98 | 0.92 |
| | 8812 | *msh4*Δ*, spp1*Δ | *S. c.* | 0.93 | 0.95 |
| **TC9 (2021-05-25)** | 6106 | *zip3*Δ | *S. c.* | 1.34 | 1.24 |
| | 5247 | *zip3*Δ*, sgs1-mn* | *S. c.* | 1.55 | 1.29 |
| | 6142 | *zip3*Δ*, sgs1-mn, spp1*Δ | *S. c.* | 1.10 | 1.20 |
| | 5539 | *spp1*Δ | *S. c.* | 1.28 | 1.28 |
| **TC11 (2021-07-13)** | 6338 | *zip4*Δ | *S. c.* | 1.08 | 1.18 |
| | 6374 | *zip4*Δ*, sgs1-mn* | *S. c.* | 1.19 | 1.23 |
| | 6371 | *zip4*Δ*, sgs1-mn, spp1*Δ | *S. c.* | 1.06 | 1.14 |
| | 6296 | *zip4*Δ*, spp1*Δ | *S. c.* | 0.98 | 1.08 |

| | | | | | |
|---|---|---|---|---|---|
| **TC15 (2022-10-05)** | 8909 | *zip3Δ, sgs1-mn, SPO11-myc18* | *S. c.* | 1.51 | 1.26 |
| | 9196 | *H3K4A, SPO11-myc18* | *S. c.* | 1.41 | 1.13 |
| | 9198 | *zip3Δ, sgs1-mn, H3K4A* | *S. c.* | 1.43 | 1.16 |
| | 9217 | *zip3Δ, sgs1-mn, H3K4A, SPO11-myc18* | *S. c.* | 1.07 | 1.19 |
| **TC23 (2023-06-01)** | 6374 | *zip4Δ, sgs1-mn* | *S. c.* | 0.98 | 1.16 |
| | 6371 | *zip4Δ, sgs1-mn, spp1Δ* | *S. c.* | 1.00 | 1.07 |
| | 6296 | *zip4Δ, spp1Δ* | *S. c.* | 1.01 | 1.08 |
| | 6377 | *zip4Δ, rec114-8D* | *S. c.* | 0.98 | 1.06 |
| | 6368 | *zip4Δ, sgs1-mn, rec114-8D* | *S. c.* | 1.00 | 1.16 |
| **TC26 (2023-08-24)** | 6374 | *zip4Δ, sgs1-mn* | *S. c.* | 1.01 | 1.21 |
| | 9341 | *zip4Δ, mer2-sid* | *S. c.* | 1.01 | 1.20 |
| | 9344 | *zip4Δ, sgs1-mn, mer2-sid* | *S. c.* | 1.07 | 1.14 |
| **TC28 (2023-09-27)** | 6634 | *SPO11-myc18* | *S. k.* | 1.27 | 1.26 |
| **TC31 (2023-11-24)** | 9407 | *zip4Δ, sgs1-mn, SPO11-myc* | *S. c.* | 1.34 | 1.26 |
| | 9410 | *zip4Δ, sgs1-mn, spp1Δ, SPO11-myc18* | *S. c.* | 1.29 | 1.27 |
| **TC32 (2023-11-29)** | 9338 | *mer2-sid* | *S. c.* | 1.36 | 1.28 |
| | 9413 | *zip4Δ, sgs1-mn, rec114-8D, spp1Δ* | *S. c.* | 1.18 | 1.25 |
| | 9416 | *zip4Δ, rec114-8D, spp1Δ* | *S. c.* | 1.26 | 1.25 |
| **TC33 (2023-12-06)** | 1358 | *SPO11-myc18* | *S. c.* | 1.25 | 1.25 |
| | 5525 | *SPO11-myc18, spp1Δ* | *S. c.* | 1.16 | 1.28 |
| **TC34 (2023-12-27)** | 9303 | *zip4Δ, sgs1-mn, H3K4A* | *S. c.* | 1.19 | 1.21 |

| | | | | | |
|---|---|---|---|---|---|
| | 9344 | *zip4Δ, sgs1-mn, mer2-sid* | *S. c.* | 1.25 | 1.26 |
| | 9396 | *zip4Δ, sgs1-mn, mer2-sid, H3K4A* | *S. c.* | 1.31 | 1.16 |
| | 9404 | *zip4Δ, sgs1-mn, mer2-sid, spp1Δ* | *S. c.* | 1.06 | 1.18 |
| **TC (2024-05-07) by Viktoria Prast** | 9196 | *SPO11-myc, H3K4A* | *S. c.* | 1.10 | 1.22 |

*S. c.* … *Saccharomyces cerevisiae* SK1

*S. k.* … *Saccharomyces kudriavzevii*

## 5.5 Sample IDs for Protec-seq

**Table 5.5-1:** Overview of all Protec-seq samples mentioned in this study

| Sample | ID | Fky | t | Genotype | TC date | TC | Prep |
|---|---|---|---|---|---|---|---|
| vp052.IP | 296558 | 1358 | t3.5 | *SPO11-myc18, wt* | 2023-12-06 | LK | LK |
| vp053.IP | 296559 | 1358 | t4 | *SPO11-myc18, wt* | 2023-12-06 | LK | LK |
| vp054.IP | 296560 | 5525 | t3.5 | *SPO11-myc18, spp1Δ* | 2023-12-06 | LK | LK |
| vp055.IP | 296561 | 5525 | t4 | *SPO11-myc18, spp1Δ* | 2023-12-06 | LK | LK |
| vp056.IP | 296562 | 9407 | t6 | *SPO11-myc18, zip4Δ, sgs1-mn* | 2023-11-24 | LK | LK |
| vp057.IP | 296563 | 9410 | t6 | *SPO11-myc18, zip4Δ, sgs1-mn, spp1Δ* | 2023-11-24 | LK | LK |
| vp058.IP | 296564 | 1358 | t5 | *SPO11-myc18, wt* | 2023-12-06 | LK | VP |
| vp059.IP | 296565 | 1358 | t6 | *SPO11-myc18, wt* | 2023-12-06 | LK | VP |
| vp060.IP | 296566 | 5525 | t5 | *SPO11-myc18, spp1Δ* | 2023-12-06 | LK | VP |
| vp061.IP | 296567 | 5525 | t6 | *SPO11-myc18, spp1Δ* | 2023-12-06 | LK | VP |
| vp063.IP | 296569 | 3088 | t6 | *untagged, wt* | 2023-12-06 | LK | VP |
| vp082.IP | 296618 | 9196 | t3.5 | *SPO11-myc18, H3K4A* | 2024-05-07 | VP | VP |
| vp083.IP | 296619 | 9196 | t4 | *SPO11-myc18, H3K4A* | 2024-05-07 | VP | VP |
| vp084.IP | 296620 | 9196 | t6 | *SPO11-myc18, H3K4A* | 2024-05-07 | VP | VP |

t … timepoint
TC … meiotic time course performed by
Prep … Protec-seq and Library preparation
LK … Lisa Kainz
VP … Viktoria Prast

## 5.6 ImageJ Macros

Scripts were designed for (Fiji Is Just) ImageJ 2.14.0/1.54f; Java 1.8.0_172 [64-bit] and run on Windows 10/11 or Mac OS X. The python-based language IJ1 Macro was chosen for the macros.

### 5.6.1 Initial assessment of intensity maximum

This macro measures the maximum intensity per image and creates an output file containing the average maximum intensity, as well as the highest and lowest maximum intensity of all analysed images. This script serves as the starting point for selecting optimal values for `upperorange`, `upperred`, and `upperblue` for the script that converts .obf files to the 16-bit and 8-bit .tif formats (**Section 5.6.2**).

The script is saved as: \\share.mfpl.ac.at\vbc\CHROM\KLEIN\Lisa_VBC\spreads\macro scripts fiji\initial assessment of global intensity of 16bit.ijm

```
parentdir = getDirectory("Choose Directory");
list = getFileList(parentdir);
listOrange = getFileList(parentdir);
listRed = getFileList(parentdir);

orangename = "STAR ORANGE_Rad51" //" - Rec8"
redname = "STAR RED_Rec8"   //" - Red1"
bluename = "Alexa_488"

j = 0;
for (i = 0; i <list.length; i++) {
 if (endsWith(list[i], ".obf")) { //change to file name
              listRed[j] = list[i];
              print(j + " " + listRed[j]);
              j=j+1;
}
       }

imagenumber = j
print("Number of different images= " + j)

run("Clear Results");
run("Close All");
for (i = 0; i <list.length; i++) {
       if (endsWith(list[i], ".obf")) {
```

```
	run("Bio-Formats Importer", "open=[" + parentdir + list[i] + "]"+ " autoscale
	color_mode=Default rois_import=[ROI manager] view=Hyperstack
	stack_order=XYCZT series_2"); //change to intended series
	run("Set Measurements...", "min display add redirect=None decimal=3");
	//selectWindow(listRed[i] + " - STAR RED.STED");
	run("Measure");
}
	}

run("Summarize");
selectWindow("Results");
saveAs("Results", parentdir + redname + " assessment of global maximum of 16bit
images.csv");

run("Clear Results");
run("Close All");
for (i = 0; i <list.length; i++) {
	if (endsWith(list[i], ".obf")) {
	run("Bio-Formats Importer", "open=[" + parentdir + list[i] + "]"+ " autoscale
	color_mode=Default rois_import=[ROI manager] view=Hyperstack
	stack_order=XYCZT series_1"); //change to intended series
	run("Set Measurements...", "min display add redirect=None decimal=3");
	//selectWindow(listRed[i] + " - STAR RED.STED");
	run("Measure");
}
	}

run("Summarize");
selectWindow("Results");
saveAs("Results", parentdir + orangename + " assessment of global maximum of 16bit
images.csv");

run("Clear Results");
run("Close All");
for (i = 0; i <list.length; i++) {
	if (endsWith(list[i], ".obf")) {
	run("Bio-Formats Importer", "open=[" + parentdir + list[i] + "]"+ " autoscale
	color_mode=Default rois_import=[ROI manager] view=Hyperstack
	stack_order=XYCZT series_3"); //change to intended series
	run("Set Measurements...", "min display add redirect=None decimal=3");
	//selectWindow(listRed[i] + " - STAR RED.STED");
	run("Measure");
}
	}

run("Summarize");
```

```
selectWindow("Results");
saveAs("Results", parentdir + bluename + " assessment of global maximum of 16bit
images.csv");
run("Clear Results");
run("Close All");


//https://imagej.nih.gov/ij/developer/macro/functions.html#S
```

### 5.6.2 Conversion of .obf files to 16-bit and 8-bit .tif files

This macro converts STED microscopy images in .obf format into 16-bit and 8-bit .tif files. It creates composites of the 8-bit .tif files containing the STAR ORANGE and STAR RED channels (2col.tif) and the STAR ORANGE, STAR RED, and Alexa 488 channels (3col.tif). flash.tif files are then created from the two or three channel composites and the STAR ORANGE channel, resulting in interactive movies.

The script is saved as: \\share.mfpl.ac.at\vbc\CHROM\KLEIN\Lisa_VBC\spreads\macro scripts fiji\obfTOtifandDNA_v4-LK.ijm

```
parentdir = getDirectory("Choose Directory");
list = getFileList(parentdir);
upperorange = 350; // has to be determined for each data set
upperred = 550;   // has to be determined for each data set (medium = 400)
upperblue = 500;   // has to be determined for each data set

orangename = " - STAR ORANGE_Rad51" //" - rec8"
redname = " - STAR RED_Rec8"   //" - red1"
bluename = " - Alexa 488_DNA"  //" - DNA"

oname = " - STAR ORANGE"
rname = " - STAR RED"
bname = " - Alexa 488"


for (i = 0; i <list.length; i++) {
       if (endsWith(list[i], ".obf")) {
       run("Bio-Formats Importer", "open=[" + parentdir + list[i] + "]"+ autoscale
       color_mode=Default rois_import=[ROI manager] view=Hyperstack
       stack_order=XYCZT series_1 series_2 series_3");

       selectWindow(list[i] + oname + ".STED");
       setMinAndMax(0, upperorange);
```

```
run("8-bit");
saveAs("Tiff", parentdir + list[i].substring(0,list[i].length()-4) +
orangename + "_8-bit.STED");
selectWindow(list[i] + rname + ".STED");
setMinAndMax(0, upperred);
run("8-bit");
saveAs("Tiff", parentdir + list[i].substring(0,list[i].length()-4) + redname
+ "_8-bit.STED");
selectWindow(list[i] + bname + ".STED");
setMinAndMax(0, upperblue);
run("8-bit");
saveAs("Tiff", parentdir + list[i].substring(0,list[i].length()-4) + bluename
+ "_8-bit.STED");


/*run("Merge Channels...", "c2=[" + list[i].substring(0,list[i].length()-4) +
redname + ".tif] c1=[" + list[i].substring(0,list[i].length()-4) + orangename
+ ".tif] c3=[" + list[i].substring(0,list[i].length()-4) + bluename + ".tif]
create keep");
saveAs("Tiff", parentdir + list[i].substring(0,list[i].length()-4) + "
3col");
run("Make Composite");
run("Stack to RGB");
run("Add Slice");
selectWindow(list[i].substring(0,list[i].length()-4) + orangename + ".tif");
run("Red");
run("Select All");
run("Copy");
selectWindow(list[i].substring(0,list[i].length()-4) + " 3col.tif (RGB)");
run("Paste");
saveAs("Tiff", parentdir + list[i].substring(0,list[i].length()-4) + " 3col
flash");*/


run("Merge Channels...", "c1=[" + list[i].substring(0,list[i].length()-4) +
orangename + "_8-bit.tif] c2=[" + list[i].substring(0,list[i].length()-4) +
redname + "_8-bit.tif] create keep");
saveAs("Tiff", parentdir + list[i].substring(0,list[i].length()-4) + "
2col");
run("Stack to RGB");
run("Add Slice");
selectWindow(list[i].substring(0,list[i].length()-4) + orangename + "_8-
bit.tif");
run("Red");
run("Copy");
selectWindow(list[i].substring(0,list[i].length()-4) + " 2col.tif (RGB)");
//selectWindow("Composite (RGB)");
```

```
        run("Paste");
        saveAs("Tiff", parentdir + list[i].substring(0,list[i].length()-4) + " 2col
        flash");

    run("Close All");
        }
}
run("Close All");

for (i = 0; i <list.length; i++) {
        if (endsWith(list[i], ".obf")) {
        run("Bio-Formats Importer", "open=[" + parentdir + list[i] + "]"+ " autoscale
        color_mode=Default rois_import=[ROI manager] view=Hyperstack
        stack_order=XYCZT series_1 series_2 series_3");

        selectWindow(list[i] + oname + ".STED");
        setMinAndMax(0, upperorange);
        saveAs("Tiff", parentdir + list[i].substring(0,list[i].length()-4) +
        orangename + "_16-bit.STED");
        run("8-bit");
        //saveAs("Tiff", parentdir + list[i].substring(0,list[i].length()-4) +
        orangename + ".STED");
        selectWindow(list[i] + rname + ".STED");
        setMinAndMax(0, upperred);
        saveAs("Tiff", parentdir + list[i].substring(0,list[i].length()-4) + redname
        + "_16-bit.STED");
        run("8-bit");
        //saveAs("Tiff", parentdir + list[i].substring(0,list[i].length()-4) +
        redname + ".STED");
        selectWindow(list[i] + bname + ".STED");
        setMinAndMax(0, upperblue);
        saveAs("Tiff", parentdir + list[i].substring(0,list[i].length()-4) + bluename
        + "_16-bit.STED");
        run("8-bit");
        //saveAs("Tiff", parentdir + list[i].substring(0,list[i].length()-4) +
        bluename + ".STED");

        run("Merge Channels...", "c2=[" + list[i].substring(0,list[i].length()-4) +
        redname + "_16-bit.tif] c1=[" + list[i].substring(0,list[i].length()-4) +
        orangename + "_16-bit.tif] c3=[" + list[i].substring(0,list[i].length()-4) +
        bluename + "_16-bit.tif] create keep");
        saveAs("Tiff", parentdir + list[i].substring(0,list[i].length()-4) + "
        3col");
        run("Make Composite");
        run("Stack to RGB");
        run("Add Slice");
```

```
        selectWindow(list[i].substring(0,list[i].length()-4) + orangename + "_16-
        bit.tif");
        run("Red");
        run("Select All");
        run("Copy");
        selectWindow(list[i].substring(0,list[i].length()-4) + " 3col.tif (RGB)");
        run("Paste");
        saveAs("Tiff", parentdir + list[i].substring(0,list[i].length()-4) + " 3col
        flash");

    run("Close All");
        }
}
run("Close All");
```

### 5.6.3 Assessing foci number and intensity

This macro was used to determine the number and intensity of foci in 16-bit .tif files, typically from the STAR ORANGE channel (STED microscopy). The area in which the foci were analysed was manually marked. A separate output file in .csv format is saved for each image, containing the size and intensity of each individual focus. The output files were then combined into a single file using R and RStudio.

The script is saved as: \\share.mfpl.ac.at\vbc\CHROM\KLEIN\Lisa_VBC\spreads\macro scripts fiji\foci_v2-LK.ijm

```
parentdir = getDirectory("Choose Directory");
list = getFileList(parentdir);
listflash  = getFileList(parentdir);
listorange  = getFileList(parentdir);

j = 0;
for (i = 0; i <list.length; i++) {
 if (endsWith(list[i], "ORANGE_16-bit.tif")) {
             listorange[j] = list[i];
             print(j + " " + listorange[j]);
}
 if (endsWith(list[i], "2col flash.tif")) {
             listflash[j] = list[i];
             print(j + " " + listflash[j]);
             j=j+1;
}
       }
```

```
imagenumber = j
print("Number of different images= " + j)

for (i = 0; i <imagenumber; i++) {
open(parentdir + listflash[i] );
open(parentdir + listorange[i] );

selectWindow(listflash[i]);
setLocation(500, 200, 2000, 1000);
setTool("freehand");
setMinAndMax(0, 92);
doCommand("Start Animation [\\]");
waitForUser("Select area -MUST INCLUDE UPPER LEFT CORNER!! for analysis by freehand
tool to exclude polycomplex!! Click OK when done");

selectWindow(listorange[i]);
run("Restore Selection");
run("Create Mask");
selectWindow(listorange[i]);
run("Duplicate...", " ");
run("Gaussian Blur...", "sigma=1");
run("Set Measurements...", "area integrated display redirect=None decimal=3");
run("Auto Local Threshold", "method=Bernsen radius=5 parameter_1=0 parameter_2=0
white");
run("Analyze Particles...", "size=4-400 pixel circularity=0.10-1.00 show=Outlines
display exclude clear include summarize add");

selectWindow(listorange[i]);
roiManager("select", 0);
roiManager("update");

roicount = roiManager("count");
run("Clear Results");
for (n = 0; n <roicount; n++) {
roiManager("select", n);
run("Measure");
}
saveAs("Results", parentdir + listflash[i].substring(0,listflash[i].length()-10) +
"_number Areas Intensities.csv");
setLocation(500, 200, 2000, 1000);
waitForUser("Press OK when done");
roiManager("delete");
run("Close All");
}
```

### 5.6.4 Analysis of associated axial fragments

This is an interactive macro in which the user manually marks all axis fragments that appear associated, typically in the STAR RED channel (STED microscopy). A .csv output file is created for each image, containing the number and length of each individual fragment. These files were later combined into a single file using R and RStudio. To transform the length measurements into µm, all lengths were divided by 0.121 (1 µm corresponds to 0.121 arbitrary units).

The script is saved as: \\share.mfpl.ac.at\vbc\CHROM\KLEIN\Lisa_VBC\spreads\macro scripts fiji\Analyze Pseudosynapsis PC Windows-LK v2.ijm

```
//pseudosynapsis
parentdir = getDirectory("Choose Directory");
list = getFileList(parentdir);
listTIF = getFileList(parentdir);
brightsetting = 50

run("Color Picker...");
setForegroundColor(255, 255, 255); //sets the color of the brush to white
setBackgroundColor(255, 255, 255); //sets the color of the brush to white
selectWindow("CP");
run("Close");

j = 0;
for (i = 0; i <list.length; i++) {
 if (endsWith(list[i], "RED 8-bit.tif")) {
              listTIF[j] = list[i];
              print(j + " " + listTIF[j]);
              j=j+1;
}
       }

imagenumber = j;
print("Number of different images= " + j)
print(parentdir)
```

```
run("Clear Results");


for (i = 0; i <imagenumber; i++) {
open(listTIF[i]);
selectWindow(listTIF[i]);
setMinAndMax(0, brightsetting);
run("Duplicate...", listTIF[i]);
run("Multiply...", "value=0.900");
rename(listTIF[i].substring(0,listTIF[i].length()-4) + " PS marked.tif");
setLocation(500, 200, 2000, 1000);
//setMinAndMax(0, brightsetting);
run("Show All");
selectWindow(listTIF[i].substring(0,listTIF[i].length()-4) + " PS marked.tif");
setThreshold(254, 255);
setTool("Paintbrush Tool");
run("Paintbrush Tool Options...", "brush=6");
selectWindow(listTIF[i].substring(0,listTIF[i].length()-4) + " PS marked.tif");
waitForUser("Select Pseudosynapsis! Don't make a mistake, you can't go back. Click
OK when done");
run("Measure");
run("Analyze Particles...", "display exclude clear include summarize add");
selectWindow("Results");
saveAs("Results", parentdir + listTIF[i].substring(0,listTIF[i].length()-4) + "
pseudosynapsis results.csv");
selectWindow(listTIF[i].substring(0,listTIF[i].length()-4) + " PS marked.tif");
saveAs("Tiff", parentdir + listTIF[i].substring(0,listTIF[i].length()-4) + " PS
marked.tif");
run("Close All");
}


selectWindow("Summary");
saveAs("Results", parentdir + listTIF[i].substring(0,listTIF[i].length()-4) + "
pseudosynapsis summary.csv");
```

## 5.7 R Scripts

The script was designed for R version 4.1.3 (2022-03-10) and RStudio 2022.07.1+554.

### 5.7.1 Detailed analysis of foci number and intensity

The script requires the output files in .csv format of the ImageJ macro that assesses the number and intensity of foci described above (**Section 5.6.3**). THe output is a .pdf file containing: a boxplot with the number of foci per nucleus, a bar plot according to foci number/nucleus as foci classes, a heatmap of the foci brightness according to the number of foci/nucleus and foci classes, a density plot and a second boxplot with all foci overall and their brightness. To make plots of the different mutants comparable, the x-axis was set to a fixed length for Rad51 and Zip3 foci. However, it can also be determined automatically (`xlimright`).

Scripts to analyse Rad51 and Zip3 foci are saved as: \\share.mfpl.ac.at\vbc\CHROM\KLEIN\Lisa_VBC\R\For Rad51 Foci Plotting different color axis length (LK adapted).R and \\share.mfpl.ac.at\vbc\CHROM\KLEIN\Lisa_VBC\R\For Zip3 Foci Plotting different color axis length (LK adapted).R

```
# Files need to be stored in subfolders named after their time course like this
"*anything* TC *Date*" (Example: TC 2017-09-17)
library(RColorBrewer)      #Color selection along a sequence of 201 steps
library(data.table)

InDirectory <-  "//share.mfpl.ac.at/vbc/CHROM/KLEIN/Lisa_VBC/spreads/TC9 zip3del
25-05-2021/t5/Rec8 Rad51/t5 5539 spp1 Rec8 Rad51/"      # Folder containing folders
with foci quantifications  (t6 6338 zip4??? Rec8 Rad51)
resultfilepattern <- " peakresult.txt"            # Ending of the peakresult .txt
files. Don't forget the space if there is one. Example: " valley5000 vol2000
peakresult.txt"
focifile <- " foci.txt"                                          # Same as in
"peakresultfile". Example: "foci.txt"
OutDirectory <- InDirectory
#meiotic_progression <- c(100, 100, 100, 100, 100)        # Percentage of nuclei
past M1 as determined via dapi counting, order date>strain>timepoint. If these have
not been determined, deactivate line 80 & 81
focitype <- "Rad51"
strains <- c("5539")                       # All strains to compare (must be in
filenames)
genotype <- c("spp1")   # (must be in filenames AND MATCH THE ORDER OF STRAINS!!!,
There is the problem of "none-uniqueness" (such as that zip4 is in all names...,
therefore we use hard coding))
```

```
timepoints <- c("t5")                                # Timepoint per strain
date <- "25-05-2022"
experiments<-length(strains)*length(timepoints)

##FK for Lisa
#Accumulating data and primary processing
tab<-0; tab<-data.table()
for(names in (list.files(InDirectory, pattern = "Intensities.csv"))) {
  print(paste0(InDirectory,names))
  tab<-rbind(tab,fread(paste0(InDirectory,names)), fill=TRUE)
}
tab<-tab[complete.cases(V1,Label,Area,IntDen), ]
tab$Label<-substring(tab$Label,1,nchar(tab$Label)-10)
tab1<-tab[,':='(focinumber=.N, strain=strains[sapply(strains, grepl, Label)],
genotype=genotype[sapply(strains, grepl, Label)],
timepoint=timepoints[sapply(timepoints, grepl, Label)]), by=Label]
colnames(tab1)[5]<-c("TotalIntensity")
setorder(tab1,strain,timepoint,focinumber,TotalIntensity)

tabimages <- tab1[,.(focinumber=unique(focinumber),strain=unique(strain),
timepoint=unique(timepoint),
straintime=paste0(unique(strain),unique(timepoint)),maxIntensityImg=max(TotalIntens
ity)), by = Label]
# write.table(tabimages,file=paste0((unlist(strsplit(InDirectory,"//"))), " ",
timepoints, " ", strains, " ", genotype, " ", focitype, " FociNumber_Nucleus.txt"),
append=FALSE, quote=FALSE, sep="\t", dec=".", row.names=FALSE, col.names=TRUE)
write.table(tabimages, file= paste(OutDirectory, " ", timepoints, " ", strains, "
", genotype, " ", focitype, " FociNumber_Nucleus.txt", sep = ""), append=FALSE,
quote=FALSE, sep="\t", dec=".", row.names=FALSE, col.names=TRUE)

maxfoci <- max(tabimages[,focinumber])    #Determins the maximal number of foci per
nucleus of al experiments
tabexperiments <-
tabimages[,.(focinumber.sum=sum(focinumber),strain=unique(strain),
genotype=genotype[which(strains==unique(strain))],
timepoint=unique(timepoint),nucnumber=.N, maxIntensityExp=max(maxIntensityImg)), by
= straintime]
focinumberdensity<-tabimages[,.(fociclass=.N), by= .(focinumber,straintime)]
classcollaps<-focinumberdensity[ ,.(classnumbers=.N), by = straintime]
setorder(focinumberdensity,straintime,focinumber)
focinumberindex<-
1+rep(c(0,(maxfoci+1),2*(maxfoci+1),3*(maxfoci+1)),classcollaps$classnumber)+focinu
mberdensity$focinumber    # creates indices from focinumber for use in density
# focinumberdensity0<-0; focinumberdensity0<-data.table()
```

```
# focinumberdensity0[,':='(focinumber=rep(0:(maxfoci),experiments),
straintime=rep(tabexperiments$straintime,each = (maxfoci+1)),
fociclass=rep(0,(maxfoci+1)*experiments))]
# setorder(focinumberdensity0,straintime,focinumber)
# focinumberdensity0$fociclass[focinumberindex]<-focinumberdensity$fociclass
# tabexperiments
# write.table(tab1, file=paste0((unlist(strsplit(InDirectory,"//"))), " ",
timepoints, " ", strains, " ", genotype, " ", focitype, " foci_data.txt"),
append=FALSE, quote=FALSE, sep="\t", dec=".", row.names=FALSE, col.names=TRUE)
write.table(tab1, file= paste(OutDirectory, " ", timepoints, " ", strains, " ",
genotype, " ", focitype, " foci_data.txt", sep = ""), append=FALSE, quote=FALSE,
sep="\t", dec=".", row.names=FALSE, col.names=TRUE)

#Plot
ramp <- colorRamp(brewer.pal(8, "RdBu"), bias = .2)            # bias 0.5 compacts
the "low colors" and spreads out the "high"2" ones
sequential <- rgb( ramp(seq(1, 0, length = 256)), max = 255)    #, max = 255
#sequential <- rgb( ramp(c(seq(1, 0.8, length = 51), seq(0.8, 0.2, length = 153),
seq(0.2,0, length = 52))))    #, max = 255

for (o in 1:length(tabexperiments$straintime)){       #The loop for the actual
plotting
  straino <-   tabexperiments$strain[o]
  genotypeo <- tabexperiments$genotype[o]
  timepointo <-   tabexperiments$timepoint[o]
  straintimeo <-  tabexperiments$straintime[o]

pdf(file=paste(OutDirectory, focitype, "_foci, ",straino, "_", timepointo,
"_summary_plot.pdf", sep = ""), height = 15, width = 10)      #Saves files as pdf.
Placing this inside the loop causes a seperate .pdf for each plot, putting it
before the loop causes all plots to be saved to the same .pdf
par(mar=c(2,0.2,0.2,0.2) + 0.1, oma= c(0,3.2,0,1) +0.1)        #Sets the parameters
of the page

  #Boxplot and title
  par(fig = c(0, 1, 0.79, 0.97))     #Sets the position of the first plot
  quantilf <- as.vector(quantile(tabimages[strain == straino &
timepoint==timepointo,focinumber], probs = c(0.05, 0.95, 0.99)))
  digits <- floor(log10(quantilf[3]))
  # xlimright <- ceiling(quantilf[3]/10^digits)*10^digits
  xlimright <- 300 #defines axis length so that all compared plots have the same
axis length
  boxplot(tabimages[strain == straino & timepoint==timepointo,focinumber],
horizontal = TRUE, ylim=c(0,xlimright), col = FALSE, xaxt = 'n', ann = FALSE, frame
= FALSE, boxlwd="2", whisklwd="2",staplelwd="2",medlwd="5",outlwd="2")   #Boxplot
with all parameters
```

```
  #Title
  mtext(paste0(focitype, " Foci, ","Strain: ", tabexperiments$strain[o], ",
Genotype: ", genotype[which(strains==straino)], ", Timepoint = ",
tabexperiments$timepoint[o], ",  \nNumber of Nuclei Analyzed: ",
tabexperiments$nucnumber[o]), outer=TRUE,  cex=1.5, side=3, line = -3)
  mtext(paste0("Boxplot: Foci Numbers, Median = ", median(tabimages[strain ==
straino & timepoint==timepointo,focinumber]),", Mean = ",
round(mean(tabimages[strain == straino & timepoint==timepointo,focinumber]),1), ",
Stdev = +-", round(sd(tabimages[strain == straino &
timepoint==timepointo,focinumber]), digits=2)), side=3, line=-1.8)     #Title of
the plot itself

  par(fig = c(0, 1, 0.73, 0.93), new = TRUE)      #Sets the position of the plot

  #barplot(value = focinumberdensity0[straintime == straintimeo, fociclass], group
= c(0,xlimright), ylim= c(0,15), xlim=c(0,xlimright), ylab = "", col =
"DarkOrange1", border = NA, cex.axis = 0.8)  #, labels = FALSE
  v1 <- focinumberdensity[straintime == straintimeo, focinumber]
  v2 <- rep(0,length(focinumberdensity[straintime == straintimeo, focinumber]))
  v3 <- focinumberdensity[straintime == straintimeo, fociclass]
  plot(x = NULL, y = NULL, xlim=c(0,xlimright), ylim= c(0,15), xaxt = 'n', yaxt =
'n', bty='n', ann = FALSE, frame = FALSE)     #Plot for the focus/global
  segments(v1,v2,v1,v3, lwd=750/maxfoci, col=  "#D6604D")
  #barplot(height = focinumberdensity0[straintime == straintimeo, fociclass],
names.arg  = paste0("",1:length(focinumberdensity0[straintime == straintimeo,
fociclass])), ylim= c(0,15), xlim=c(0,xlimright), ylab = "", col = "DarkOrange1",
border = NA, cex.axis = 0.5)
  text(x=125, y=6, labels = "Barplot: Class Frequencies According to Foci Number")
#Title of the plot itself
  mtext("Class frequencies", side=2, cex = 0.8, line=2, at = 2)     #Y-axis label
  axis(1,at=seq(0,xlimright), line= -0.3, labels = FALSE, lwd.ticks = 0.2)
  axis(1,at=seq(0,xlimright, 20), line = -0.3, labels = round(seq(0,xlimright,
20)), lwd.ticks = 1)
  axis(2,seq(0,5,1), line=-2)

  #1st Brightness plot without bars
  par(fig = c(0, 1, 0.52, 0.70), new = TRUE)      #Sets the position of the plot
  plot(x = NULL, y = NULL, xlim=c(0,xlimright),ylim=c(0,100), ylab = "", cex.axis =
0.8)     #Plot for the focus/global
  mtext("Heatmap: Foci Normalized by Global Maximum", side=3, line=0.2)     #Title
of the plot itself
  mtext("Foci percentile", side=2, cex = 0.8, line=2)     #Y-axis label

  maxIntensityExpV<-tabexperiments$maxIntensityExp[o]
```

```
  fociperExp <-focinumberdensity[straintime ==
tabexperiments$straintime[o],focinumber]
  classperExp <- focinumberdensity[straintime ==
tabexperiments$straintime[o],fociclass]
  v1<-rep(fociperExp,fociperExp*classperExp)  #origin, destination x
  v2<-sequence(nvec = fociperExp*classperExp,from =
0)/v1/rep(classperExp,classperExp*fociperExp)*100                    #y-
starts__sequence(nvec =2:4, from=0, by=1) --> 0 1 0 1 2 0 1 2 3
  v3<-sequence(nvec = fociperExp*classperExp,from =
1)/v1/rep(classperExp,classperExp*fociperExp)*100                    #y-
ends__  in steps of 1/fociperClass (/v1/class...)
  vcol <- tab1[strain == tabexperiments$strain[o] & timepoint ==
tabexperiments$time[o],TotalIntensity]
  #segments(v1,v2,v1,v3, col= rgb(0,0,0,alpha = vcol/max(vcol)), lwd=750/maxfoci)
#single bars of averages for the first brightness plot (linear)
  segments(v1,v2,v1,v3, col= sequential[ceiling(vcol/max(vcol)*256)],
lwd=750/maxfoci)   #single bars of averages for the first brightness plot (linear)
  # segments(v1,v2,v1,v3, col= sequential[log2(vcol/maxIntensityExpV[o]*256)*32],
lwd=500/maxfoci)   #single bars of averages for the first brightness plot (log
scale)

  #legend of global
  par(fig = c(0, 0.5, 0.46, 0.56), lend=1, new = TRUE)      #Sets the position of
the next plot
  plot(x = NULL, y = NULL, ylim=c(0.5,maxfoci+0.5), xlim=c(0, 1), xaxt = 'n', yaxt
= 'n', bty='n')    #Provides the plot that houses the legend. "bty='n'" causes the
plot boundaries to be invisible
  segments((0:249)/250,1,(1:250)/250,1, col= sequential[1:250], lwd=15)   #single
bars of averages for the first brightness plot (linear)
  axis(1,at=seq(0,250,25)/250,seq(0,250,25), cex.axis = 0.8, line = 0.2)
#Draws a log2 scale below the legend with the lowest brightness result as the
lowest value

  #2nd Brightness plot without bars
  par(fig = c(0, 1, 0.25, 0.44), new = TRUE)      #Lines 127-153 have the same
annotations as in lines 99-123 except where stated otherwise
  #plot(x = NULL, y = NULL, xlim=c(-0.5,maxfoci+0.5),ylim=c(0,100), ylab = "",
cex.axis = 0.8)
  subtab1o <- tab1[strain == straino & timepoint==timepointo,]
  setorder(subtab1o,TotalIntensity)
  focinumbero <- length(subtab1o[,TotalIntensity])
  maxTotalo <- max(subtab1o[,TotalIntensity])
  quantilo <- as.vector(quantile(subtab1o[,TotalIntensity], probs = c(0.05, 0.95,
0.99)))
  digits <- floor(log10(quantilo[3]))
 # xlimright <- ceiling(quantilo[3]/10^digits)*10^digits
```

```
  xlimright <- 10000 #defines axis length so that all compared plots have the same
axis length
  maxdenso1 <- max(density(x = subtab1o[,TotalIntensity], bw = xlimright/50)$y)
  maxdenso2 <- max(density(x = subtab1o[,TotalIntensity], bw = xlimright/250)$y)
  par(fig = c(0, 1, 0.25, 0.43), mgp=c(3,1,0), new = TRUE)     #Sets position for
the next plot
  plot(density(x = subtab1o[,TotalIntensity], bw = xlimright/50),
xlim=c(0,xlimright), ylim=c(-maxdenso1/2,maxdenso1*1.2), yaxt = 'n', xaxt = 'n',
ann = FALSE, frame = FALSE)      #Plots the vertical brightness boxplot
  polygon(density(x = subtab1o[,TotalIntensity], bw = xlimright/50), col=
"#92C5DE")      #Plots the vertical brightness boxplot
  axis(1,cex.axis = 0.8, line = 0.1)     #Adds an axis below the boxplot that goes
from 0 to 100
  v_expand <- hist(x = subtab1o[,TotalIntensity], breaks =
seq(0,xlimright/250+maxTotalo,xlimright/250), plot =
FALSE)$counts[findInterval(subtab1o[,TotalIntensity],seq(0,maxTotalo,xlimright/250)
)]

points(subtab1o[,TotalIntensity],(jitter(rep(0,focinumbero))*6*maxdenso2/max(v_expa
nd)*v_expand)-maxdenso1/4, col = rgb(0,0,0,alpha=0.4), cex=.3)      #Plots the
vertical brightness boxplot
  modo <- density(x = subtab1o[,TotalIntensity], bw =
xlimright/50)$x[which.max(density(x = subtab1o[,TotalIntensity], bw =
xlimright/50)$y)]
  text(modo,1.1*maxdenso1, paste0("Mode = ",round(modo)))
  #points(tab1[strain == straino &
timepoint==timepointo,TotalIntensity],jitter(rep(0,focinumbero), factor = density(x
= tab1[strain == straino & timepoint==timepointo,TotalIntensity], bw = 2000)), col
= rgb(0,0,0,alpha=0.1), cex=.3)      #Plots the vertical brightness boxplot
  mtext("Foci: Total Intensities", side=3, line=0.2)
  mtext("Density of foci intensities", side=2, cex = 0.8, line=2)

  #Brightness Plot
  par(fig = c(0, 1, 0.02, 0.22), new = TRUE)     #Sets position for the next plot
  boxplot(subtab1o[,TotalIntensity], horizontal = TRUE, ylim=c(0,xlimright), col =
FALSE, yaxt = 'n', xaxt = 'n', ann = FALSE, frame = FALSE, boxlwd="2",
whisklwd="2",staplelwd="2",medlwd="5",outlwd="2")      #Plots the vertical
brightness boxplot
  #abline(v=mean(tab[which(tab[,3] == strain & tab[,4] == timepoint & tab[,5] ==
date),6]*100))       #Plots a line through the boxplot at the mean, but it looks
like shit so keep it deactivated unless you need it
  segments(quantilo,rep(0.9,3),quantilo,rep(1.1,3), col= "#B2182B", lwd = 2)
  text(x = quantilo, y=rep(1.15,3), c(0.05, 0.95, 0.99), cex = 0.8, col =
"#B2182B")
  text(x = median(subtab1o[,TotalIntensity]), y = 1.3, paste("Median = ",
median(subtab1o[,TotalIntensity]), ", Mean = ",
```

```
round(mean(subtab1o[,TotalIntensity])), "+/-",
round(sd(subtab1o[,TotalIntensity]))), cex = 0.8, adj = 0)     #Adds the median
above the boxplot
  axis(1,cex.axis = 0.8, mgp=c(3,1,0), line = -2)     #Adds an axis below the
boxplot that goes from 0 to 100
 # text(x = 2*median(subtab1o[,TotalIntensity]), y = 1.5, paste("Foci: Total
Intensities"))     #Adds a title above the boxplot
  text(x = 2*median(subtab1o[,TotalIntensity]), y = 1.5)
   mtext("Boxplot of foci intensities", side=2, cex = 0.8, line=2)

  dev.off()     #Turns off the current device. Needed to tell the pdf function that
it's time to save.
}
```

## 5.8 Zusammenfassung

Homologe Chromosomen müssen in der ersten meiotischen Teilung durch Crossovers verbunden werden, um eine korrekte Segregation zu ermöglichen. Diese Crossovers entstehen durch die Reparatur von programmierten DNA-Doppelstrangbrüche (DSBs). DSBs treten vorwiegend in H3K4me3-angereicherten Promotorregionen auf, die üblicherweise in Chromatinschleifen lokalisiert sind, während die DSB-Maschinerie – Spo11 und seine Hilfsproteine Rec114, Mei4 und Mer2 – mit der Chromosomenachse assoziiert ist. Das PHD-Finger-Protein Spp1 wurde als Verbindungselement zwischen zukünftigen DSB-Stellen und der DSB-Maschinerie vorgeschlagen, da es gleichzeitig H3K4me3 und Mer2 binden kann. Interessanterweise ist *spp1*∆ synthetisch letal mit den zmm$^-$ Mutanten (ZMM-Proteine: Zip1–4, Msh4–5, Mer3, Spo16), die für die Reparatur von DSBs und die Festlegung von Crossovers erforderlich sind.

Diese Masterarbeit zeigt, dass Spp1 und H3K4me3 zur meiotischen DSB-Reparatur über eine Funktion beitragen, die über die reine DSB-Bildung hinausgeht. Der Verlust von Spp1 oder H3K4me3 führt zu deutlichen Verzögerungen in der meiotischen Progression, was auf eine beeinträchtigte Reparatur hinweist. STED-Mikroskopie konnte zeigen, dass in einem Hintergrund, in dem Zellen auf den unregulierten Joint Molecule (JM) Weg zurückgreifen, die Bildung stabiler axialer Assoziationen stark von Spp1 und H3K4me3 abhängt. Die Interaktion zwischen Mer2 und Spp1 ist für diese Stabilisierung jedoch nicht erforderlich. Zytologische Analysen und Genome-weite Protec-seq Daten verdeutlichen zudem, dass weder DSB-Anzahl, -Zeitpunkt noch -Positionierung allein die Defekte in *spp1*∆- und *H3K4A*-Mutanten erklären können. Diese Mutanten akkumulieren eine beträchtliche Menge an DSBs, die Reparaturfaktoren rekrutieren können, während eine veränderte DSB-Landschaft allein nur geringe Auswirkungen zeigt.

Wir schlagen daher vor, dass in der kombinierten Abwesenheit von ZMM-Proteinen und H3K4me3/Spp1, Helikasen oder Nukleasen unangemessen Zugang zu Stranginvasionsintermediaten erhalten, was zu deren Destabilisierung und zum Verlust axialer Assoziationen führt.

# 6 References

**Theses**

Kainz, L. (2022). Depletion analysis of meiotic H3K4me3 binding protein Spp1. Bachelor Thesis (University of Vienna).

Prast, V. (2016). A novel systematic screen for synthetic spore lethality with *spp1*Δ identifies the ZMM pathway and Vpr1, a new player in meiotic recombination. Master Thesis (University of Vienna).

**Journal Articles**

Acquaviva, L., Székvölgyi, L., Dichtl, B., Dichtl, B. S., de La Roche Saint André, C., Nicolas, A. and Géli, V. (2013) 'The COMPASS subunit Spp1 links histone methylation to initiation of meiotic recombination', *Science,* 339(6116), pp. 215-8.

Adam, C., Guérois, R., Citarella, A., Verardi, L., Adolphe, F., Béneut, C., Sommermeyer, V., Ramus, C., Govin, J., Couté, Y. and Borde, V. (2018) 'The PHD finger protein Spp1 has distinct functions in the Set1 and the meiotic DSB formation complexes', *PLOS Genetics,* 14(2), pp. e1007223.

Agarwal, S. and Roeder, G. S. (2000) 'Zip3 provides a link between recombination enzymes and synaptonemal complex proteins', *Cell,* 102(2), pp. 245-55.

Alani, E., Padmore, R. and Kleckner, N. (1990) 'Analysis of wild-type and rad50 mutants of yeast suggests an intimate relationship between meiotic chromosome synapsis and recombination', *Cell,* 61(3), pp. 419-36.

Alberts, B., Johnson, A., Lewis, J., Morgan, D. and Raff, M. (2015) 'Meiosis', *Molecular Biology of the Cell.* 6th ed: Norton & Company, pp. 1004-1010.

Allers, T. and Lichten, M. (2001) 'Differential timing and control of noncrossover and crossover recombination during meiosis', *Cell,* 106(1), pp. 47-57.

Antony, E., Tomko, E. J., Xiao, Q., Krejci, L., Lohman, T. M. and Ellenberger, T. (2009) 'Srs2 disassembles Rad51 filaments by a protein-protein interaction triggering ATP turnover and dissociation of Rad51 from DNA', *Mol Cell,* 35(1), pp. 105-15.

Arora, C., Kee, K., Maleki, S. and Keeney, S. (2004) 'Antiviral protein Ski8 is a direct partner of Spo11 in meiotic DNA break formation, independent of its cytoplasmic role in RNA metabolism', *Mol Cell,* 13(4), pp. 549-59.

Arora, K. and Corbett, Kevin D. (2018) 'The conserved XPF:ERCC1-like Zip2:Spo16 complex controls meiotic crossover formation through structure-specific DNA binding', *Nucleic Acids Research,* 47(5), pp. 2365-2376.

Bae, H. J., Dubarry, M., Jeon, J., Soares, L. M., Dargemont, C., Kim, J., Geli, V. and Buratowski, S. (2020) 'The Set1 N-terminal domain and Swd2 interact with RNA polymerase II CTD to recruit COMPASS', *Nat Commun,* 11(1), pp. 2181.

Berger, J. M., Fass, D., Wang, J. C. and Harrison, S. C. (1998) 'Structural similarities between topoisomerases that cleave one or both DNA strands', *Proc Natl Acad Sci U S A,* 95(14), pp. 7876-81.

Bergerat, A., de Massy, B., Gadelle, D., Varoutas, P.-C., Nicolas, A. and Forterre, P. (1997) 'An atypical topoisomerase II from archaea with implications for meiotic recombination', *Nature,* 386(6623), pp. 414-417.

Bergerat, A., Gadelle, D. and Forterre, P. (1994) 'Purification of a DNA topoisomerase II from the hyperthermophilic archaeon Sulfolobus shibatae. A thermostable enzyme with both bacterial and eucaryal features', *J Biol Chem,* 269(44), pp. 27663-9.

Bernstein, K. A., Reid, R. J., Sunjevaric, I., Demuth, K., Burgess, R. C. and Rothstein, R. (2011) 'The Shu complex, which contains Rad51 paralogues, promotes DNA repair through inhibition of the Srs2 anti-recombinase', *Mol Biol Cell,* 22(9), pp. 1599-607.

Bienz, M. (2006) 'The PHD finger, a nuclear protein-interaction domain', *Trends Biochem Sci,* 31(1), pp. 35-40.

Bishop, D. K. (1994) 'RecA homologs Dmc1 and Rad51 interact to form multiple nuclear complexes prior to meiotic chromosome synapsis', *Cell,* 79(6), pp. 1081-92.

Bishop, D. K., Park, D., Xu, L. and Kleckner, N. (1992) 'DMC1: a meiosis-specific yeast homolog of E. coli recA required for recombination, synaptonemal complex formation, and cell cycle progression', *Cell,* 69(3), pp. 439-56.

Blanco, M. G., Matos, J., Rass, U., Ip, S. C. and West, S. C. (2010) 'Functional overlap between the structure-specific nucleases Yen1 and Mus81-Mms4 for DNA-damage repair in S. cerevisiae', *DNA Repair (Amst),* 9(4), pp. 394-402.

Blat, Y., Protacio, R. U., Hunter, N. and Kleckner, N. (2002) 'Physical and functional interactions among basic chromosome organizational features govern early steps of meiotic chiasma formation', *Cell,* 111(6), pp. 791-802.

Borde, V., Lin, W., Novikov, E., Petrini, J. H., Lichten, M. and Nicolas, A. (2004) 'Association of Mre11p with double-strand break sites during yeast meiosis', *Mol Cell,* 13(3), pp. 389-401.

Börner, G. V., Barot, A. and Kleckner, N. (2008) 'Yeast Pch2 promotes domainal axis organization, timely recombination progression, and arrest of defective recombinosomes during meiosis', *Proc Natl Acad Sci U S A,* 105(9), pp. 3327-32.

Borner, G. V., Kleckner, N. and Hunter, N. (2004) 'Crossover/noncrossover differentiation, synaptonemal complex formation, and regulatory surveillance at the leptotene/zygotene transition of meiosis', *Cell,* 117(1), pp. 29-45.

Börner, G. V., Kleckner, N. and Hunter, N. (2004) 'Crossover/noncrossover differentiation, synaptonemal complex formation, and regulatory surveillance at the leptotene/zygotene transition of meiosis', *Cell,* 117(1), pp. 29-45.

Brar, G. A., Yassour, M., Friedman, N., Regev, A., Ingolia, N. T. and Weissman, J. S. (2012) 'High-resolution view of the yeast meiotic program revealed by ribosome profiling', *Science,* 335(6068), pp. 552-7.

Brick, K., Smagulova, F., Khil, P., Camerini-Otero, R. D. and Petukhova, G. V. (2012) 'Genetic recombination is directed away from functional genomic elements in mice', *Nature,* 485(7400), pp. 642-5.

Briggs, S. D., Bryk, M., Strahl, B. D., Cheung, W. L., Davie, J. K., Dent, S. Y., Winston, F. and Allis, C. D. (2001) 'Histone H3 lysine 4 methylation is mediated by Set1 and required for cell growth and rDNA silencing in Saccharomyces cerevisiae', *Genes Dev,* 15(24), pp. 3286-95.

Brill, S. J. and Stillman, B. (1991) 'Replication factor-A from Saccharomyces cerevisiae is encoded by three essential genes coordinately expressed at S phase', *Genes Dev,* 5(9), pp. 1589-600.

Callender, T. L., Laureau, R., Wan, L., Chen, X., Sandhu, R., Laljee, S., Zhou, S., Suhandynata, R. T., Prugar, E., Gaines, W. A., Kwon, Y., Börner, G. V., Nicolas, A., Neiman, A. M. and Hollingsworth, N. M. (2016) 'Mek1 Down Regulates Rad51 Activity during Yeast Meiosis by Phosphorylation of Hed1', *PLOS Genetics,* 12(8), pp. e1006226.

Cannavo, E. and Cejka, P. (2014) 'Sae2 promotes dsDNA endonuclease activity within Mre11-Rad50-Xrs2 to resect DNA breaks', *Nature,* 514(7520), pp. 122-5.

Cannavo, E., Sanchez, A., Anand, R., Ranjha, L., Hugener, J., Adam, C., Acharya, A., Weyland, N., Aran-Guiu, X., Charbonnier, J. B., Hoffmann, E. R., Borde, V., Matos, J. and Cejka, P. (2020) 'Regulation of the MLH1-MLH3 endonuclease in meiosis', *Nature,* 586(7830), pp. 618-622.

Carballo, J. A., Johnson, A. L., Sedgwick, S. G. and Cha, R. S. (2008) 'Phosphorylation of the axial element protein Hop1 by Mec1/Tel1 ensures meiotic interhomolog recombination', *Cell,* 132(5), pp. 758-70.

Carballo, J. A., Panizza, S., Serrentino, M. E., Johnson, A. L., Geymonat, M., Borde, V., Klein, F. and Cha, R. S. (2013) 'Budding Yeast ATM/ATR Control Meiotic Double-Strand Break (DSB) Levels by Down-Regulating Rec114, an Essential Component of the DSB-machinery', *PLOS Genetics,* 9(6), pp. e1003545.

Casari, E., Rinaldi, C., Marsella, A., Gnugnoli, M., Colombo, C. V., Bonetti, D. and Longhese, M. P. (2019) 'Processing of DNA Double-Strand Breaks by the MRX Complex in a Chromatin Context', *Front Mol Biosci,* 6, pp. 43.

Charpentier, E. and Doudna, J. A. (2013) 'Rewriting a genome', *Nature,* 495(7439), pp. 50-51.

Chavdarova, M., Marini, V., Sisakova, A., Sedlackova, H., Vigasova, D., Brill, S. J., Lisby, M. and Krejci, L. (2015) 'Srs2 promotes Mus81-Mms4-mediated resolution of recombination intermediates', *Nucleic Acids Res,* 43(7), pp. 3626-42.

Chen, H., Lisby, M. and Symington, L. S. (2013) 'RPA coordinates DNA end resection and prevents formation of DNA hairpins', *Mol Cell,* 50(4), pp. 589-600.

Chen, X., Suhandynata, R. T., Sandhu, R., Rockmill, B., Mohibullah, N., Niu, H., Liang, J., Lo, H.-C., Miller, D. E., Zhou, H., Börner, G. V. and Hollingsworth, N. M. (2015) 'Phosphorylation of the Synaptonemal Complex Protein Zip1 Regulates the Crossover/Noncrossover Decision during Yeast Meiosis', *PLOS Biology,* 13(12), pp. e1002329.

Cheng, C. H., Lo, Y. H., Liang, S. S., Ti, S. C., Lin, F. M., Yeh, C. H., Huang, H. Y. and Wang, T. F. (2006) 'SUMO modifications control assembly of synaptonemal complex and polycomplex in meiosis of Saccharomyces cerevisiae', *Genes Dev,* 20(15), pp. 2067-81.

Chua, P. R. and Roeder, G. S. (1998) 'Zip2, a meiosis-specific protein required for the initiation of chromosome synapsis', *Cell,* 93(3), pp. 349-59.

Ciosk, R., Shirayama, M., Shevchenko, A., Tanaka, T., Toth, A., Shevchenko, A. and Nasmyth, K. (2000) 'Cohesin's binding to chromosomes depends on a separate complex consisting of Scc2 and Scc4 proteins', *Mol Cell,* 5(2), pp. 243-54.

Claeys Bouuaert, C., Pu, S., Wang, J., Oger, C., Daccache, D., Xie, W., Patel, D. J. and Keeney, S. (2021a) 'DNA-driven condensation assembles the meiotic DNA break machinery', *Nature,* 592(7852), pp. 144-149.

Claeys Bouuaert, C., Tischfield, S. E., Pu, S., Mimitou, E. P., Arias-Palomo, E., Berger, J. M. and Keeney, S. (2021b) 'Structural and functional characterization of the Spo11 core complex', *Nat Struct Mol Biol,* 28(1), pp. 92-102.

Cloud, V., Chan, Y. L., Grubb, J., Budke, B. and Bishop, D. K. (2012) 'Rad51 is an accessory factor for Dmc1-mediated joint molecule formation during meiosis', *Science,* 337(6099), pp. 1222-5.

Cruz, C., Della Rosa, M., Krueger, C., Gao, Q., Horkai, D., King, M., Field, L. and Houseley, J. (2018) 'Tri-methylation of histone H3 lysine 4 facilitates gene expression in ageing cells', *Elife,* 7.

D'Andrea, L. D. and Regan, L. (2003) 'TPR proteins: the versatile helix', *Trends Biochem Sci,* 28(12), pp. 655-62.

Daee, D. L., Ferrari, E., Longerich, S., Zheng, X.-f., Xue, X., Branzei, D., Sung, P. and Myung, K. (2012) 'Rad5-dependent DNA Repair Functions of the Saccharomyces cerevisiae FANCM Protein Homolog Mph1*', *Journal of Biological Chemistry,* 287(32), pp. 26563-26575.

Davidson, I. F., Bauer, B., Goetz, D., Tang, W., Wutz, G. and Peters, J. M. (2019) 'DNA loop extrusion by human cohesin', *Science,* 366(6471), pp. 1338-1345.

de Jager, M., van Noort, J., van Gent, D. C., Dekker, C., Kanaar, R. and Wyman, C. (2001) 'Human Rad50/Mre11 is a flexible complex that can tether DNA ends', *Mol Cell,* 8(5), pp. 1129-35.

de los Santos, T., Hunter, N., Lee, C., Larkin, B., Loidl, J. and Hollingsworth, N. M. (2003) 'The Mus81/Mms4 endonuclease acts independently of double-Holliday junction resolution to promote a distinct subset of crossovers during meiosis in budding yeast', *Genetics,* 164(1), pp. 81-94.

De Muyt, A., Jessop, L., Kolar, E., Sourirajan, A., Chen, J., Dayani, Y. and Lichten, M. (2012) 'BLM helicase ortholog Sgs1 is a central regulator of meiotic recombination intermediate metabolism', *Mol Cell,* 46(1), pp. 43-53.

De Muyt, A., Pyatnitskaya, A., Andréani, J., Ranjha, L., Ramus, C., Laureau, R., Fernandez-Vega, A., Holoch, D., Girard, E., Govin, J., Margueron, R., Couté, Y., Cejka, P., Guérois, R. and Borde, V. (2018) 'A meiotic XPF-ERCC1-like complex recognizes joint molecule recombination intermediates to promote crossover formation', *Genes Dev,* 32(3-4), pp. 283-296.

Dehé, P. M., Dichtl, B., Schaft, D., Roguev, A., Pamblanco, M., Lebrun, R., Rodríguez-Gil, A., Mkandawire, M., Landsberg, K., Shevchenko, A., Shevchenko, A., Rosaleny, L. E., Tordera, V., Chávez, S., Stewart, A. F. and Géli, V. (2006) 'Protein interactions within the Set1 complex and their roles in the regulation of histone 3 lysine 4 methylation', *J Biol Chem,* 281(46), pp. 35404-12.

Deltcheva, E., Chylinski, K., Sharma, C. M., Gonzales, K., Chao, Y., Pirzada, Z. A., Eckert, M. R., Vogel, J. and Charpentier, E. (2011) 'CRISPR RNA maturation by trans-encoded small RNA and host factor RNase III', *Nature,* 471(7340), pp. 602-7.

Ding, D. Q., Sakurai, N., Katou, Y., Itoh, T., Shirahige, K., Haraguchi, T. and Hiraoka, Y. (2006) 'Meiotic cohesins modulate chromosome compaction during meiotic prophase in fission yeast', *J Cell Biol,* 174(4), pp. 499-508.

Dong, H. and Roeder, G. S. (2000) 'Organization of the yeast Zip1 protein within the central region of the synaptonemal complex', *J Cell Biol,* 148(3), pp. 417-26.

Dover, J., Schneider, J., Tawiah-Boateng, M. A., Wood, A., Dean, K., Johnston, M. and Shilatifard, A. (2002) 'Methylation of histone H3 by COMPASS requires ubiquitination of histone H2B by Rad6', *J Biol Chem,* 277(32), pp. 28368-71.

Duroc, Y., Kumar, R., Ranjha, L., Adam, C., Guérois, R., Md Muntaz, K., Marsolier-Kergoat, M. C., Dingli, F., Laureau, R., Loew, D., Llorente, B., Charbonnier, J. B., Cejka, P. and Borde, V. (2017) 'Concerted action of the MutLβ heterodimer and Mer3 helicase regulates the global extent of meiotic gene conversion', *Elife,* 6.

Engebrecht, J. A., Voelkel-Meiman, K. and Roeder, G. S. (1991) 'Meiosis-specific RNA splicing in yeast', *Cell,* 66(6), pp. 1257-68.

Fabre, F., Chan, A., Heyer, W. D. and Gangloff, S. (2002) 'Alternate pathways involving Sgs1/Top3, Mus81/ Mms4, and Srs2 prevent formation of toxic recombination intermediates from single-stranded gaps created by DNA replication', *Proc Natl Acad Sci U S A,* 99(26), pp. 16887-92.

Fricke, W. M. and Brill, S. J. (2003) 'Slx1-Slx4 is a second structure-specific endonuclease functionally redundant with Sgs1-Top3', *Genes Dev,* 17(14), pp. 1768-78.

Fudenberg, G., Imakaev, M., Lu, C., Goloborodko, A., Abdennur, N. and Mirny, L. A. (2016) 'Formation of Chromosomal Domains by Loop Extrusion', *Cell Rep,* 15(9), pp. 2038-49.

Fung, J. C., Rockmill, B., Odell, M. and Roeder, G. S. (2004) 'Imposition of crossover interference through the nonrandom distribution of synapsis initiation complexes', *Cell,* 116(6), pp. 795-802.

Ganji, M., Shaltiel, I. A., Bisht, S., Kim, E., Kalichava, A., Haering, C. H. and Dekker, C. (2018) 'Real-time imaging of DNA loop extrusion by condensin', *Science,* 360(6384), pp. 102-105.

Garcia, V., Phelps, S. E., Gray, S. and Neale, M. J. (2011) 'Bidirectional resection of DNA double-strand breaks by Mre11 and Exo1', *Nature,* 479(7372), pp. 241-4.

Gasior, S. L., Wong, A. K., Kora, Y., Shinohara, A. and Bishop, D. K. (1998) 'Rad52 associates with RPA and functions with rad55 and rad57 to assemble meiotic recombination complexes', *Genes Dev,* 12(14), pp. 2208-21.

Gietz, R. D. and Schiestl, R. H. (2007) 'High-efficiency yeast transformation using the LiAc/SS carrier DNA/PEG method', *Nature Protocols,* 2(1), pp. 31-34.

Gobbini, E., Cassani, C., Villa, M., Bonetti, D. and Longhese, M. P. (2016) 'Functions and regulation of the MRX complex at DNA double-strand breaks', *Microb Cell,* 3(8), pp. 329-337.

Goldstein, A. L. and McCusker, J. H. (1999) 'Three new dominant drug resistance cassettes for gene disruption in Saccharomyces cerevisiae', *Yeast,* 15(14), pp. 1541-53.

Goloborodko, A., Imakaev, M. V., Marko, J. F. and Mirny, L. (2016) 'Compaction and segregation of sister chromatids via active loop extrusion', *Elife,* 5.

Govin, J., Dorsey, J., Gaucher, J., Rousseaux, S., Khochbin, S. and Berger, S. L. (2010) 'Systematic screen reveals new functional dynamics of histones H3 and H4 during gametogenesis', *Genes Dev,* 24(16), pp. 1772-86.

Gray, S. and Cohen, P. E. (2016) 'Control of Meiotic Crossovers: From Double-Strand Break Formation to Designation', *Annu Rev Genet,* 50, pp. 175-210.

Gruber, S., Haering, C. H. and Nasmyth, K. (2003) 'Chromosomal cohesin forms a ring', *Cell,* 112(6), pp. 765-77.

Haber, J. E. (2012) 'Mating-Type Genes and MAT Switching in Saccharomyces cerevisiae', *Genetics,* 191(1), pp. 33-64.

Halbach, F., Reichelt, P., Rode, M. and Conti, E. (2013) 'The yeast ski complex: crystal structure and RNA channeling to the exosome complex', *Cell,* 154(4), pp. 814-26.

Harju, S., Fedosyuk, H. and Peterson, K. R. (2004) 'Rapid isolation of yeast genomic DNA: Bust n' Grab', *BMC Biotechnol,* 4, pp. 8.

Hartsuiker, E., Bähler, J. and Kohli, J. (1998) 'The role of topoisomerase II in meiotic chromosome condensation and segregation in Schizosaccharomyces pombe', *Mol Biol Cell,* 9(10), pp. 2739-50.

Hayashi, K., Yoshida, K. and Matsui, Y. (2005) 'A histone H3 methyltransferase controls epigenetic events required for meiotic prophase', *Nature,* 438(7066), pp. 374-8.

Henderson, K. A., Kee, K., Maleki, S., Santini, P. A. and Keeney, S. (2006) 'Cyclin-dependent kinase directly regulates initiation of meiotic recombination', *Cell,* 125(7), pp. 1321-32.

Herskowitz, I. (1988) 'Life cycle of the budding yeast Saccharomyces cerevisiae', *Microbiological reviews,* 52(4), pp. 536-553.

Ho, C. K., Mazón, G., Lam, A. F. and Symington, L. S. (2010) 'Mus81 and Yen1 promote reciprocal exchange during mitotic recombination to maintain genome integrity in budding yeast', *Mol Cell,* 40(6), pp. 988-1000.

Hollingsworth, N. M. and Byers, B. (1989) 'HOP1: a yeast meiotic pairing gene', *Genetics,* 121(3), pp. 445-62.

Hollingsworth, N. M., Ponte, L. and Halsey, C. (1995) 'MSH5, a novel MutS homolog, facilitates meiotic reciprocal recombination between homologs in Saccharomyces cerevisiae but not mismatch repair', *Genes Dev,* 9(14), pp. 1728-39.

Hong, E. L., Shinohara, A. and Bishop, D. K. (2001) 'Saccharomyces cerevisiae Dmc1 Protein Promotes Renaturation of Single-strand DNA (ssDNA) and Assimilation of ssDNA into Homologous Super-coiled Duplex DNA', *Journal of Biological Chemistry,* 276(45), pp. 41906-41912.

Hong, S., Sung, Y., Yu, M., Lee, M., Kleckner, N. and Kim, K. P. (2013) 'The logic and mechanism of homologous recombination partner choice', *Mol Cell,* 51(4), pp. 440-53.

Hooker, G. W. and Roeder, G. S. (2006) 'A Role for SUMO in meiotic chromosome synapsis', *Curr Biol,* 16(12), pp. 1238-43.

Houlard, M., Godwin, J., Metson, J., Lee, J., Hirano, T. and Nasmyth, K. (2015) 'Condensin confers the longitudinal rigidity of chromosomes', *Nature Cell Biology,* 17(6), pp. 771-781.

Huang, T., Yuan, S., Gao, L., Li, M., Yu, X., Zhan, J., Yin, Y., Liu, C., Zhang, C., Lu, G., Li, W., Liu, J., Chen, Z.-J. and Liu, H. (2020) 'The histone modification reader ZCWPW1 links histone methylation to PRDM9-induced double-strand break repair', *eLife,* 9, pp. e53459.

Hunt, L. J., Ahmed, E. A., Kaur, H., Ahuja, J. S., Hulme, L., Chou, T. C., Lichten, M. and Goldman, A. S. H. (2019) 'S. cerevisiae Srs2 helicase ensures normal recombination intermediate metabolism during meiosis and prevents accumulation of Rad51 aggregates', *Chromosoma,* 128(3), pp. 249-265.

Hunter, N. (2015) 'Meiotic Recombination: The Essence of Heredity', *Cold Spring Harb Perspect Biol,* 7(12).

Hunter, N. and Kleckner, N. (2001) 'The single-end invasion: an asymmetric intermediate at the double-strand break to double-holliday junction transition of meiotic recombination', *Cell,* 106(1), pp. 59-70.

Ivanov, E. L., Korolev, V. G. and Fabre, F. (1992) 'XRS2, a DNA repair gene of Saccharomyces cerevisiae, is needed for meiotic recombination', *Genetics,* 132(3), pp. 651-64.

Jessop, L. and Lichten, M. (2008) 'Mus81/Mms4 endonuclease and Sgs1 helicase collaborate to ensure proper recombination intermediate metabolism during meiosis', *Mol Cell,* 31(3), pp. 313-23.

Jessop, L., Rockmill, B., Roeder, G. S. and Lichten, M. (2006) 'Meiotic chromosome synapsis-promoting proteins antagonize the anti-crossover activity of sgs1', *PLoS genetics,* 2(9), pp. e155-e155.

Jinek, M., Chylinski, K., Fonfara, I., Hauer, M., Doudna, J. A. and Charpentier, E. (2012) 'A programmable dual-RNA-guided DNA endonuclease in adaptive bacterial immunity', *Science,* 337(6096), pp. 816-21.

Johnson, D., Crawford, M., Cooper, T., Claeys Bouuaert, C., Keeney, S., Llorente, B., Garcia, V. and Neale, M. J. (2021) 'Concerted cutting by Spo11 illuminates meiotic DNA break mechanics', *Nature,* 594(7864), pp. 572-576.

Kaback, D. B., Guacci, V., Barber, D. and Mahon, J. W. (1992) 'Chromosome size-dependent control of meiotic recombination', *Science,* 256(5054), pp. 228-32.

Kane, S. M. and Roth, R. (1974) 'Carbohydrate Metabolism During AsCOpore Development in Yeast', *Journal of Bacteriology,* 118(1), pp. 8-14.

Kapuscinski, J. (1995) 'DAPI: a DNA-Specific Fluorescent Probe', *Biotechnic & Histochemistry,* 70(5), pp. 220-233.

Karányi, Z., Halász, L., Acquaviva, L., Jónás, D., Hetey, S., Boros-Oláh, B., Peng, F., Chen, D., Klein, F., Géli, V. and Székvölgyi, L. (2018) 'Nuclear dynamics of the Set1C subunit Spp1 prepares meiotic recombination sites for break formation', *J Cell Biol,* 217(10), pp. 3398-3415.

Kariyazono, R., Oda, A., Yamada, T. and Ohta, K. (2019) 'Conserved HORMA domain-containing protein Hop1 stabilizes interaction between proteins of meiotic DNA break hotspots and chromosome axis', *Nucleic Acids Research,* 47(19), pp. 10166-10180.

Kaur, H., De Muyt, A. and Lichten, M. (2015) 'Top3-Rmi1 DNA single-strand decatenase is integral to the formation and resolution of meiotic recombination intermediates', *Molecular cell,* 57(4), pp. 583-594.

Kee, K., Protacio, R. U., Arora, C. and Keeney, S. (2004) 'Spatial organization and dynamics of the association of Rec102 and Rec104 with meiotic chromosomes', *Embo j,* 23(8), pp. 1815-24.

Keeney, S. (2001) 'Mechanism and control of meiotic recombination initiation', *Curr Top Dev Biol,* 52, pp. 1-53.

Keeney, S. (2008) 'Spo11 and the Formation of DNA Double-Strand Breaks in Meiosis', *Genome Dyn Stab,* 2, pp. 81-123.

Keeney, S., Giroux, C. N. and Kleckner, N. (1997) 'Meiosis-specific DNA double-strand breaks are catalyzed by Spo11, a member of a widely conserved protein family', *Cell,* 88(3), pp. 375-84.

Keeney, S. and Kleckner, N. (1995) 'Covalent protein-DNA complexes at the 5' strand termini of meiosis-specific double-strand breaks in yeast', *Proc Natl Acad Sci U S A,* 92(24), pp. 11274-8.

Keeney, S., Lange, J. and Mohibullah, N. (2014) 'Self-organization of meiotic recombination initiation: general principles and molecular pathways', *Annu Rev Genet,* 48, pp. 187-214.

Khan, Y. A., White, K. I. and Brunger, A. T. (2022) 'The AAA+ superfamily: a review of the structural and mechanistic principles of these molecular machines', *Crit Rev Biochem Mol Biol,* 57(2), pp. 156-187.

Kim, J., Kim, J. A., McGinty, R. K., Nguyen, U. T., Muir, T. W., Allis, C. D. and Roeder, R. G. (2013) 'The n-SET domain of Set1 regulates H2B ubiquitylation-dependent H3K4 methylation', *Mol Cell,* 49(6), pp. 1121-33.

Kim, K. P., Weiner, B. M., Zhang, L., Jordan, A., Dekker, J. and Kleckner, N. (2010) 'Sister cohesion and structural axis components mediate homolog bias of meiotic recombination', *Cell,* 143(6), pp. 924-37.

Kim, Y., Rosenberg, S. C., Kugel, C. L., Kostow, N., Rog, O., Davydov, V., Su, T. Y., Dernburg, A. F. and Corbett, K. D. (2014) 'The chromosome axis controls meiotic events through a hierarchical assembly of HORMA domain proteins', *Dev Cell,* 31(4), pp. 487-502.

Kim, Y., Shi, Z., Zhang, H., Finkelstein, I. J. and Yu, H. (2019) 'Human cohesin compacts DNA by loop extrusion', *Science,* 366(6471), pp. 1345-1349.

Kirmizis, A., Santos-Rosa, H., Penkett, C. J., Singer, M. A., Vermeulen, M., Mann, M., Bähler, J., Green, R. D. and Kouzarides, T. (2007) 'Arginine methylation at histone H3R2 controls deposition of H3K4 trimethylation', *Nature,* 449(7164), pp. 928-32.

Klapholz, S., Waddell, C. S. and Esposito, R. E. (1985) 'The role of the SPO11 gene in meiotic recombination in yeast', *Genetics,* 110(2), pp. 187-216.

Klar, T. A. and Hell, S. W. (1999) 'Subdiffraction resolution in far-field fluorescence microscopy', *Optics Letters,* 24(14), pp. 954-956.

Kleckner, N. (2006) 'Chiasma formation: chromatin/axis interplay and the role(s) of the synaptonemal complex', *Chromosoma,* 115(3), pp. 175-94.

Klein, F., Mahr, P., Galova, M., Buonomo, S. B., Michaelis, C., Nairz, K. and Nasmyth, K. (1999) 'A central role for cohesins in sister chromatid cohesion, formation of axial elements, and recombination during yeast meiosis', *Cell,* 98(1), pp. 91-103.

Krejci, L., Van Komen, S., Li, Y., Villemain, J., Reddy, M. S., Klein, H., Ellenberger, T. and Sung, P. (2003) 'DNA helicase Srs2 disrupts the Rad51 presynaptic filament', *Nature,* 423(6937), pp. 305-9.

Kumar, R., Bourbon, H. M. and de Massy, B. (2010) 'Functional conservation of Mei4 for meiotic DNA double-strand break formation from yeasts to mice', *Genes Dev,* 24(12), pp. 1266-80.

Lam, I. and Keeney, S. (2014) 'Mechanism and regulation of meiotic recombination initiation', *Cold Spring Harb Perspect Biol,* 7(1), pp. a016634.

Lao, J. P., Oh, S. D., Shinohara, M., Shinohara, A. and Hunter, N. (2008) 'Rad52 promotes postinvasion steps of meiotic double-strand-break repair', *Mol Cell,* 29(4), pp. 517-24.

Lee, J. S., Shukla, A., Schneider, J., Swanson, S. K., Washburn, M. P., Florens, L., Bhaumik, S. R. and Shilatifard, A. (2007) 'Histone crosstalk between H2B monoubiquitination and H3 methylation mediated by COMPASS', *Cell,* 131(6), pp. 1084-96.

Li, J., Hooker, G. W. and Roeder, G. S. (2006) 'Saccharomyces cerevisiae Mer2, Mei4 and Rec114 form a complex required for meiotic double-strand break formation', *Genetics,* 173(4), pp. 1969-81.

Lin, F. M., Lai, Y. J., Shen, H. J., Cheng, Y. H. and Wang, T. F. (2010) 'Yeast axial-element protein, Red1, binds SUMO chains to promote meiotic interhomologue recombination and chromosome synapsis', *Embo j,* 29(3), pp. 586-96.

Lipinski, K. A., Kaniak-Golik, A. and Golik, P. (2010) 'Maintenance and expression of the S. cerevisiae mitochondrial genome—From genetics to evolution and systems biology', *Biochimica et Biophysica Acta (BBA) - Bioenergetics,* 1797(6-7), pp. 1086-1098.

Liu, J., Ede, C., Wright, W. D., Gore, S. K., Jenkins, S. S., Freudenthal, B. D., Todd Washington, M., Veaute, X. and Heyer, W.-D. (2017) 'Srs2 promotes synthesis-dependent strand annealing by disrupting DNA polymerase δ-extending D-loops', *eLife,* 6, pp. e22195.

Liu, J., Wu, T. C. and Lichten, M. (1995) 'The location and structure of double-strand DNA breaks induced during yeast meiosis: evidence for a covalently linked DNA-protein intermediate', *Embo j,* 14(18), pp. 4599-608.

Loidl, J., Klein, F. and Engebrecht, J. (1998) 'Genetic and morphological approaches for the analysis of meiotic chromosomes in yeast', *Methods Cell Biol,* 53, pp. 257-85.

Loidl, J., Nairz, K. and Klein, F. (1991) 'Meiotic chromosome synapsis in a haploid yeast', *Chromosoma,* 100(4), pp. 221-8.

Ma, H., Kunes, S., Schatz, P. J. and Botstein, D. (1987) 'Plasmid construction by homologous recombination in yeast', *Gene,* 58(2-3), pp. 201-16.

Macaisne, N., Novatchkova, M., Peirera, L., Vezon, D., Jolivet, S., Froger, N., Chelysheva, L., Grelon, M. and Mercier, R. (2008) 'SHOC1, an XPF endonuclease-related protein, is essential for the formation of class I meiotic crossovers', *Curr Biol,* 18(18), pp. 1432-7.

Mahajan, R., Delphin, C., Guan, T., Gerace, L. and Melchior, F. (1997) 'A small ubiquitin-related polypeptide involved in targeting RanGAP1 to nuclear pore complex protein RanBP2', *Cell,* 88(1), pp. 97-107.

Mahgoub, M., Paiano, J., Bruno, M., Wu, W., Pathuri, S., Zhang, X., Ralls, S., Cheng, X., Nussenzweig, A. and Macfarlan, T. S. (2020) 'Dual histone methyl reader ZCWPW1 facilitates repair of meiotic double strand breaks in male mice', *eLife,* 9, pp. e53360.

Maleki, S., Neale, M. J., Arora, C., Henderson, K. A. and Keeney, S. (2007) 'Interactions between Mei4, Rec114, and other proteins required for meiotic DNA double-strand break formation in Saccharomyces cerevisiae', *Chromosoma,* 116(5), pp. 471-86.

Manhart, C. M. and Alani, E. (2016) 'Roles for mismatch repair family proteins in promoting meiotic crossing over', *DNA Repair (Amst),* 38, pp. 84-93.

Mao-Draayer, Y., Galbraith, A. M., Pittman, D. L., Cool, M. and Malone, R. E. (1996) 'Analysis of Meiotic Recombination Pathways in the Yeast Saccharomyces cerevisiae', *Genetics,* 144(1), pp. 71-86.

Matos, J., Blanco, M. G., Maslen, S., Skehel, J. M. and West, S. C. (2011) 'Regulatory control of the resolution of DNA recombination intermediates during meiosis and mitosis', *Cell,* 147(1), pp. 158-72.

Matunis, M. J., Coutavas, E. and Blobel, G. (1996) 'A novel ubiquitin-like modification modulates the partitioning of the Ran-GTPase-activating protein RanGAP1 between the cytosol and the nuclear pore complex', *J Cell Biol,* 135(6 Pt 1), pp. 1457-70.

Mazina, O. M., Mazin, A. V., Nakagawa, T., Kolodner, R. D. and Kowalczykowski, S. C. (2004) 'Saccharomyces cerevisiae Mer3 helicase stimulates 3'-5' heteroduplex extension by Rad51; implications for crossover control in meiotic recombination', *Cell,* 117(1), pp. 47-56.

Mazón, G. and Symington, L. S. (2013) 'Mph1 and Mus81-Mms4 prevent aberrant processing of mitotic recombination intermediates', *Mol Cell,* 52(1), pp. 63-74.

McGinn, J. and Marraffini, L. A. (2019) 'Molecular mechanisms of CRISPR-Cas spacer acquisition', *Nat Rev Microbiol,* 17(1), pp. 7-12.

McKee, A. H. and Kleckner, N. (1997) 'A general method for identifying recessive diploid-specific mutations in Saccharomyces cerevisiae, its application to the isolation of mutants blocked at intermediate stages of meiotic prophase and characterization of a new gene SAE2', *Genetics,* 146(3), pp. 797-816.

Mersman, D. P., Du, H. N., Fingerman, I. M., South, P. F. and Briggs, S. D. (2012) 'Charge-based interaction conserved within histone H3 lysine 4 (H3K4) methyltransferase complexes is needed for protein stability, histone methylation, and gene expression', *J Biol Chem,* 287(4), pp. 2652-65.

Michaelis, C., Ciosk, R. and Nasmyth, K. (1997) 'Cohesins: Chromosomal Proteins that Prevent Premature Separation of Sister Chromatids', *Cell,* 91(1), pp. 35-45.

Miller, T., Krogan, N. J., Dover, J., Erdjument-Bromage, H., Tempst, P., Johnston, M., Greenblatt, J. F. and Shilatifard, A. (2001) 'COMPASS: a complex of proteins associated with a trithorax-related SET domain protein', *Proc Natl Acad Sci U S A,* 98(23), pp. 12902-7.

Mimitou, E. P., Yamada, S. and Keeney, S. (2017) 'A global view of meiotic double-strand break end resection', *Science,* 355(6320), pp. 40-45.

Mohibullah, N. and Keeney, S. (2017) 'Numerical and spatial patterning of yeast meiotic DNA breaks by Tel1', *Genome Res,* 27(2), pp. 278-288.

Moore, J. K. and Haber, J. E. (1996) 'Cell cycle and genetic requirements of two pathways of nonhomologous end-joining repair of double-strand breaks in Saccharomyces cerevisiae', *Mol Cell Biol,* 16(5), pp. 2164-73.

Morawska, M. and Ulrich, H. D. (2013) 'An expanded tool kit for the auxin-inducible degron system in budding yeast', *Yeast,* 30(9), pp. 341-351.

Mu, X., Murakami, H., Mohibullah, N. and Keeney, S. (2020) 'Chromosome-autonomous feedback down-regulates meiotic DNA break competence upon synaptonemal complex formation', *Genes Dev,* 34(23-24), pp. 1605-1618.

Murakami, H. and Keeney, S. (2008) 'Regulating the formation of DNA double-strand breaks in meiosis', *Genes Dev,* 22(3), pp. 286-92.

Murakami, H. and Keeney, S. (2014) 'Temporospatial coordination of meiotic DNA replication and recombination via DDK recruitment to replisomes', *Cell,* 158(4), pp. 861-873.

Nagy, P. L., Griesenbeck, J., Kornberg, R. D. and Cleary, M. L. (2002) 'A trithorax-group complex purified from Saccharomyces cerevisiae is required for methylation of histone H3', *Proc Natl Acad Sci U S A,* 99(1), pp. 90-4.

Nairz, K. and Klein, F. (1997) 'mre11S--a yeast mutation that blocks double-strand-break processing and permits nonhomologous synapsis in meiosis', *Genes Dev,* 11(17), pp. 2272-90.

Nakagawa, T., Flores-Rozas, H. and Kolodner, R. D. (2001) 'The MER3 helicase involved in meiotic crossing over is stimulated by single-stranded DNA-binding proteins and unwinds DNA in the 3' to 5' direction', *J Biol Chem,* 276(34), pp. 31487-93.

Nakagawa, T. and Kolodner, R. D. (2002) 'Saccharomyces cerevisiae Mer3 is a DNA helicase involved in meiotic crossing over', *Mol Cell Biol,* 22(10), pp. 3281-91.

Nakagawa, T. and Ogawa, H. (1999) 'The Saccharomyces cerevisiae MER3 gene, encoding a novel helicase-like protein, is required for crossover control in meiosis', *Embo j,* 18(20), pp. 5714-23.

Nandabalan, K. and Roeder, G. S. (1995) 'Binding of a cell-type-specific RNA splicing factor to its target regulatory sequence', *Mol Cell Biol,* 15(4), pp. 1953-60.

Nasmyth, K. (2001) 'Disseminating the genome: joining, resolving, and separating sister chromatids during mitosis and meiosis', *Annu Rev Genet,* 35, pp. 673-745.

Naumova, N., Imakaev, M., Fudenberg, G., Zhan, Y., Lajoie, B. R., Mirny, L. A. and Dekker, J. (2013) 'Organization of the mitotic chromosome', *Science,* 342(6161), pp. 948-53.

Neale, M. J., Pan, J. and Keeney, S. (2005) 'Endonucleolytic processing of covalent protein-linked DNA double-strand breaks', *Nature,* 436(7053), pp. 1053-7.

Neale, M. J., Ramachandran, M., Trelles-Sticken, E., Scherthan, H. and Goldman, A. S. H. (2002) 'Wild-Type Levels of Spo11-Induced DSBs Are Required for Normal Single-Strand Resection during Meiosis', *Molecular Cell,* 9(4), pp. 835-846.

Ng, H. H., Dole, S. and Struhl, K. (2003) 'The Rtf1 component of the Paf1 transcriptional elongation complex is required for ubiquitination of histone H2B', *J Biol Chem,* 278(36), pp. 33625-8.

Ng, H. H., Robert, F., Young, R. A. and Struhl, K. (2003) 'Targeted recruitment of Set1 histone methylase by elongating Pol II provides a localized mark and memory of recent transcriptional activity', *Mol Cell,* 11(3), pp. 709-19.

Nichols, M. D., DeAngelis, K., Keck, J. L. and Berger, J. M. (1999) 'Structure and function of an archaeal topoisomerase VI subunit with homology to the meiotic recombination factor Spo11', *Embo j,* 18(21), pp. 6177-88.

Nishimura, K., Fukagawa, T., Takisawa, H., Kakimoto, T. and Kanemaki, M. (2009) 'An auxin-based degron system for the rapid depletion of proteins in nonplant cells', *Nature Methods,* 6(12), pp. 917-922.

Nitiss, J. L. (2009) 'DNA topoisomerase II and its growing repertoire of biological functions', *Nat Rev Cancer,* 9(5), pp. 327-37.

Niu, H., Li, X., Job, E., Park, C., Moazed, D., Gygi, S. P. and Hollingsworth, N. M. (2007) 'Mek1 kinase is regulated to suppress double-strand break repair between sister chromatids during budding yeast meiosis', *Mol Cell Biol,* 27(15), pp. 5456-67.

Niu, H., Wan, L., Baumgartner, B., Schaefer, D., Loidl, J. and Hollingsworth, N. M. (2005) 'Partner choice during meiosis is regulated by Hop1-promoted dimerization of Mek1', *Mol Biol Cell,* 16(12), pp. 5804-18.

Niu, H., Wan, L., Busygina, V., Kwon, Y., Allen, J. A., Li, X., Kunz, R. C., Kubota, K., Wang, B., Sung, P., Shokat, K. M., Gygi, S. P. and Hollingsworth, N. M. (2009) 'Regulation of meiotic recombination via Mek1-mediated Rad54 phosphorylation', *Mol Cell,* 36(3), pp. 393-404.

Ogawa, T., Shinohara, A., Nabetani, A., Ikeya, T., Yu, X., Egelman, E. H. and Ogawa, H. (1993) 'RecA-like recombination proteins in eukaryotes: functions and structures of RAD51 genes', *Cold Spring Harb Symp Quant Biol,* 58, pp. 567-76.

Oger, C. and Claeys Bouuaert, C. (2025) 'SPO11 dimers are sufficient to catalyse DNA double-strand breaks in vitro', *Nature,* 639(8055), pp. 792-799.

Oh, J., Al-Zain, A., Cannavo, E., Cejka, P. and Symington, L. S. (2016) 'Xrs2 Dependent and Independent Functions of the Mre11-Rad50 Complex', *Mol Cell,* 64(2), pp. 405-415.

Oh, S. D., Lao, J. P., Hwang, P. Y.-H., Taylor, A. F., Smith, G. R. and Hunter, N. (2007) 'BLM Ortholog, Sgs1, Prevents Aberrant Crossing-over by Suppressing Formation of Multichromatid Joint Molecules', *Cell,* 130(2), pp. 259-272.

Oh, S. D., Lao, J. P., Taylor, A. F., Smith, G. R. and Hunter, N. (2008) 'RecQ Helicase, Sgs1, and XPF Family Endonuclease, Mus81-Mms4, Resolve Aberrant Joint Molecules during Meiotic Recombination', *Molecular Cell,* 31(3), pp. 324-336.

Oldenburg, K. R., Vo, K. T., Michaelis, S. and Paddon, C. (1997) 'Recombination-mediated PCR-directed plasmid construction in vivo in yeast', *Nucleic Acids Res,* 25(2), pp. 451-2.

Orr-Weaver, T. L., Szostak, J. W. and Rothstein, R. J. (1981) 'Yeast transformation: a model system for the study of recombination', *Proc Natl Acad Sci U S A,* 78(10), pp. 6354-8.

Paigen, K. and Petkov, P. M. (2018) 'PRDM9 and Its Role in Genetic Recombination', *Trends Genet,* 34(4), pp. 291-300.

Pan, J., Sasaki, M., Kniewel, R., Murakami, H., Blitzblau, H. G., Tischfield, S. E., Zhu, X., Neale, M. J., Jasin, M., Socci, N. D., Hochwagen, A. and Keeney, S. (2011) 'A hierarchical combination of factors shapes the genome-wide topography of yeast meiotic recombination initiation', *Cell,* 144(5), pp. 719-31.

Panizza, S., Mendoza, M. A., Berlinger, M., Huang, L., Nicolas, A., Shirahige, K. and Klein, F. (2011) 'Spo11-accessory proteins link double-strand break sites to the chromosome axis in early meiotic recombination', *Cell,* 146(3), pp. 372-83.

Paull, T. T. (2018) '20 Years of Mre11 Biology: No End in Sight', *Mol Cell,* 71(3), pp. 419-427.

Paull, T. T. and Gellert, M. (1998) 'The 3' to 5' exonuclease activity of Mre 11 facilitates repair of DNA double-strand breaks', *Mol Cell,* 1(7), pp. 969-79.

Perry, J., Kleckner, N. and Börner, G. V. (2005) 'Bioinformatic analyses implicate the collaborating meiotic crossover/chiasma proteins Zip2, Zip3, and Spo22/Zip4 in ubiquitin labeling', *Proc Natl Acad Sci U S A,* 102(49), pp. 17594-9.

Petela, N. J., Gligoris, T. G., Metson, J., Lee, B. G., Voulgaris, M., Hu, B., Kikuchi, S., Chapard, C., Chen, W., Rajendra, E., Srinivisan, M., Yu, H., Löwe, J. and Nasmyth, K. A. (2018) 'Scc2 Is a Potent Activator of Cohesin's ATPase that Promotes Loading by Binding Scc1 without Pds5', *Mol Cell,* 70(6), pp. 1134-1148.e7.

Pochart, P., Woltering, D. and Hollingsworth, N. M. (1997) 'Conserved properties between functionally distinct MutS homologs in yeast', *J Biol Chem,* 272(48), pp. 30345-9.

Pokholok, D. K., Harbison, C. T., Levine, S., Cole, M., Hannett, N. M., Lee, T. I., Bell, G. W., Walker, K., Rolfe, P. A., Herbolsheimer, E., Zeitlinger, J., Lewitter, F., Gifford, D. K. and Young, R. A. (2005) 'Genome-wide map of nucleosome acetylation and methylation in yeast', *Cell,* 122(4), pp. 517-27.

Pommier, Y., Sun, Y., Huang, S.-y. N. and Nitiss, J. L. (2016) 'Roles of eukaryotic topoisomerases in transcription, replication and genomic stability', *Nature Reviews Molecular Cell Biology,* 17(11), pp. 703-721.

Prakash, R., Satory, D., Dray, E., Papusha, A., Scheller, J., Kramer, W., Krejci, L., Klein, H., Haber, J. E., Sung, P. and Ira, G. (2009) 'Yeast Mph1 helicase dissociates Rad51-made D-loops: implications for crossover control in mitotic recombination', *Genes Dev,* 23(1), pp. 67-79.

Prieler, S., Chen, D., Huang, L., Mayrhofer, E., Zsótér, S., Vesely, M., Mbogning, J. and Klein, F. (2021) 'Spo11 generates gaps through concerted cuts at sites of topological stress', *Nature,* 594(7864), pp. 577-582.

Prieler, S., Penkner, A., Borde, V. and Klein, F. (2005) 'The control of Spo11's interaction with meiotic recombination hotspots', *Genes Dev,* 19(2), pp. 255-69.

Prinz, S., Amon, A. and Klein, F. (1997) 'Isolation of COM1, a new gene required to complete meiotic double-strand break-induced recombination in Saccharomyces cerevisiae', *Genetics,* 146(3), pp. 781-95.

Priyanka, P. P. and Yenugu, S. (2021) 'Coiled-Coil Domain-Containing (CCDC) Proteins: Functional Roles in General and Male Reproductive Physiology', *Reprod Sci,* 28(10), pp. 2725-2734.

Pyatnitskaya, A., Andreani, J., Guérois, R., De Muyt, A. and Borde, V. (2022) 'The Zip4 protein directly couples meiotic crossover formation to synaptonemal complex assembly', *Genes Dev,* 36(1-2), pp. 53-69.

Pyatnitskaya, A., Borde, V. and De Muyt, A. (2019) 'Crossing and zipping: molecular duties of the ZMM proteins in meiosis', *Chromosoma,* 128(3), pp. 181-198.

Rao, S. S. P., Huang, S. C., Glenn St Hilaire, B., Engreitz, J. M., Perez, E. M., Kieffer-Kwon, K. R., Sanborn, A. L., Johnstone, S. E., Bascom, G. D., Bochkov, I. D., Huang, X., Shamim, M. S., Shin, J.,

Turner, D., Ye, Z., Omer, A. D., Robinson, J. T., Schlick, T., Bernstein, B. E., Casellas, R., Lander, E. S. and Aiden, E. L. (2017) 'Cohesin Loss Eliminates All Loop Domains', *Cell,* 171(2), pp. 305-320.e24.

Robert, T., Dervins, D., Fabre, F. and Gangloff, S. (2006) 'Mrc1 and Srs2 are major actors in the regulation of spontaneous crossover', *Embo j,* 25(12), pp. 2837-46.

Robert, T., Nore, A., Brun, C., Maffre, C., Crimi, B., Bourbon, H. M. and de Massy, B. (2016) 'The TopoVIB-Like protein family is required for meiotic DNA double-strand break formation', *Science,* 351(6276), pp. 943-9.

Rockmill, B., Fung, J. C., Branda, S. S. and Roeder, G. S. (2003) 'The Sgs1 helicase regulates chromosome synapsis and meiotic crossing over', *Curr Biol,* 13(22), pp. 1954-62.

Rockmill, B., Sym, M., Scherthan, H. and Roeder, G. S. (1995) 'Roles for two RecA homologs in promoting meiotic chromosome synapsis', *Genes Dev,* 9(21), pp. 2684-95.

Rojowska, A., Lammens, K., Seifert, F. U., Direnberger, C., Feldmann, H. and Hopfner, K. P. (2014) 'Structure of the Rad50 DNA double-strand break repair protein in complex with DNA', *Embo j,* 33(23), pp. 2847-59.

Rosonina, E. and Manley, J. L. (2005) 'From Transcription to mRNA: PAF Provides a New Path', *Molecular Cell,* 20(2), pp. 167-168.

Ross-Macdonald, P. and Roeder, G. S. (1994) 'Mutation of a meiosis-specific MutS homolog decreases crossing over but not mismatch correction', *Cell,* 79(6), pp. 1069-80.

Rousová, D., Nivsarkar, V., Altmannova, V., Raina, V. B., Funk, S. K., Liedtke, D., Janning, P., Müller, F., Reichle, H., Vader, G. and Weir, J. R. (2021) 'Novel mechanistic insights into the role of Mer2 as the keystone of meiotic DNA break formation', *Elife,* 10.

San-Segundo, P. A. and Roeder, G. S. (1999) 'Pch2 Links Chromatin Silencing to Meiotic Checkpoint Control', *Cell,* 97(3), pp. 313-324.

Sanborn, A. L., Rao, S. S., Huang, S. C., Durand, N. C., Huntley, M. H., Jewett, A. I., Bochkov, I. D., Chinnappan, D., Cutkosky, A., Li, J., Geeting, K. P., Gnirke, A., Melnikov, A., McKenna, D., Stamenova, E. K., Lander, E. S. and Aiden, E. L. (2015) 'Chromatin extrusion explains key features of loop and domain formation in wild-type and engineered genomes', *Proc Natl Acad Sci U S A,* 112(47), pp. E6456-65.

Sandhu, R., Monge Neria, F., Monge Neria, J., Chen, X., Hollingsworth, N. M. and Börner, G. V. (2020) 'DNA Helicase Mph1(FANCM) Ensures Meiotic Recombination between Parental Chromosomes by Dissociating Precocious Displacement Loops', *Dev Cell,* 53(4), pp. 458-472.e5.

Sanger, F., Nicklen, S. and Coulson, A. R. (1977) 'DNA sequencing with chain-terminating inhibitors', *Proceedings of the National Academy of Sciences of the United States of America,* 74(12), pp. 5463-5467.

Santos-Rosa, H., Schneider, R., Bannister, A. J., Sherriff, J., Bernstein, B. E., Emre, N. C., Schreiber, S. L., Mellor, J. and Kouzarides, T. (2002) 'Active genes are tri-methylated at K4 of histone H3', *Nature,* 419(6905), pp. 407-11.

Santucci-Darmanin, S., Neyton, S., Lespinasse, F., Saunières, A., Gaudray, P. and Paquis-Flucklinger, V. (2002) 'The DNA mismatch-repair MLH3 protein interacts with MSH4 in meiotic cells, supporting a role for this MutL homolog in mammalian meiotic recombination', *Human Molecular Genetics,* 11(15), pp. 1697-1706.

Saponaro, M., Callahan, D., Zheng, X., Krejci, L., Haber, J. E., Klein, H. L. and Liberi, G. (2010) 'Cdk1 targets Srs2 to complete synthesis-dependent strand annealing and to promote recombinational repair', *PLoS Genet,* 6(2), pp. e1000858.

Sasanuma, H., Hirota, K., Fukuda, T., Kakusho, N., Kugou, K., Kawasaki, Y., Shibata, T., Masai, H. and Ohta, K. (2008) 'Cdc7-dependent phosphorylation of Mer2 facilitates initiation of yeast meiotic recombination', *Genes Dev,* 22(3), pp. 398-410.

Sasanuma, H., Murakami, H., Fukuda, T., Shibata, T., Nicolas, A. and Ohta, K. (2007) 'Meiotic association between Spo11 regulated by Rec102, Rec104 and Rec114', *Nucleic Acids Res,* 35(4), pp. 1119-33.

Sasanuma, H., Sakurai, H. S. M., Furihata, Y., Challa, K., Palmer, L., Gasser, S. M., Shinohara, M. and Shinohara, A. (2019) 'Srs2 helicase prevents the formation of toxic DNA damage during late prophase I of yeast meiosis', *Chromosoma,* 128(3), pp. 453-471.

Sasanuma, H., Tawaramoto, M. S., Lao, J. P., Hosaka, H., Sanda, E., Suzuki, M., Yamashita, E., Hunter, N., Shinohara, M., Nakagawa, A. and Shinohara, A. (2013) 'A new protein complex promoting the assembly of Rad51 filaments', *Nature Communications,* 4(1), pp. 1676.

Schellenberg, M. J., Appel, C. D., Adhikari, S., Robertson, P. D., Ramsden, D. A. and Williams, R. S. (2012) 'Mechanism of repair of 5'-topoisomerase II-DNA adducts by mammalian tyrosyl-DNA phosphodiesterase 2', *Nat Struct Mol Biol,* 19(12), pp. 1363-71.

Schindelin, J., Arganda-Carreras, I., Frise, E., Kaynig, V., Longair, M., Pietzsch, T., Preibisch, S., Rueden, C., Saalfeld, S., Schmid, B., Tinevez, J.-Y., White, D. J., Hartenstein, V., Eliceiri, K., Tomancak, P. and Cardona, A. (2012) 'Fiji: an open-source platform for biological-image analysis', *Nature Methods,* 9(7), pp. 676-682.

Schneider, C. A., Rasband, W. S. and Eliceiri, K. W. (2012) 'NIH Image to ImageJ: 25 years of image analysis', *Nature Methods,* 9(7), pp. 671-675.

Schneider, J., Wood, A., Lee, J. S., Schuster, R., Dueker, J., Maguire, C., Swanson, S. K., Florens, L., Washburn, M. P. and Shilatifard, A. (2005) 'Molecular regulation of histone H3 trimethylation by COMPASS and the regulation of gene expression', *Mol Cell,* 19(6), pp. 849-56.

Schwacha, A. and Kleckner, N. (1995) 'Identification of double Holliday junctions as intermediates in meiotic recombination', *Cell,* 83(5), pp. 783-91.

Schwacha, A. and Kleckner, N. (1997) 'Interhomolog Bias during Meiotic Recombination: Meiotic Functions Promote a Highly Differentiated Interhomolog-Only Pathway', *Cell,* 90(6), pp. 1123-1135.

Serrentino, M.-E., Chaplais, E., Sommermeyer, V. and Borde, V. (2013) 'Differential Association of the Conserved SUMO Ligase Zip3 with Meiotic Double-Strand Break Sites Reveals Regional Variations in the Outcome of Meiotic Recombination', *PLOS Genetics,* 9(4), pp. e1003416.

Shahbazian, M. D., Zhang, K. and Grunstein, M. (2005) 'Histone H2B ubiquitylation controls processive methylation but not monomethylation by Dot1 and Set1', *Mol Cell,* 19(2), pp. 271-7.

Shinohara, A., Gasior, S., Ogawa, T., Kleckner, N. and Bishop, D. K. (1997) 'Saccharomyces cerevisiae recA homologues RAD51 and DMC1 have both distinct and overlapping roles in meiotic recombination', *Genes Cells,* 2(10), pp. 615-29.

Shinohara, A., Ogawa, H. and Ogawa, T. (1992) 'Rad51 protein involved in repair and recombination in S. cerevisiae is a RecA-like protein', *Cell,* 69(3), pp. 457-70.

Shinohara, M., Hayashihara, K., Grubb, J. T., Bishop, D. K. and Shinohara, A. (2015) 'DNA damage response clamp 9-1-1 promotes assembly of ZMM proteins for formation of crossovers and synaptonemal complex', *J Cell Sci,* 128(8), pp. 1494-506.

Shinohara, M., Oh, S. D., Hunter, N. and Shinohara, A. (2008) 'Crossover assurance and crossover interference are distinctly regulated by the ZMM proteins during yeast meiosis', *Nat Genet,* 40(3), pp. 299-309.

Shor, E., Weinstein, J. and Rothstein, R. (2005) 'A genetic screen for top3 suppressors in Saccharomyces cerevisiae identifies SHU1, SHU2, PSY3 and CSM2: four genes involved in error-free DNA repair', *Genetics,* 169(3), pp. 1275-89.

Silva, S., Altmannova, V., Luke-Glaser, S., Henriksen, P., Gallina, I., Yang, X., Choudhary, C., Luke, B., Krejci, L. and Lisby, M. (2016) 'Mte1 interacts with Mph1 and promotes crossover recombination and telomere maintenance', *Genes Dev,* 30(6), pp. 700-17.

Singh, T. R., Saro, D., Ali, A. M., Zheng, X. F., Du, C. H., Killen, M. W., Sachpatzidis, A., Wahengbam, K., Pierce, A. J., Xiong, Y., Sung, P. and Meetei, A. R. (2010) 'MHF1-MHF2, a histone-fold-containing protein complex, participates in the Fanconi anemia pathway via FANCM', *Mol Cell,* 37(6), pp. 879-86.

Smith, A. V. and Roeder, G. S. (1997) 'The yeast Red1 protein localizes to the cores of meiotic chromosomes', *J Cell Biol,* 136(5), pp. 957-67.

Snowden, T., Acharya, S., Butz, C., Berardini, M. and Fishel, R. (2004) 'hMSH4-hMSH5 recognizes Holliday Junctions and forms a meiosis-specific sliding clamp that embraces homologous chromosomes', *Mol Cell,* 15(3), pp. 437-51.

Soares, L. M., He, P. C., Chun, Y., Suh, H., Kim, T. and Buratowski, S. (2017) 'Determinants of Histone H3K4 Methylation Patterns', *Mol Cell,* 68(4), pp. 773-785.e6.

Solinger, J. A., Kiianitsa, K. and Heyer, W. D. (2002) 'Rad54, a Swi2/Snf2-like recombinational repair protein, disassembles Rad51:dsDNA filaments', *Mol Cell,* 10(5), pp. 1175-88.

Sommermeyer, V., Béneut, C., Chaplais, E., Serrentino, M. E. and Borde, V. (2013) 'Spp1, a member of the Set1 Complex, promotes meiotic DSB formation in promoters by tethering histone H3K4 methylation sites to chromosome axes', *Mol Cell,* 49(1), pp. 43-54.

Srinivasan, M., Petela, N. J., Scheinost, J. C., Collier, J., Voulgaris, M., M, B. R., Beckouët, F., Hu, B. and Nasmyth, K. A. (2019) 'Scc2 counteracts a Wapl-independent mechanism that releases cohesin from chromosomes during G1', *Elife,* 8.

Srinivasan, M., Scheinost, J. C., Petela, N. J., Gligoris, T. G., Wissler, M., Ogushi, S., Collier, J. E., Voulgaris, M., Kurze, A., Chan, K. L., Hu, B., COtanzo, V. and Nasmyth, K. A. (2018) 'The Cohesin Ring Uses Its Hinge to Organize DNA Using Non-topological as well as Topological Mechanisms', *Cell,* 173(6), pp. 1508-1519.e18.

Storlazzi, A., Gargano, S., Ruprich-Robert, G., Falque, M., David, M., Kleckner, N. and Zickler, D. (2010) 'Recombination proteins mediate meiotic spatial chromosome organization and pairing', *Cell,* 141(1), pp. 94-106.

Storlazzi, A., Xu, L., Schwacha, A. and Kleckner, N. (1996) 'Synaptonemal complex (SC) component Zip1 plays a role in meiotic recombination independent of SC polymerization along the chromosomes', *Proc Natl Acad Sci U S A,* 93(17), pp. 9043-8.

Subramanian, V. V., MacQueen, A. J., Vader, G., Shinohara, M., Sanchez, A., Borde, V., Shinohara, A. and Hochwagen, A. (2016) 'Chromosome Synapsis Alleviates Mek1-Dependent Suppression of Meiotic DNA Repair', *PLOS Biology,* 14(2), pp. e1002369.

Sun, X., Huang, L., Markowitz, T. E., Blitzblau, H. G., Chen, D., Klein, F. and Hochwagen, A. (2015) 'Transcription dynamically patterns the meiotic chromosome-axis interface', *Elife,* 4.

Sun, Z. W. and Allis, C. D. (2002) 'Ubiquitination of histone H2B regulates H3 methylation and gene silencing in yeast', *Nature,* 418(6893), pp. 104-8.

Sung, P. (1994) 'Catalysis of ATP-dependent homologous DNA pairing and strand exchange by yeast RAD51 protein', *Science,* 265(5176), pp. 1241-3.

Sym, M., Engebrecht, J. A. and Roeder, G. S. (1993) 'ZIP1 is a synaptonemal complex protein required for meiotic chromosome synapsis', *Cell,* 72(3), pp. 365-78.

Sym, M. and Roeder, G. S. (1995) 'Zip1-induced changes in synaptonemal complex structure and polycomplex assembly', *J Cell Biol,* 128(4), pp. 455-66.

Tang, S., Wu, M. K. Y., Zhang, R. and Hunter, N. (2015) 'Pervasive and essential roles of the Top3-Rmi1 decatenase orchestrate recombination and facilitate chromosome segregation in meiosis', *Mol Cell,* 57(4), pp. 607-621.

Tang, X., Hu, Z., Ding, J., Wu, M., Guan, P., Song, Y., Yin, Y., Wu, W., Ma, J., Huang, Y. and Tong, M.-H. (2025) 'In vitro reconstitution of meiotic DNA double-strand-break formation', *Nature,* 639(8055), pp. 800-807.

Taverna, S. D., Li, H., Ruthenburg, A. J., Allis, C. D. and Patel, D. J. (2007) 'How chromatin-binding modules interpret histone modifications: lessons from professional pocket pickers', *Nat Struct Mol Biol,* 14(11), pp. 1025-1040.

Tay, Y. D., Sidebotham, J. M. and Wu, L. (2010) 'Mph1 requires mismatch repair-independent and -dependent functions of MutSα to regulate crossover formation during homologous recombination repair', *Nucleic Acids Research,* 38(6), pp. 1889-1901.

Tessé, S., Bourbon, H. M., Debuchy, R., Budin, K., Dubois, E., Liangran, Z., Antoine, R., Piolot, T., Kleckner, N., Zickler, D. and Espagne, E. (2017) 'Asy2/Mer2: an evolutionarily conserved mediator of

meiotic recombination, pairing, and global chromosome compaction', *Genes Dev,* 31(18), pp. 1880-1893.

Thacker, D., Mohibullah, N., Zhu, X. and Keeney, S. (2014) 'Homologue engagement controls meiotic DNA break number and distribution', *Nature,* 510(7504), pp. 241-6.

Tisi, R., Vertemara, J., Zampella, G. and Longhese, M. P. (2020) 'Functional and structural insights into the MRX/MRN complex, a key player in recognition and repair of DNA double-strand breaks', *Comput Struct Biotechnol J,* 18, pp. 1137-1152.

Truebestein, L. and Leonard, T. A. (2016) 'Coiled-coils: The long and short of it', *Bioessays,* 38(9), pp. 903-16.

Tsubouchi, H. and Ogawa, H. (2000) 'Exo1 roles for repair of DNA double-strand breaks and meiotic crossing over in Saccharomyces cerevisiae', *Mol Biol Cell,* 11(7), pp. 2221-33.

Tsubouchi, T., Macqueen, A. J. and Roeder, G. S. (2008) 'Initiation of meiotic chromosome synapsis at centromeres in budding yeast', *Genes Dev,* 22(22), pp. 3217-26.

Tsubouchi, T., Zhao, H. and Roeder, G. S. (2006) 'The meiosis-specific zip4 protein regulates crossover distribution by promoting synaptonemal complex formation together with zip2', *Dev Cell,* 10(6), pp. 809-19.

Tsukamoto, Y., Mitsuoka, C., Terasawa, M., Ogawa, H. and Ogawa, T. (2005) 'Xrs2p regulates Mre11p translocation to the nucleus and plays a role in telomere elongation and meiotic recombination', *Mol Biol Cell,* 16(2), pp. 597-608.

Tung, K. S. and Roeder, G. S. (1998) 'Meiotic chromosome morphology and behavior in zip1 mutants of Saccharomyces cerevisiae', *Genetics,* 149(2), pp. 817-32.

Veaute, X., Jeusset, J., Soustelle, C., Kowalczykowski, S. C., Le Cam, E. and Fabre, F. (2003) 'The Srs2 helicase prevents recombination by disrupting Rad51 nucleoprotein filaments', *Nature,* 423(6937), pp. 309-12.

Vitaliano-Prunier, A., Menant, A., Hobeika, M., Géli, V., Gwizdek, C. and Dargemont, C. (2008) 'Ubiquitylation of the COMPASS component Swd2 links H2B ubiquitylation to H3K4 trimethylation', *Nat Cell Biol,* 10(11), pp. 1365-71.

Wan, L., Niu, H., Futcher, B., Zhang, C., Shokat, K. M., Boulton, S. J. and Hollingsworth, N. M. (2008) 'Cdc28-Clb5 (CDK-S) and Cdc7-Dbf4 (DDK) collaborate to initiate meiotic recombination in yeast', *Genes Dev,* 22(3), pp. 386-97.

Wang, J. C. (2002) 'Cellular roles of DNA topoisomerases: a molecular perspective', *Nature Reviews Molecular Cell Biology,* 3(6), pp. 430-440.

Wang, Y., Li, S. Y., Wang, Y. Z. and He, Y. (2023) 'ZmASY1 interacts with ZmPRD3 and is crucial for meiotic double-strand break formation in maize', *New Phytol,* 237(2), pp. 454-470.

Wells, D., Bitoun, E., Moralli, D., Zhang, G., Hinch, A., Jankowska, J., Donnelly, P., Green, C. and Myers, S. R. (2020) 'ZCWPW1 is recruited to recombination hotspots by PRDM9 and is essential for meiotic double strand break repair', *eLife,* 9, pp. e53392.

Wells, J. N., Gligoris, T. G., Nasmyth, K. A. and Marsh, J. A. (2017) 'Evolution of condensin and cohesin complexes driven by replacement of Kite by Hawk proteins', *Curr Biol,* 27(1), pp. R17-r18.

Wiedenheft, B., Sternberg, S. H. and Doudna, J. A. (2012) 'RNA-guided genetic silencing systems in bacteria and archaea', *Nature,* 482(7385), pp. 331-8.

Wild, P., Susperregui, A., Piazza, I., Dörig, C., Oke, A., Arter, M., Yamaguchi, M., Hilditch, A. T., Vuina, K., Chan, K. C., Gromova, T., Haber, J. E., Fung, J. C., Picotti, P. and Matos, J. (2019) 'Network Rewiring of Homologous Recombination Enzymes during Mitotic Proliferation and Meiosis', *Mol Cell,* 75(4), pp. 859-874.e4.

Woglar, A. and Villeneuve, A. M. (2018) 'Dynamic Architecture of DNA Repair Complexes and the Synaptonemal Complex at Sites of Meiotic Recombination', *Cell,* 173(7), pp. 1678-1691.e16.

Xaver, M., Huang, L., Chen, D. and Klein, F. (2013) 'Smc5/6-Mms21 prevents and eliminates inappropriate recombination intermediates in meiosis', *PLoS Genet,* 9(12), pp. e1004067.

Xue, X., Choi, K., Bonner, J. N., Szakal, B., Chen, Y. H., Papusha, A., Saro, D., Niu, H., Ira, G., Branzei, D., Sung, P. and Zhao, X. (2015) 'Selective modulation of the functions of a conserved DNA motor by a histone fold complex', *Genes Dev,* 29(10), pp. 1000-5.

Yan, Z., Delannoy, M., Ling, C., Daee, D., Osman, F., Muniandy, P. A., Shen, X., Oostra, A. B., Du, H., Steltenpool, J., Lin, T., Schuster, B., Décaillet, C., Stasiak, A., Stasiak, A. Z., Stone, S., Hoatlin, M. E., Schindler, D., Woodcock, C. L., Joenje, H., Sen, R., de Winter, J. P., Li, L., Seidman, M. M., Whitby, M. C., Myung, K., Constantinou, A. and Wang, W. (2010) 'A histone-fold complex and FANCM form a conserved DNA-remodeling complex to maintain genome stability', *Mol Cell,* 37(6), pp. 865-78.

Yang, H., Zhang, T., Tao, Y., Wu, L., Li, H.-t., Zhou, J.-q., Zhong, C. and Ding, J. (2012) 'Saccharomyces Cerevisiae MHF Complex Structurally Resembles the Histones (H3-H4)2 Heterotetramer and Functions as a Heterotetramer', *Structure,* 20(2), pp. 364-370.

Yu, H. G. and Koshland, D. E. (2003) 'Meiotic condensin is required for proper chromosome compaction, SC assembly, and resolution of recombination-dependent chromosome linkages', *J Cell Biol,* 163(5), pp. 937-47.

Zakharyevich, K., Ma, Y., Tang, S., Hwang, P. Y., Boiteux, S. and Hunter, N. (2010) 'Temporally and biochemically distinct activities of Exo1 during meiosis: double-strand break resection and resolution of double Holliday junctions', *Mol Cell,* 40(6), pp. 1001-15.

Zakharyevich, K., Tang, S., Ma, Y. and Hunter, N. (2012) 'Delineation of joint molecule resolution pathways in meiosis identifies a crossover-specific resolvase', *Cell,* 149(2), pp. 334-47.

Zheng, Z., Zheng, L., Arter, M., Liu, K., Yamada, S., Ontoso, D., Kim, S. and Keeney, S. (2025) 'Reconstitution of SPO11-dependent double-strand break formation', *Nature,* 639(8055), pp. 784-791.

Zhu, Z., Chung, W. H., Shim, E. Y., Lee, S. E. and Ira, G. (2008) 'Sgs1 helicase and two nucleases Dna2 and Exo1 resect DNA double-strand break ends', *Cell,* 134(6), pp. 981-94.

Zickler, D. and Kleckner, N. (1998) 'The leptotene-zygotene transition of meiosis', *Annu Rev Genet,* 32, pp. 619-97.

Zickler, D. and Kleckner, N. (2015) 'Recombination, Pairing, and Synapsis of Homologs during Meiosis', *Cold Spring Harbor perspectives in biology,* 7(6), pp. a016626.